Copyright Notices

Notice 1

Notice 2

Generation, Propagation and Detection of Multi-bound Solitons for Optical Communications

Nguyen Duc Nhan

A Thesis submitted in fulfilment of the requirements for the degree of Doctor of Philosophy

Department of Electrical and Computer Systems Engineering
Monash University
Australia

June 2011

Table of Contents

Abstract

Optical fibres can transmit terabit per second of information over thousands of kilometres. Although impressive, this performance is quickly being used up by new internet applications. Thus there is a constant need for innovation in optical communications systems. One such innovation is multi-bound solitons, which are groups of pulses that maintain their spacing over extremely long distances, so do not interfere with one another.

This thesis provides detailed studies of the generation, propagation and detection of bound solitons for telecommunications applications.

For generation, nonlinear actively-mode-locked fibre lasers are studied in detail, using analysis, numerical simulations and experiments. Their stability under a wide variety of operating conditions is investigated. Stable bound solitons can be generated when the laser's power is increased sufficiently. Excellent agreement between the simulated results and the experimental measurements for pulse width, pulse spectrum and RF spectrum is obtained.

These bound solitons were then propagated through standard single-mode transmission fibre. Experimental measurements show that the solitons remain bound in a single span of fibre. Numerical simulations illustrate the dynamics of the solitons at various powers. Again, excellent agreement is found between experimental and numerical results.

A novel technique for the detection and analysis of bound solitons is proposed. This uses bi-spectral analysis. A method of implementing bispectral analysis using four-wave mixing in optical fibres is investigated.

Declaration

I declare that this thesis is my own work, and it contains no material which has been accepted for the award of any other degree or diploma in any university or other institution. To the best of my knowledge this thesis contains no material previously published or written by another person, except where due reference is made in the text of the thesis.

June 2011

Nhan Duc Nguyen.

Acknowledgements

Firstly I would like to express deepest gratitude to my supervisor, Dr. Le Nguyen Binh, for his invaluable support and encouragement. Without his guidance through my research, this work cannot be done. I have learned from him lessons not only in science but also in life.

Next, I would like to express special thank to Prof. Arthur Lowery who has accepted to be my supervisor after Dr. Le Nguyen Binh retired. I really appreciate his help for helpful discussions and for the time he spent to read and correct the manuscripts.

I also would like to thank Dr. Khee Khok Pang, my associate supervisor although he passed away two years ago. He helped me during absence of Dr. Le Nguyen Binh. I had his useful advice about signal processing and communications.

I would like to acknowledge the financial support of my research at Monash University by the Programme No 322 of the Government of Socialist Republic of Vietnam. Thanks to the officers, Lan and Lien, of the program for their help.

I would like to thank the technicians in the ECSE Department for their help in my experiments, especially Mr. Tony Brosinsky who helped me a lot to build my experiment boards.

Many thanks go to my best friends, Liem Huynh and Trung Vo. They helped me familiarize with living in Melbourne, when I came to Monash University for the first time. We had a lot of interesting discussion in regards to my research topics.

I also take a chance to thank Huy Quang Lam who helped me know how to build a numerical model of mode-locked lasers at the early stage of my research.

To my friends and colleagues in Vietnam, too many to be named here, I appreciate their encouragement that helped me gain confidence in my academic life.

Finally and most importantly, I would like to express my gratitude to my whole family, especially my parents for their love and encouragement throughout my academic road I have gone. Unfortunately, my father passed away before I am fulfil his desire. He is always in my mind and this thesis is dedicated to him. I am very grateful to my wife, Minh Tran and my children for their love, patient and their support. They are the power in my life.

List of Figures

List of Tables

Abbreviations

AM	Amplitude modulation
APL	Additive pulse limiting
APM	Additive pulse mode locking
ASE	Amplified spontaneous emission
CGLE	Complex Ginzburg-Landau equation
CW	Continuous wave
DBS	Dual-bound soliton
DDF	Dispersion decreasing fibre
DI-NOLM	Dispersion imbalanced – nonlinear optical loop mirror
DM	Dispersion management
DQPSK	Differential quadrature phase shift keying
DSF	Dispersion shifted fibre
EDFA	Erbium-doped fibre amplifier
EO	Electro-optic
FM	Frequency modulation
FWM	Four-wave mixing
GLE	Ginzburg-Landau equation
GVD	Group velocity dispersion
HNLF	Highly nonlinear fibre
MLFRL	Mode-locked fibre ring laser
NOLM	Nonlinear optical loop mirror
NPC	Nonlinear phase conjugation
NPR	Nonlinear polarization rotation

NSE	Nonlinear Schrödinger Equation
OFDM	Orthogonal frequency division multiplexing
OOK	On-off keying
OSA	Optical spectrum analyser
OTDM	Optical time-division multiplexing
PC	Polarization controller
PCF	Photonic crystal fibre
PIC	Photonic integrated circuit
PMSL	Phase modulated Sagnac loop
QBS	Quadruple-bound soliton
RO	Relaxation oscillation
SBS	Stimulated Brillouin scattering
SMSR	Supermode noise suppression ratio
SPM	Self phase modulation
SRS	Stimulated Raman scattering
SSMF	Standard single mode fibre
TBS	Triple-bound soliton
THG	Third-harmonic generation
WDM	Wavelength division multiplexing
XPM	Cross phase modulation

Chapter 1

Introduction

Optical fibre communication technologies can now support terabits per seconds (Tbps) data rate [1-3]; however, the network capacity is approaching the Shannon limit, which is imposed by the signal-to-noise ratio and the nonlinear effects [4]. In order to increase the limit, some technologies have been proposed recently such as advanced modulation formats [5-6], multi-carrier transmission of orthogonal frequency division multiplexing (OFDM) [7-10] and digital coherent detection [6, 9, 11]. Another technique could be soliton transmission, a special pulse propagation scheme in balance between dispersion and nonlinear effect [12]. Nakazawa *et al.* [13] has demonstrated the 80 Gbit/s per channel soliton transmission at ultra-long transmission distance of ten thousands kilometres. Furthermore, this technique could be also preferred for optical packet switching due to fast switching rate and optical buffering of solitons [14-17].

One of the most important components in soliton transmission technique is the ultra-short pulse generator which is normally based on mode locking [18]. Ultra-short pulse generators can be used as data transmitters not only in soliton transmission systems [18], but also other systems such as optical time-division multiplexing (OTDM) systems [1, 19-20] and optical code-division multiple access (O-CDMA) systems [21]. They are also becoming more important in telecommunication systems

through various processing functions such as broad comb generation [10, 22], optical sampling or optical analog-to-digital conversion [23-28].

Bound solitons [29-33] are groups of a few solitons that influence each other's propagation velocities so that they maintain a constant timing between the solitons in the group. Multi-bound solitons suggest the group has three or more solitons within it. The relative phase of the solitons in the group can take on different values, such as 0, π, 0. This means that they could be used to convey information over large distances.

This thesis reports on multi-bound solitons laser with an emphasis on actively mode-locked fibre lasers. As a new form of solitons, multi-bound solitons generated from the actively FM mode-locked fibre laser is considered as a potential data carrier in soliton transmission systems. Three main functions according to three basic parts of a communication system will be investigated. They are generation, propagation and detection of multi-bound solitons.

1.1 MODE-LOCKED FIBRE LASERS AS ULTRA-SHORT PULSE GENERATORS

Ultra-short pulse lasers are commonly classified by their gain medium such as, solid-state, semiconductor or fibre. Each medium has its own advantages and disadvantages. In optical telecommunications, semiconductor and fibre gain media are most commonly used for generation of ultra-short pulses using techniques such as mode locking [34], gain switching [35] or external modulation [36]. Although semiconductor lasers offer a good engineering solution, mode-locked fibre lasers are being developed for optical communication systems [19, 37].

Mode locking is a technique for generating ultra-short pulses in fibre systems. When hundreds or thousands of longitudinal oscillation modes in a fibre cavity are forced to be in phase, short pulses are formed. The pulsewidth decreases when more longitudinal modes are phase-locked. It is important that mode-locked fibre lasers can directly produce hyperbolic secant pulses, which can propagate along transmission fibres as optical solitons. Soliton pulses are desirable in ultra-long haul transmission systems because they remain stability against perturbations of transmitting medium and keep the pulse shape undistorted during propagation.

Like any mode-locked lasers, mode-locked fibre lasers can be classified into two basic categories: actively and passively mode-locked.

1.1.1 Passive mode locking

Passively mode-locked fibre lasers do not use an external driving signal. Mode locking is achieved using loss modulation mechanisms of the passive elements. Figure 1-1 shows several configurations of passively mode-locked fibre lasers. The loss modulation is provided by: saturable absorption (SA) [38], nonlinear optical loop mirror (NOLM) [39] and nonlinear polarization rotation (NPR) [40]. The pulse shaping in all passively mode locked fibre lasers is based on intensity dependent discrimination, where the peak of optical pulse acquires the lowest loss while the temporal wings of the pulse experience a higher loss per roundtrip in the fibre cavity. After many roundtrips, the pulse is shortened until its bandwidth is limited by the gain bandwidth of the medium [34]. Because the operation of the NOLM and NPR are considered as fast saturable absorption processes, the width of their pulses is often very narrow, in the order of sub-300 fs [41-45]. Furthermore, it has been theoretically

and experimentally shown that a ring configuration of a mode-locked fibre laser will initiate mode-locking more easily at a lower threshold [46-47].

Although passively mode-locked fibre lasers can easily generate very short pulses with high peak powers, the repetition rates of their generated pulse trains is limited to around 100 MHz. The reason of limited repetition rate is due to that the length of the fibre cavity, which determines the fundamental frequency, is in the order of metres. This limitation prevents the passively mode-locked fibre lasers from being used in high data rate transmission applications. To increase the repetition rate in these fibre lasers, harmonic mode-locking, where multiple pulses coexist inside the fibre cavity can be employed. However, the output pulses may have amplitude and timing fluctuations, so they are unable to meet strict requirements in communication systems [48].

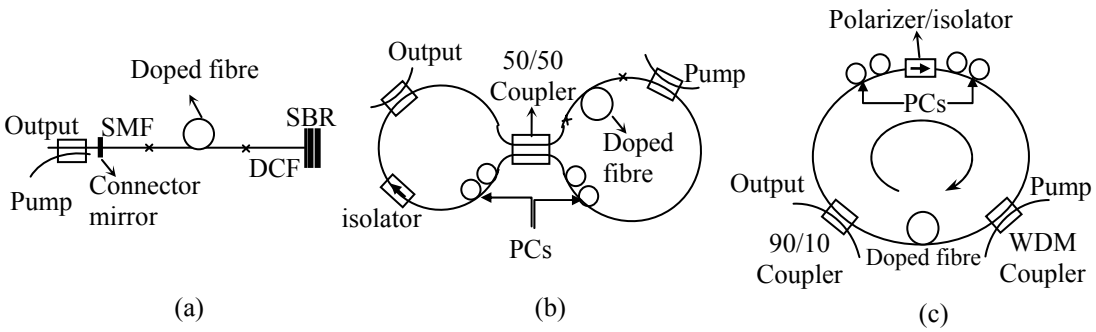

Figure 1-1 Typical configurations of passively mode-locked fibre laser: (a) Linear cavity configuration using a saturable Bragg reflector (SBR); (b) Figure-8 configuration based on nonlinear fibre loop mirror; (c) Ring configuration based on nonlinear polarization rotation. (PC: Polarization controller).

1.1.2 Active mode locking

Unlike passive mode-locking, active mode-locking has an element driven by an external electrical signal to modulate the loss or gain inside the fibre cavity. Most

actively mode-locked fibre lasers use integrated electro-optic $LiNbO_3$ modulators for mode locking. There are two types of modulator: amplitude modulators and phase modulators. These correspond to two active mode-locking mechanisms: amplitude modulation (AM) and frequency modulation (FM). A typical configuration of an actively mode-locked fibre laser using an amplitude or phase modulator is shown in Figure 1-2(a). To provide a high repetition rate pulse train, the modulator is driven at a harmonic of the fundamental mode spacing of the fibre loop. In AM mode-locking, the loss of the cavity is periodically modulated and the pulse is built up at the times that correspond to minimum loss in the fibre cavity as described in Figure 1-2(b). FM mode-locking is carried out by repeatedly up or down frequency chirping, so after many roundtrips the pulse is built up and shortened because the chirped tails of the pulses experience higher loss than the unchirped centre of the pulse. Recent studies [49-51] have shown the superiority of the FM mode-locked fibre laser compared to the AM mode-locked fibre laser. Firstly, a phase modulator is easier to control than an amplitude modulator because it has no DC bias point, so it avoids the problem of DC bias drift. Secondly, the pulses obtained from the FM mode-locked fibre laser are generally shorter than those obtained from the AM mode-locked fibre laser, due to the pulse compression induced by group velocity dispersion (GVD) and chirping from phase modulation [52]. The performance of a FM mode-locked fibre laser can be improved further in optimal combination between GVD, phase modulation and nonlinear effects in design of the fibre cavity [53]. Furthermore, FM mode-locked fibre lasers using rational harmonic mode locking to increase repetition rate, produce pulses with stable amplitudes due to the uniformity of the phase modulation [54]. Some other advantages such as the reduction of timing jitter or smaller quantum

limited jitter [55] also make the FM mode-locked fibre laser more attractive in high-capacity optical communication systems.

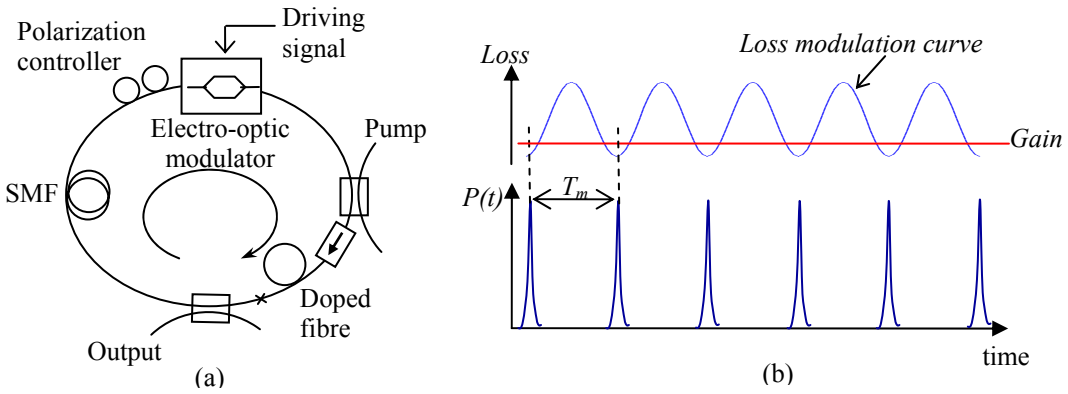

Figure 1-2 Typical configuration of actively mode-locked fibre laser (a) A fibre ring configuration, (b) a description of pulse formation in active mode locking.

Although actively mode-locked fibre lasers can produce short pulses at repetition rates of 10 – 40 Gigapulses/s, their pulsewidths are relatively wide, around a picosecond. The generation of sub-picosecond pulses at Gigapulses/s rates is especially important for Tbps transmission systems using OTDM [1]. Therefore it would be desirable to produce a sub-picosecond pulse train at a repetition rate of 10 – 40 Gigapulses/s with a conventional high speed modulator. Hence there are some techniques to compress optical pulses from actively mode-locked fibre lasers, such as hybrid mode locking, which combines passive and active mode locking [56], asynchronous mode locking [57-58] and adiabatic soliton pulse compression through dispersion decreasing fibres [59].

1.2 NONLINEAR PULSE PROPAGATION IN FIBRE OPTICS

Nonlinearity is a fundamental property of optical waveguides including optical fibres. The origin of the nonlinear response is related to the high order susceptibility of

optical material under the influence of an applied field [60-62]. For silica glasses, used for optical fibres and some nonlinear waveguides, only the third-order susceptibility is responsible for nonlinear effects, through its contribution to the total polarization [60]. In general, nonlinear effects in optical fibre can be classified into two classes. One class refers to the energy transfer from the optical field to the propagation medium that is the result of stimulated inelastic scattering such as stimulated Raman scattering (SRS) and stimulated Brillouin scattering (SBS) [60]. Another class is governed by the third-order susceptibility $\chi^{(3)}$ and responsible for most important nonlinear effects, which are called Kerr effects [61].

The Kerr effect is related to the intensity dependence of the refractive index or the nonlinear refractive index [60-61]. Important effects which originate from the nonlinear refractive index include third-harmonic generation (THG), four-wave mixing (FWM) and self-phase modulation (SPM), cross-phase modulation (XPM). Firstly, SPM refers to the self-induced phase shift experienced by an optical field during its propagation [60]. Because the phase change is proportional to the intensity, an optical pulse modulates its own phase with its intensity. The modulation of optical phase leads to frequency chirping related to the pulse shape. Therefore SPM is responsible for spectral broadening. In contrast to SPM, XPM and FWM effects require the participation of more than one optical fields, each having different wavelengths, direction or polarization state. The main difference between XPM and FWM is that the occurrence of FWM requires a specific phase matching condition [60, 62]. For XPM, an optical field with high intensity imposes a nonlinear phase shift on another field and this results in a spectral broadening similar to SPM. In FWM the interaction between optical fields creates new optical waves according to conservation

rules of energy-momentum. These Kerr effects are normally one type of the main impairments in optical transmission systems [62-63]. However, they are also very significant in photonic signal processing due to the instantaneous response of the third-order nonlinearity [64].

In certain conditions, the propagation of a special optical wave in a nonlinear medium, called an optical soliton, can occur. A first-order optical soliton is a solitary wave with an unchanging shape, because of the balance of nonlinear and linear effects in the medium. Optical solitons are normally classified into spatial and temporal solitons depending on the confinement of optical wave in time or space during propagation [65]. Spatial solitons remain confined and constant size of optical beams along propagation direction under the balance between spatial self-focusing and diffraction-induced spreading effects. Temporal optical solitons occur when there is a balance of the SPM with dispersion, to keep the pulse shape unchanged [65]. Due to this special feature, temporal solitons are very important in optical transmission applications, as well as the operation of mode-locked fibre lasers.

The optical Kerr nonlinearity plays an important role in mode-locked fibre lasers. Using high-power amplification, the pulses in the fibre cavity attain high enough intensities to cause a sufficiently-large nonlinear phase shift to affect the pulse formation in the cavity. In particular, SPM and XPM are the most important effects, which determine the mechanism of pulse formation of most passively mode-locked fibre lasers through NOLM and NPR operations [39-40]. Together with dispersion, the nonlinear phase shift plays an important role in the evolution of mode-locked pulses, as well as in shaping the output pulses. Particularly, in the normal dispersion regime, parabolic pulses with high energy are normally formed rather than the

Gaussian pulses [66-67]. In the anomalous dispersion regime, soliton pulses are formed [39-40]. Although nonlinear effects are not required for active mode locking, they also significantly influence the shape of the output pulses. Some reports that analysed the actively mode-locked fibre laser, including the nonlinear effects, demonstrated the influence of SPM on ultrashort pulse generation [37, 68-70]. In general, SPM in the active mode-locked fibre causes pulse compression, based on the soliton effect [69], and suppression of supermode noise, which would cause an amplitude fluctuation induced by ASE noise [71]. Thus, a stable operating regime is only attained when the pulse power exceeds a certain value. Furthermore, for actively FM mode-locked fibre lasers, the presence of SPM in the cavity greatly modifies the up- and down-chirp caused by the phase modulation and so suppresses the relaxation oscillation which would cause intensity fluctuations [53, 72].

1.3 DETECTION OF ULTRA-SHORT PULSES IN FIBER OPTICS

For broadband signals like ultra-short soliton pulses, their detection and characterization are challenging due to the limitation of instrumentation bandwidth in electrical domain. The bandwidth of signal can be broadened from hundreds of GHz to tens of THz using OTDM [1, 19-20] and multi-carrier transmission technologies [6-10]. Moreover, advanced modulation formats can be applied in these technologies [10, 20], hence they can set new challenges such as phase information detection and phase preservation in signal processing.

In order to overcome above challenges, ultra-fast photonic processing is required for detection. By shifting signal processing from the electronic domain to the photonic domain, the limitation of operation bandwidth is easily eliminated. Ultra-fast

photonic signal processing can be implemented by exploiting nonlinearity in optical guided systems such as optical fibres and nonlinear waveguides [61-62]. The autocorrelation methods, which are the most popular in ultra-short pulse characterization, can exploit optical nonlinear effects such as the second-harmonic generation [73] and the third-harmonic generation [74]. Dorrer and Maywar [75] have proposed RF spectrum analysis of broadband signal using nonlinear effects. A RF spectrum analysis of the signal with bandwidth of greater than 1 THz has been performed [76]. Besides many other signal processing functions exploiting Kerr effects can be implemented to overcome the bandwidth limitation in future networks [77-81].

This rapid progress of nonlinear signal processing is due to the development of nonlinear devices. Initially, the dispersion shifted (DS) fibre was used as a highly nonlinear fibre (HNLF), because of its modified the fibre geometry [82]. The value of the nonlinear coefficient of this fibre is normally tens times higher than standard single mode fibre (SSMF), which is mainly achieved by reducing the fibre core area. Consequently, a length of DS-HNLF of hundreds of metres is required in some nonlinear signal processing applications. Recent advances in the development of HNLFs have attempted to reduce their required length and operating power in practical applications. Through modifying the fibre's structure as well as the glass composition, many novel HNLFs such as photonic crystal fibres [83], microstructure fibres [84] and Bismuth-based or chalcogenide glass fibres [85-86] have been developed with the achieved nonlinear coefficients beyond hundreds to thousands times higher than that of SSMF. Another option is based on nonlinear waveguides to enable photonic signal processing in compact devices which has recently attracted a

lot attention in research [87-88]. The benefit of using nonlinear waveguides is the feasibility of the development of photonic integrated circuits (PICs) for all-optical signal processing. Recently, it has been shown that a dispersion engineered planar chalcogenide waveguide is an attractive candidate for photonic signal processing devices in future optical networks [87]. With the nonlinear coefficient of approximately 10000 $W^{-1}km^{-1}$, which is ten thousand times greater than that of SSMF, multi-function processing of optical signal at ultra-high speed has been demonstrated in compact devices [80-81].

1.4 MOTIVATION AND OBJECTIVES OF THE THESIS

As demonstrated above, an actively FM mode-locked fibre laser can offer many advantages such as generation of a stable ultra-short pulse sequence at common transmission rates, synchronization with other electronic components in communication systems and low timing jitter. Moreover, active phase modulation has made an important contribution to shortening and stability of mode-locked pulses, especially in presence of dispersion and nonlinear effects [56-58]. Although actively mode-locked fibre lasers have been available commercial, they are still the subject for fundamental research, such as pulse dynamics in various operating conditions. On the other hand, it is important to explore the principles of operation of actively FM mode-locked fibre lasers in order to discover new operation regimes.

This thesis covers not only the generation of bound solitons, a new state in actively mode-locked fibre rings, but also investigates the dynamic characteristics of bound solitons when they propagate along optical transmission fibres. In periodic systems such as within mode-locked fibre lasers, solitons, or more correctly

dissipative solitons, experience periodically loss and gain effects and they behave in various interesting regimes. When the fibre ring cavity operates in strongly nonlinear regime, soliton pulses can exhibit several exciting characteristics such as bifurcation, period-doubling, chaos and specially bound states observed recently [29-33]. However, most research effort has focused on the passively mode-locked fibre laser systems [29-33, 89], it is only recently that attention has been paid to the actively mode-locked fibre laser system [90]. On the other hand, understanding the dynamic aspects of actively mode-locked soliton fibre lasers remains very challenging. The dynamic behaviours of soliton in the active mode-locked fibre laser are different from that in the passive mode-locked fibre laser due to the presence of a modulator. Moreover, the limitations of repetition rate and instability of bound solitons can be eliminated by active mode locking.

The stability of bound solitons relates to the interactions in mode-locked fibre ring cavity that depends strongly on the phase difference between the individual solitons [91]. For a conventional system, a power spectrum or a Fourier transform of autocorrelation is popular technique to characterize the signal [92]. However this is not sufficient for phase modulated signals because the phase information is hidden in common power spectrum analysis. Instead of power spectrum characterization, the bi-spectrum which is the Fourier transform of the triple-order correlation, can provide us not only magnitude information but also phase information [93]. It is especially useful in characterizing non-Gaussian nonlinear processes and so is applicable in many various fields such as signal processing, biomedicine and image reconstruction [94]. Therefore, using this technique to characterize the dynamic states of solitons in mode-

locked fibre lasers is attractive. This thesis shows it can be a useful tool to analyse the behaviour of signals generated from these systems, such as multi-bound solitons.

This thesis focuses on three issues: the generation, propagation and detection of multi-bound solitons. The first issue is the generation of multi-bound solitons using actively FM mode-locked fibre ring lasers. Mechanisms of multi-bound soliton formation in an actively fibre ring under high nonlinear scheme are investigated. In addition, the phase relationship between bound solitons and the influence of active phase modulation on the formation and the stability of multi-bound solitons are also discussed. The second issue is the propagation of multi-bound solitons along fibres. The dynamic behaviour of multi-bound solitons during propagation along the fibres will be investigated to examine them as potential data carriers. Finally, bispectrum techniques are proposed to characterize multi-bound solitons. By exploiting parametric process for signal processing, bispectrum estimation based on FWM effect will be examined.

1.5 ORGANIZATION OF THE THESIS AND RESEARCH CONTRIBUTIONS

This thesis is divided into three main parts. The first part is devoted to experimentally and numerically investigations of actively FM mode-locked fibre ring lasers as a multi-bound solitons generator. The second part focuses on experimental and numerical investigations of propagation of multi-bound solitons in fibres. The last part is numerical investigations of bispectrum technique for analysis of multi-bound soliton states and the third-order nonlinearity parametric process. Therefore, the thesis is organized in following manner:

Chapter 2 reviews the theory of mode-locked fibre laser. Firstly, the fundamentals of pulse propagation in nonlinear dispersive medium are introduced through important nonlinear Schrödinger equations and their analytical solutions. These equations also provide the theoretical basis for building theoretical models of mode-locked fibre lasers. A theoretical foundation of soliton generation in the nonlinear fibre ring resonators based on both passive and active mode-locking techniques is given in this chapter.

Chapter 3 presents original experimental work on the actively FM mode-locked fibre lasers to investigate soliton generation in single pulse scheme. Numerical simulations are also used to investigate the pulse formation inside the fibre cavity as well as to verify the experimental results. The effect of detuning of the FM mode-locked fibre laser is experimentally and numerically investigated. The results obtained in this chapter are the foundations for the next chapters.

Chapter 4 investigates multi-bound solitons in nonlinear fibre ring lasers. Firstly, a review of bound solitons generated by passively mode-locked fibre lasers is given. The mechanisms of bound soliton formation in the fibre ring cavity are introduced. Then the conditions of multi-bound soliton formation in an actively fibre ring laser are determined and discussed due to presence of the active phase modulation. Experiments on, and simulations of, the generation of multi-bound solitons in actively FM mode-locked fibre ring lasers are described in this chapter. For the first time, the existence of multi-bound solitons up to the fourth-order has been demonstrated. These results have been published in my papers [N1], [N5] and [N8]. Multi-bound solitons up to the sixth-order have been published in my papers [N3] and [N10].

In actively FM mode-locked fibre ring lasers, the electro-optic (EO) phase modulator is a key component for not only mode locking but also multi-bound soliton generation. Therefore Chapter 5 is devoted to the influence of EO phase modulators on pulse shaping of multi-bound solitons. Measurements of the phase modulator's dynamic response and half-wave voltage are implemented to show the difference between two typical types of EO phase modulators: lumped type and travelling-wave type. The influence of the EO phase modulator on the operating states of actively FM mode-locked fibre ring laser concentrates on two aspects; the artificial comb-filtering generated from the modal birefringence of the phase modulator and the chirping caused by the RF driving signal. These results show the modulator's effect on wavelength tunability and stability of multi-bound solitons. These results have been published in my papers [N3], [N5], [N9] and [N12].

An advantage of the actively mode-locked fibre ring is that it can generate a stable periodic train of multi-bound solitons. Therefore Chapter 6 experimentally investigates propagation of multi-bound solitons in optical fibres. A theoretical basis of soliton transmission in optical fibres is also reviewed. Numerical simulations are also implemented to investigate the dynamic behaviour of different multi-bound solitons during propagation along the fibres. The results of this chapter have been presented in [N3], [N11].

Chapter 7 concentrates on photonic signal processing. Although an approach of temporal imaging based signal processing using EO phase modulator has been presented in [N6], most content of this chapter focus on photonic signal processing exploiting the parametric process in the third-order nonlinearity. Hence a fundamental theory of FWM is reviewed and then important applications based on FWM such as

parametric amplification and OTDM demultiplexing using nonlinear waveguides are examined via simulation. A part of these works has been presented in my paper [N13]. In another approach to characterize the phase modulated signal, bispectrum analysis is proposed. Therefore, the basis of bispectrum analysis is introduced before this technique is applied to the analysis of multi-bound solitons. This chapter also considers the possibility of bispectrum estimation based on FWM. The limitations of this estimation as well as its application in optical receivers have been discussed and presented in [N15].

Finally, the summary of all works and important conclusion obtained in this thesis are given and some directions of research for future works are presented in the last chapter.

A list of publications achieved through the stages of the thesis project is given in Appendix A.

Chapter 2

Theory of mode-locked fibre lasers

2.1 INTRODUCTION

Mode-locked fibre lasers can be modelled as a quasi-lossless fibre transmission system. Therefore propagation of optical pulse inside a mode-locked fibre laser can be described by the nonlinear Schrödinger equation similar to that used in optical fibre links [95]. In this chapter, nonlinear Schrödinger equations are reviewed to describe the propagation of optical pulse in optical fibres. The generalized nonlinear Schrödinger equation can be easily modified to derive the master equations for mode locking and to develop a numerical model for a specific mode-locked fibre laser as described the next chapters. The conditions for mode locking and important operation modes of mode-locked fibre lasers are reviewed through analytical solutions of simplified master equations.

2.2 THE NONLINEAR SCHRÖDINGER EQUATIONS

2.2.1 Nonlinear Schrödinger equation

For a full description of optical pulse propagation, we start with the generalized nonlinear Schrödinger equation (NSE) which can be derived from the wave equation by using method of separating variables [60]. This derivation follows Agrawal [60] and is included for completeness.

$$\frac{\partial A(z,t)}{\partial z}+\frac{\alpha}{2}A(z,t)-j\sum_{n=1}^{\infty}\frac{j^n\beta_n}{n!}\frac{\partial^n A(z,t)}{\partial t^n} = j\gamma\left(1+\frac{j}{\omega_0}\frac{\partial}{\partial t}\right)\times A(z,t)\int_{-\infty}^{\infty}R(t')\left|A(z,t-t')\right|^2 dt' \quad (2\text{-}1)$$

where *A(z,t)* is the slowly varying complex envelope propagating along *z* in the propagation medium, the effect of propagation constant β around the optical carrier frequency ω_0 is Taylor-series expanded, *R(t)* is the nonlinear response function, and $\gamma=\omega_0 n_2/cA_{eff}$ is the nonlinear coefficient. In most optical communication applications, optical pulses with the widths broader than 100 fs are employed, so Eq.(2-1) can be further simplified as [60]

$$\frac{\partial A}{\partial z}+\frac{\alpha}{2}A+\frac{j\beta_2}{2}\frac{\partial^2 A}{\partial\tau^2}-\frac{\beta_3}{6}\frac{\partial^3 A}{\partial\tau^3}=j\gamma\left[\left|A\right|^2 A+\frac{j}{\omega_0}\frac{\partial\left(\left|A\right|^2 A\right)}{\partial\tau}-T_R A\frac{\partial\left(\left|A\right|^2\right)}{\partial\tau}\right] \quad (2\text{-}2)$$

where a frame of reference moving with the pulse at the group velocity v_g is used by making the transformation $\tau=t-z/v_g\equiv t-\beta_1 z$, and the propagation constant is expanded up to the third order term that includes the group velocity dispersion (β_2) and the third order dispersion (β_3). In (2-2), the first moment of the nonlinear response function is defined as [60]

$$T_R\equiv\int_0^{\infty}tR(t')dt' \quad (2\text{-}3)$$

which is responsible for Raman scattering effect and the second term in the right side of (2-2) is responsible for self-steepening effect. However, if the width of optical pulses is of the order of picoseconds, high-order effects such as self-steepening and Raman scattering can be ignored. Hence Eq.(2-2) becomes [60]

$$\frac{\partial A}{\partial z}+\frac{\alpha}{2}A+\frac{j\beta_2}{2}\frac{\partial^2 A}{\partial\tau^2}-\frac{\beta_3}{6}\frac{\partial^3 A}{\partial\tau^3}=j\gamma\left|A\right|^2 A \quad (2\text{-}4)$$

This equation can describe the most important linear and nonlinear propagation effects of optical pulse in optical fibres.

If we further simplify the Eq.(2-4) by setting the attenuation factor and the third-order dispersion coefficient to zero, then the traditional NSE can be obtained as

$$\frac{\partial A}{\partial z}+\frac{j\beta_2}{2}\frac{\partial^2 A}{\partial \tau^2}=i\gamma\left|A\right|^2 A \qquad (2\text{-}5)$$

Eq.(2-5) is a well known equation in nonlinear fibre optics which is employed to explain propagation of optical solitary waves or solitons in nonlinear dispersive medium [60].

2.2.2 Ginzburg-Landau equation: A modified nonlinear Schrödinger equation

Although the NSEs described above can be used to explain most of nonlinear effects including higher-order effects, they only describe the pulse propagation in passive nonlinear media without gain. In a propagation medium with gain as fibre amplifiers, the gain effect is required to be included into the NSE. The NSE equation with gain effect is also called the Ginzburg-Landau equation (GLE), which can be also derived from the wave equation [96]. Beside the cubic GLE, an extended version is the quintic cubic G-L equation (QCGLE) which has also attracted considerable attention [97]. The GLEs play an important role in description of nonlinear systems including nonlinear fibre optics [64, 95, 97] as well as fibre lasers [98-99].

In general an amplification of optical pulse in active fibres with gain coefficient $g(\omega)$ can be simply given as follows [100]

$$\frac{\partial A(z,\omega)}{\partial z}=\frac{1}{2}g(\omega)A(z,\omega) \qquad (2\text{-}6)$$

For an approximation of homogeneously broadened system, the gain spectral shape takes a Lorentzian profile [64]:

$$g(\omega) = \frac{g_0}{1 + (\omega - \omega_g)^2 / \Delta\omega_g^2} \tag{2-7}$$

where g_0 is the maximum small signal gain, ω_g is the atomic transition frequency and $\Delta\omega_g$ is the gain bandwidth which relates to the dipole relaxation time. The gain spectrum can be approximated by a Taylor series expansion in around ω_g:

$$g(\omega) \approx g_0 \left(1 - (\omega - \omega_g)^2 / \Delta\omega_g^2\right) \tag{2-8}$$

By substituting (2-8) into (2-6), and taking the inverse Fourier transform with assumption of the carrier frequency ω_0 close to ω_g, the propagation equation with amplification is obtained as follows

$$\frac{\partial A(z,t)}{\partial z} = \frac{g_0}{2}\left[A(z,t) + \frac{1}{\Delta\omega_g^2}\frac{\partial^2 A(z,t)}{\partial t^2} \right] \tag{2-9}$$

However, in many cases of pulse propagation, especially in the mode-locked fibre laser systems, the gain saturation plays an important role in pulse amplification. Therefore, the saturation need to be included in (2-9) by replacing g_0 in g_{sat} [64]

$$g_{sat}(z) = \frac{g_0(z)}{1 + P_{av}(z)/P_{sat}} \tag{2-10}$$

and (2-9) is modified by using (2-10) as

$$\frac{\partial A(z,t)}{\partial z} = \frac{g_{sat}}{2}\left[A(z,t) + \frac{1}{\Delta\omega_g^2}\frac{\partial^2 A(z,t)}{\partial t^2} \right] \approx \frac{g_0}{2\left(1 + P_{av}(z)/P_{sat}\right)}\left[A(z,t) + \frac{1}{\Delta\omega_g^2}\frac{\partial^2 A(z,t)}{\partial t^2} \right] \tag{2-11}$$

where g_0 is assumed to be constant along the active fibre or unsaturated gain coefficient, P_{sat} is the saturated power of the gain medium, P_{av} is the average power of the signal at position z in the active fibre as [101]

$$P_{av}(z)=\frac{1}{T_m}\int_{-T_m/2}^{T_m/2}\left|A(z,t)\right|^2 dt \tag{2-12}$$

For a full model of the pulse evolution in gain medium, other effects such as dispersion, nonlinear effects are also required to be included in (2-11). Hence, by combining two equations (2-11) and (2-4), a modified NSE can be obtained:

$$\frac{\partial A}{\partial z}+\frac{j}{2}\left(\beta_2+\frac{jg_{sat}}{\Delta\omega_g^2}\right)\frac{\partial^2 A}{\partial\tau^2}-\frac{\beta_3}{6}\frac{\partial^3 A}{\partial\tau^3}=i\gamma\left|A\right|^2 A+\frac{1}{2}\left(g_{sat}-\alpha\right)A \tag{2-13}$$

This is the cubic GLE which is normally used to describe pulse propagation in mode-locked fibre lasers [95, 98-99].

2.2.3 Coupled nonlinear Schrödinger equations

In some fibre systems where there are more than one polarization state present in the fibre, pulse propagation is described by two coupled nonlinear Schrodinger equations [60]. These equations are significant in the models relating to polarization states such as polarization mode dispersion in fibre transmission and nonlinear polarization rotation in passive mode locking [102-104].

By the same manner similar to the NSE for single mode, two coupled equations for the slowly varying polarization components of the optical field can be derived as follows [102]:

$$\begin{aligned}\frac{\partial A_x}{\partial z}+\frac{\Delta\beta_1}{2}\frac{\partial A_x}{\partial\tau}+\frac{j}{2}\left(\beta_2+\frac{jg_{sat}}{\Delta\omega_g^2}\right)\frac{\partial^2 A_x}{\partial\tau^2}-\frac{\beta_3}{6}\frac{\partial^3 A_x}{\partial\tau^3}&=\frac{1}{2}\left(g_{sat}-\alpha\right)A_x\\ &+j\gamma\left[\left(\left|A_x\right|^2+\tfrac{2}{3}\left|A_y\right|^2\right)A_x+\tfrac{j}{3}A_x^* A_y^2\exp(-2j\Delta\beta_0 z)\right]\end{aligned} \tag{2-14}$$

$$\begin{aligned}\frac{\partial A_y}{\partial z}-\frac{\Delta\beta_1}{2}\frac{\partial A_y}{\partial\tau}+\frac{j}{2}\left(\beta_2+\frac{jg_{sat}}{\Delta\omega_g^2}\right)\frac{\partial^2 A_y}{\partial\tau^2}-\frac{\beta_3}{6}\frac{\partial^3 A_y}{\partial\tau^3}&=\frac{1}{2}\left(g_{sat}-\alpha\right)A_y\\ &+j\gamma\left[\left(\left|A_y\right|^2+\tfrac{2}{3}\left|A_x\right|^2\right)A_y+\tfrac{j}{3}A_y^* A_x^2\exp(+2j\Delta\beta_0 z)\right]\end{aligned} \tag{2-15}$$

where A_x, A_y are the slowly varying envelopes of orthogonal polarization components, $\Delta\beta_1 = \beta_{1,x} - \beta_{1,y} = \Delta n_g / c$ is the , Δn_g is the group birefringence.

With highly birefringent fibres, the terms $\exp(-2j\Delta\beta_0 z)$ and $\exp(+2j\Delta\beta_0 z)$ can be neglected due to their rapid oscillations and equations (2-14)-(2-15) become:

$$\frac{\partial A_x}{\partial z} + \frac{\Delta\beta_1}{2}\frac{\partial A_x}{\partial \tau} + \frac{j}{2}\left(\beta_2 + \frac{j g_{sat}}{\Delta\omega_g^2}\right)\frac{\partial^2 A_x}{\partial \tau^2} - \frac{\beta_3}{6}\frac{\partial^3 A_x}{\partial \tau^3} = j\gamma\left(\left|A_x\right|^2 + \tfrac{2}{3}\left|A_y\right|^2\right)A_x + \frac{1}{2}\left(g_{sat} - \alpha\right)A_x \quad (2\text{-}16)$$

$$\frac{\partial A_y}{\partial z} - \frac{\Delta\beta_1}{2}\frac{\partial A_y}{\partial \tau} + \frac{j}{2}\left(\beta_2 + \frac{j g_{sat}}{\Delta\omega_g^2}\right)\frac{\partial^2 A_y}{\partial \tau^2} - \frac{\beta_3}{6}\frac{\partial^3 A_y}{\partial \tau^3} = j\gamma\left(\left|A_y\right|^2 + \tfrac{2}{3}\left|A_x\right|^2\right)A_y + \frac{1}{2}\left(g_{sat} - \alpha\right)A_y \quad (2\text{-}17)$$

For an optical fibre with the length L, the phase variation of polarization components due to nonlinearity can be derived by considering the nonlinear term only in (2-16)-(2-17) for simplicity

$$\phi_{NL}^x = \gamma L\left(\left|A_x\right|^2 + \tfrac{2}{3}\left|A_y\right|^2\right) \text{ and } \phi_{NL}^y = \gamma L\left(\left|A_y\right|^2 + \tfrac{2}{3}\left|A_x\right|^2\right) \quad (2\text{-}18)$$

and hence the angle of polarization rotation is given by

$$\varphi_{NPR} = \varphi_{NL}^y - \varphi_{NL}^x = \frac{\gamma L}{3}\left(\left|A_y\right|^2 - \left|A_x\right|^2\right) \quad (2\text{-}19)$$

Note that this angle is zero when the light input is linearly polarized due to $\left|A_x\right|^2 = \left|A_y\right|^2$. On the other hand, the polarization ellipse rotates with nonlinear propagation in the fibre.

2.3 OPTICAL SOLITONS

2.3.1 Temporal solitons

As mentioned in Chapter 1, optical solitons in fibre systems are temporal solitons formed by the balance between SPM and GVD effects during propagation. The propagation of optical soliton in nonlinear dispersive media such as optical

waveguides or fibres is governed by the standard NSE (2-5) derived in Section 2.2.1. By using the transformation of variables as following [64]:

$$T = \tau / \tau_0 \ , \ \xi = z / L_D \ , \ u = \sqrt{\gamma L_D}\, A \tag{2-20}$$

where τ_0 is a temporal scaling parameter often taken to be the input pulse width and $L_D = \tau_0^2 / |\beta_2|$ is the dispersion length. Eq.(2-5) can be normalized to the (1+1)-dimensional NSE as follows [64]

$$j\frac{\partial u}{\partial Z} - \frac{s}{2}\frac{\partial^2 u}{\partial T^2} \pm |u|^2 u = 0 \tag{2-21}$$

where $s = sgn(\beta_2) = \pm 1$ stands for the sign of the GVD parameter which can be positive or negative, depending on the wavelength. The nonlinear term is positive (+1) for optical fibres but may become negative (-1) for waveguides made of semiconductor materials. Thus there are two cases of basic propagation in optical fibres relating to the dispersion which is normally measured by the parameter

$$D = \frac{d}{d\lambda}\left(\frac{1}{v_g}\right) = -\frac{2\pi c}{\lambda^2}\beta_2 \tag{2-22}$$

where the dispersion parameter D is expressed in units of ps/(nm.km). For standard single mode fibre, D is positive or GVD is anomalous at wavelengths > 1.3 μm and D is negative or GVD is normal at wavelengths shorter than 1.3 μm.

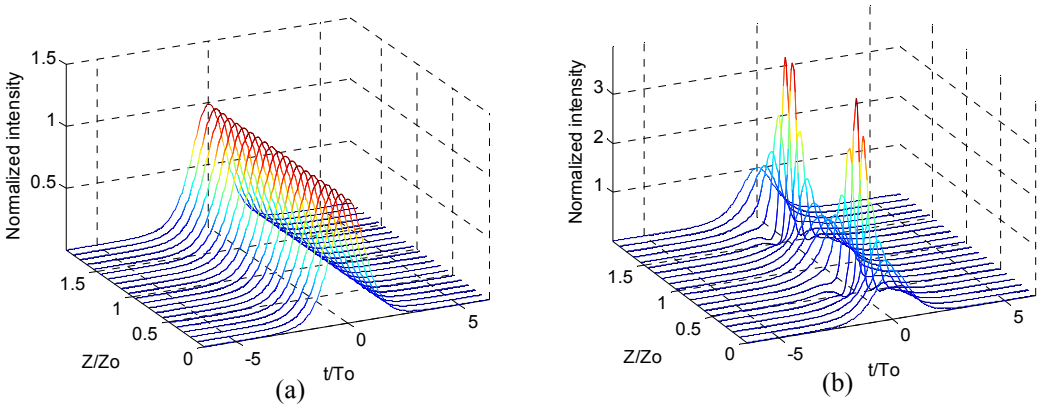

Figure 2-1 Evolution of (a) the first order soliton, and (b) the second order soliton over 2 soliton periods. (Results obtained using MATLAB)

Because of two possible signs of the GVD parameter, optical fibres can support two different types of solitons which are solutions of Eq.(2-21). In particular, Eq.(2-21) has solutions in the form of dark temporal solitons in case of normal GVD (s = +1) and bright temporal solitons in case of anomalous GVD (s = -1). These solutions can be found by the inverse scattering method [105]. In case of anomalous GVD, Eq.(2-21) takes the form

$$j\frac{\partial u}{\partial Z}+\frac{1}{2}\frac{\partial^2 u}{\partial T^2}+|u|^2 u=0 \qquad (2\text{-}23)$$

and the most interesting solution of (2-23) is the fundamental soliton with general form given by

$$u(\xi,T)=\operatorname{sech}(T)\exp(j\xi/2) \qquad (2\text{-}24)$$

Thus at the input of the fibre, the soliton is given as $u(0,T)=\operatorname{sech}(T)$ and it can be converted into real units as follows:

$$A(0,\tau)=\sqrt{P_0}\operatorname{sech}\left(\frac{\tau}{\tau_0}\right)=\left(\frac{|\beta_2|}{\gamma\tau_0^2}\right)^{1/2}\operatorname{sech}\left(\frac{\tau}{\tau_0}\right) \qquad (2\text{-}25)$$

Solution (2-25) indicates that if a hyperbolic-secant pulse with peak power P_0 which satisfies expression in (2-25), it can propagate undistorted without change in temporal and spectral shapes in an ideal lossless fibre at arbitrary distances as shown in Figure 2-1(a). This result is obtained by using a simple MATLAB simulation with the code listed in Appendix B. This important feature results from the balance between GVD and SPM effects. When the peak power launched into the fibre is much higher, a higher-order soliton can be excited with the input form [60]

$$u(0,T) = N\text{sech}(T) \tag{2-26}$$

where N is an integer represents for the soliton order and determined by

$$N^2 = \frac{L_D}{L_{NL}} = \frac{\gamma P_0 \tau_0^2}{|\beta_2|} \tag{2-27}$$

Different from the fundamental soliton, the temporal and spectral shapes of higher-order solitons ($N > 1$) vary periodically during propagation with the period $\xi_0 = \pi/2$ or in real units $z_0 = \pi L_D/2$. Figure 2-1(b) shows a periodic variation of second order soliton as an example.

With $s = +1$ in case of normal GVD, Eq.(2-21) takes the form

$$j\frac{\partial u}{\partial Z} - \frac{1}{2}\frac{\partial^2 u}{\partial T^2} + |u|^2 u = 0 \tag{2-28}$$

and solutions of (2-28) are dark solitons which is found by the inverse scattering method similar to the case of bright solitons. Solution of a fundamental dark soliton is given by [60, 106]

$$u(\xi,T) = \cos\phi \tanh\left[\cos\phi(T - \xi\sin\phi) - j\sin\phi\right]\exp(j\xi) \tag{2-29}$$

The features of the dark soliton are a high constant power level with an intensity dip and an abrupt phase change at the centre depending on parameter ϕ. For $\phi = 0$, the dark soliton is a black soliton with the zero dip and a phase jump of π at the centre. When $\phi \neq 0$, the dip intensity is non-zero and such solitons are called the grey solitons as shown in Figure 2-2.

In general, solitons in fibre have attracted a lot of interest from researchers. In communication systems, the understanding of solitons is of importance in both transmission and signal processing [64, 106-107].

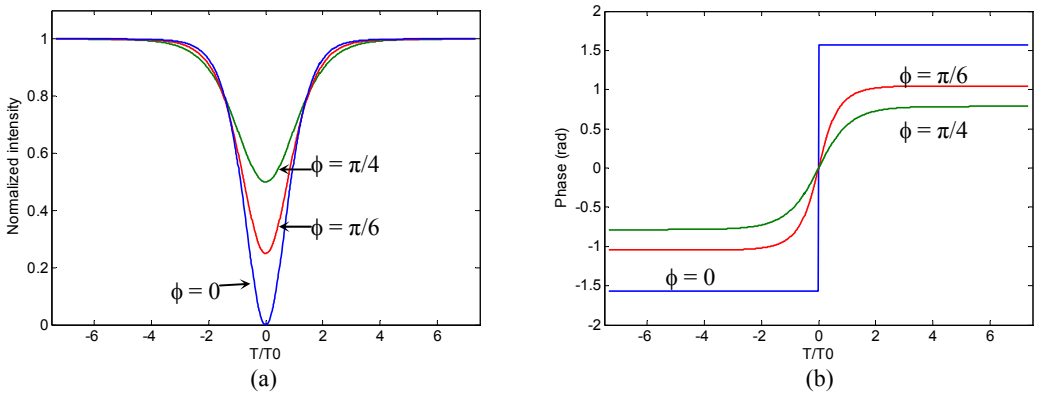

Figure 2-2 (a) Intensity and (b) phase profiles of dark solitons for various values of the internal phase ϕ.

2.3.2 Dissipative solitons

The optical solitons mentioned above only exist in an ideal propagation medium that has no any perturbations such as loss and gain. In practical systems such as mode-locked fibre lasers, the optical signal is periodically amplified to compensate the loss that it experiences in the fibre cavity. Thus there is a periodic variation of the pulse power which can form an index grating and induce modulation stability. It has been demonstrated that solitons are able to exist in these systems [64]. Therefore, propagation of optical pulse in this case should be described by the GLE (2-13) which

includes the loss and gain effects. Similar to the standard NSE, it is useful to introduce the dimensionless variables and Eq.(2-13) becomes

$$j\frac{\partial u}{\partial \xi}-\frac{1}{2}(s+jd)\frac{\partial^2 u}{\partial T^2}+|u|^2 u=\frac{j}{2}\mu u \tag{2-30}$$

$$\text{where } d=g_{sat}L_D\Big/\left(\Delta\omega_g^2\tau_0^2\right),\ \mu=\left(g_{sat}-\alpha\right)L_D \tag{2-31}$$

Because Eq.(2-30) is not integrable, so a solitary-wave solution is guessed and its form is [64]

$$u(\xi,\tau)=N_s\left[\operatorname{sech}\left(\tau\Big/\tau_0\right)\right]^{(1+jq)}\exp\left(j\kappa\xi\right) \tag{2-32}$$

In this solution, N_s is represented for the order or amplitude of soliton, τ_0 is the soliton width, q is the chirp parameter and κ is the phase shift during propagation. These parameters are determined by substituting it in Eq.(2-30) and balancing terms. They are [64]

$$N_s^2=\frac{1}{2\tau_0^2}\left[s\left(q^2-2\right)+3qd\right] \tag{2-33}$$

$$\tau_0^2=-\frac{\left[d\left(1-q^2\right)+2sq\right]}{\mu} \tag{2-34}$$

$$\kappa=-\frac{1}{2\tau_0^2}\left[s\left(1-q^2\right)-2qd\right] \tag{2-35}$$

$$q=\frac{3s\pm\sqrt{9+8d^2}}{2d} \tag{2-36}$$

Thus the width and the peak power of the soliton are determined by the system parameters such as loss, gain and its finite bandwidth. Different to solitons supported by NSE, the influence of these parameters plays an important role in the existence of solitons in these fibre systems. Due to periodic perturbations during propagation,

solitons dissipate their energy and this dissipation plays an essential role for their formation and stabilization. Such a soliton is often called a dissipative soliton, or an autosoliton due to its mechanism of self-organization [95]. In order to preserve the shape and energy, a balance between gain and loss mechanisms is required beside the balance between GVD and SPM. A frequency chirping can help to maintain the balance between gain and loss during propagation in a bandwidth-limited system and this explains why dissipative solitons are normally chirped pulses.

2.4 GENERATION OF SOLITONS IN NONLINEAR OPTICAL FIBRE RING RESONATORS

2.4.1 Master equation for mode locking

Mode locking is a technique to force longitudinal oscillation modes of a laser in phase to generate short pulses. For mode-locked fibre ring lasers, an optical pulse in every round-trip experiences the same effects such as loss and gain as that in an equivalent transmission fibre span. Thus a circulation of the pulse inside the ring resonators is approximately equivalent to a propagation of the pulse in a fibre transmission link with infinite number of spans. That is, the circular cavity can be thought of as being rolled out into a long transmission system. Therefore the Eq.(2-13) can be used to describe mode locking in fibre lasers. However the variation of the pulse in round-trip time scale is considered, rather than in a distance scale. In addition, a modulation function *M*, which is responsible for various mode locking mechanisms, is necessary to be added into (2-13). Then Eq.(2-13) is modified by introducing new variables $T = \xi / v_g$, where v_g is the group velocity of the optical pulse, to obtain [68, 101, 108]

$$\frac{1}{v_g}\frac{\partial A(T,\tau)}{\partial T}+\frac{j}{2}\left(\beta_2+\frac{jg_{sat}}{\Delta\omega_g^2}\right)\frac{\partial^2 A(T,\tau)}{\partial\tau^2}-\frac{\beta_3}{6}\frac{\partial^3 A(T,\tau)}{\partial\tau^3}=j\gamma\left|A(T,\tau)\right|^2 A(T,\tau) \qquad (2\text{-}37)$$
$$+\frac{1}{2}\left(g_{sat}-\alpha\right)A(T,\tau)+M(A,T,\tau)$$

A further modification is implemented by multiplication of both sides in (2-37) with L_c, the ring cavity length, and setting $T_c = L_c / v_g$ which is the cavity period. Then (2-37) becomes

$$T_c\frac{\partial A(T,\tau)}{\partial T}+\frac{j}{2}\left(\beta_2+\frac{jg_{sat}}{\Delta\omega_g^2}\right)L_c\frac{\partial^2 A(T,\tau)}{\partial\tau^2}-\frac{\beta_3 L_c}{6}\frac{\partial^3 A(T,\tau)}{\partial\tau^3}=j\gamma L_c\left|A(T,\tau)\right|^2 A(T,\tau) \qquad (2\text{-}38)$$
$$+\frac{L_c}{2}\left(g_{sat}-\alpha\right)A(T,\tau)+M(A,T,\tau)$$

Eq.(2-38) is the well-known master equation which was first derived by Haus [109] to describe mode locking in time domain. Thus there are two time scales in this equation: the time T is measured in terms of the cavity period or the round-trip time T_c, while the time τ is measured in terms of a pulse window. The term M, which depends on the mode locking mechanism: passive or active, is a function of amplitude and time in terms of time scale τ in every round-trip. In many theoretical studies on mode locking, Eq.(2-38) has been applied for the investigation of the pulse evolution in the cavity [34]. We note that the parameters in the master equation are averaged over the cavity for analysis.

2.4.2 Passive mode-locking

Passive mode locking in fibre ring lasers is normally based on the mechanisms of NOLM and NPR in the cavity as described in Figure 2-3(a)&(b). NOLM and NPR act as mode lockers due to their artificial saturable absorption. For a NOLM, a Sagnac interferometer, its transmittance varies as a function of pulse power P via [110-111]

$$T = 1-0.5\left\{1+\cos\left[0.5\gamma(G-1)PL\right]\right\} \qquad (2\text{-}39)$$

where G is the amplification factor and L is the length of Sagnac loop. While the transmittance of NPR structure using nonlinear birefringence can be given by [112]

$$T = \cos^2\alpha\cos^2\varphi + \sin^2\alpha\sin^2\varphi + \frac{1}{2}\sin 2\alpha\sin 2\varphi\cos(\Delta\phi_L + \Delta\phi_{NL}) \quad (2\text{-}40)$$

where α is the angle between the polarization direction of the input light and the fast axis of optical fibre, φ is the angle between the fast axis of optical fibre and the polarization direction of the polarizer, $\Delta\phi_L$ and $\Delta\phi_{NL}$ are linear and the nonlinear phase difference between the two orthogonal polarization components, respectively. They are given by

$$\Delta\phi_L = \phi_L^y - \phi_L^x = \frac{2\pi L}{\lambda}(n_y - n_x) \quad (2\text{-}41)$$

$$\Delta\phi_{NL} = \phi_{NL}^x - \phi_{NL}^y = -\frac{\gamma LP\cos 2\alpha}{3} \quad (2\text{-}42)$$

where n_x and n_y are the refractive indices of the fast and slow axes of the optical fibre respectively, L is the length of the fibre in the cavity.

Figure 2-3(c)-(d) shows the transmittances of fast saturable absorption based on NOLM and NPR respectively. Thus the peak of the pulse experiences a higher net gain than its wings, which shortens the pulse in every roundtrip. This mode locking mechanism is sometimes known as additive pulse mode locking (APM) [113] because pulse shaping is produced by the interference between the component pulses circulating in the cavity.

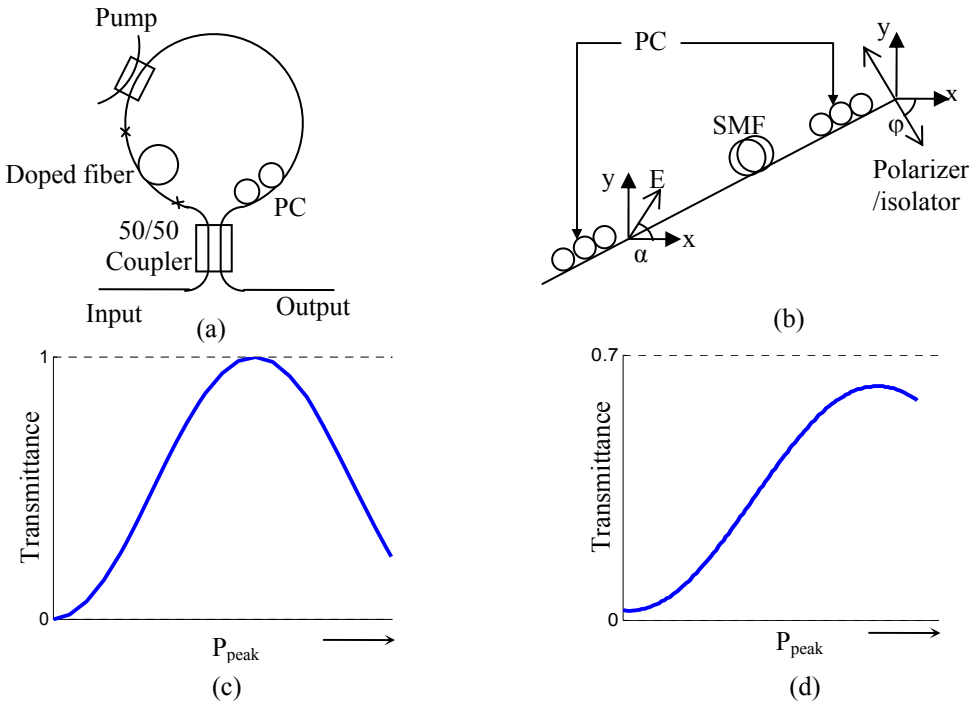

Figure 2-3 Really operation and transmittance of artificial fast saturable absorption based on (a&c) NOLM and (b&d) NPR, respectively.

Fast saturable absorption mode locking can be theoretically described by introducing the saturable loss modulation into the master equation (2-38) [34]. The modulation of a fast saturable absorber $M_{sa}(t)$ can be modelled by [34]

$$M_{sa}(t) = \frac{s_0}{1 + |A|^2 / (A_{eff} I_{sat})} \tag{2-43}$$

where s_0 is the unsaturated loss, I_{sat} is the saturation intensity of the absorber. In the case of weak saturation ($|A|^2 \cong I_{sat}$), expression (2-43) can be expanded into a Taylor series to give

$$M_{sa}(t) \approx s_0 - \frac{s_0}{A_{eff} I_{sat}} |A|^2 = s_0 - s_{SAM} |A|^2 \tag{2-44}$$

where s_{SAM} is called the self amplitude modulation (SAM) coefficient [34]. The master equation of passive mode locking thus can be derived by using (2-38) and (2-44)

$$T_c\frac{\partial A}{\partial T}+\frac{j}{2}\left(\beta_2+\frac{jg_{sat}}{\Delta\omega_g^2}\right)L_c\frac{\partial^2 A}{\partial\tau^2}-\frac{\beta_3 L_c}{6}\frac{\partial^3 A}{\partial\tau^3}=j\gamma L_c|A|^2A+\frac{L_c}{2}(g_{sat}-\alpha)A \qquad (2\text{-}45)$$
$$-\frac{s_0}{2}A+s_{SAM}|A|^2A$$

We can simplify Eq.(2-45) by incorporating the unsaturated loss s_0 into the loss coefficient and ignoring the effects of dispersion and nonlinearity [34]

$$T_c\frac{\partial A}{\partial T}-\frac{g_{sat}}{2\Delta\omega_g^2}L_c\frac{\partial^2 A}{\partial\tau^2}=\frac{L_c}{2}(g_{sat}-\alpha')A+s_{SAM}|A|^2A \qquad (2\text{-}46)$$

This is the simplest case of passive mode locking where the pulse shaping is based on purely saturable absorption. The solution of Eq.(2-46) is a simple soliton pulse given by

$$A(\tau)=A_0\,\mathrm{sech}\left(\tau/\tau_0\right) \qquad (2\text{-}47)$$

By substitution of (2-47) into (2-46), the pulse width τ_0 and relations between parameters of the system can be obtained [34]

$$\tau_0^2=\frac{g_{sat}L_c}{s_{SAM}\Delta\omega_g^2|A_0|^2} \qquad (2\text{-}48)$$

and $$g_{sat}-\alpha'=-\frac{g_{sat}}{\Delta\omega_g^2\tau_0^2} \qquad (2\text{-}49)$$

Expression (2-48) can explain why the pulse width in passive mode locking is much shorter than that in active mode locking [34], because the loss modulation curve is

proportional to $s_{SAM}\left|A_0\right|^2/\tau_0^2$, then the curvature of loss modulation increases faster when the pulse is shorter while it remains unchanged in active mode locking.

However the effects of GVD and SPM are always significant to pulse shaping in practical passively mode-locked fibre lasers. Hence the master equation need to include these effects and is given by [34]

$$T_c\frac{\partial A}{\partial T}+\frac{j}{2}\left(\beta_2+\frac{jg_{sat}}{\Delta\omega_g^2}\right)L_c\frac{\partial^2 A}{\partial\tau^2}=j\gamma L_c\left|A\right|^2A+\frac{L_c}{2}\left(g_{sat}-\alpha'\right)A+s_{SAM}\left|A\right|^2A \qquad (2\text{-}50)$$

This equation has a simple steady state solution as following [114]:

$$A(T,\tau)=A_0\left[\operatorname{sech}\left(\tau/\tau_0\right)\right]^{1+jq}\mathrm{e}^{j\kappa T} \qquad (2\text{-}51)$$

where q is the chirp parameter and κ is the phase shift in every roundtrip. By using (2-51) as an anzat and balancing terms, the following pulse parameters and relations are obtained

$$\tau_0^2=\frac{L_c\left[g_{sat}\left(2-q^2\right)/\Delta\omega_g^2+3\beta_2 q\right]}{2s_{SAM}\left|A_0\right|^2} \qquad (2\text{-}52)$$

$$q=-\frac{3g_{sat}}{2\beta_2\Delta\omega_g^2}\pm\sqrt{\left(\frac{3g_{sat}}{2\beta_2\Delta\omega_g^2}\right)^2+\frac{2(\beta_2+\gamma\tau_0\left|A_0\right|^2)}{\beta_2}} \qquad (2\text{-}53)$$

$$\kappa=\frac{L_c}{2\tau_0^2T_c}\left(\beta_2(q^2-1)+\frac{g_{sat}q}{\Delta\omega_g^2}\right) \qquad (2\text{-}54)$$

$$g_{sat}-\alpha'=\frac{1}{\tau_0^2}\left(\frac{g_{sat}(q^2-1)}{\Delta\omega_g^2}-2\beta_2 q\right) \qquad (2\text{-}55)$$

Expression (2-53) indicates that a combination of anomalous GVD ($\beta_2<0$) and SPM can give a zero chirp solution and the shortest pulses can be obtained in this case. For a small SAM coefficient and weak filtering, a soliton can be formed via the balance of

anomalous GVD and SPM. The SAM and filtering effects can be considered as weak perturbations in the fibre cavity. However they play an important role in stabilization of the pulse against noise build-up in the intervals between the pulses [34].

When solitons are periodically perturbed by the gain, loss, filtering and SAM effects inside the fibre ring cavity, they radiate, or generate continuum or dispersive waves [95]. If the continuum components shed by the soliton are phase matched from pulse to pulse, its energy can build up and sidebands appear in the spectrum where the frequency components with the relative phase of soliton and dispersive wave changes by an integer multiple (n) of 2π per round trip. These parasitic sidebands were first described and explained by Kelly [115]. This phenomenon is observed in most passively soliton fibre lasers. The positions of sidebands in the spectrum depend strongly on the dispersion of the fibre cavity via [116]

$$\Delta\lambda_n = \pm n\lambda_0\sqrt{\frac{2n}{cDL_c} - 0.0787\frac{\lambda_0^2}{\left(c\tau_{FWHM}\right)^2}} \tag{2-56}$$

where n is the order of sideband, D is the fibre dispersion parameter in the cavity, τ_{FWHM} is the full-width at half-maximum of the pulse and λ_0 is the centre wavelength. Thus from the positions of sidebands in the obtained optical spectrum the dispersion of the cavity can be estimated.

2.4.3 Actively mode-locking

Similar to passive mode locking, active mode locking can be described by a master equation with a proper AM or FM function. Actively mode-locked fibre lasers can experience different operation modes from linear to nonlinear depending on the power

level in the cavity. Therefore, these modes are represented by various master equations and their solutions show characteristics of mode-locked pulse.

2.4.3.1 AM mode locking

In AM mode locking, the amplitude modulation provides a time dependent loss. The pulse will form at time slots where the loss dips are below the gain level. The modulation of an amplitude modulator can be mathematically described by [68]

$$M_A(T,\tau) = -m_{AM}\left[1-\cos(\omega_m \tau)\right] \tag{2-57}$$

and the pulse evolution equation can be derived from general master equation (2-38) to describe AM mode locking as following [68]

$$T_c\frac{\partial A}{\partial T}+\frac{j}{2}\left(\beta_2+\frac{jg_{sat}}{\Delta\omega_g^2}\right)L_c\frac{\partial^2 A}{\partial\tau^2}-\frac{\beta_3 L_c}{6}\frac{\partial^3 A}{\partial\tau^3}=j\gamma L_c|A|^2 A+\frac{L_c}{2}\left(g_{sat}-\alpha\right)A - m_{AM}\left[1-\cos(\omega_m\tau)\right]A \tag{2-58}$$

where m_{AM} is the modulation index, $\omega_m = 2\pi f_m$ is the angular modulation frequency. For actively AM mode locking, the modulation frequency (f_m) is normally much higher than the cavity fundamental frequency (f_c) and a harmonic of f_c: $f_m = Nf_c$, N is the order of the harmonic.

In case of pure AM mode locking, the effects of GVD and SPM are ignored. Additionally, a second order Taylor series expansion can be applied to the modulation function due to the pulse is only positioned at the minimum of the modulation curve. Then Eq.(2-58) becomes [117]:

$$T_c\frac{\partial A}{\partial T}-\frac{g_{sat}L_c}{\Delta\omega_g^2}\frac{\partial^2 A}{\partial\tau^2}=\frac{L_c}{2}\left(g_{sat}-\alpha\right)A-\frac{m_{AM}}{2}\omega_m^2\tau^2 A \tag{2-59}$$

The solution of this equation is a Gaussian pulse given by [117]:

$$A = A_0 \exp\left[-\frac{\tau^2}{2\tau_0^2}\right] \tag{2-60}$$

$$\text{where} \quad \tau_0 = \sqrt[4]{\frac{g_{sat}L_c}{\Delta\omega_g^2 m_{AM}\omega_m^2}} \tag{2-61}$$

This is the result predicted by Kuizenga-Siegman [52] and shows the pulse width τ_0 is proportional to the inverse of the gain bandwidth and the modulation frequency. The eigenvalue of the equation can give the important condition of the mode-locked laser through the expression:

$$g - l = \sqrt{\frac{m_{AM}\omega_m^2 g}{2\Delta\omega_g^2}} \qquad \text{(2-62) where } g = \frac{g_{sat}L_c}{2} \text{ and } l = \frac{\alpha L_c}{2}$$

g and l parameters are considered as the gain and the loss within one round trip of the fibre cavity. Thus the expression (2-62) also indicates that the gain must be fixed at a certain value higher than the loss to compensate for the excess loss caused by the modulator and the filtering from the limited gain bandwidth [117]. This condition requires that the gain is sufficient for compensating the loss of the ring cavity. Optical fibre amplifiers are thus preferred to operate in the saturation region in the cases when the ring is either under modulation or no modulation states, to achieve stability of the total energy distributed in the ring.

With presence of the GVD effect in the fibre lasers, the evolution of the pulse inside the fibre ring cavity satisfies the following equation [34]:

$$T_r\frac{\partial A}{\partial T} + \frac{j}{2}\left(\beta_2 + \frac{jg_{sat}}{\Delta\omega_g^2}\right)L_c\frac{\partial^2 A}{\partial\tau^2} = \frac{L_c}{2}\left(g_{sat} - \alpha\right)A - \frac{m_{AM}}{2}(\omega_m\tau)^2 A \tag{2-63}$$

This is a Hermite's differential equation and a stable solution of this equation takes the form [34]

$$A = A_0 \exp\left[-\frac{\tau^2(1+jq)}{2\tau_0^2}\right]\exp(j\kappa T) \tag{2-64}$$

where A_0, τ_0 are the amplitude and the width of the pulse respectively, q is the chirp parameter and κ is the phase shift in every roundtrip. This is a chirped Gaussian pulse with the pulse parameters obtained by balancing terms in (2-63) [117]

$$\tau_0 = \sqrt[4]{\frac{L_c\left[g_{sat}\left(1-q^2\right)+2q\beta_2\Delta\omega_g^2\right]}{m_{AM}\omega_m^2\Delta\omega_g^2}} \tag{2-65}$$

$$q = -\frac{g_{sat}}{\Delta\omega_g^2\beta_2} \pm \sqrt{\left(\frac{g_{sat}}{\Delta\omega_g^2\beta_2}\right)^2+1} \tag{2-66}$$

$$\kappa = \frac{L_c}{\tau_0^2 T_c}\left(\beta_2 - \frac{g_{sat}q}{\Delta\omega_g^2}\right) \tag{2-67}$$

$$g_{sat} - \alpha = \frac{1}{\tau_0^2}\left(\beta_2 q + \frac{g_{sat}}{\Delta\omega_g^2}\right) \tag{2-68}$$

The result shows that if $\beta_2 = 0$ (ignoring GVD effect), then the chirp factor $q = 0$ and $\kappa = 0$, subsequently the pulse width in (2-65) returns (2-61). Thus the presence of GVD can cause the generated pulse chirped.

When the fibre cavity is pumped with sufficiently high power, the SPM effect is not negligible and included into the master equation as fully described in (2-58). With the addition of sufficiently negative GVD and SPM, the solitary pulse formation can be obtained and the solution of (2-58) is assumed to be a chirped secant hyperbolic pulse [117]

$$A = A_0\left[\operatorname{sech}\left(\frac{\tau}{\tau_0}\right)\right]^{(1+jq)} \tag{2-69}$$

In nonlinear regime, the pulse is shortened by a combination of SPM and negative GVD similar to passive mode locking. However in order to shorten the pulse by soliton compression, two following conditions must be satisfied [118]:

- The synchronisation between the modulator and the pulse train must be maintained or the solitons must be exactly retimed on each round trip. This is a common condition for stable operation of mode-locked fibre lasers against the thermal drift of the cavity length. This condition also ensures the phase matching that is the total phase of the lightwaves circulating in the ring cavity must be a multiple number of 2π.
- The excess loss of the continuum which is determined by the eigenvalue of (2-58) must be higher than that of the soliton. The resulting condition is [108]

$$\mathrm{Re}\sqrt{\frac{m_{AM}\omega_m^2}{2L_c}\left[\frac{g_{sat}}{\Delta\omega_g^2}-j\beta_2\right]} > \frac{\pi^2}{24}m_{AM}\omega_m^2\tau_0^2+\frac{g_{sat}}{3\Delta\omega_g^2\tau_0^2} \tag{2-70}$$

  In (2-70), on the right side is the loss experienced by the soliton, and on the left side is the loss of the continuum. In addition, the modulation must not drive the soliton into instability. The condition for suppression of energy fluctuations of the soliton can be obtained from soliton perturbation theory [108, 118-119]:

$$\frac{g_{sat}}{3\Delta\omega_g^2\tau_0^2} > \frac{\pi^2}{24}m_{AM}\omega_m^2\tau_0^2 \tag{2-71}$$

From above conditions, the mode-locked pulse can be compressed with the width much shorter than that predicted by Kuizenga-Siegman [52]. The factor of pulse width shortening *R* can be found as follows [68]

$$R \le 1.37\left(\frac{\beta_2 L}{g_{sat}\Big/\left(\Delta\omega_g\right)^2}\right)^{1/4} \tag{2-72}$$

The condition (2-72) determines the lower limit of the pulse width with the help of SPM and negative GVD. The possible pulse width reduction is proportional to the fourth root of dispersion that indicates the need of excessive amount of dispersion to maintain a stable soliton while suppressing the continuum [68].

2.4.3.2 FM mode locking

In contrast to AM mode locking, FM mode locking is based on a periodic chirping caused by phase modulation [52]. When the modulation frequency is exactly a harmonic of the fundamental frequency, the phase matching condition is satisfied for resonance of optical waves in the cavity. In frequency domain, the sidebands generated by phase modulation are matched to the axial modes of the cavity. While in time domain, the pulses are built up at the extremes of the modulation cycles. At these temporal positions, the optical waves are no chirped and thus the optical waves are constructively summed when they are in phase, while they are destructively interfered at other temporal positions due to repeatedly linear chirping in the cavity.

Phase modulation of the optical field can be described by the function [101, 120]

$$M_F(T,\tau) = jm_{FM}\cos(\omega_m \tau) \tag{2-73}$$

where m_{FM} is the phase modulation index. When using the expression of phase modulation for mode locker, FM mode locking can be described by the master equation as following [120]

$$T_c\frac{\partial A}{\partial T} + \frac{j}{2}\left(\beta_2 + \frac{jg_{sat}}{\Delta\omega_g^2}\right)L_c\frac{\partial^2 A}{\partial \tau^2} - \frac{\beta_3 L_c}{6}\frac{\partial^3 A}{\partial \tau^3} = j\gamma L_c |A|^2 A + \frac{L_c}{2}(g_{sat} - \alpha)A + jm_{FM}\cos(\omega_m \tau)A \tag{2-74}$$

Because the pulse is formed in only the narrow part of modulation period, the modulation function can be approximated to the second order of the Taylor expansion. Then Eq.(2-74) can be simplified by ignoring the nonlinear effect [53]:

$$T_c \frac{\partial A}{\partial T} + \frac{j}{2}\left(\beta_2 + \frac{j g_{sat}}{\Delta\omega_g^2}\right) L_c \frac{\partial^2 A}{\partial \tau^2} = \frac{L_c}{2}\left(g_{sat} - \alpha\right) A + j m_{FM}\left(1 - \frac{\omega_m^2 \tau^2}{2}\right) A \quad (2\text{-}75)$$

Therefore Eq.(2-75) describes the FM mode locking in linear regime. Similar to AM mode locking, the solution of this equation is a chirped Gaussian pulse given by (2-64) [34]. By the same techniques as in previous sections, the pulse parameters in this case can be obtained

$$\tau_0 = \sqrt[4]{\frac{L_c\left[\beta_2 \Delta\omega_g^2\left(1-q^2\right) + 2q g_{sat}\right]}{m_{FM}\omega_m^2 \Delta\omega_g^2}} \quad (2\text{-}76)$$

$$q = \frac{\beta_2 \Delta\omega_g^2}{g_{sat}} \pm \sqrt{\left(\frac{\beta_2 \Delta\omega_g^2}{g_{sat}}\right)^2 + 1} \quad (2\text{-}77)$$

$$\kappa = \frac{m_{FM}}{T_c} - \frac{L_c}{2\tau_0^2 T_c}\left(\frac{g_{sat} q}{\Delta\omega_g^2} - \beta_2\right) \quad (2\text{-}78)$$

$$g_{sat} - \alpha = \frac{1}{\tau_0^2}\left(\beta_2 q + \frac{g_{sat}}{\Delta\omega_g^2}\right) \quad (2\text{-}79)$$

In the simplest case, i.e the pure FM mode locking with $\beta_2 = 0$, the generated pulse is always chirped with $q = \pm 1$ due to phase modulation. On the other hand, the pulses generated from a FM mode-locked laser can be located at either extreme up-chirp ($q > 0$) or down-chirp ($q < 0$) of the modulation cycle in the absence of dispersion and nonlinearity that can create a switching between these two states in a random manner [52]. However in presence of dispersion effect, this switching can be suppressed as possibly indicated in (2-79) which is the expression of the excess loss

of the cavity. If $\beta_2 < 0$ (anomalous dispersion), the excess loss at the up-chirp half cycle is lower than that at down-chirp cycle ($q > 0$) and vice versa. Thus the pulses located at positive half-cycles are preferred in the anomalous dispersive fibre cavity while they located at negative half-cycles are preferred in the normal dispersive fibre cavity [51]. On the other hand, the pulse in the up-chirp cycle is compressed by the dispersion while the down-chirp pulse is broadened in the anomalous GVD cavity. This shortened up-chirp pulse experiences less chirp after passing the phase modulator which reduces the loss due to the filtering and gain bandwidth limitation effects. The up-chirp pulse is finally dominant in the anomalous GVD cavity. This stability of the mode-locked pulse in the FM fibre ring laser has been theoretically studied in [53].

In nonlinear regime, the SPM is also significant in pulse shaping [121]. Similar to AM mode locking, the solitons are formed inside the fibre cavity with the balance between GVD and SPM effects. To generate stable solitons, the required gain for noise must be higher than that for the soliton and the condition for stability can be obtained by the perturbation soliton theory [120]

$$\mathrm{Re}\sqrt{\frac{jm_{FM}\omega_m^2}{2L_c}\left[\frac{g_{sat}}{\Delta\omega_g^2}+j\beta_2\right]} > \frac{2g_{sat}}{3\Delta\omega_g^2\tau_0^2} \qquad (2\text{-}80)$$

In (2-80) the left side is the loss of the ASE noise and the right side is the loss of the soliton. Tamura and Nakazawa [53, 71] also indicated that the pulse energy equalization occurs in the support of SPM and filtering effect when the dispersion of the cavity is anomalous. This stability of the soliton in presence of the third-order dispersion in a FM mode-locked fibre laser have been numerically investigated in [51].

Beside the synchronous mode-locking in FM mode-locked fibre laser, another mechanism for mode-locking based on asynchronous phase modulation has been proposed by Doerr *et al.* [56]. In this scheme, asynchronous modulation is obtained by detuning of modulation frequency with a proper amount. However, in order to generate a stable soliton train, the detuning is required to remain within a limit which satisfies the following condition [120]:

$$|\Delta f_{\lim}| \ll \frac{1}{T_c} \mathrm{Re} \sqrt{\frac{j m_{FM} \omega_m^2}{2L_c} \left[\frac{g_{sat}}{\Delta \omega_g^2} + j\beta_2 \right]} \tag{2-81}$$

With a small detuning within this limit, the soliton can overcome the frequency shift to remain the mode-locked state [120]. When the detuning exceeds the above limit, the noise can build up and destroy the solitons. The fibre laser will operate in FM oscillation state if the modulation frequency is moderately detuned. In this regime, the output has a constant intensity but a periodical chirp and its optical spectrum is hugely broadened [122]. The transition from the FM oscillation state to phase mode locking has complex behaviour at smaller detuning where the relaxation oscillations can occur with different properties [72]. In this state, the noise can build up faster than the soliton to become the new pulse and replace the old one. The cause of relaxation oscillation is the change of the cavity loss when the modulation frequency is detuned [122]. The pulse passes through the modulator with a small time shift from the extremes of the modulation cycles which increase the loss of the pulse while the ASE noise gets more gain at the extremes of modulation cycles where the loss in the cavity is lowest. When the detuning becomes larger, a new pulse can build up from the ASE noise while the old pulse decays and disappears finally. This process is periodically repeated and this repetition can satisfy the phase matching condition for resonance in

the fibre ring cavity which leads to the relaxation oscillation [72]. In this state, the output is periodically strong spikes but with lower average power because more power is stored in the cavity from resonance. The relaxation oscillation can occur several times due to the central mode hopping in detuning process [123]. The supermode noise can be dramatically enhanced between these transitions by getting the excess energy from the cavity through matching between the relaxation oscillation frequency and the frequency of beating between the modulation sidebands and lasing modes [123].

2.4.3.3 Rational harmonic mode locking

In active mode locking, one way to increase the repetition rate is to use the rational harmonic mode locking by tuning the modulation frequency to a rational number of the cavity fundamental frequency [124]:

$$f_m = Nf_c \pm \frac{f_c}{M} \tag{2-82}$$

where N, M are integers and N is the harmonic order; M can be considered as multiplication factor.

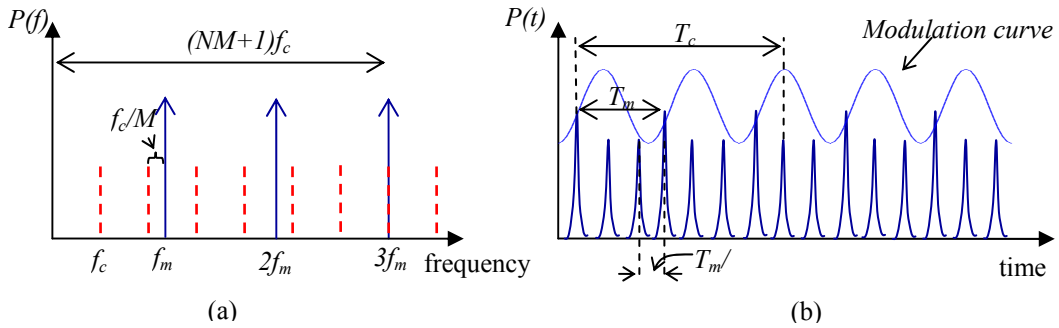

Figure 2-4 A rational harmonic mode locking (a) in frequency domain, (b) in time domain with $N = 2$ and $M = 3$ as an example.

To understand the rate multiplication in rational harmonic mode locking, a simple description in frequency domain is shown in Figure 2-4(a). In the frequency domain, the harmonics of modulation frequency would be only matched to the different multiples of the cavity modes when the modulation frequency is detuned by f_c/M. Thence the repetition rate of the output pulse can be multiplied by a factor of M. The mechanism can be understood in time domain as described in Figure 2-4(b). When the fibre laser is detuned by a ratio f_c/M, the difference between the cavity round-trip time and N times the modulation frequency is equal to the time delay experienced by a pulse after one round trip. On the other hand, the phase delay of a pulse between consecutive round trips is proportional to $2\pi N/M$ and the pulse returns to its original positions after M round trips. As a result, there are M sets of pulses in one round trip window resulting in a multiplied repetition rate.

Because of the pulse distribution over a non-uniform modulation profile, the output pulses suffer from large amplitude fluctuations which limit the application of rational harmonic AM mode locking in practical systems. Several methods such as nonlinear optic methods [125-126] and modulator transmittance adjustment [127-129] have been proposed for pulse amplitude equalization.

For FM mode locking, the situation is different to the AM mode locking, as it has been shown that the rational harmonic mode locking is due to the contributions of harmonics of the modulation frequency in the amplified electrical driving signal [54]. The higher order harmonics are generated from the power amplifier operating in saturated scheme. Therefore, the phase of the optical field at the output of the phase modulator can be modulated via

$$E_{out} = E_{in} e^{j\varphi(t)} \tag{2-83}$$

where E_{in}, E_{out} are the optical field at the input and output of the phase modulator respectively, and $\varphi(t)$ varies corresponding to the driving signal. In the case of the amplified signal, this variation can be represented by a summation of a series of cosine functions as following

$$\varphi(t) = \sum_{k=1}^{\infty} m_k \cos(k 2\pi f_m t + \theta_k) \tag{2-84}$$

where f_m is the modulation frequency, m_k and θ_k are the modulation index and the phase delay bias for each frequency component respectively. From analysis in [54], the field of the optical signal experiences an average phase modulation after M round trips of

$$\bar{\varphi}_M(t) = \sum_{k=1}^{\infty} M m_{kM} \cos(kM 2\pi f_m t + \theta_{kM}) \tag{2-85}$$

Thus when the modulation frequency f_m is detuned as specified in Eq.(2-82), the modulation effect of lower order harmonics of the f_m are cancelled and only the frequency component of M times the modulation frequency is enhanced, and becomes dominant after M round trips [54]. On the other hand, the effective phase modulation curve with the number of cycles multiplied by M times in the same transmission window is proven in Figure 2-5. Because of mode locking based on frequency chirping, the generated pulse train in FM rational mode locking does not suffer from unequal amplitude problem [54].

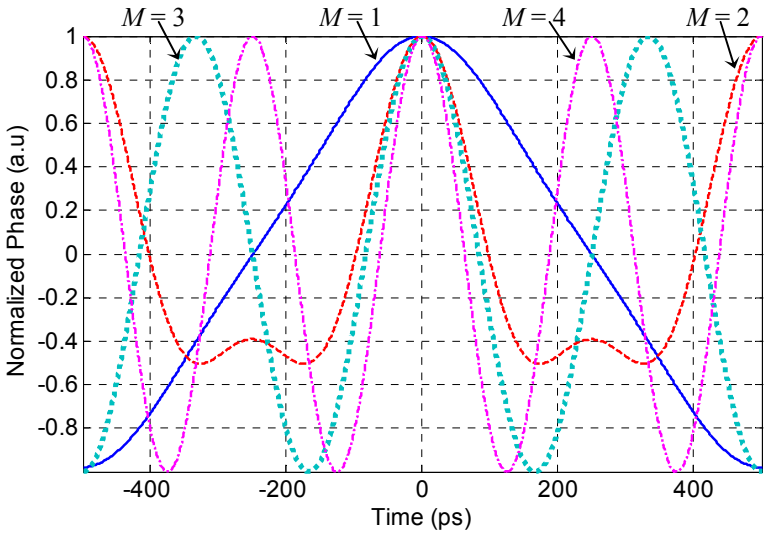

Figure 2-5 Average phase modulation profile at different detuning f_c/M with M = 1-4 to achieve rational harmonic mode locking in the FM mode-locked fibre laser. The driving signal of phase modulator is modelled with magnitudes of higher harmonic components as follows: $m_2 = 0.008m_1$, $m_3 = 0.07m_1$, $m_4 = 0.0035m_1$.

2.5 CONCLUDING REMARKS

In this chapter, the fundamentals of optical pulse propagation and mode locking mechanisms have been reviewed. In order to obtain a stable pulse train from active mode locking, some conditions have been summarized and explained. In an active mode-locked fibre laser with sufficiently high gain, the SPM effect becomes significant for pulse compression inside the anomalous dispersion average cavity to generate solitons.

Chapter 3

Actively FM mode-locked fibre lasers: Experiment and Simulation

3.1 INTRODUCTION

By using an electro-optic phase modulator as a mode locker, the actively mode-locked fibre ring laser can generate a high speed pulse train with high performance such as narrower pulsewidth, higher stability in both harmonic mode locking and rational harmonic mode locking. Moreover, many interesting operation modes only exist in the FM mode-locked fibre ring lasers such as asynchronous mode locking [56], transitions states from CW scheme to mode-locked scheme [122-123].

In this chapter, an actively FM mode-locked fibre ring laser (FM-MLFRL) will be constructed to demonstrate soliton generation in which the erbium gain medium is used for amplification inside the cavity. Different states from detuning to mode-locked will be experimentally investigated to show the complex behaviour of a FM-MLFRL. In addition, a numerical model is also developed to simulate the FM-MLFRL. This model is used to verify the experimental characterization of the FM-MLFRL. The results obtained in this chapter provide a basis for further research in the next chapters.

3.2 ACTIVELY FM MODE-LOCKED FIBRE RINGS: EXPERIMENT

3.2.1 Experimental setup

Figure 3-1 shows the experimental setup of the FM-MLFRL. In this setup, an erbium doped fibre amplifier (EDFA) MOABF-17 (Lightwaves2020) pumped at 980 nm is used in the fibre ring to moderate the optical power in the loop for mode locking. This amplifier operates in the saturation region and the output power can be adjusted by varying the pump power or the current of the pump laser diode. A 50 m Corning SMF-28 fibre is inserted after the EDFA with the aim of enhancing the nonlinear phase shift through the SPM effect as well as ensuring that the average dispersion in the fibre ring is anomalous which is important in designing a stable soliton fibre laser [53]. By measuring the input and output power of the EDFA, the total loss of the cavity can be estimated. This loss consisting of the insertion loss of the phase modulator and connections is approximately 10.5 dB to 11 dB in our setup. We note that the loss can vary due to change in the polarization state.

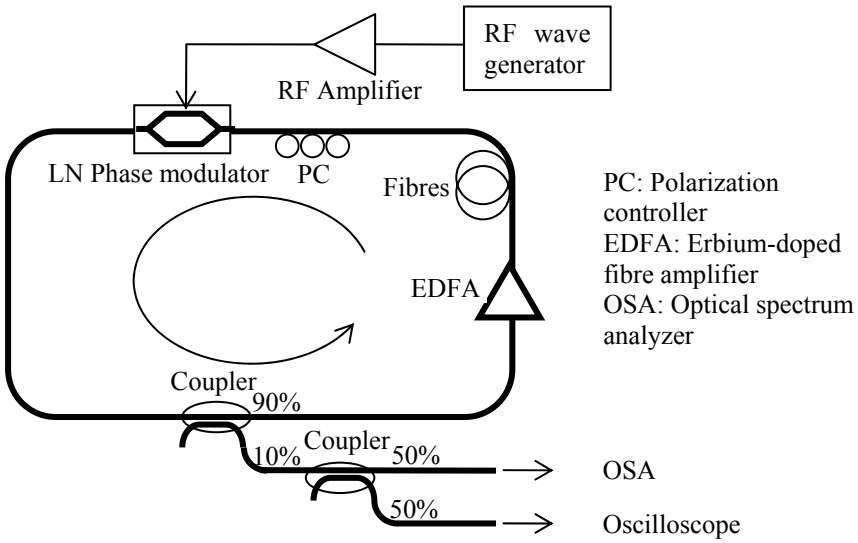

Figure 3-1 Experimental setup of the actively FM mode-locked fibre laser.

An electro-optic integrated phase modulator (PM-315P, Crystal Technology) is used as a mode locker and controls the states of locking in the fibre ring. At the input of the phase modulator, a polarization controller (PC), consisting of two quarter-wave plates and one half-wave plate, is used to control the polarization of light which is required to minimize the loss cavity and influences to stable formation of solitons. The phase modulator with half-wave voltage (V_π) of 9 V is driven by a sinusoidal signal generated from a signal generator (HP-8647A) in the region of 1 GHz frequency. The RF sinusoidal wave is amplified by a broadband RF power amplifier (DC7000H) with 18 dB gain which can provide a maximum saturated power of approximately 19 dBm at the output. Thus the phase modulation index of ~1 radian can be achieved for mode locking. The fundamental frequency of the fibre laser cavity is determined by tuning the modulation frequency to lock the fibre laser at different harmonics. In this setup the fundamental frequency of the fibre cavity is 2.2802 MHz, which is equivalent to the delay of the 90 m total length of the fibre ring.

The output of the mode locked laser is extracted using the 90:10 coupler. This is monitored by an optical spectrum analyser (HP-70952B) and a repetitive sampling oscilloscope (Agilent DCA-J 86100C) with an optical bandwidth of 65 GHz. Because fibre laser operates at only 1 GHz, the bandwidth of the oscilloscope is wide enough to measure pulse widths greater than 10 ps. For pulse widths less than 10 ps, the rise time of the oscilloscope (7.4 ps) should be considered using $\tau_p = \sqrt{\tau_{meas}^2 - \tau_{equi}^2}$, where τ_p, τ_{meas} and τ_{equi} are the estimated and measured pulse widths and the rise time of the oscilloscope respectively. A RF spectrum analyser (FS315 Rohde&Schwarz) with frequency range up to 3 GHz was also used to determine the stability of the generated pulse train.

Beside the conventional ring structure as described above, another setup of the actively MLFRL using EO phase modulator which is based on the Sagnac loop interferometer (PMSL) also has been implemented in our experiment. In this setup as shown in Figure 3-2, the phase modulator is placed at the middle of a fibre Sagnac loop. Because of the insertion of the 3 dB coupler in the PMSL, the total loss of the ring cavity is about 16 dB which is much higher than that of the conventional FM-MLFRL.

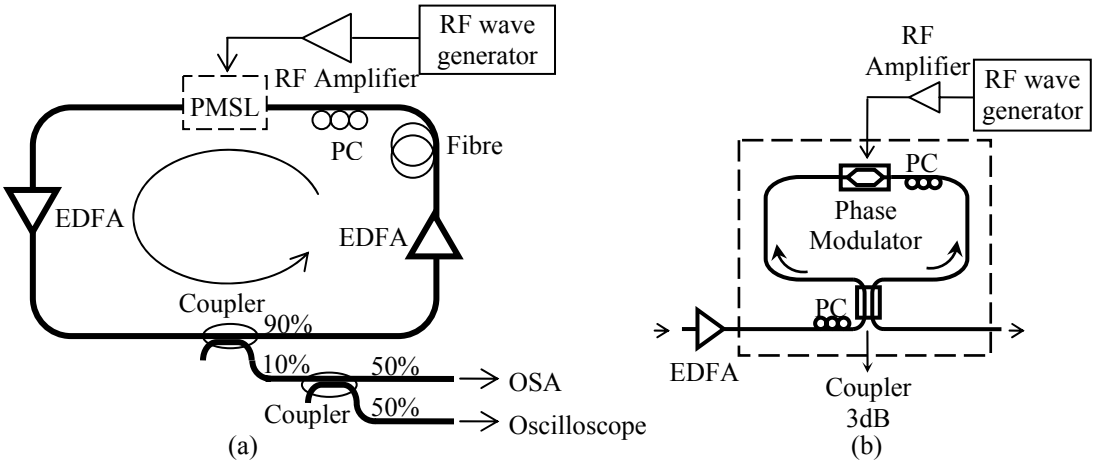

Figure 3-2 Experimental setup of the actively mode-locked fibre laser using phase modulated Sagnac loop (PMSL) (a) Schematic diagram of whole fibre ring laser, (b) Detailed diagram of the PMSL. (PC: Polarization controller).

3.2.2 Results and discussion

This section presents the results obtained from characterization of the FM-MLFRL setup above to show different operation modes including soliton generation, detuning effect and rational harmonic mode locking.

3.2.2.1 Soliton generation

By setting the saturated power of the EDFA of 5 dBm, a stable pulse train was generated at the 438th harmonic of the fundamental cavity frequency. Figure 3-3(a-c) shows the time trace and spectrum of the generated mode-locked pulse. The temporal and spectral widths of the pulse are 12.5 ps and 0.23 nm respectively. This result indicates that the pulse is transform-limited with a time-bandwidth product of 0.36. Because no optical band-pass filter is used in the setup, the emission wavelength of the fibre laser is around 1560 nm where the gain of the EDFA is maximum. The stability of the mode-locked pulse train is demonstrated by the RF spectrum shown in Figure 3-3(d). A supermode noise suppression ratio (SMSR) of higher than 45 dB was achieved without any feedback circuit for stabilization.

With the aim of increasing the phase modulation index, the phase modulator PM-315P was replaced by the phase modulator Covega's Mach-40-27 which has a half-wave voltage of only 4 V at the 1 GHz modulation frequency. It is surprising that a wider pulse sequence at the higher modulation index of 2.3 radians was obtained in this setup, with the same intracavity optical power as in the previous setup. Figure 3-4 shows the waveform and the corresponding optical spectrum of the mode-locked pulse generated from this setup. The pulse broadening in this case indicates a limitation of the gain bandwidth in the cavity, which could relate to the phase modulators, and will be explained more detail in Chapter 4.

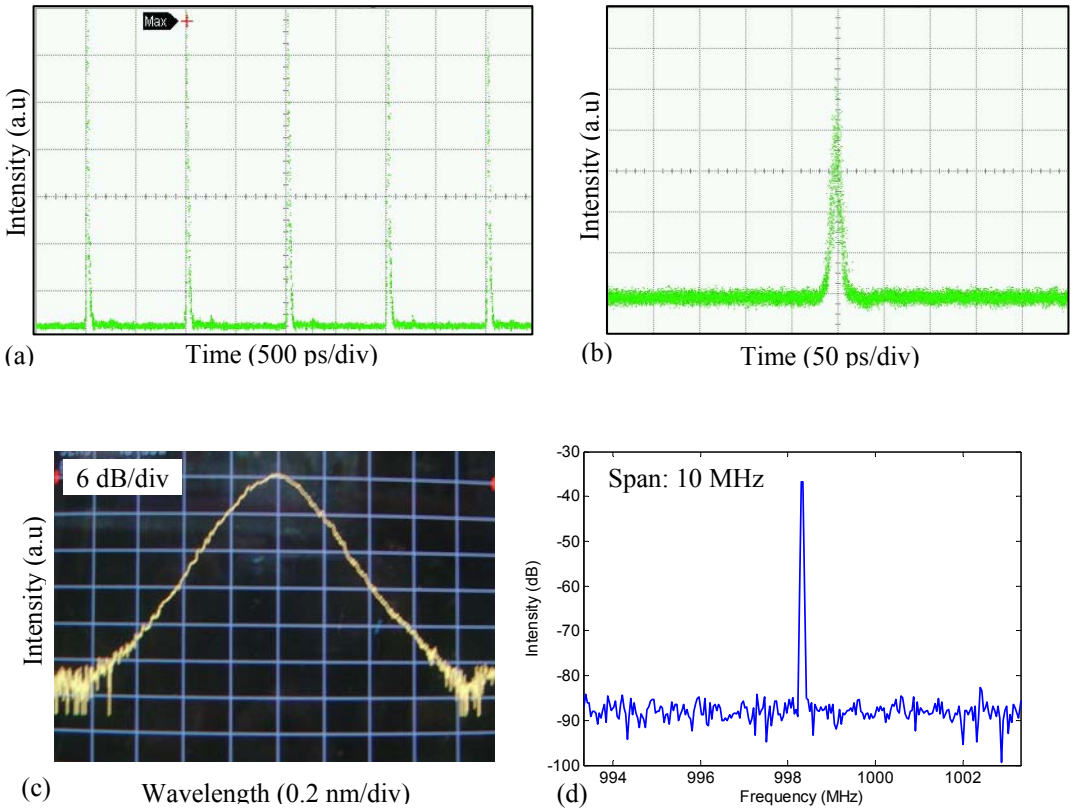

Figure 3-3 Waveforms of (a) the pulse train, and (b) the single pulse, (c) corresponding optical spectrum, (d) RF spectrum of the mode-locked pulse generated from the FM-MLFRL.

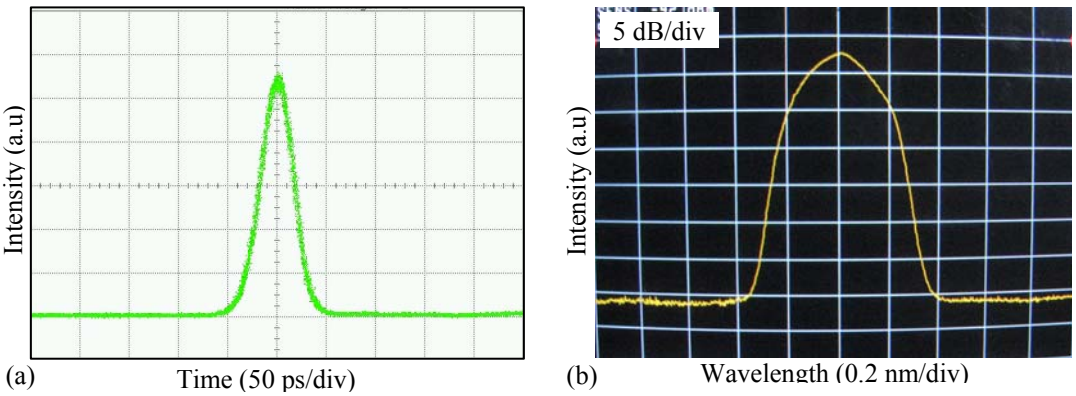

Figure 3-4 (a) Waveform and (b) spectrum of the mode-locked pulse generated from the FM mode-locked fibre ring laser using the phase modulator Mach-40-27.

In the configuration of mode-locked fibre laser using PMSL, phase modulation is converted into amplitude modulation by interference between clockwise light and counter clockwise light, which have a phase difference between them [130]. This

effect comes from the fact that the phase modulator is optimized for only one transmission direction. The transmission of the PMSL output is given by [130]

$$T(t) = \sin^2\left[\frac{\Delta\varphi(t) + \phi}{2}\right] \qquad (3\text{-}1)$$

where $\Delta\varphi(t)$ is the differential phase caused by the driving signal between two passage directions, ϕ is the bias differential phase. Thus in this configuration of the actively MLFRL, the PMSL can be considered as an amplitude modulator without the bias drift problem and possibly polarization dependence [130-131]. Expression (3-1) shows that the intensity modulation of the PMSL can operate at double the modulation frequency [132]; however, the mode-locked pulses at the peaks of the transmission acquire residual chirp from phase modulation [133]. This chirp will affect to the pulse characteristics as well as stability in the same way as in the actively FM-MLFRL. Figure 3-5 shows the time trace of the pulse train at 1 GHz generated from this configuration. High cavity loss reduces the efficiency of soliton compression effect in the fibre laser. Additionally, the PMSL is equivalent to an amplitude modulator, so that the modulation index depends on the intensity modulation curve converted from the phase modulation. With small phase modulation index the modulation index of the PMSL is also small. Therefore the width of the generated pulse is about 100 ps and the pulse shape with the product of time-bandwidth of 0.7 is a chirped pulse rather than a soliton.

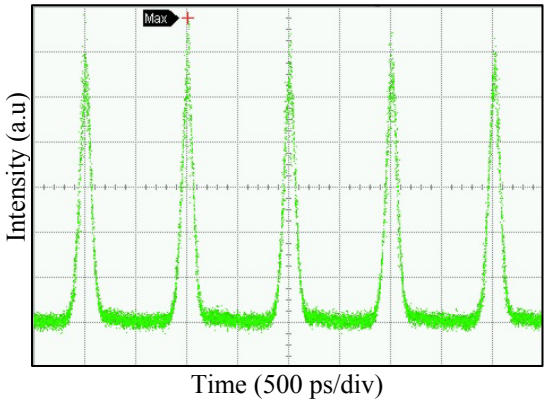

Figure 3-5 Waveform of the pulse train generated from the mode-locked fibre laser using PMSL

3.2.2.2 Detuning effect and relaxation oscillation

When the modulation frequency f_m is detuned, the fibre laser can experience various regimes. The transition state shows complex behaviours such as relaxation oscillation and excess noise enhancement as mentioned in Chapter 2. In our setup, the fibre laser experiences three main regimes: mode-locked regime, FM oscillation and transition states depending on detuning amount $|\Delta f_m|$. Because the range of $|\Delta f_m|$ in each regime depends on the cavity length or the cavity dispersion, we have inserted 100 m SMF-28 fibre into the fibre ring (Case A) replacing 50 m SMF-28 fibre in the original setup (Case B). The aim of changing the length of the SMF-28 fibre is to enhance sensitivity of detuning because of smaller $|\Delta f_m|$ as well as to change the phase differences of polarization components that can lead to a sufficiently NPR for a hybrid mode-locking. By detuning the f_m, the important regimes in both cases are identified as follows:

- When $|\Delta f_m| > 2$ kHz for Case A and $|\Delta f_m| > 4$ kHz for Case B, the fibre ring laser operates in FM oscillation regime which can be identified by its optical

spectrum. At large $|\Delta f_m|$, the optical spectrum is similar to CW signal due to the limitation of resolution in the OSA, while the RF spectrum cannot identify the first harmonic component of f_m as shown in Figure 3-8(a). When the effective modulation index is sufficient, by decreasing $|\Delta f_m|$, the optical spectrum is broadened with a double-peak shape due to the energy going to the optical frequencies far from the centre carrier mode as shown in Figure 3-6 (a). The spectrum keeps broadening when $|\Delta f_m|$ is reduced close to 2 kHz for Case A and 4 kHz for Case B. Figure 3-8(b) also shows the typical RF spectrum in this regime, which indicates strong supermode noise and a broad linewidth of each sidemode due to the beating between the cavity modes and the modulation frequency. Moreover the strength of the first harmonic is increased according to the reduction of $|\Delta f_m|$.

- When $0.3\ \text{kHz} < |\Delta f_m| < 2\ \text{kHz}$ for Case A and $0.8\ \text{kHz} < |\Delta f_m| < 4\ \text{kHz}$ for Case B, the fibre laser enters a transition regime where many complex behaviours such as the relaxation oscillations as well as the enhanced supermode noise status can occur [123]. The double-peak spectrum broadening becomes maximum before the energy at the main carrier grows according to the reduction of detuning as shown in Figure 3-6(b). Between the FM oscillation and mode locking regimes, the relaxation oscillations (RO) as well as the enhanced supermode noise status have been also observed. In the first half of the detuning range where $|\Delta f_m|$ is large, the time trace shows a high intensity with a nearly constant envelope in which the signal under the envelope varies continuously and rapidly in time domain. When the detuning

deceases further, the envelope of the high intensity is more deeply modulated as shown in Figure 3-7(a). Because the supermode noise is still dominant noise source, the RF spectrum exhibits behaviour similar to shown in Figure 3-8(b). Using a narrower resolution bandwidth, the beat noise between the modulation sidebands and the cavity modes of about 10 kHz can be observed as in Figure 3-8(c). At the lower limit of the detuning range, in the transition regime, when the detuning is decreased to around 500 Hz, the RO becomes stronger as an enhanced excess noise [123]. In this state, the building up of new pulses and the decay of old pulses can occur at the same time, thus the pulses exhibit a rapid variation of both amplitude and time position within the modulation cycle. Therefore, in this state the time trace of the signal is observed as noisy pulses as shown in Figure 3-7(b). The corresponding optical spectrum shows ripples in the envelope as shown in Figure 3-6(c). If the optical power in the cavity is further increased, the optical spectrum can exhibit sidebands as seen in Figure 3-6(d), which indicates the existence of ultra-short pulses with high peak power in this state. Figure 3-8(d) show the RF spectrum with strong sidebands of 2 kHz formed by beating between the modulation frequency and the RO frequency.

- When $|\Delta f_m| < 0.3$ kHz for Case A and $|\Delta f_m| < 0.8$ kHz for Case B, the mode-locked state can be identified by a clear pulse shape in the time trace, a sudden disappearance of the ripple in the optical spectrum and a sufficient suppression of supermode noise. When the detuning is reduced to a small amount that is within a specific limitation as specified in (2.81) or no detuning, the mode locking can be achieved to generate the stable pulse train as shown in Figure

3-3. By providing a sufficient gain in the cavity the RO noise suppression greater than 40 dB and the supermode noise suppression greater than 45 dB can be achieved in our setup without using any stabilization technique.

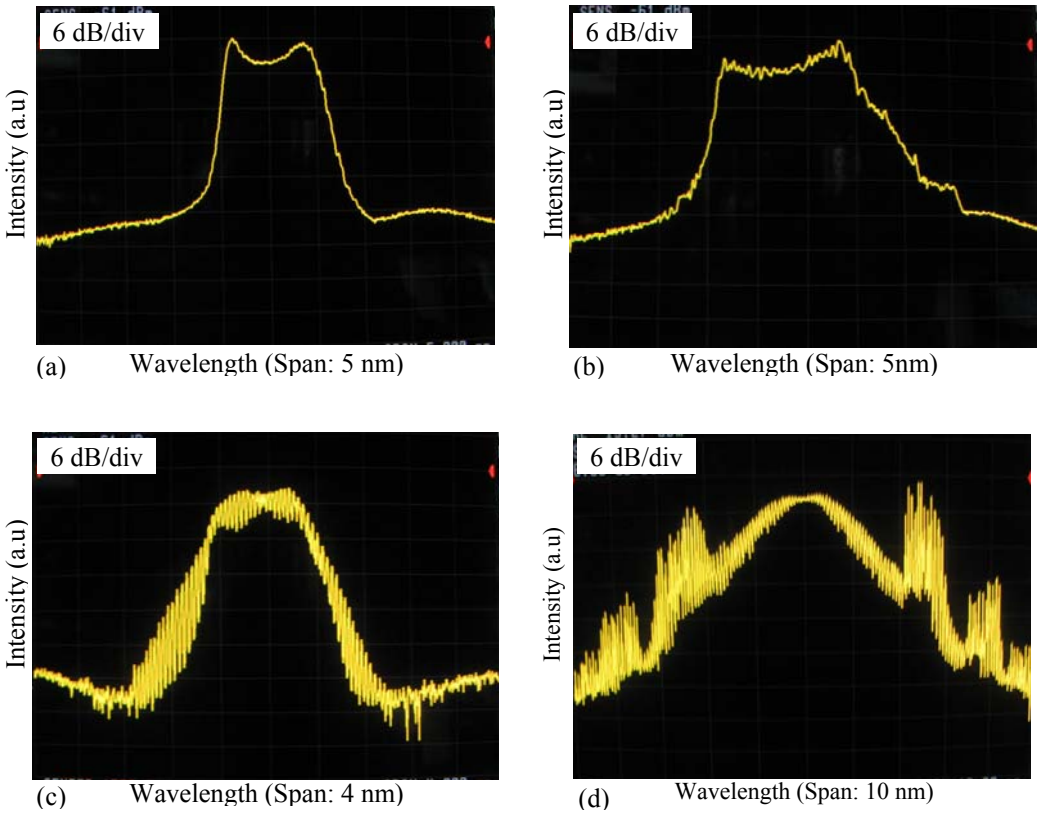

Figure 3-6 Optical spectra at different frequency detuning regimes: (a) FM oscillation, (b) Entering the transition regime, (c) Enhanced relaxation oscillation in the transition regime, and (d) Relaxation oscillation at higher optical power level.

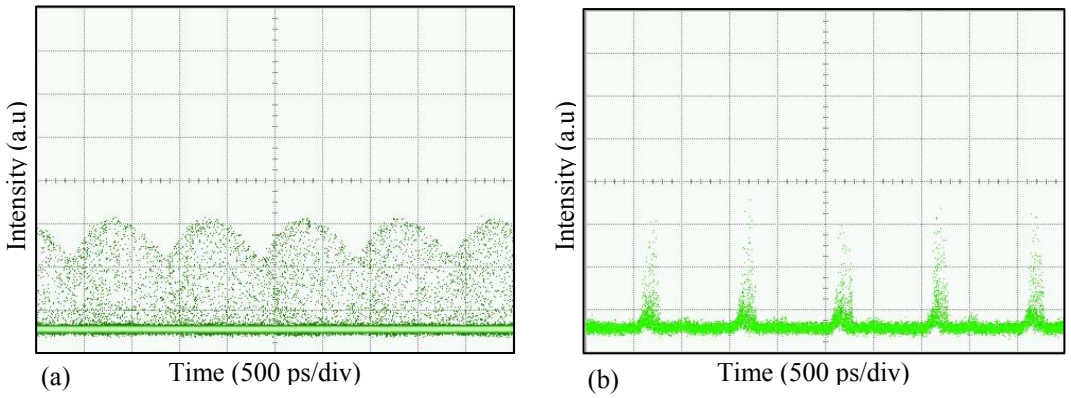

Figure 3-7 Time traces in the transition regime: (a) at larger half of the detuning range, and (b) at smaller half of the detuning range when the relaxation oscillation is enhanced.

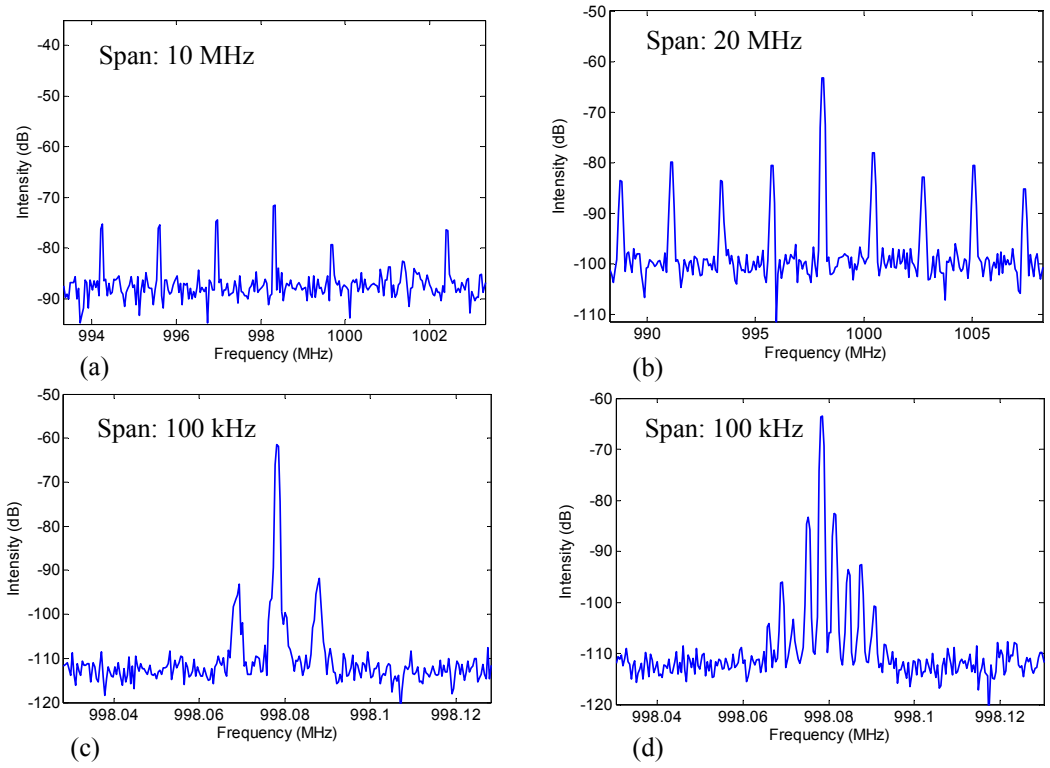

Figure 3-8 RF spectra in different regimes: (a) CW-like regime, (b) FM oscillation regime and transition regime in span of 20 MHz, (c) at larger half of the detuning rang in the transition regime in span of 100 kHz, and (d) Enhanced relaxation oscillation in transition regime in span of 100 kHz.

In the transition regime, it is really interesting that the existence of ultra-short pulses with very high peak power is observed when the detuning is about 500 Hz, with appropriate adjustment of polarization controller. Figure 3-9 shows the spectrum

and the time trace of this state in Case A. In this figure the time trace shows the generated pulses with very narrow width and a constant high peak power but a strong timing jitter, while the optical spectrum shows a broad spectral width and Kelly sidebands [115] generated by the resonance of dispersive waves and the generated pulses. These results indicate clearly the existence of solitons in this state. Based on the spectral width of 1.58 nm, the pulse width is approximately about 1.8 ps which is obviously impossible to resolve by the oscilloscope. From the sideband locations, the total cavity dispersion estimated by expression (2.56) is of about -0.0172 ps^2/m. High stability of the optical spectrum also demonstrates that solitons are stably formed inside the cavity. It is believed that the passive mode locking based on NPR plays a key role in this state. This process can be explained as follows: when the cavity is slightly detuned, the relaxation oscillation occurs in which the pulses in form of spikes acquire so high peak power that the NPR becomes significant in the weak birefringence cavity. In a favourable condition, by changing the settings of the polarization controller, the passive mode locking based on NPR can be achieved to shape the pulse circulating in the cavity. Thus the fibre laser in this state operates similar to a hybrid passive-active mode-locked laser [134-136]. In order to verify this passive mechanism, the RF modulation signal was turned off, however the optical spectrum with sidebands still remained for at least five minutes before it disappeared. Owing to the detuning, solitons experience a frequency shift that results in temporal variation of the pulses or timing jitter. Moreover this state operates in additive-pulse mode locking (APM) regime, it is easily prone to dropout as demonstrated in Figure 3-9(b) by the base line at the bottom of the pulse trace. This state is also observed in Case B, although it is more difficult for adjustment due to insufficient NPR effect in a

shorter fibre cavity. By carefully adjusting the polarization controller, solitons generated by this mechanism in Case B can be obtained as shown in Figure 3-10, however they are less stable. With the first sideband spacing of 3.95 nm, the average GVD of the cavity estimated by Expression (2.56) is about -0.0144 ps^2/m. The estimation of the average GVD is valid due to a reduction of the dispersion in Case B of -1.1 ps^2 which is exactly equivalent to a 50 m SMF-28 fibre.

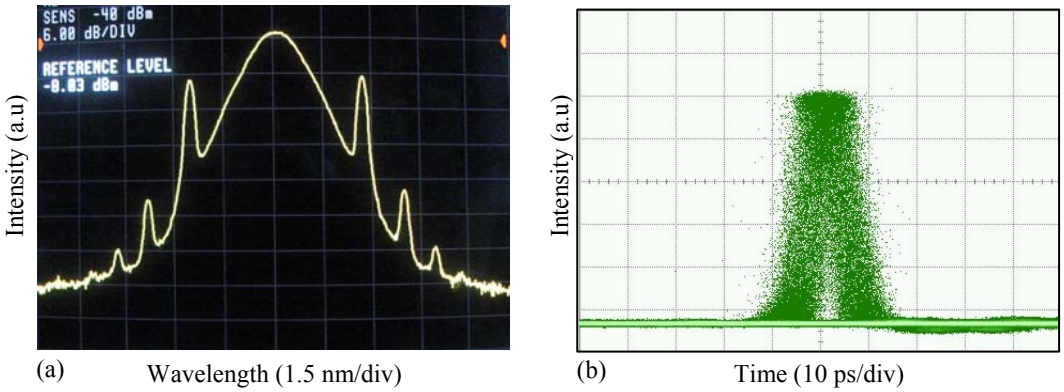

Figure 3-9 Spectrum and time trace of the hybrid mode locking state in Case A with an insertion of 100-m SMF-28 fibre into the ring cavity.

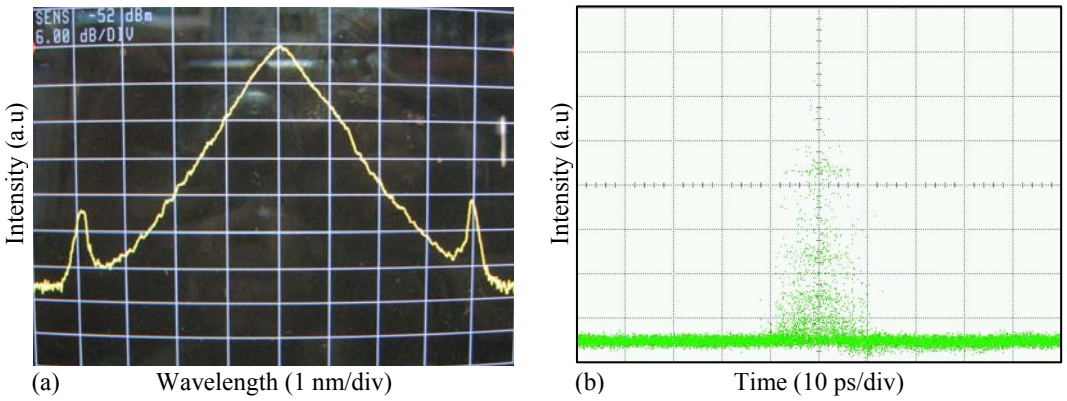

Figure 3-10 Spectrum and time trace of the hybrid mode locking state in Case B with an insertion of 50-m SMF-28 fibre into the ring cavity.

3.2.2.3 Rational harmonic mode locking

As described in Section 2.4.3.3, rational harmonic mode locking can be implemented in the actively FM mode-locked fibre laser by the higher-order harmonics of the amplified driving signal. By using a RF spectrum analyser, the magnitude of the harmonics at the output of the power amplifier is measured as a function of the RF input power. Figure 3-11 shows the measured results which indicate a strong increase of the second harmonic while the magnitude of the first harmonic remains unchanged at 19 dBm when the RF input power is greater than 2 dBm. Higher-order harmonics such as the third- and fourth-order harmonics are slightly enhanced at input powers higher than 5 dBm. The magnitudes of the high-order harmonics determine the modulation index of the corresponding rational harmonic mode locking.

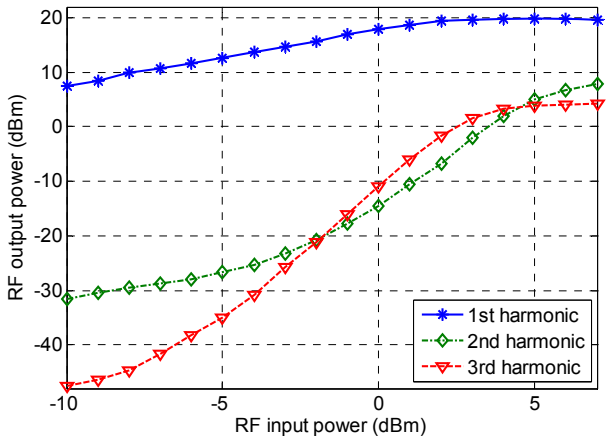

Figure 3-11 Output power of the 1st, 2nd and 3rd harmonics as a function of the RF input power

When the modulation frequency is detuned by amount of $\pm f_c/2$ and $\pm f_c/3$ from the 438th harmonic of the cavity frequency, pulse trains at the repetition rate of double and triple modulation frequency are generated as shown in Figure 3-12 at the RF input power of the power amplifier of 7 dBm. The pulse train for the second-order rational harmonic mode locking shows a better quality than that at the third order rational

harmonic mode locking due to higher modulation index of the second harmonic component. Other order rational harmonic mode locking such as the 4th and the 5th orders also can be obtained by an appropriate detuning but gives very low stability due to weak strength of the corresponding harmonic components in the driving signal.

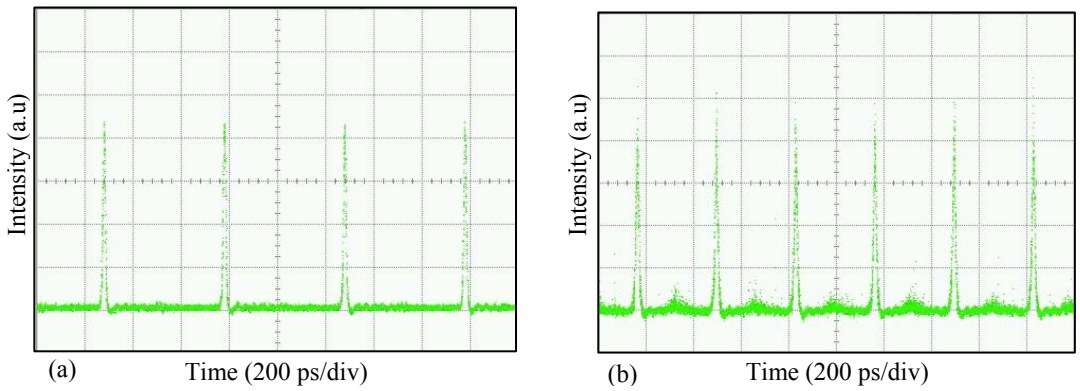

Figure 3-12 Time traces of the pulse trains in (a) the second- and (b) the third-order rational harmonic mode locking.

Similarly, the rational harmonic mode-locking can be achieved in the mode-locked fibre laser using PMSL for the repetition rate multiplication by detuning to different rational number of harmonics of the cavity. The detuning allows the pulses experienced the opposite chirp in consecutive round trips and consequently a uniform intensity transmission window can be obtained. In fact, the intensity modulation curve of the PMSL depends strongly on the phase modulation profile. If the phase modulation curve is distorted, the higher order harmonics in the resulted intensity modulation signal are also strongly enhanced to facilitate the rational harmonic mode locking. By detuning the modulation frequency of $\pm f_c/M$ with M from 2 to 6, the repetition rate of the pulse train is multiplied by a factor M as shown in Figure 3-13. However the amplitude of pulses is unequal because of the non-uniformity of the intensity modulation profile.

Thus the pulse trains at the output of the mode-locked fibre ring laser using PMSL show the problem of non-uniform amplitude which is disadvantage of rational harmonic mode locking using amplitude modulation. While the uniform pulse trains are always generated by phase modulation in rational harmonic mode locking if the strength of higher order harmonic component is sufficiently high in the driving signal.

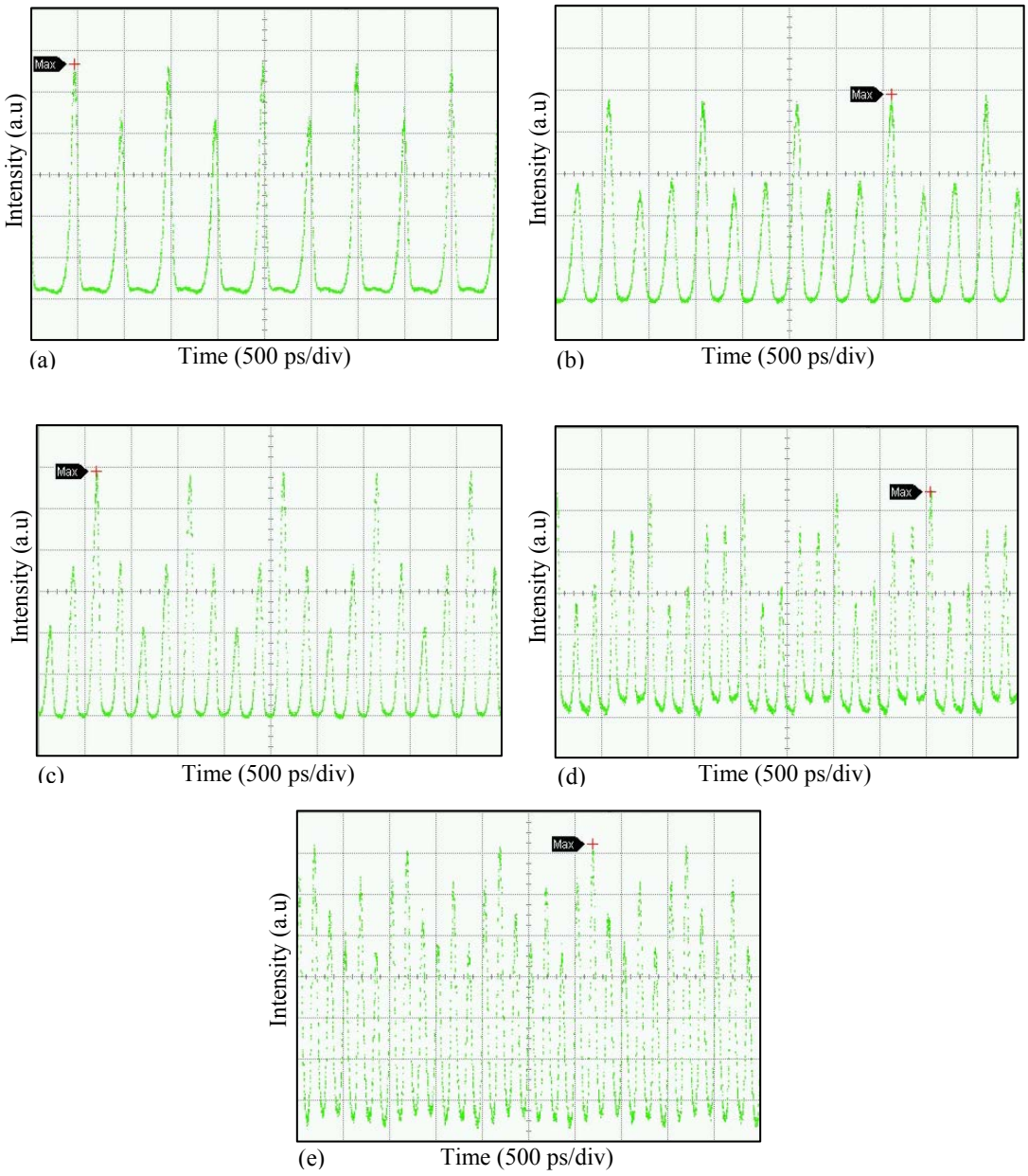

Figure 3-13 Time traces of (a) the second-order, (b) the third-order, (c) the fourth-order, (d) the fifth-order, and (e) the sixth-order rational harmonic mode locking in the fibre ring laser using PMSL.

3.3 SIMULATION OF ACTIVELY FM MODE-LOCKED FIBRE LASER

3.3.1 Numerical simulation model

Although a FM mode locking can be theoretically described by the master equation with averaged parameters, it is difficult to solve this equation to find an analytical solution including all of important effects. Therefore in order to understand the physical processes occurring inside the fibre ring cavity, a numerical model is developed in this chapter. The model of mode-locked fibre laser with a ring configuration consists of basic components similar to that in the experimental setup.

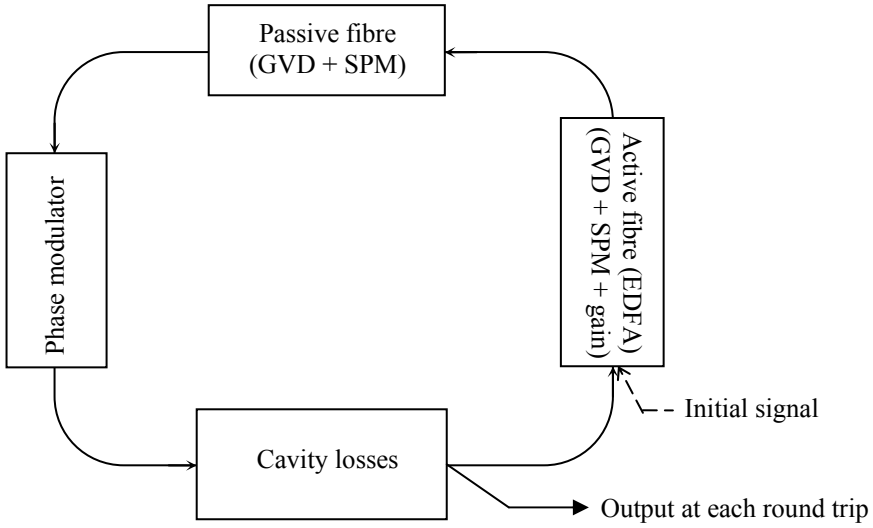

Figure 3-14 Schematic diagram of the numeric model for an actively FM mode-locked fibre ring laser.

Figure 3-14 shows the block diagram of the numerical model for an actively FM mode-locked fibre ring laser. In this model, a slowly varying envelope of the optical pulse passes through each component once in each round trip. This process will be repeated until a desired solution is obtained. Thus the envelope function of the pulse at the n^{th} round-trip can be given by

$$A^n(t) = \hat{L}\hat{M}\hat{F}\hat{F}_g . A^{n-1}(t) \qquad (3\text{-}2)$$

where A^n, A^{n-1} are the complex amplitude of the pulse at the nth and the (n-1)th round-trips respectively, $\hat{L}$, $\hat{M}$, $\hat{F}$ and $\hat{F}_g$ are the operators representing for the loss of the cavity, the modulation mechanism, the passive and active fibres respectively. Based on physical mechanisms well understood, the operators or the models of the components inside the ring cavity can be exactly described and the effect of each component is individually considered in the model.

Firstly, the operators $\hat{F}$ and $\hat{F}_g$ which describe propagation of the optical field in optical fibres can be modelled by the generalized NSE (2.13) which can be rewritten for convenience as follows [96]

$$\frac{\partial A}{\partial z}+\frac{j}{2}\left(\beta_2+\frac{jg_{sat}}{\Delta\omega_g^2}\right)\frac{\partial^2 A}{\partial\tau^2}-\frac{\beta_3}{6}\frac{\partial^3 A}{\partial\tau^3}=i\gamma\left|A\right|^2 A+\frac{1}{2}\left(g_{sat}-\alpha\right)A \tag{3-3}$$

In case of passive fibre, the gain factor is set to zero, but the gain factor with saturation is nonzero in active fibre for amplification in the EDFA, and modelled by using Eqs.(2.10) and (2.12). The ASE noise generated from the EDFA is also included at the end of the active fibre. The ASE noise in one polarisation is modelled as an additive complex Gaussian-distributed noise with a variance given by

$$\sigma_{ASE}^2=h\nu n_{sp}(G-1)B_{ASE} \tag{3-4}$$

where h is Plank's constant, ν is the optical carrier frequency, G is the gain coefficient and B_{ASE} is the optical noise bandwidth and n_{sp} is the spontaneous factor which relates to the noise figure NF of the EDFA as follows

$$n_{sp}=\frac{NF.G-1}{2(G-1)} \tag{3-5}$$

Eq.(3-3) for both active and passive fibres can be solved by using well-known split-step Fourier method in which the fibre is split into small sections of length and the linear and nonlinear effects are alternatively evaluated between two Fourier-transform domains respectively [60].

Secondly, the operator $\hat{M}$ for an EO phase modulator is given by

$$\hat{M} = \exp[jm\cos(\omega_m(\tau + \Delta\tau_s) + \phi_0)] \tag{3-6}$$

where m is the phase modulation index, ϕ_0 is the initial phase and $\omega_m = 2\pi f_m$ is the angular modulation frequency, assumed to be a harmonic of the fundamental frequency of the fibre ring, $\Delta\tau_s$ is the time shift which is caused by detuning and given by

$$\Delta\tau_s = \frac{T_m - T_h}{T_c} T \tag{3-7}$$

where $T_m = 1/f_m$ is the modulation period, $T_h = T_c/N$ with T_c is the cavity period and N is the harmonic order, T is the time in terms of the round trip duration.

Beside the attenuation of optical fibres, there are some losses inside the cavity such as coupling loss, insertion losses of the modulator and connectors. All these losses need to be included into the simulation and combined into the total cavity loss factor. The influence of this loss is given as

$$\hat{L} = 10^{l_{dB}/20} \tag{3-8}$$

where l_{dB} is the total loss of the cavity in dB. Thus this effect in turn determines the required gain coefficient of the EDFA to ensure that the gain is sufficient to compensate the total loss in a single round trip for stable lasing operation.

Equations (3-3)-(3-8) provide a full set of equations for numerical simulation of an actively FM mode-locked fibre ring laser. Due to the recursive nature of pulse propagation in a ring cavity, the operators are repeatedly applied to the complex envelope of the pulse to find a stable solution. The complex amplitude of the output is used as the input of the next round-trip and stored for display and analysis. In simulation of pulse formation, a complex Gaussian-distributed noise of -10 dBm is used as a seeding signal. Depending on the strength of the effects in the model, a stable pulse can be found in 500 round trips or even up to 10000 round trips. Number of samples in simulation window as well as the step-size in spatial domain is properly chosen to minimize numerical errors in calculation. Particularly, the number of samples in a modulation period is 4096 and the spatial step-size is from 2 m to 5 m to keep the maximum nonlinear phase shift below 0.05 rad in each step.

Table 3-1 Parameter values used in simulations of the FM mode-locked fibre laser

β_2^{SMF} = -21.7 ps^2/km for $\bar{\beta}_2 < 0$,	β_2^{EDF} = 19 ps^2/km,	$\Delta\omega_g$ = 16 nm,
β_2^{SMF} = +21.7 ps^2/km for $\bar{\beta}_2 > 0$	γ^{EDF} = 0.0023 W^{-1}/m,	$f_m \approx$ 1GHz,
γ^{SMF} = 0.0014 W^{-1}/m,	α^{EDF} = 0.5 dB/km	m = 0.05π - 1π rad
α^{SMF} = 0.2 dB/km	P_{sat} = 5 ÷ 8 dBm	λ = 1559 nm
L_{SMF} = 80 m	g_0 = 0.315 m^{-1}	
L_{EDF} = 10 m	NF = 5 dB	

SMF – Standard single mode fiber, EDF – Erbium doped fiber, NF – noise figure of the EDFA

3.3.2 Results and discussion

3.3.2.1 Mode-locked pulse formation

By using the numerical model described above, the pulse formation in the FM mode-locked fibre ring laser can be investigated. Table 3-1 summarizes all parameters used

in the simulations. Figure 3-15(a) shows an evolution of the mode-locked pulse built up from the noise at $m \sim 1$ radian in the ring cavity with an anomalous $\overline{\beta}_2$ of -0.0171 ps^2/m. Figure 3-15(b) plots the peak power as a function of round trip number. The steady state is only reached after 5000 round trips and a damped oscillation occurs in initial stage of pulse formation process. Figure 3-16 shows the time trace and the spectrum of mode-locked pulse at steady state. It is noted that the pulse with the width of 11.6 ps is well fitted to a secant hyperbolic pulse rather than a Gaussian pulse; however, its spectrum exhibits no sideband due to weak dispersive waves in the cavity.

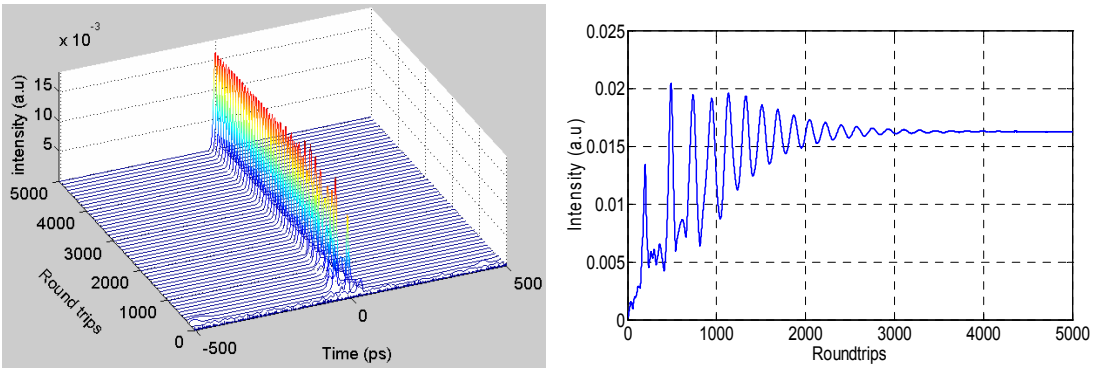

(a) (b)

Figure 3-15 (a) Numerical simulated evolution of the mode-locked pulse formation from the noise, (b) Variation of the peak power 5000 round trips in the anomalous average dispersion cavity.

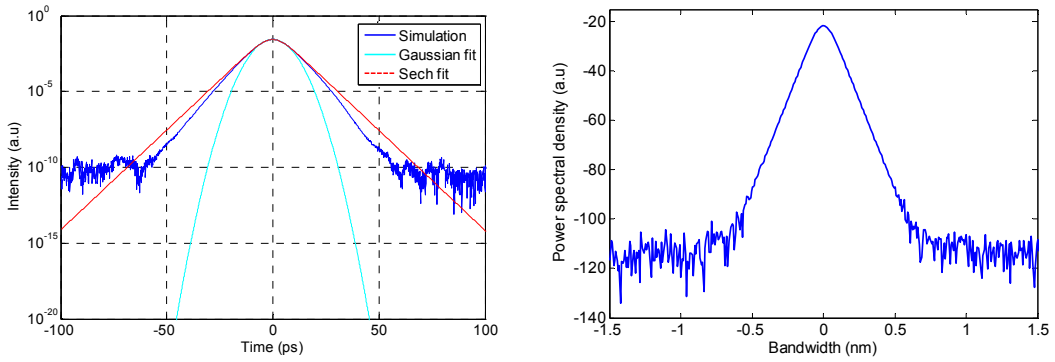

(a) (b)

Figure 3-16 (a) Numerical simulated time trace and (b) the corresponding spectrum of mode-locked pulse at steady state in the anomalous average dispersion cavity.

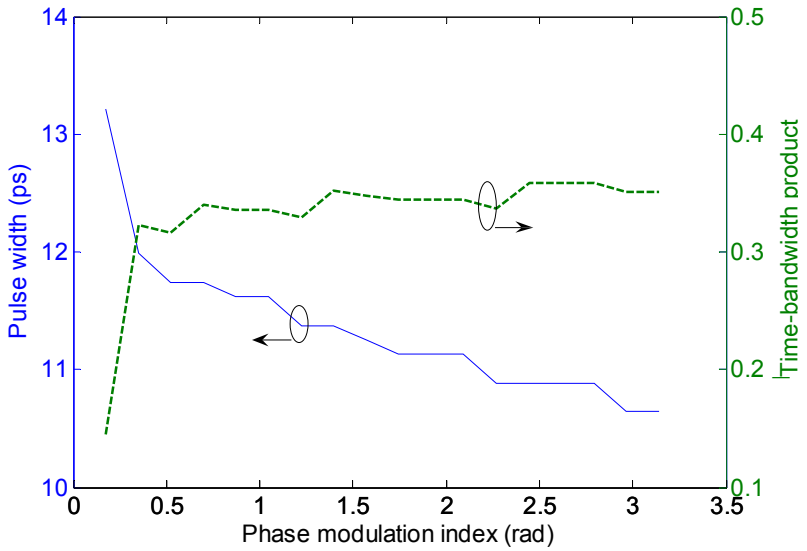

Figure 3-17 Variation of mode-locked pulse parameters as a function of the phase modulation index in the anomalous average dispersion cavity.

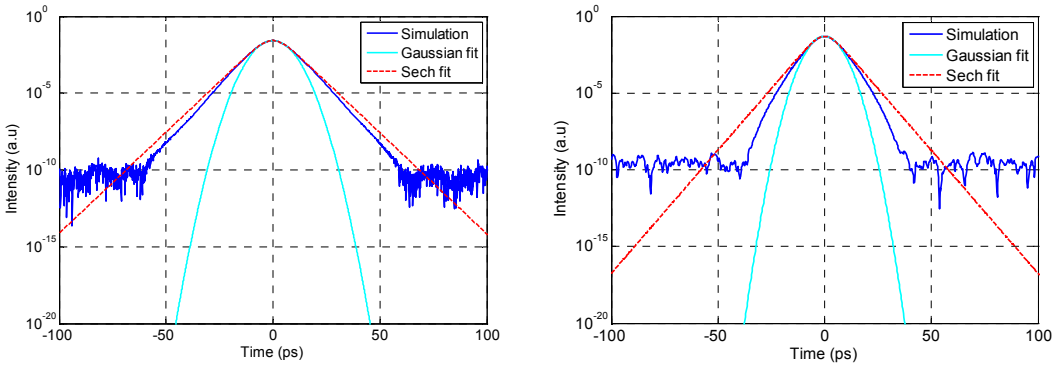

Figure 3-18 Numerical simulated waveforms in steady state of mode-locked pulses at two different modulation indices (a) m = 0.87 radian, and (b) m = π radian.

The effect of the phase modulation index *m* on the mode-locked pulse is also numerically investigated by varying the index in a range from 0.175 radian to π radian and the results are shown in Figure 3-17. The increase in modulation index shortens the pulse width. At the index lower than 0.5 radian, the rate of pulse shortening is stronger due to the soliton compression effect which results from the dominant SPM effect in pulse shaping. However, at a modulation index higher than 0.5 radian where

the active phase modulation becomes a stronger contributor to pulse shaping, the reduction of the pulse width is slow and almost linear. The chirp of the pulse increases with the increase in the phase modulation index and the pulse diverges from the secant hyperbolic profile and becomes closer to a Gaussian pulse at a higher modulation index. Figure 3-18 shows the waveforms of the generated pulse at two different modulation indices with the Gaussian fit and secant hyperbolic fit curves.

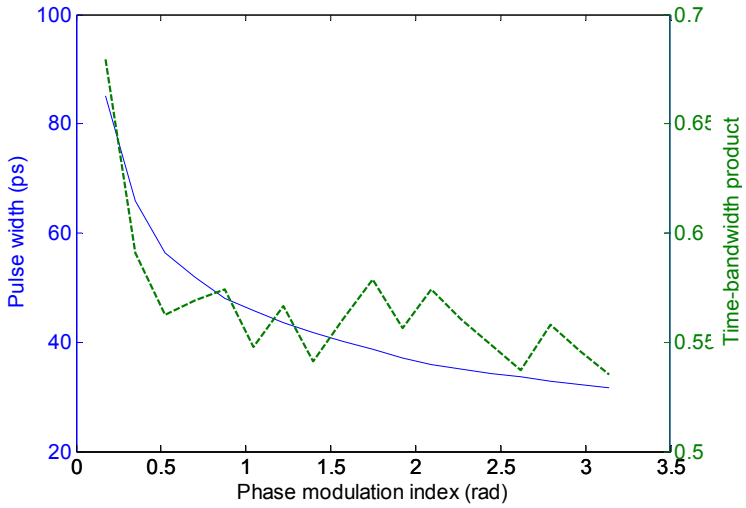

Figure 3-19 Variation of mode-locked pulse as a function of the phase modulation index in the normal average dispersion cavity.

Instead of an anomalous dispersion cavity, the sign of dispersion in the fibres is reversed to provide a normal dispersion cavity with $\overline{\beta}_2$ of +0.0213 ps^2/m. With the same conditions of mode locking, the mode-locked pulse in the normal dispersion cavity is wider and higher chirped than that in the anomalous dispersion cavity. The parameters of the mode-locked pulse as a function of the modulation index in the normal dispersion cavity are depicted in Figure 3-19. The pulse is also shortened with the increase in the phase modulation index. Evolution of mode-locked pulse in the normal average dispersion cavity at $m \sim 1$ radian is shown in Figure 3-20(a). Figure

3-21 shows the pulse profile in time domain and its spectrum at steady state, that indicates a parabolic pulse rather than a soliton or Gaussian pulse. Furthermore, in the initial stage of the pulse formation, there is an existence of dark soliton embedded into the background pulse growing up as shown in Figure 3-20(b). It is understood that in this stage the accumulated phase modulation is relatively weak, so that the SPM effect is dominant due to the high gain from the EDFA. The dark soliton formation occurs from the balance of normal GVD and SPM effects, yet the dark soliton is unstable. It experiences a periodic variation of time position (dotted line in Figure 3-20(b)) and decays due to the chirping caused by active phase modulation. Figure 3-22 shows the waveform with a dip at near centre of the background pulse and its phase profile with a phase change of about $\pi/2$ at the dip at the 2900th round trip. Because the intensity of the dip which also varies along the evolution is nonzero, the formed dark soliton is referred to as the gray soliton rather than the black soliton [65]. The existence of dark soliton only remains until the accumulated phase shift is sufficient to lock a pulse at the minimum of modulation cycle.

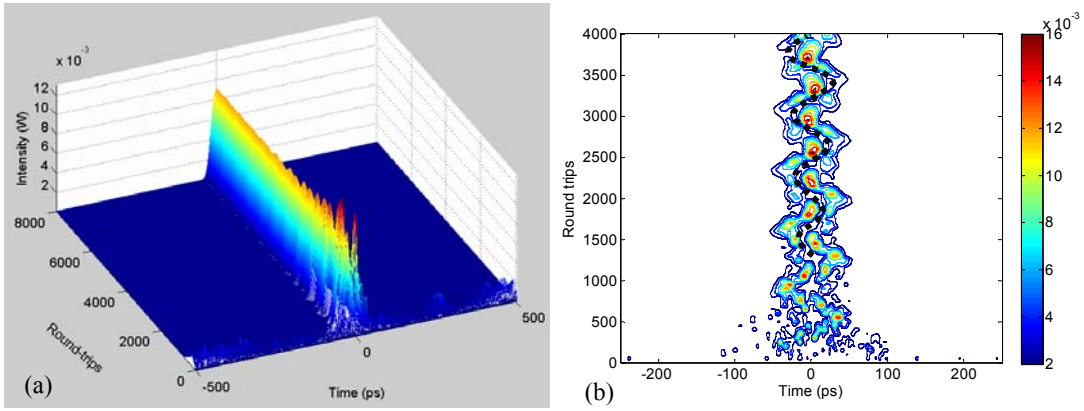

Figure 3-20 (a) Numerical simulated evolution of mode-locked pulse formation from noise in the normal average dispersion cavity over 8000 round trips, (b) The evolution in the first 4000 round trips showing the dark soliton formation (black dotted line) embedded in the background pulse.

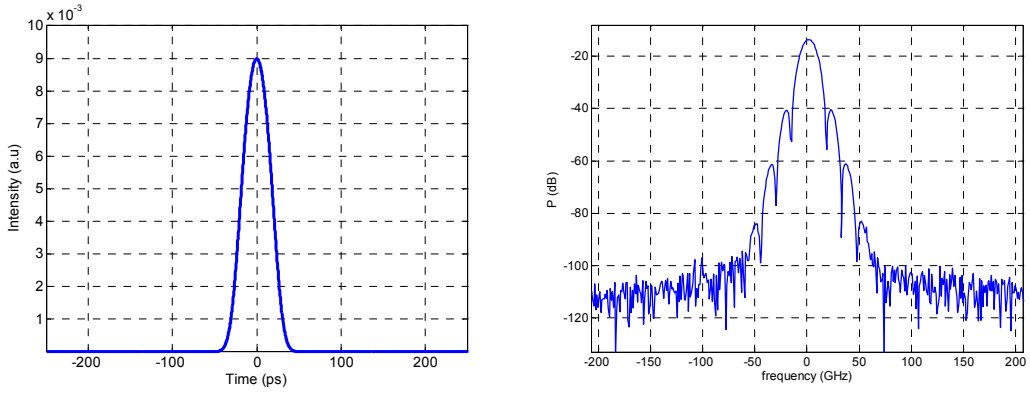

(a) (b)

Figure 3-21 (a) Simulated waveform and (b) spectrum of mode-locked pulse at steady state in the normal average dispersion cavity.

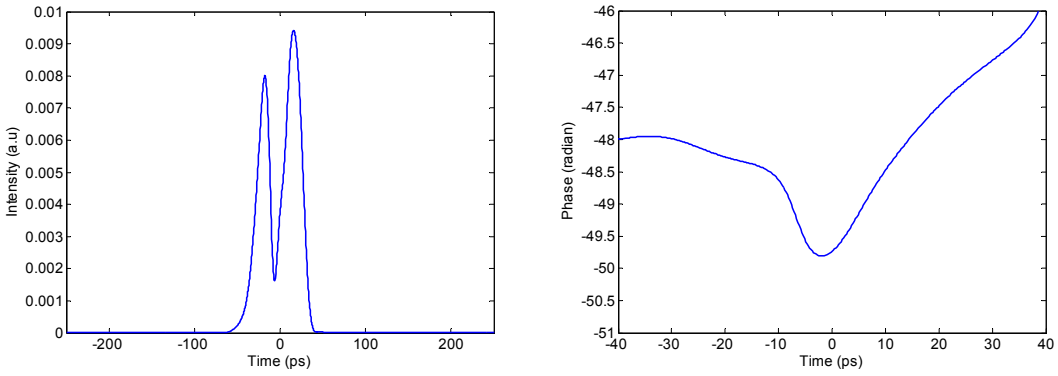

(a) (b)

Figure 3-22 (a) Simulated waveform and (b) its phase profile at the 2900th round trip showing a gray soliton embedded in the building-up pulse.

In the FM mode-locked fibre laser, the pulse formation at up-chirping or down-chirping cycles depends on the dispersion of the cavity which is anomalous or normal [51, 53]. On the other way, the pulse switching between positive and negative modulation cycles is suppressed due to the presence of GVD effect. Figure 3-23 shows evolutions of the mode-locked pulses built up from noise in normal and anomalous dispersive fibre rings in one modulation period. The modulation curve is phase shifted by $\pi/2$ to display both up-chirp and down-chirp cycles in the same simulation window. The dashed lines in the graphs indicate the phase modulation

curve applied in every round-trip. Thus the pulse is built up only at the extreme of the up-chirp cycle in the anomalous dispersion cavity or only at the extreme of the down-chirp cycle in the normal dispersion cavity.

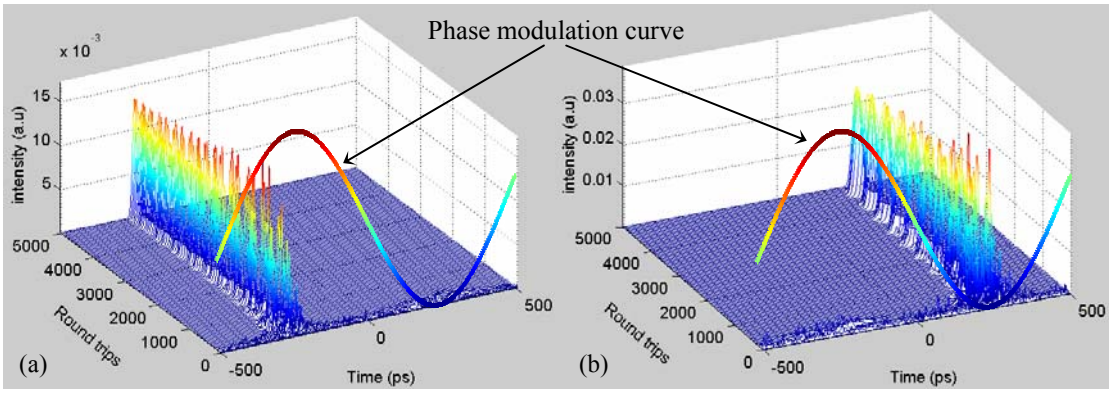

Figure 3-23 Numerical simulated evolution of mode-locked pulse built up from noise in (a) anomalous dispersion cavity, and (b) normal dispersion cavity at the same phase of modulation curve.

3.3.2.2 Detuning operation

Detuning moves the modulation frequency away from a harmonic of the cavity frequency. The pulse passes through the modulator at different times relative to the modulation each round trip and so experiences a frequency shifting [137]. During propagation through the dispersive fibre, the frequency shift imparts a temporal shift relative to the modulation curve. However, a large detuning can destroy a stable mode locking state due to a fast varying of the modulation cycle between successive round-trips and so the fibre laser falls into the FM oscillation regime, which generates a highly chirped signal [122]. Figure 3-24 shows the numerical simulated results in time and frequency domains when the modulation frequency is detuned by 6 kHz. The pulse evolution shown in Figure 3-24(a) indicates spike-like patterns, changing from one round trip to the next one. An example of unstable waveform in time domain at the 5000th round trip is shown in Figure 3-24(b) and its spectrum in Figure 3-24(c) is

broadened with two peaks as observed in the experiment. By taking the average of the waveforms over the last 500 round trips, a waveform with the envelope modulated at f_m can be observed in Figure 3-24(d).

When the detuning is slightly moderate, the phase variation of the modulation cycle between successive round trips is sufficiently slow to enable the pulse to build up in the cavity with adequately high gain. However the built-up pulses experience the frequency shift induced by detuning that leads to the variation of temporal position and higher loss to be decayed [72]. Relaxation oscillation behaviour occurs in this state as shown in Figure 3-25(a) at the detuning of 1 kHz. Repetition of the process consisting of the pulse decay and the pulse building up exhibits turbulence-like behaviour as seen in contour plot view in Figure 3-25(b). Figure 3-25(c) show a typical time trace of this state at the 5000^{th} round trip in which there are three pulses existing simultaneously in the same modulation cycle. In this figure, the lowest pulse close to the extreme of modulation cycle is the new pulse building up from noise, the middle pulse with highest peak power and narrow width is experiencing the time shift, while the last pulse with lower peak, which is far from the extreme is decaying due to higher loss. The built-up pulses can survive in around 500 to 1000 round trips. Because very narrow pulses of 2.5 ps are generated in this case, the corresponding spectrum exhibits sidebands as shown in Figure 3-25(d).

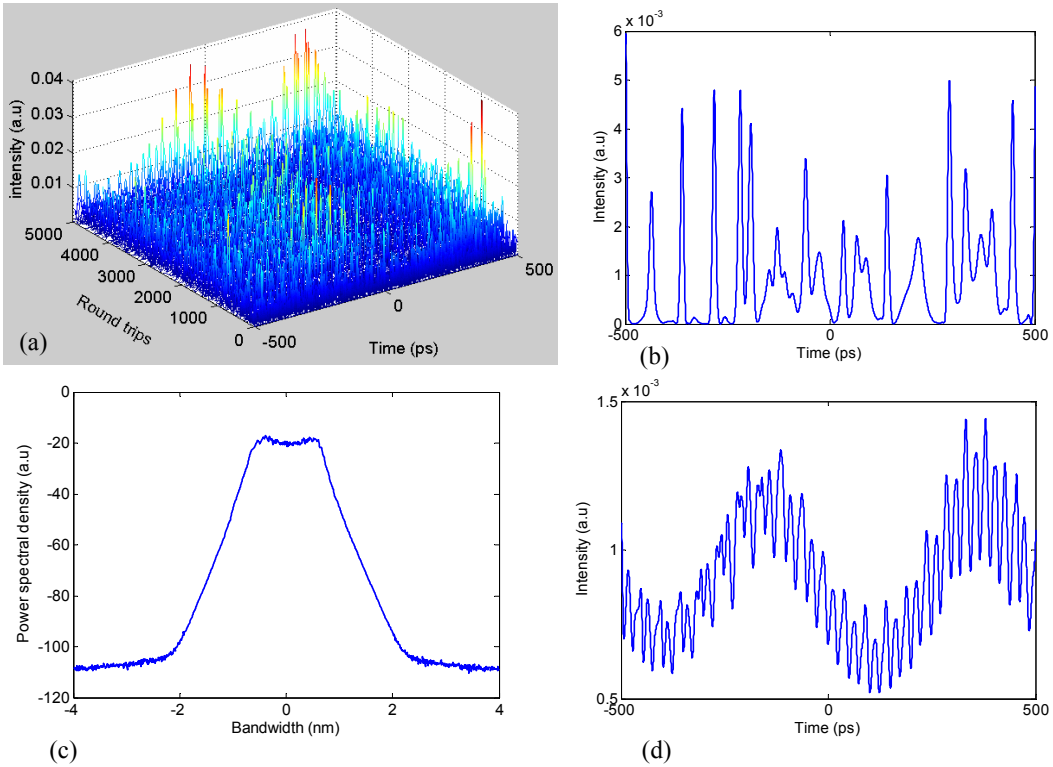

Figure 3-24 (a) Numerical simulated evolution of the signal circulating in the cavity, (b) the waveform of the output over 5000 round trips, (c) the spectrum and (d) the waveform averaged over last 500 round trips when the modulation frequency is detuned by 6 kHz.

When the detuning is small enough, the cavity still remains mode-locked state as in asynchronous mode locking [56]. However the mode-locked pulse can experience a variation of temporal position induced by the frequency shift and the dispersion of the cavity. Figure 3-26 shows the behaviour of the mode-locked pulse when the modulation frequency is detuned by 0.25 kHz. The contour plot in Figure 3-26(b) indicates that the pulse still can overcome the detuning problem to stabilize in the cavity.

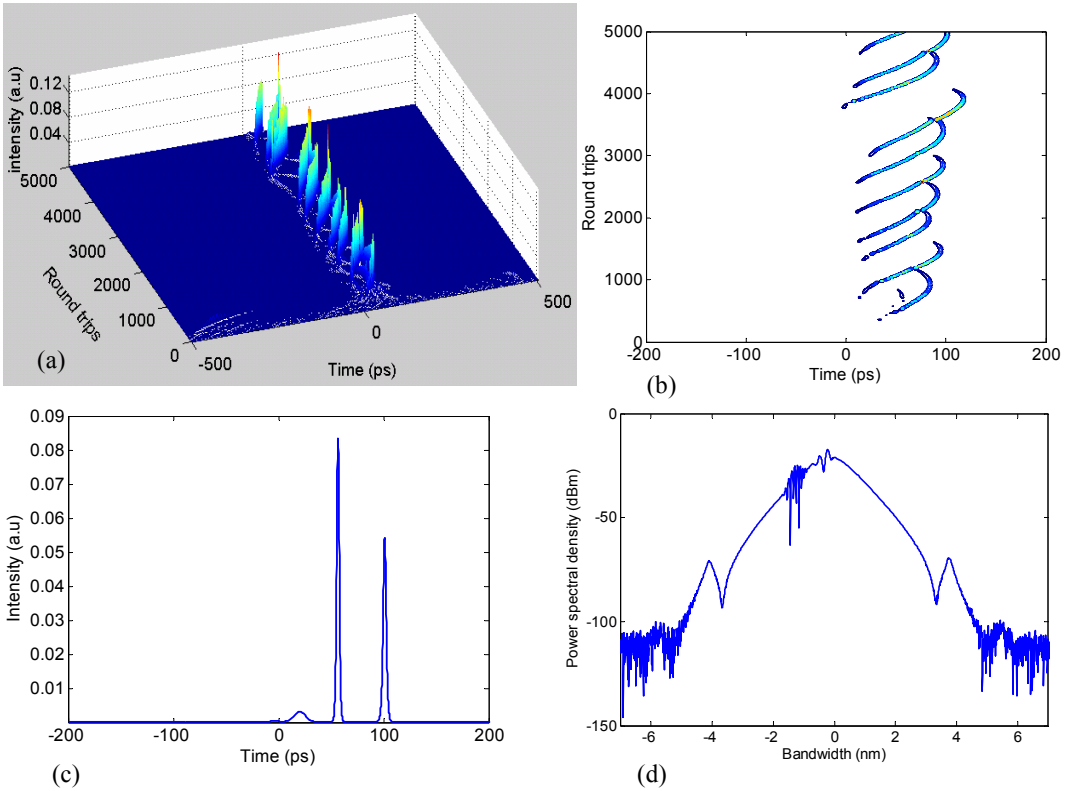

Figure 3-25 (a) Numerical simulated evolution of the signal circulating in the cavity, (b) contour plot view of the evolution, (c) the time trace of the output over 5000 round trips, (d) the spectrum averaged over last 500 round trips when the modulation frequency is detuned by 1 kHz with a higher gain factor $g_0 = 0.315$ m^{-1} and $P_{sat} = 8$ dBm.

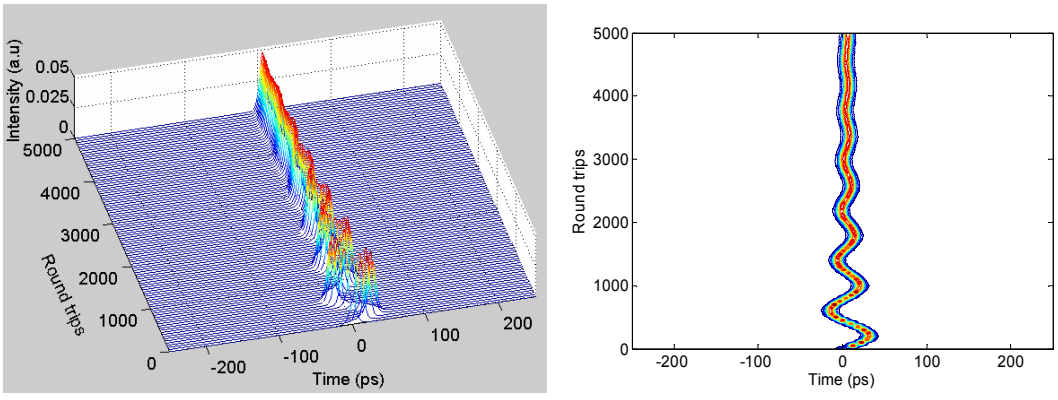

Figure 3-26 (a) Numerical simulated evolution of the mode-locked pulse circulating in the cavity, (b) contour plot view of the evolution when the modulation frequency is detuned by 250 Hz.

3.4 CONCLUDING REMARKS

Actively mode-locked fibre ring lasers using EO phase modulators have been experimentally demonstrated for generation of sequence of short pulses. The obtained results also indicate that the FM mode-locked fibre laser offers a better performance in terms of pulse width and stability than the mode-locked fibre laser using PMSL which acts as an amplitude modulator. The rational harmonic mode locking has been achieved by the enhancement of higher order harmonics in the electrical driving signal applied to the optical modulator. Moreover, detuning effects in the fibre laser have been characterized through the time traces, optical spectrum and RF spectrum analysis. All obtained results indicated complex behaviour in the transition regime in which the hybrid passive-active mode locking can be achieved to generate solitons with narrow pulse width.

Furthermore, a numerical model of the FM mode-locked fibre ring laser has also been developed to investigate the physical processes occurring inside the fibre cavity. The formation of mode-locked pulse in various conditions of the cavity has been numerically studied to demonstrate that indeed, short pulses generated from the FM mode-locked fibre laser system are chirped solitons. The model has also been used to reproduce all possible operations of the FM mode-locked fibre laser including the detuning effect in the experiment to demonstrate the validity of the model that will be used for the next chapters.

Chapter 4

Multi-bound solitons

4.1 INTRODUCTION

Optical solitons have attracted considerable attention in research not only for their generation techniques but also for their propagation dynamics. The understanding of soliton dynamics is of much significance for soliton applications in communications and signal processing. Therefore, extensive studies on soliton interactions have been performed [1-9]. For practical dissipative systems such as mode-locked fibre lasers, the interaction between solitons can be theoretically described by the complex Ginzburg-Landau equation (CGLE) [91, 138-139] instead of the standard nonlinear Schrödinger equation, which is only valid in conservative systems. Hence the interaction of solitons described by the CGLE has attracted considerable attention in theoretical studies. Malomed [140-141] analysed the interaction of slightly overlapping CGLE solitons and firstly predicted about the formation of stable dual- and multipulse bound states of solitons. Then Akhmediev *et al.* [139] numerically investigated the interaction of the CGLE solitons by using two-dimensional phase space approach. They also found the stable solution of dual and multi-pulse bound solitons with a $\pi/2$ phase difference between them. These theoretical results opened a new research direction on states and dynamics of short pulses in the mode-locked fibre lasers.

It has taken one decade since Malomed's prediction to experimentally demonstrate the existence of the bound solitons in the passively mode-locked fibre laser using NPR technique [29]. Then, bound solitons were also reported in a passively mode-locked fibre laser using NOLM [142]. Most numerical and experimental investigations on various operation modes and dynamics of bound solitons have been implemented in the passively mode-locked fibre lasers [29-32, 45, 142-151]. However, there was an interesting question about the existence of bound solitons in actively mode-locked fibre lasers. The bound soliton pairs but not multi-bound solitons with more than two solitons in bound states was experimentally observed for the first time in the actively FM mode-locked fibre laser [152]. Multi-bound solitons can be considered as a special state in which many solitons bind together to form a stable bunch of solitons through effective interactions in specific propagation conditions. Unlike high-order solitons whose shapes vary periodically during propagation, multi-bound solitons can remain their parameters such as temporal separation and shape unchanged in the propagation condition.

In this chapter, we will demonstrate the existence of multi-bound solitons with more than two solitons in bound states generated from the actively FM mode-locked fibre laser. The formation mechanism and the characteristics of multi-bound solitons are also described and discussed.

4.2 BOUND SOLITONS IN PASSIVE MODE LOCKING

4.2.1 Multi-pulsing operation

Bound soliton states can be considered as one of the multiple soliton operation modes of the passively mode-locked fibre laser [153]. On the other hand, the formation of

bound solitons relates to multi-soliton operation and effective interactions between solitons inside the nonlinear fibre cavity. In strongly nonlinear regime of operation, passively mode-locked fibre lasers exhibit a multi-pulsing behaviour. The existence of multiple solitons in the cavity also refers to the soliton energy quantization effect which limits the peak power of solitons in specific conditions. Efforts have been achieved [32, 96, 154-156] to find mechanisms of multi-pulse formation that is important for optimization and design of passively soliton fibre lasers.

There are three main mechanisms of multi-pulse formation that limit the peak power of the pulse circulating in the cavity:

- The first mechanism relates to the pulse splitting due to the limited gain bandwidth [154]. Under highly nonlinearity due to strong pumping, the mode-locked pulse is compressed by SPM effect so that its spectrum is broadened so wide that some frequency components can exceed limited bandwidth of the gain medium. Consequently, the pulse experiences higher extra loss of the cavity and splits into two pulses with wider pulse-widths or narrower spectral width to avoid this loss.

- According to the above mechanism, a pulse would experience a compression process until its width is so narrow that to be split into two wider pulses. In conditions of the fibre laser; however, solitons are considerably chirped by SPM and the gain bandwidth limitation effect. A generation of sub-pulses from an initial pulse can occur because of strong chirping after a number of roundtrips [96]. These sub-pulses can keep growing to have the same width and amplitude. According to dissipative soliton theory [65, 95], this second mechanism of the multi-pulse generation can be also identified. Due to

dissipative nature of the fibre lasers, the dispersive waves are generated by shedding the energy of the soliton during circulating in the cavity. In a strongly pumped gain medium, a part of the dispersive waves acquires sufficient gain to grow and evolve into a new dissipative soliton with the width and amplitude specified by the fibre cavity parameters [156].

- The third mechanism of multi-pulsing is based on the cavity effect which relates to the transmittance of the cavity formed by NPR or NOLM. As explained in Chapter 2 (Section 2.3.2), the transmittance of the fibre cavity in both techniques using NPR and NOLM is a sinusoidal function of the nonlinear phase delay. Thus there are two distinct regimes of operation in a period of the transmittance curve (see Figure 2-1). In the first half, the transmittance increases with increasing intensity. While the transmittance decreases with increasing intensity in the second half. The maximum of the transmittance curve is also the transition point between two regimes. For mode locking, the cavity operates in the first regime due to the characteristic of saturable absorption [112]. When the nonlinear phase delay is sufficient in soliton operation of the fibre laser, the cavity can be dynamically switched from the saturable absorption mode to the saturable amplification mode that limits the peak of solitons generated inside the cavity [136]. For NPR technique, the switching point between two modes can be adjusted by changing the setting of polarization controllers to change the linear phase delay. As a result of the cavity feedback, the peak power of soliton is limited which is responsible for the multi-pulse operation in the cavity [153].

4.2.2 Bound states in a passively mode-locked fibre ring

Although multi-pulsing operation was experimentally observed in early 1990s [157-158], it was only in 2001 that the bound state of solitons was confirmed experimentally on soliton formation in a passively mode-locked fibre laser using NPR technique [29]. This observation started to stimulate research interest in new states of solitons in the mode-locked fibres. Grelu *et al.* [31, 144] then has also reported the experimental observation of two, three and multi-bound solitons with the separation between adjacent pulses varying from case to case. By using a strictly dispersion managed fibre cavity, multi-pulse solitons can be formed with a fixed pulse separation [150]. In the bound state, the multi-pulse bound solitons function as a unit and they also behave similar to a single soliton in the cavity such as forming states of bound multi-pulse solitons or period-doubled, period-quadrupled and chaotic states [32]. The investigation of bound solitons was extended in fibre lasers operating in large normal cavity dispersion regimes where the pulse shape is parabolic rather than hyperbolic secant [159]. Besides, bound soliton pairs were also observed in dispersion imbalanced – nonlinear optical loop mirror (DI-NOLM) figure-8 fibre lasers [143]. The research efforts on bound solitons are still in progress and the latest report has shown the observation of bound state of 350 pulses or a "soliton crystal" in a NPR mode-locked fibre laser; a record in number of pulses in bound state [160].

The formation of bound states following the pulse splitting process in passive mode locking can be affected by various interaction mechanisms among solitons inside the cavity. Depending on the setup of the fibre laser, one or more than one interaction mechanisms become stronger than the others and determine the formation and the dynamics of bound solitons. In passively mode-locked fibre lasers, there are a

variety of possible interaction mechanisms that relate to different modes of bound solitons as follows:

- Gain depletion and recovery [161]: The interaction between pulses with the transient depletion and recovery dynamics of the gain medium. The pulses effectively repel each other due to a group velocity drift caused by the time-dependent gain depletion acting in conjunction with the gain recovery. This mechanism is significant in stabilization of pulse spacing in harmonic mode locking.
- Acoustic effect and electrostriction [162]: Due to the intense electric field, the pulses can distort the fibre material to generate acoustic waves during propagation of the next pulse. This electrostriction induces a small frequency shift between pulses that leads to an effective attraction.
- CW component – soliton interaction: In some given settings of the passively mode-locked fibre laser using NPR, a CW component can coexist with the solitons in the cavity. It has been experimentally shown that the CW component causes the central frequency shift in each soliton [147]. When the CW component becomes unstable, solitons acquire different frequency shifts which result in their various relative velocities in the cavity. This interaction is also responsible for motion mode and harmonic mode locking in passively mode locked lasers [163].
- Soliton-soliton interaction [60]: This direct interaction between solitons is from the nature of fundamental solitons which can attract or repel each other depending on their relative phases. A repulsive force appears between solitons when their phase difference is $\pi/2$ or higher, while an attraction occurs

between in-phase solitons. In general, this interaction is considerably effective only when the solitons is sufficiently close together.

- Soliton-dispersive wave interaction: During circulating in the cavity, solitons radiate dispersive waves or continuum due to periodically varying perturbations of the cavity such as losses, bandwidth limited gain [60]. The dispersive waves create a local interaction which can generate an attractive or repulsive force between solitons [164-165]

When solitons interact together through these mechanisms, different bound states can be formed inside the fibre cavity. Depending on the strength of binding between solitons, bound solitons can be classified into two basic types [45]: loosely and tightly bound solitons. For the former type, solitons are often bound together into a bunch of solitons with the temporal separation between pulses which is much larger than their pulse width. Therefore the loosely bound solitons have weak binding energy and they would be easily destroyed by environmental perturbations [148, 166]. Due to wide separation between solitons, the long-range interactions such as two first mechanisms play a dominant role in formation of loosely bound solitons. Self-stabilization of this state can be achieved by the balanced interplay between these mechanisms [167].

For tightly bound solitons, two last mechanisms play a major role in formation of bound states. Because solitons in this type are closely separated, the local interactions are attributed to the binding energy between solitons which determines characteristics and dynamics of bound solitons. It has been shown that the direct soliton interaction mainly contributes to the formation of tightly bound solitons with discrete fixed separations [150]. It should be noted that pulses formed in the fibre

lasers are often chirped solitons, so the direct interaction among them is not like that of standard unchirped solitons. Therefore, the overlap of oscillating tails of solitons results in an effective binding between them to obtain a stable bound state. However, it was believed that the dispersive wave-soliton interaction also affects to the state to generate various dynamics of bound solitons [165]. Due to strong binding energy, the tightly bound soliton behaves as a unit and exhibits all features of single soliton pulse such as collision, harmonic mode locking, and evenly bound state.

Summarily, all various interactions among solitons always coexist in the passive mode-locked fibre laser, however only one or two of them play a key role in formation and characteristic of bound solitons. And existence of other interactions also contributes to the dynamics of bound states. In other words, the bound soliton is only one of multi-pulse operations in specific conditions of the cavity settings.

4.3 BOUND SOLITONS IN ACTIVE MODE LOCKING

4.3.1 Multi-bound solitons condition

In active mode locking, although the multi-pulsing operation is harder than that in passive mode locking due to higher loss of the cavity, it still occurs under strong pumping mode of the gain medium. Mechanisms of pulse splitting in active mode locking are also similar to the mechanisms described in passive mode locking [153, 156]. However the width of pulse in active mode locking is much wider than that in passive mode locking, the contribution of the limited bandwidth of the gain medium in the peak power limiting effect is negligible except either a band-pass filter inserted into the ring or an intrinsically filtering effect from the ring cavity narrow sufficiently the gain bandwidth. Therefore splitting of a single pulse into multi pulses only occurs

in an actively fibre cavity when the power in the fibre ring increases above a certain mode locking threshold. At higher power, higher order solitons can be excited and in addition the accumulated nonlinear phase shift in the loop can be so high that a single pulse breaks up into many pulses [96, 157]. The number of pulses depends on the optical power in the ring, so there is a specific range of power for each splitting level. The fluctuation of pulses may occur at region of power where there is a transition from the lower splitting level to the higher. Moreover, the chirping caused by phase modulator in the loop also makes the process of pulse conversion from a chirped single pulse into multi-pulses taking place more easily [168-169]. In hybrid mode-locked fibre lasers using NPR for pulse shaping, the peak power limiting effect is caused by the additive pulse limiting (APL) effect [136]. By a proper setting of the cavity parameters, the cavity can be switched from additive-pulse mode locking (APM) regime to APL regime that can clamp the peak of solitons at a certain level.

Because the pulse splitting only occurs at specific positions around the loss minima of the modulation curve in the cavity, the split pulses are closely separated and the tightly bound states are supposed to be the only mode existing in the actively mode-locked fibre lasers. Hence there are effective interactions among these pulses to stabilize the multi-bound states in the cavity, in other word, the multi-bound solitons are formed and stabilized by the balanced interplay between these interactions. The direct soliton interaction, which is influenced by the relative phase difference of the carrier under the envelope of adjacent pulses, is believed to contribute significantly in formation of bound solitons. However, for a actively FM mode locked fibre laser, another interaction among pulses needs to be considered due to the linear chirping caused by active phase modulation. Particularly, the multi-bound soliton sequence is

only stably formed at the up-chirping half-cycle in the case of an anomalous path-averaged dispersion fibre ring [53]. On the other hand the bound soliton pulses should be symmetrically distributed around the extreme of the positive phase modulation half-cycle where the pulses acquire up-chirping as described in Figure 4-1. Thus the group velocity of the lightwave, induced by anomalous dispersion, contained within the first pulse of the soliton bunch is decreased after passing through the phase modulator; while the last pulse of the bunch receives opposite effect, which is enhancement of group velocity [152, 170]. The variation of the group velocity between pulses creates an attractive force that pulls them to the extreme of modulation half-cycle similar to the jittering control in soliton transmission systems [170-172]. Thus another interaction between the solitons is required to balance the effective attraction by linear chirping and it is the direct soliton interaction. A repulsive force which is sufficient enough to balance with the effective attractive force appears only in case of the π phase difference between adjacent pulses [173-175]. For other phase differences, there is an energy exchange or an attraction between pulses that possibly do not conform to a stable multi-bound pulse sequence. Thus we can generate the multi-soliton bound states using an appropriate phase modulation profile that can even be the high order harmonics of the modulation frequency. Therefore, in a specific mode-locked fibre laser setup, beside the optical power level and net dispersion of the fibre cavity, the modulator-induced chirp or the phase modulation index determine not only the pulse width but also the temporal separation of bound-soliton pulses at which the interactive effects cancel each other.

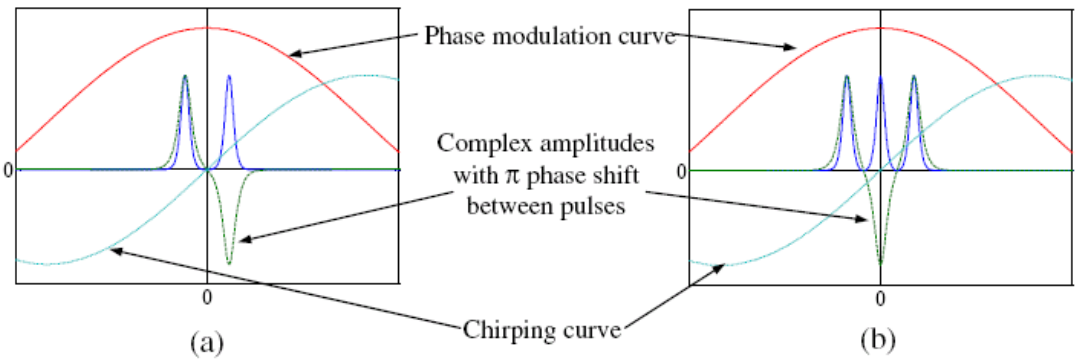

Figure 4-1 Effective interactions in multi-bound solitons (a) Dual-soliton bound state, and (b) Triple-soliton bound state.

The presence of a phase modulator in the cavity to balance the effective interactions among bound-soliton pulses is similar to the use of this device in a long haul soliton transmission system to reduce the timing jitter or to suppress soliton interactions [170-172], for this reason the simple perturbation theory can be applied to understand the role of phase modulation on mechanism of multi-bound solitons formation. The field of a multi-soliton bound state can be described as following:

$$u_{bs} = \sum_{i=1}^{N} u_i(z,t) \tag{4-1}$$

and $$u_i = A_i \operatorname{sech}\{(t - T_i)/T_0\} \exp(j\theta_i - j\omega_i t) \tag{4-2}$$

where N is number of solitons in the bound state, T_0 is pulse width of soliton and A_i, T_i, θ_i, ω_i represent the amplitude, position, phase and frequency of soliton respectively. In the simplest case of multi-soliton bound state, N equals 2 or we consider the dual-soliton bound state with the identical amplitude of pulse and the phase difference of π value ($\Delta\theta = \theta_{i+1} - \theta_i = \pi$), the ordinary differential equations for the frequency difference and the pulse separation can be derived by using the perturbation method [170]

$$\frac{d\omega}{dz} = -\frac{4\beta_2}{T_0^3}\exp\left[-\frac{\Delta T}{T_0}\right] - 2\alpha_m \Delta T \tag{4-3}$$

$$\frac{d\Delta T}{dz} = \beta_2 \omega \tag{4-4}$$

where β_2 is the averaged group-velocity dispersion of the fibre loop, ΔT is pulse separation between two adjacent solitons ($T_{i+1} - T_i = \Delta T$) and $\alpha_m = m\omega_m^2/(2L_c)$, L_c is the total length of the ring, m is the phase modulation index, ω_m is the angular modulation frequency. Eqs. (4-3) and (4-4) show the evolution of frequency difference and position of bound solitons in the fibre ring in which the first term on the right hand side represents the accumulated frequency difference of two adjacent pulses during a round trip of the fibre ring and the second one represents the relative frequency difference of these pulses when passing through the phase modulator. In the steady state, the pulse separation is constant and the induced frequency differences cancel each other. On the other hand, if setting Eq. (4-3) to zero we have

$$-\frac{4\beta_2}{T_0^3}\exp\left[-\frac{\Delta T}{T_0}\right] - 2\alpha_m \Delta T = 0 \text{ or } \Delta T \exp\left[\frac{\Delta T}{T_0}\right] = -\frac{4\beta_2}{T_0^3}\frac{L_c}{m\omega_m^2} \tag{4-5}$$

We can see from (4-5) the effect of phase modulation to the pulse separation and β_2 and α_m must have opposite signs which mean that in an anomalous dispersion fibre ring with negative value of β_2, the pulses should be up chirped. With a specific setup of the actively FM fibre laser, when the magnitude of chirping increases, the bound pulse separation decreases subsequently. The pulse width also reduces according to the increase in the phase modulation index and modulation frequency, so that the ratio $\Delta T/T_0$ can change not much. Thus, the binding of solitons in the FM mode-locked fibre laser is assisted by the phase modulator. Bound solitons in the ring

experience periodically the frequency shift and hence their velocity in response to changes in their temporal positions by the interactive forces in equilibrium state.

In principle, thus multi-bound solitons can be also generated in any actively mode-locked fibre laser including amplitude mode locking with an appropriate frequency chirping in the cavity. Controllability of linear chirping in the amplitude modulator is hence required in order to maintain a balance in steady state. Moreover, a frequency shifting facilitates a pulse splitting due to broadening the pulse spectrum in a limited gain bandwidth [169].

4.4 GENERATION OF MULTI-BOUND SOLITONS IN ACTIVELY FM MODE-LOCKED FIBER LASER

4.4.1 Experimental setup

An actively FM-MLFRL which is similar to that described details in Chapter 3 has been setup to generate multi-bound solitons. Initially, we used the experimental setup of the FM mode-locked fibre laser as shown in Figure 4-2(a). Because the EDFA in this setup has low gain and saturated power that was insufficient for multi-pulse operation, hence two EDFAs with 12 dBm maximum output were used for the experiment of multi-bound soliton generation [176]. However this setup was limited in its number of bound solitons due to the limitation of the saturation power of the EDFA. Moreover, the ASE noise was enhanced by the presence of two EDFAs in the ring that degraded the performance of the bound solitons. Therefore the setup described in Chapter 3 for the generation of asingle-soliton train is used (See Figure 3-1). The experimental setup of the actively FM-MLFRL for generation of multi-bound solitons is shown again in Figure 4-2(b). In this setup, only one EDFA with higher gain and maximum saturated power of 17 dBm is used. The modulation

frequency of about 1 GHz is selected to generate the bound solitons. The output is characterized to estimate the performance of the bound states by the instruments HP-70952B for optical spectrum measurement, an Agilent DCA-J 86100C with optical bandwidth of 65 GHz for waveform measurement and a FS315 for RF spectrum measurement (see Chapter 3 for more details).

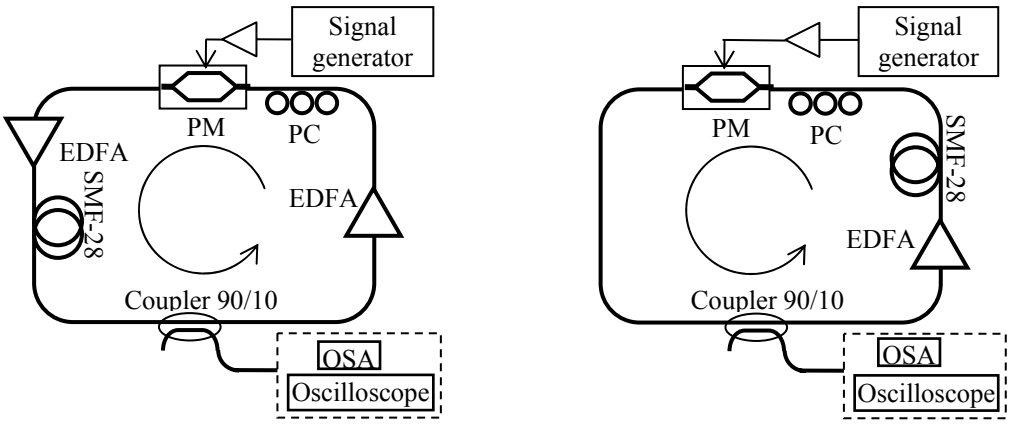

Figure 4-2 The experimental setups for multi-bound soliton generation (a) using two EDFA with low gain and saturated power, (b) using one EDFA with high gain and saturated power.

4.4.2 Results and discussion

In the initial setup, the generation of multi-bound solitons in the active MLFL has been achieved [176], yet the number of bound solitons was limited up to the quadruple state due to the limitation of the saturated power of the EDFA. In the next setup, we have extended the experimental investigation with the bound states of up to the 6^{th} order. By adjusting the polarization states together with the total stored optical power in the cavity, the multi-soliton bound states are obtained as shown in Figure 4-3. When the average optical power is increased to a certain level, the bound states are correspondingly switched to higher order states with larger number of solitons. A slight adjustment of polarization controller is necessary to stabilize the bound states.

Figure 4-3(a)-(e) shows the traces and spectra of the lowest to highest order bound states, the sextuple-soliton bound state. The significant advantage of the active fibre laser is the ease of generation of multi-soliton bound sequence at moderately high modulation frequency as shown in Figure 4-4.

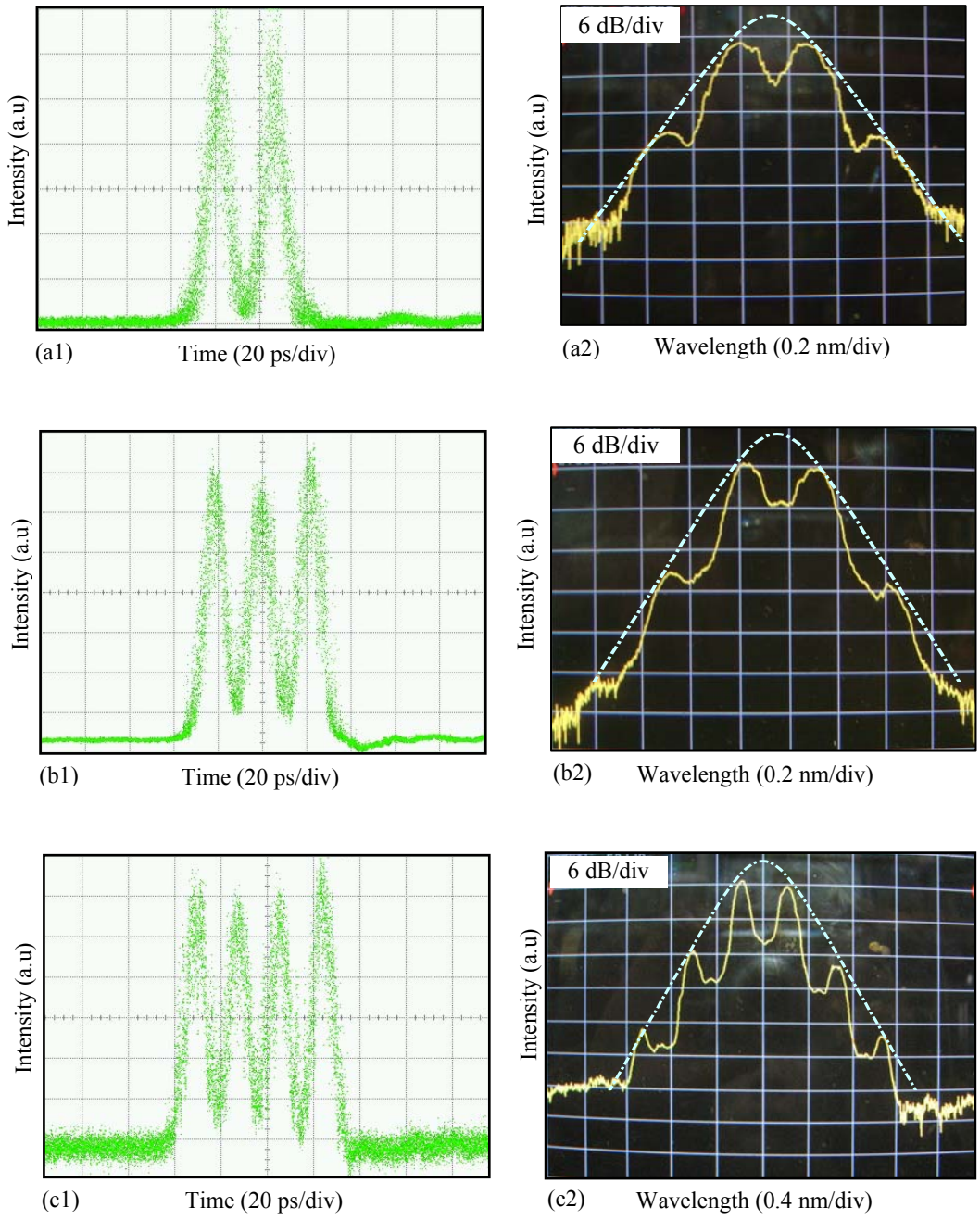

Figure 4-3 Oscilloscope traces (1) and optical spectra (2) of (a) dual-soliton, (b) triple-soliton, (c) quadruple-soliton, (d) quintuple-soliton and (e) sextuple-soliton bound states.

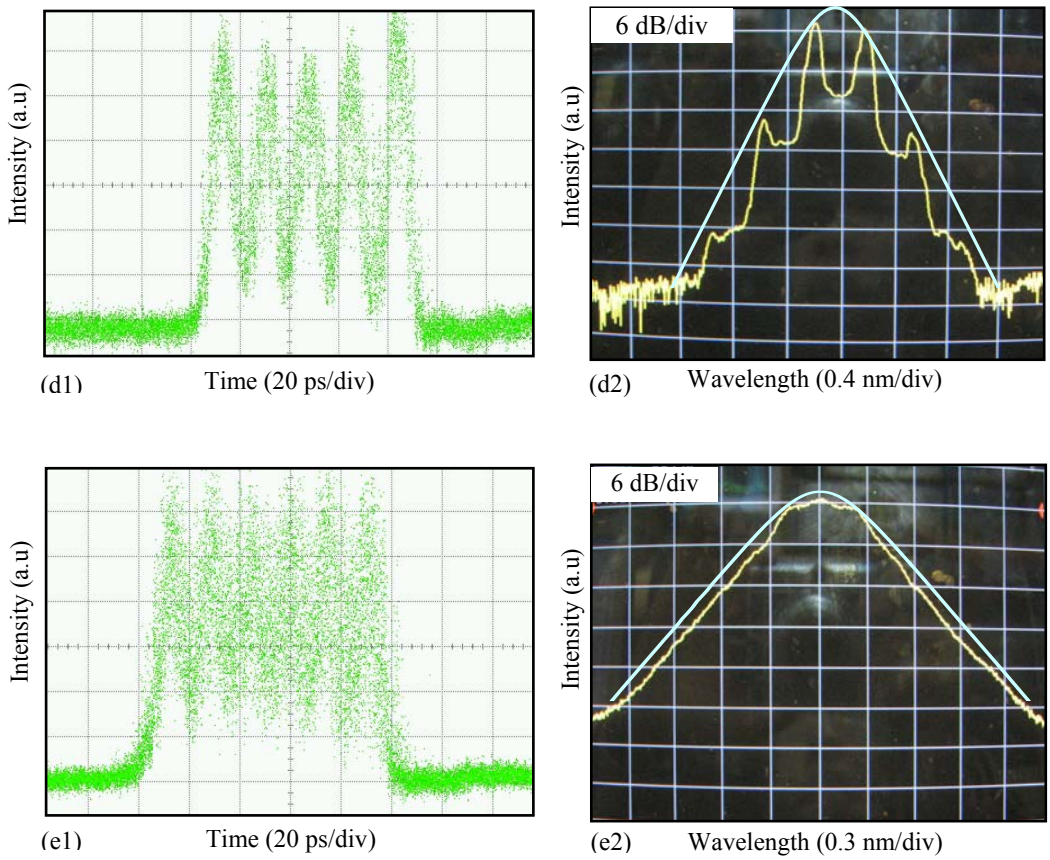

Figure 4-3 Continued.

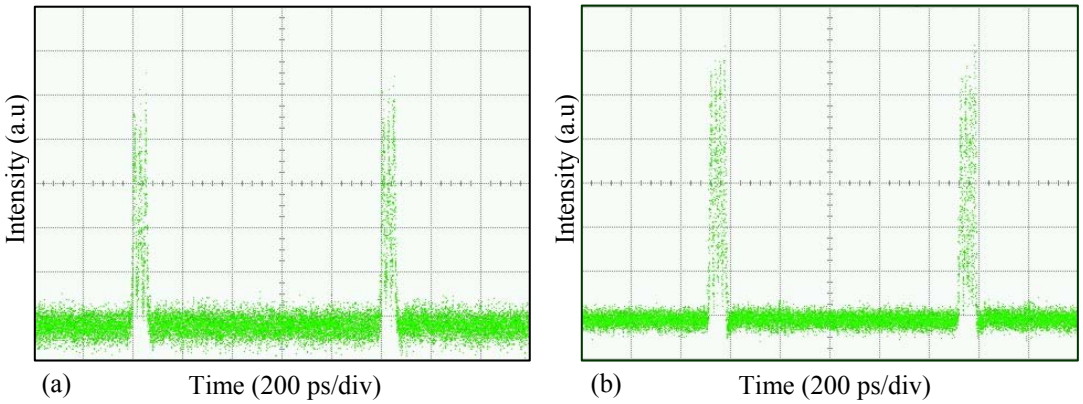

Figure 4-4 Time-domain oscilloscope traces of (a) triple-soliton,and (b) quadruple-soliton sequence at modulation frequency ~ 1GHz.

In the tightly bound states, the solitons are closely separated, and then the overlap between solitons causes their spectra to be modulated with a shape and symmetry depending on their relative phase difference. Hence the existence of the

bound states is also confirmed through the shapes of modulated optical spectra as compared to the conventional spectrum of the single soliton state. When the multi-bound states appear after the optical power in the cavity is increased to an appropriate level, there is a sudden change of the optical spectrum. The symmetry of spectra in Figure 4-3(a2)-(e2) indicates a relative phase difference of π between two adjacent bound solitons. The dashed-dot lines show the envelope of modulated spectra that correspond to the spectrum of a single soliton pulse. The suppression of the carrier at the centre of the pass-band spectrum further confirms the π phase difference between adjacent pulses, especially the pair of the dual-bound solitons. The distance between the two spectral main lobes is exactly correlated to the temporal separation between two adjacent pulses in time domain. The specific shape of spectrum depends on number of solitons in the bound states which can be odd or even. In the case of even-soliton bound states such as dual-soliton and quadruple-soliton bound states there is always a dip at the centre of spectrum, while there is a small hump in the case of odd-soliton bound state such as triple-soliton bound state and quintuple-soliton bound state. The small hump at centre of spectrum is formed by interaction between next neighbouring pulses which are in-phase in bound states. This is similar to the case for quadrature phase shift keying modulation format which is well known in the field of digital communications [177]. When the phase difference moves away from π value, the modulation and symmetry of spectrum vary accordingly. For the sextuple-soliton bound state, its spectrum is weakly modulated due to the variation of phase difference induced by ASE noise. The change in relative phase locking influences to the interaction of adjacent pulses or the performance of bound soliton output as in Figure 4-3(e).

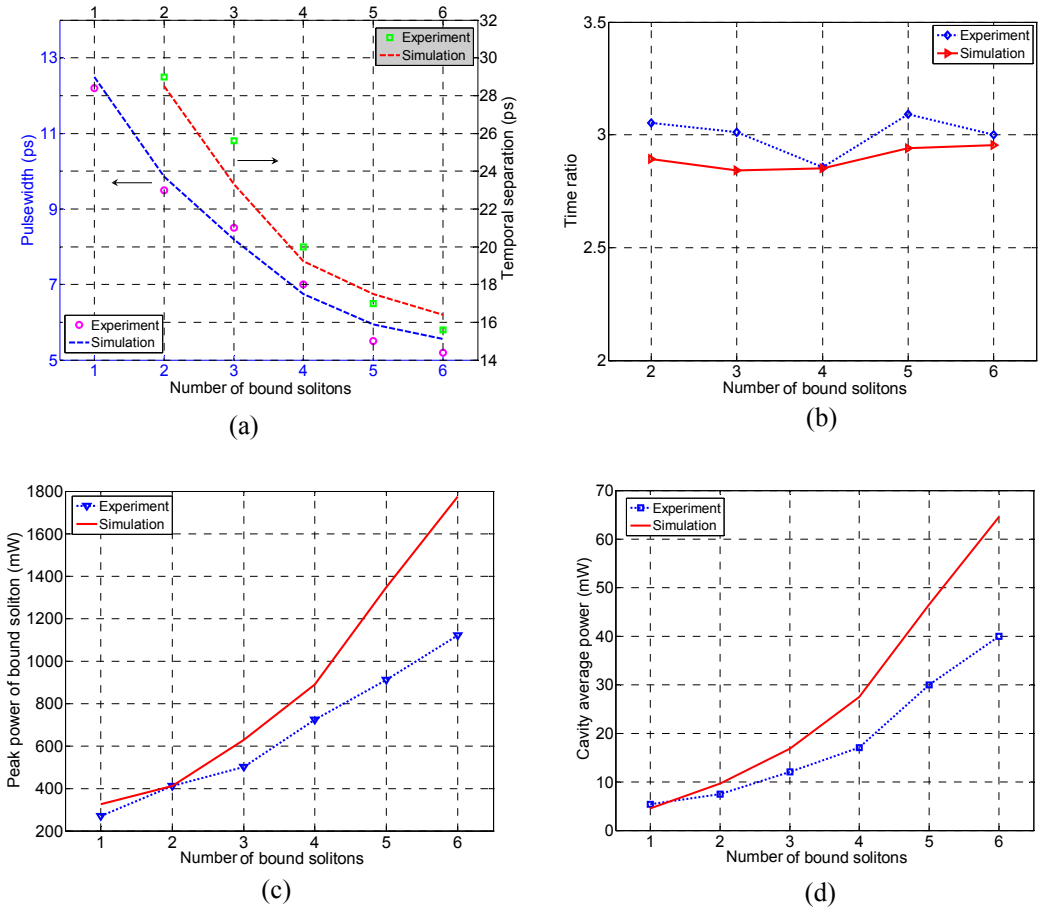

Figure 4-5 The variation of the characteristics with the number of solitons in the bound states (a) pulsewidth and temporal separation, (b) ratio between pulsewidth and separation, (c) peak power, (d) corresponding average power of the cavity.

All the important measurements of the multi-bound solitons are summarised in Figure 4-5, which plots the average values of the pulsewidth ($\overline{\tau}$), the time separation between pulses ($\Delta\tau$), the maximum peak power of a soliton pulse (P_0) and average optical power ($\overline{P}$) inside the fibre ring against the number of bound solitons. Figure 4-5(a) shows the variation of the pulsewidth decreasing with respect to the increase in number of pulses in bound states. This is due to pulse compression effect, the self phase modulation, enhanced by higher optical power level in the cavity at higher order bound states. Whilst the temporal separation between pulses in the multi-bound state also accordingly decreases to remain a ratio between separation and pulsewidth

nearly unchanged which is approximately three as shown in Figure 4-5(b). The onset power level of the energy stored in the ring is 7.5, 12, 17, 30 and 40 mW for the generation of dual, triple, quadruple, quintuple and sextuple states respectively.

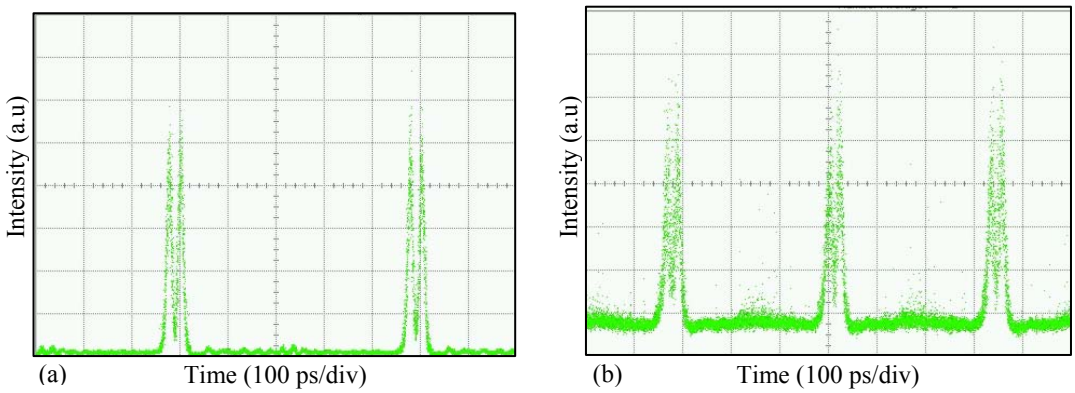

Figure 4-6 Time traces of dual-bound solitons in rational harmonic mode locking schemes: (a) the second order rational harmonic (~2GHz), (b) the third order rational harmonic (~3GHz).

Similar to a single-soliton state, rational harmonic mode locking of multi-bound solitons can be also obtained. Figure 4-6 shows the time traces of dual- and triple-bound solitons at the second and third rational harmonic mode locking after increasing properly the intra-cavity saturated power as well as the RF input power to enhance the second harmonic of modulation frequency. With an appropriate phase modulation profile which is formed by detuning amount of $\pm f_c/2$, the multi-bound solitons in rational harmonic mode locking are generated in the same interaction mechanism with the same characteristic as those in the conventional harmonic mode-locking. However the temporal separation between solitons in this case is smaller than that in conventional harmonic mode locking due to higher chirp rate of higher order harmonics of modulation frequency. Thus, the multi-bound solitons can exist in various regimes of operation similar to the conventional single pulse mode.

When the higher order bound solitons operate at higher power level, they are more sensitive to the change in polarization state even multi-wavelength operation can occur [178-180]. This effect is disadvantageous to the multi-bound soliton operation due to the reduction of energy of the operating wavelength from other excited wavelengths [179]. On the other hand, higher order bound solitons are more sensitive to fluctuations of the environmental condition. In experimental conditions, these polarization effects are usually controlled by a polarization controller [134-135], especially at the input of integrated optical modulator so as only one polarized state can be normally preferred through the modulator and hence the forcing of the matching condition of this polarized state. Moreover, the increase in saturated power in the fibre cavity allows generation of higher order bound soliton states, yet the ASE noise is also enhanced under strong pumping scheme in the EDFAs [181]. If the phase noise induced by ASE noise is sufficient, it affects not only to the phase matching conditions of the fibre ring but also to the phase locking between adjacent pulses as discussed above. Figure 4-7 shows the RF spectra of the dual- and quadruple-bound soliton trains to estimate the stability of the multi-bound soliton train. From the results of RF spectrum analysis, the SMSR is higher 45 dB for the dual-bound soliton, but it is reduced to 40 dB for the quadruple-bound soliton. Obviously, there are more fluctuations in higher order bound states or they are more sensitive to the environmental conditions. However there are small fluctuations in amplitude and temporal position of the solitons in the bound states as indicated by a broadening of the spectral line in insets of Figure 4-7. In the experiment, it has been found that the tuning of polarization controller becomes harder to obtain a stable bound state when number of solitons in the bound state is larger.

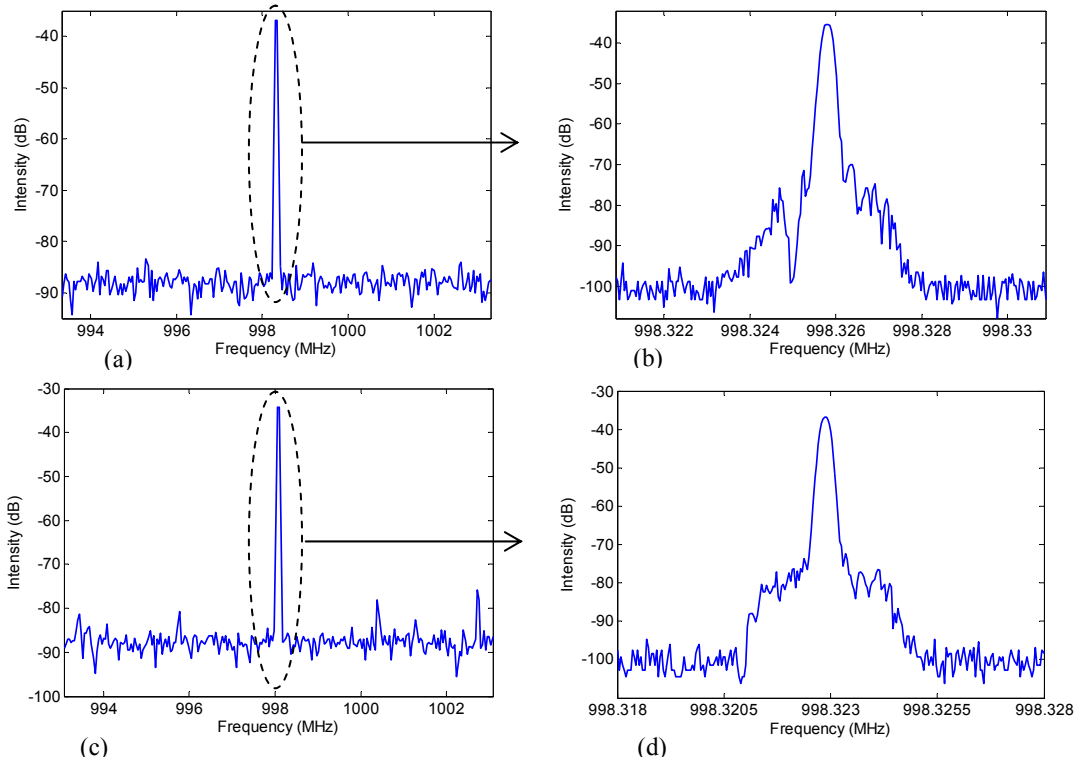

Figure 4-7 The RF spectra of the dual-bound soliton (a&b), and (c&d) the quadruple-bound soliton in spans of 10 MHz and 10 kHz.

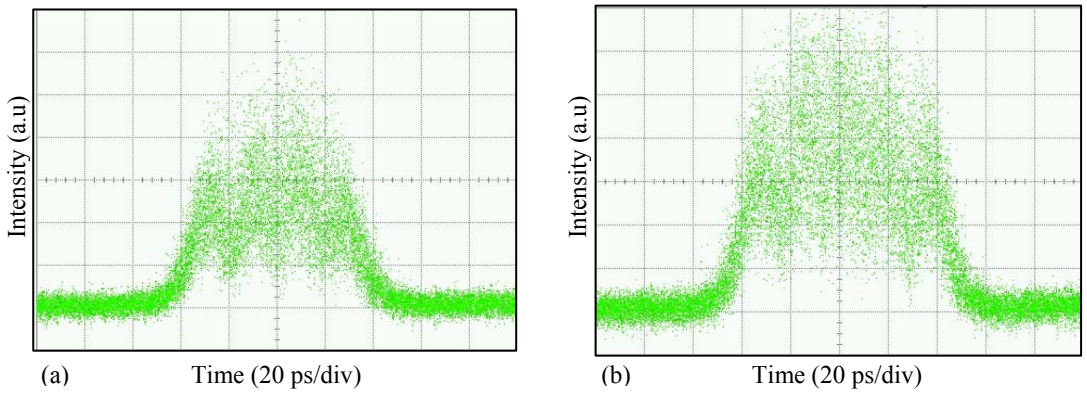

Figure 4-8 Time traces of the unstable pulse at the optical power levels of (a) quadruple-bound and (b) quintuple-bound solitons respectively.

Although the EO phase modulator plays a key role as a mode locker in our active mode-locked fibre laser, we should note that the polarization effect shows an important influence to multi-bound solitons. At high power levels of the cavity, the

polarization dependent mechanisms such as polarization dependent loss (PDL) and polarization dependent gain (PDG) are enhanced due to the phase modulator is also a polarizing element [182-183]. Hence the variation of the polarization state, which can be caused by fluctuations of the environmental condition, changes the total loss or the gain of the cavity which affects to the shaping, the formation as well as the parameters of multi-bound solitons. We have found that a stable of multi-bound state is only obtained by proper polarization settings. If changing setting of the polarization controller, beside the stable multi-bound states observed above, a unstable pulse regime has been obtained. Figure 4-8 shows the time traces of the noisy pulses at the power levels of the quadruple- and quintuple-bound solitons respectively. Although the pulses cannot be resolved in the traces, the widths of these pulses are exactly the same width as the bunch of corresponding bound solitons. This regime seems to be multi-pulsing operation but unstable. Optical spectra of these states are slightly modulated and varied similar to Figure 4-3(e2). The pulses in the bunch, which might be in phase, move and even collide together or oscillate very fast around the extreme of the modulation cycle. As a result the pulses cannot be clearly isolated in the bunch. Therefore, the traces of these states on oscilloscope are seen like noisy waveforms.

Different from passively mode-locked fibre lasers, the active phase modulation contributes significantly to the formation and the stability of multi-bound soliton states. Figure 4-9 shows experimental results of the influence of chirping, which is directly proportional to phase modulation index, on temporal separation between adjacent pulses at different bound states. The phase modulation index is calculated from the driving voltage level of the phase modulator. When the chirp rate increases, the relative variation of group velocity between adjacent pulses is

enhanced. Thus the increase in frequency chirping reduces the temporal separation which is necessary to keep the frequency shift between these pulses unchanged in the cavity with a specific average dispersion. The decrease in time separation in experimental results show a nearly linear function of the phase modulation index that should be an exponential function as shown in (4-5). This can be due to the small range of the phase modulation index. In addition, because the pulse width of the triple-bound soliton is narrower that of the dual-bound soliton, the pulses acquire a smaller chirp that results in the lower rate of decrease in the time separation in the triple-bound soliton as seen in Figure 4-9.

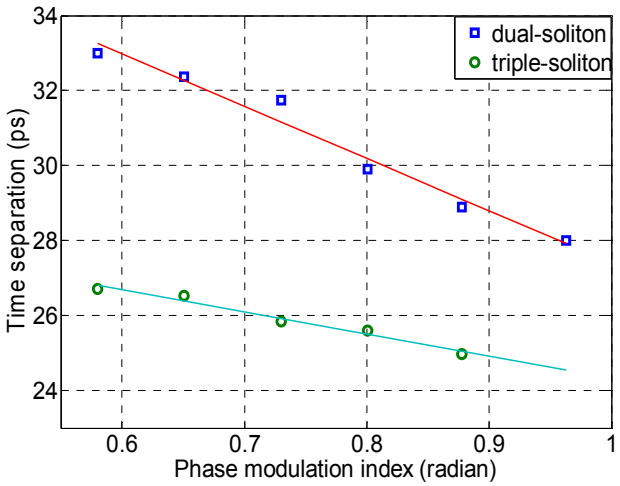

Figure 4-9 Variation of time-separation of dual and triple bound soliton states with respect to the phase modulation index. (Lines are linear fits).

4.4.3 Simulation

4.4.3.1 The formation of multi-soliton bound states

To understand the operation of multi-bound solitons in the actively FM mode-locked fibre laser, we have numerically investigated the process of multi-bound soliton generation in the FM-MLFRL by using the numerical simulation model developed in Chapter 3 for actively FM mode-locked fibre laser. Firstly, we have simulated the formation process of bound states in the FM mode-locked fibre laser whose main parameters are shown in Table 4-1. The lengths of the active fibre and passive fibre are chosen to get the cavity's average dispersion $\overline{\beta}_2$ = -10.7 ps^2/km. Figure 4-10 shows a simulated dual-soliton bound state building up from initial Gaussian-distributed noise as an input seed over the first 2000 round-trips with P_{sat} value of 8 dBm and g_0 of 0.36 m^{-1}. The built-up pulse experiences transitions with large fluctuations of intensity, position and pulse width during the first 1000 roundtrips before formation of the bound soliton state. Figure 4-10 (b&c) shows the time waveform and spectrum of the output signal at the 2000th round trip.

Table 4-1 Simulation parameters of the multi-bound soliton formation

β_2^{SMF} = -21 ps^2/km,	β_2^{ErF} = 6.43 ps^2/km,	$\Delta\omega_g$ = 16 nm,
γ_{SMF} = 0.0019 W^{-1}/m,	γ_{EDF} = 0.003 W^{-1}/m,	$f_m \approx$ 1GHz,
α_{SMF} = 0.2 dB/km	α_{EDF} = 0.5 dB/km	$m = \pi/3$
L_{SMF} = 80 m	P_{sat} = 8-14 dBm,	λ = 1559 nm
L_{EDF} = 10 m	g_0 = 0.35-0.45 m^{-1}, NF = 5 dB	l_{cav} = 11 dB

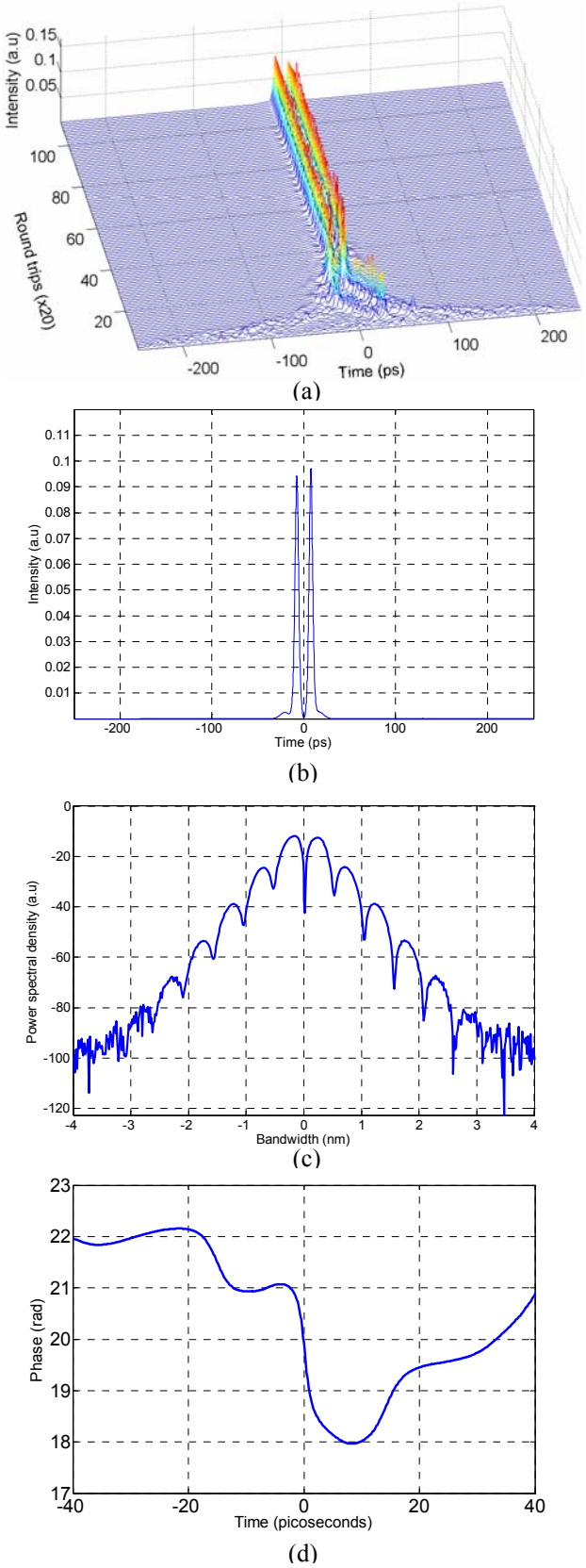

Figure 4-10 (a) Numerically simulated evolution of the dual-soliton bound state formation from noise, (b) The waveform, (c) the spectrum, and (d) the phase at the 2000th roundtrip.

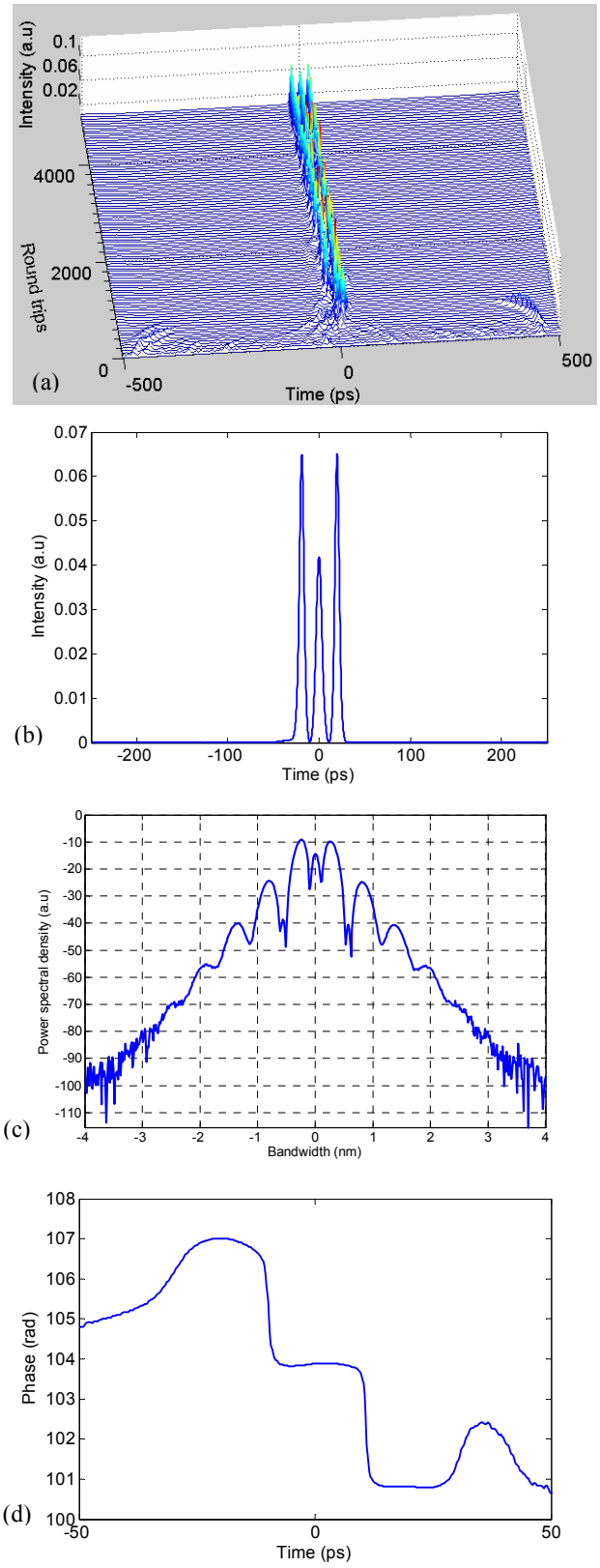

Figure 4-11 (a) Numerically simulated evolution of the triple-soliton bound state formation from noise, (b) The waveform, (c) the spectrum, and (d) the phase at the 5000th roundtrip.

The bound states with higher number of pulses can be formed at higher gain of the cavity, hence when the P_{sat} and unsaturated gain g_0 are increased to 11 dBm and 0.38 m^{-1} respectively, which is enhancing the average optical power in the ring, the triple-soliton bound steady-state is formed from the noise seeded via simulation as shown in Figure 4-11. In the case of higher optical power, the fluctuation of signal at initial transitions is stronger and it needs more round trips to reach to a more stable triple-bound state. The waveform and spectrum of the output signal from the FM mode-locked fibre laser at the 5000^{th} round trip are shown in the Figure 4-11 (b) & (c) respectively.

Although the amplitudes of the pulses are not equal, indicating the bound state can require a larger number of round trips before the effects in the ring balance, the phase difference of pulses accumulated during circulating in the fibre loop is approximately π, which is indicated by strongly-modulated spectra. In particular from the simulation result, the phase difference between adjacent pulses is 0.98π in case of the dual-pulse bound state and 0.89π in case of the triple-pulse bound state. These simulation results reproduce the experimental results (shown in Figure 4-10(d) & Figure 4-11(d)) discussed above to confirm the existence of multi-soliton bound states in a FM mode-locked fibre laser.

The cavity requires higher gain to form multi-bound states than that in stable or steady states. By adjusting the parameters of gain medium after multi-pulse state formed in the cavity, stable multi-bound soliton states can be generated after at least 10000 round trips. Figure 4-11(a) shows the contour of the dual-bound soliton formation in 10000 round trips of the ring cavity. In this simulation, the gain factor is reduced from 0.37 m^{-1} to 0.35 m^{-1} at the 2000^{th} roundtrip (the dash line). In the first

2000 round trips, the dual-bound soliton is formed, yet unstable with strong fluctuation of the peak power. Then the fluctuation is reduced by the reduction of gain factor and the generated dual-bound soliton converges to stable state after 10000 round trips as shown in Figure 4-11(b). Figure 4-11 (c) and (d) shows the waveform and the phase of the output at the 10000^{th} round trip. Similarly, the parameters of gain medium are also adjusted to obtain stable higher order multi-bound solitons. Figure 4-12 and Figure 4-13 show the simulated results of the triple-bound soliton and the quadruple-bound soliton formation processes respectively. For the triple-bound soliton, the gain factors are kept the same values as those in case of the dual-bound soliton, but the saturated power P_{sat} is increased to 11 dBm instead of 8 dBm. A variation of peak power and evolution of the triple-bound soliton formation with the gain switching at the 2000^{th} round trip are shown in Figure 4-13(a) and (b). For the quadruple-bound soliton, both the initial gain and adjusted gain factors are increased to higher values which are 0.4 m^{-1} and 0.377 m^{-1} respectively at the P_{sat} of 11 dBm. Figure 4-13 (b) shows a damping of the peak power variation after the gain adjustment to reach to a stable triple-bound soliton state, however the peak power of the quadruple-bound soliton still oscillates evenly after 10000 round trips as seen in Figure 4-14 (b). Thus it indicates a more sensitivity of the higher order multi-bound soliton to the operating condition. The sensitivity also exhibits through the uniform of pulse intensity in the bound state and the relative phase difference which is decreased from π in the dual-bound soliton to 0.87π in the quadruple-bound soliton as shown in Figure 4-12(c)-(d), Figure 4-13(c)-(d) and Figure 4-14(c)-(d).

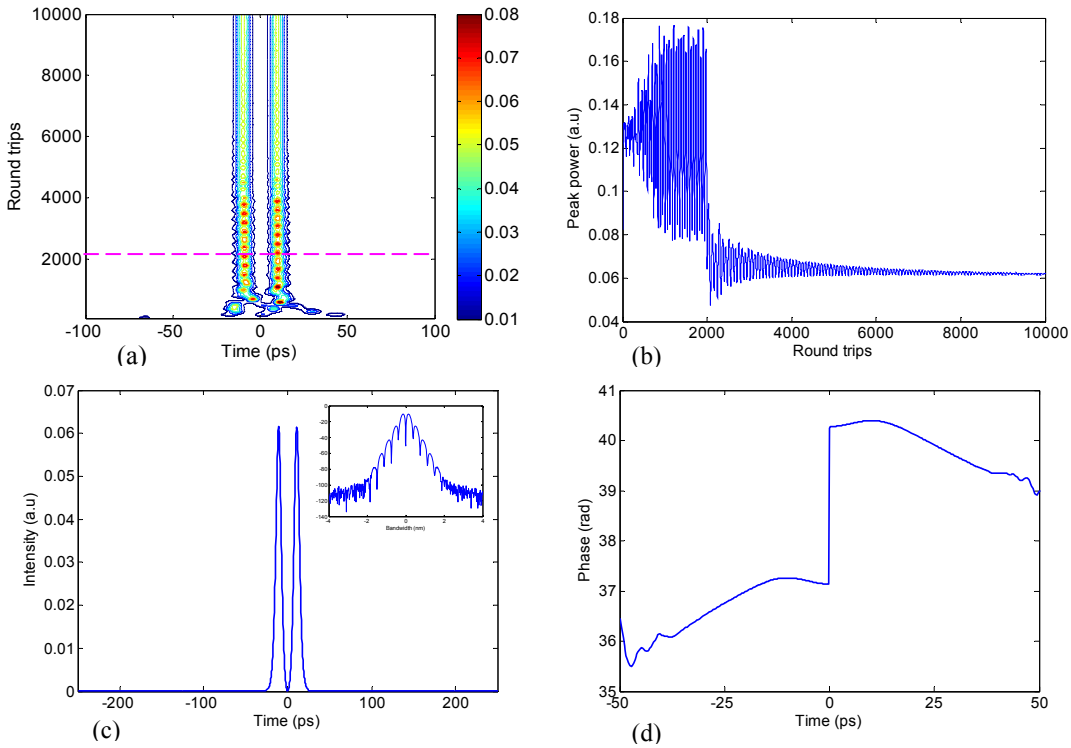

Figure 4-12 (a) Contour plot of simulated evolution of the dual-soliton bound state formation from noise, and (b) variation of the peak power with the gain switching at the 2000th round trip, (c) the waveform (Inset: the corresponding spectrum), and (d) the phase at the 10000th roundtrip.

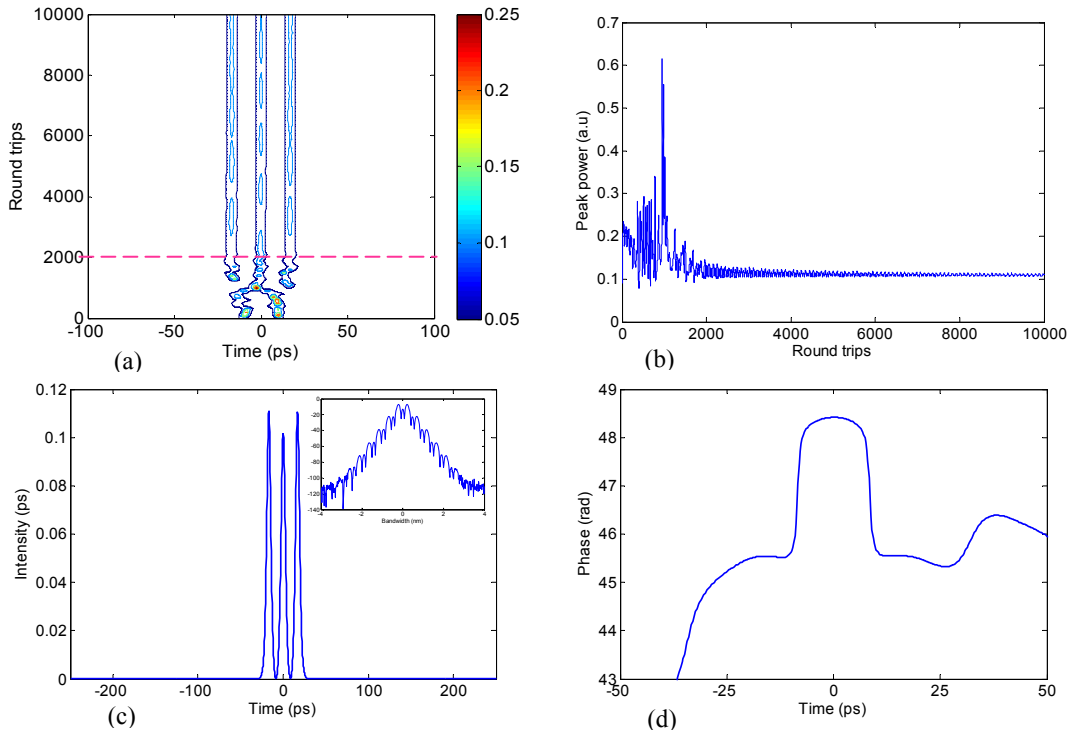

Figure 4-13 (a) Contour plot of simulated evolution of the triple-soliton bound state formation from noise, and (b) Variation of the peak power with the gain switching at the 2000th round trip, (c) The waveform (Inset: the corresponding spectrum), and (d) the phase at the 10000th roundtrip.

We note that a stable multi-bound soliton is difficult to be formed in the cavity without the adjustment of the gain parameters. With the high gain, the multi-bound soliton can be generated but unstable or becomes a quasi-stable with a periodic variation of soliton parameters in bound state. With the low gain, the nonlinear phase shift is not sufficient to generate desirable higher order multi-pulse state, while it is too strong for stable lower order multi-bound state. Different from passive mode locking, the pulse splitting in our system is caused by the excitation of higher order soliton and nonlinear chirping rather than an energy quantization mechanism.

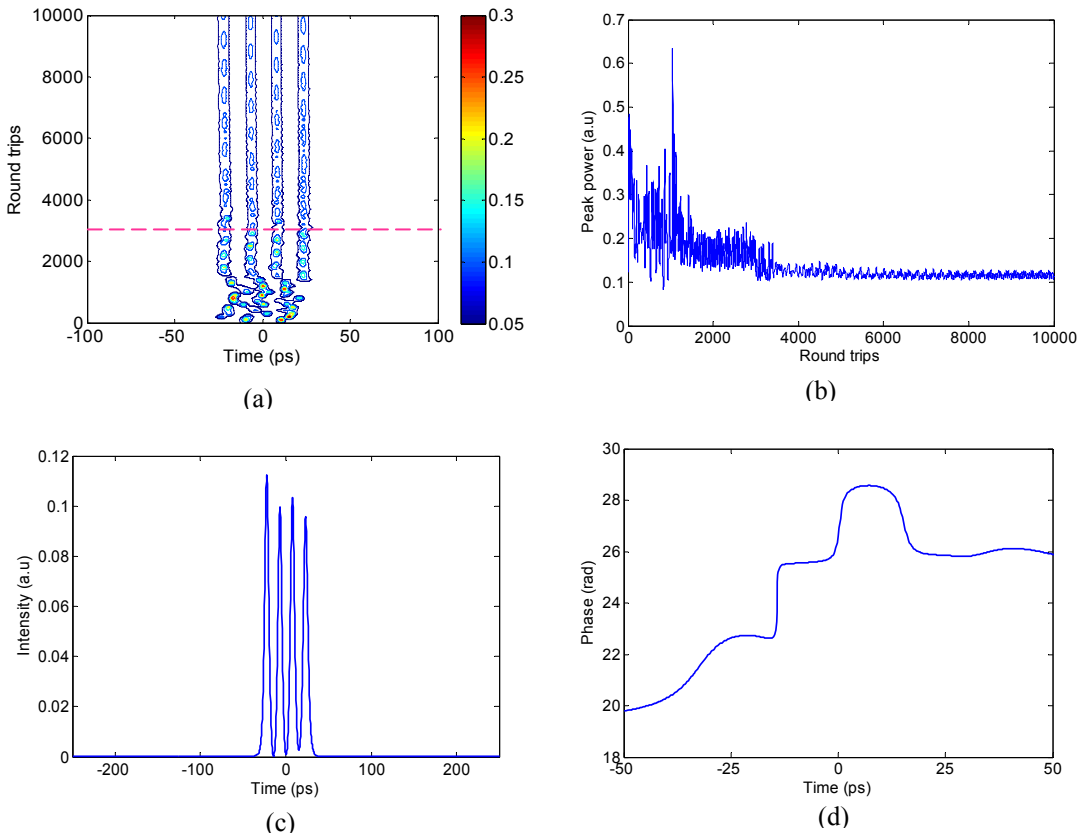

Figure 4-14 (a) Contour plot of simulated evolution of the quadruple-soliton bound state formation from noise, and (b) Variation of the peak power with the gain switching at the 3000th round trip, (c) The waveform (Inset: the corresponding spectrum), and (d) the phase at the 10000th roundtrip.

4.4.3.2 Evolution of the bound soliton states in a FM fibre loop

Obviously, multi-bound solitons can be stably generated in the phase modulated fibre cavity. On the other hand, bound solitons with the relative difference of π given by (4-1)-(4-2) are considered as a stable solution of the actively FM mode-locked fibre laser. By using the multi-soliton waveform in (4-1)-(4-2) as input, we have simulated the stability of multi-bound solitons in the active FM mode-locked fibre laser. Figure 4-15 shows the evolutions over 2000 roundtrips of the dual- and triple-bound solitons in the cavity. Because the bound solitons are really chirped pulses, while the input in simulation is unchirped, there is a damping oscillation of bound solitons in the initial stage that is considered as a transition of solitons to adjust their own parameters to match to the parameters of the cavity. However the multi-bound solitons easily reach a stable state after only a few hundred round trips.

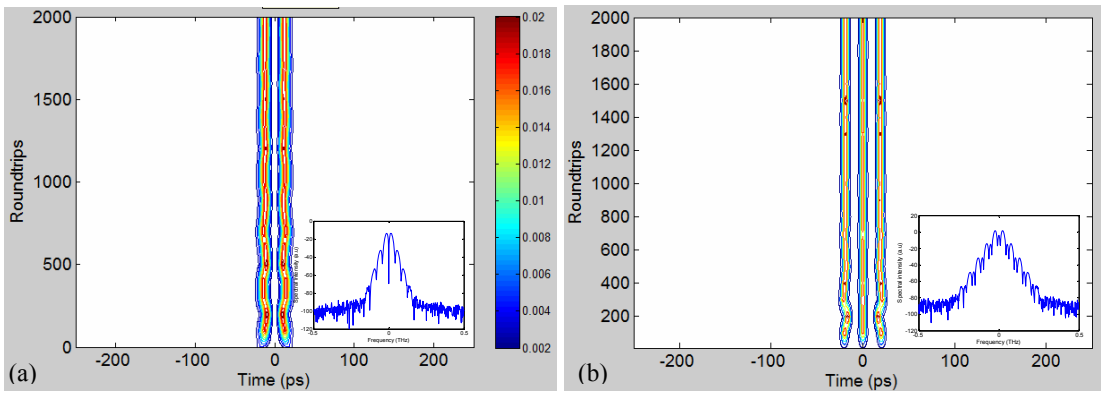

Figure 4-15 Evolution of (a) dual-bound soliton and (b) triple-bound soliton with a relative phase difference of π in the FM fibre ring cavity.

Simulation results on characteristics of multi-bound solitons after 5000 roundtrips are also shown in Figure 4-5 for comparison by using the experimental parameters of multi-bound solitons as the initial parameters. Generally, the simulated results agree with the experimental results. However, as observed in Figure 4-5(c)-(d),

there are discrepancies of the peak and average power levels between the simulated and experimental pulses, especially at higher order soliton bound states. The level of discrepancy varies from 0.1 dB to 3 dB for peak power of 1000 to 1800 mW respectively. While the experimental results show a nearly linear dependence of the peak power on the order of bound state, the simulation results show an exponential variation. Hence there is also a difference of average power of the cavity between them. However both sets of results indicate an exponential dependence of the cavity average power on the order of bound soliton state. There are some reasons taking into account the discrepancy as follows: Firstly, the parameters of the fibre cavity used in the simulation is not totally matched to those in our experiment; Secondly, when the real pulse width at higher order bound soliton state is narrower, the accuracy in the pulse width measured on the oscilloscope is reduced, although the influence of rise-time of the oscilloscope was considered in estimation. Furthermore, the variation of the polarization state becomes stronger at higher power level of the cavity that also increases the error in the power measurement. Hence the error between simulation and experimental results increases at higher order of the soliton bound state.

In addition, the higher order multi-bound soliton is more sensitive to the cavity parameter settings. Figure 4-16(a) shows an unstable state evolving in the FM fibre ring cavity. Multiple pulses are generated in the cavity, yet it is difficult to acquire the phase difference of π and uniform between pulses. In other words, the balance in the effective interaction between pulses is difficult to be achieved, the pulses can therefore collide and vary rapidly in both amplitude and time position. However this rapid variation only occurs in a limited time window around the extreme of the modulation cycle as indicated by the dash lines in Figure 4-16(b). By taking average

over last 2000 round trips, the waveform and its spectrum, which can be represented for a dynamical state, are shown in Figure 4-16(c) and (d) respectively. The wave form which is like a noisy pulse and the spectrum which is slightly modulated are similar to what is observed in the experiment (see Figure 4-8).

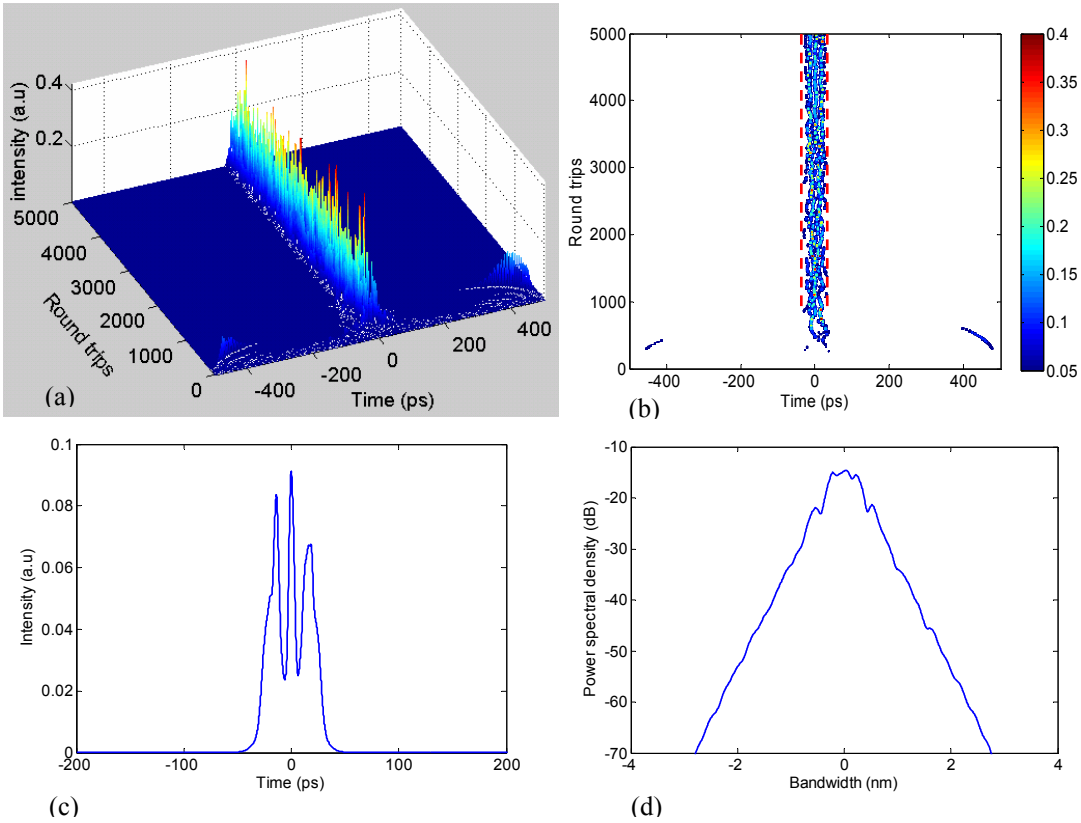

Figure 4-16 (a) Simulated evolution of multi-bound soliton in unstable condition over 5000 round trips, (b) Contour plot view of the evolution, (c) The waveform, and (d) corresponding spectrum averaged over last 2000 round trips.

4.5 RELATIVE PHASE DIFFERENCE OF MULTI-BOUND SOLITONS

4.5.1 Interferometer measurement and experimental setup

The relative phase difference plays a key factor in stability as well as determination of various modes of the bound soliton states. For passive mode locking, although the relative phase between the bound solitons of π has been confirmed in some

experimental works [143, 146], other relative phases have been also demonstrated [31, 143, 145]. The relative phase difference is of importance in determination of dynamics of the bound solitons in the fibre laser system. In particular, the bound solitons with π/2 phase difference can collide either elastically or inelastically with a single soliton depending on its initial phase [144]. On the other hand, the bound solitons can change their relative phase when the setting of the cavity change.

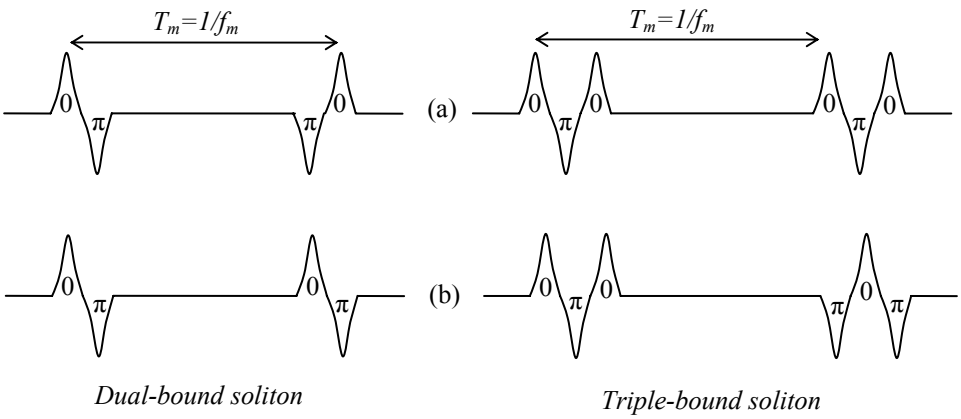

Figure 4-17 A description of two possibilities of phase difference between neighbouring pulses (a) Solitons between neighbouring bunches are in phase, (b) Solitons between neighbouring bunches are out of phase.

In contrast to passive mode locking, only the bound solitons with a π phase difference are generated stably in the actively mode-locked fibre laser system. This has been confirmed by their symmetrically modulated spectra (See Figure 4-3). In each bunch of bound solitons, adjacent pulses are out of phase to form a stable bound state through the balanced interplay of effective interactions. However, if the multi-bound soliton is considered as a unit like single pulse state, there might be two possibilities of the multi-bound soliton trains: one in which solitons between neighbouring bunches are in phase and another in which solitons between neighbouring bunches are out of phase as described in Figure 4-17. On other hand,

there may be a phase inversion between bunches of bound solitons. To check the dynamics of the relative phase difference in multi-bound soliton train which is impossible to be identified through the optical spectrum measurement, an interferometer measurement has been proposed and implemented. Figure 4-18 shows the schematic of the measurement based on an asymmetrical Mach-Zehnder fibre interferometer (MZI). The intensities of the interference patterns at two output ports of the asymmetrical MZI can be given by

$$I^{1'} = \left|E_{out}^{1'}\right|^2 = \left|\tfrac{1}{2} j^2 E_{in}(t) + \tfrac{1}{2} E_{in}(t - T_d)\right|^2 \tag{4-6}$$

$$I^{2'} = \left|E_{out}^{2'}\right|^2 = \left|\tfrac{1}{2} jE_{in}(t) + \tfrac{1}{2} jE_{in}(t - T_d)\right|^2 \tag{4-7}$$

where E_{in} is the input field of the MZI which is the field of multi-bound soliton train, T_d is the variable time delay between two arms. Depending on adjustment of the time delay, the pulses of two multi-bound solitons on two arms would interfere constructively or destructively over the overlapped positions at the output coupler.

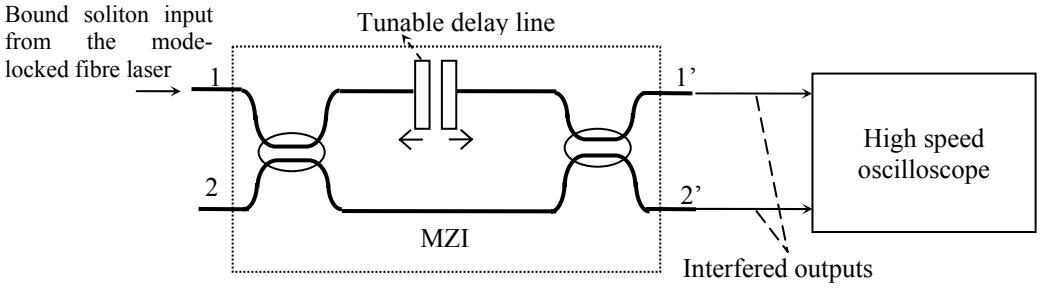

Figure 4-18 Experimental setup and principle of the interferometer measurement

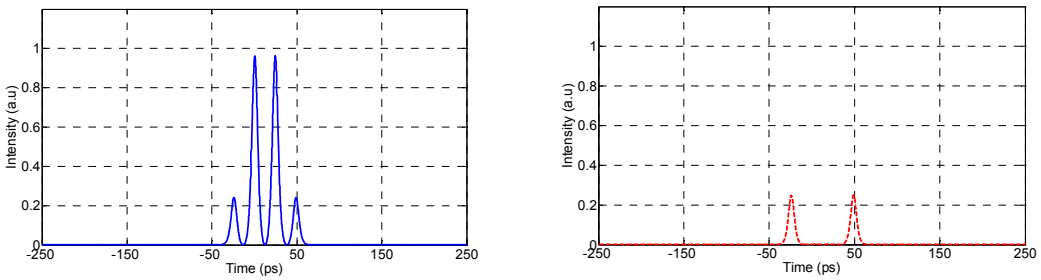

Figure 4-19 Calculated patterns of the triple-bound solitons overlapped over two pulses at two outputs of MZI (a) Constructive interference, and (b) Destructive interference.

Thus if there is no dynamically phase inversion between bunches of bound solitons or the phase difference of $\pm\pi$ between multi-bound solitons keeps unchanged, the interference patterns of two outputs would be fixed and contrary to each other when the multi-bound solitons between two arms are overlapped over one or two pulses. In case of the triple-bound solitons as an example, the calculated patterns of constructive and destructive interferences with two overlapped pulses at the outputs are shown in Figure 4-19. On the contrary, the interference patterns are dynamically varied between two output ports depending on the phase states of multi-bound solitons between two arms.

In the experimental setup as shown in Figure 4-18, the asymmetric fiber interferometer is built by two 3 dB couplers which are connected together by optical fibers to form two arms of MZI. A tunable delay line of 80 ps delay time is inserted into an arm of MZI to sufficiently provide an overlapping of MBS between two arms at the output coupler. The amplitude of overlapped pulses at the output ports (1'and 2') of MZI depends on phase difference of solitons in bound states. This determines either constructive and/or destructive interferences in time domain at overlapped positions. The interference patterns at two output ports are simultaneously monitored by two ports on the high speed oscilloscope.

4.5.2 Results and discussion

The initial phase delay between two arms of the MZI is adjusted by the fibre length difference between two arms, on the other way, the time difference between multi-bound solitons in two arms is initially about 75 ps as shown in Figure 4-20(a). By adjusting the tuneable delay line, a specific overlapping between two triple-bound solitons can be achieved. Figure 4-20(b) and (c) show, as an example, the interference patterns of triple-bound soliton state over two overlapped pulses at port 1' and 2' respectively. The results also indicates that the practical value of phase difference is not totally equal to π due to the peak power of overlapped pulses at port 1' and port 2' which is only three times higher and lower than that of input pulses respectively. However the interference patterns are not steady but alternatively changed between two ports. The alternating change of the patterns between two ports indicates that a phase inversion periodically occurs. For single pulse scheme in active mode locking, J. O'Neil *et al.* [90] has theoretically demonstrated that only the pulse train in which neighbouring pulses are out of phase is stable in the cavity. Therefore in multi-bound states, it is understandable when solitons are out of phase not only in the bunch but also between bunches. Because there is a phase shift in each roundtrip that is accumulated during circulating in the cavity, the phase inversion occurs after the accumulated phase shift is integer multiple of 2π. This is also confirmed by simulation result as shown in Figure 4-21 to indicate a periodic variation of the phase difference between $-\pi$ and π.

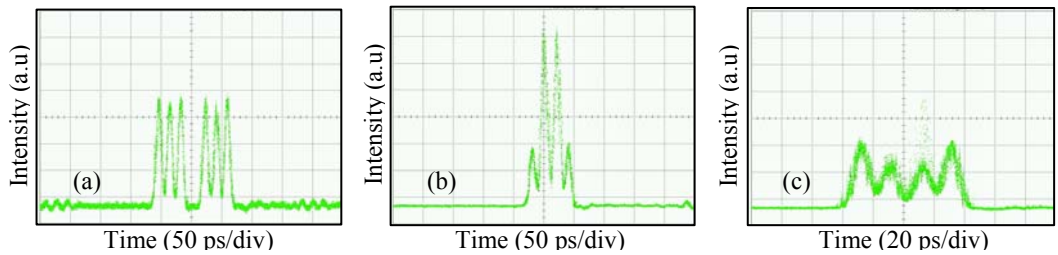

Figure 4-20 The time traces of triple-bound solitons (a) before overlapped, (b) overlapped at port 1' and (c) overlapped at port 2' of MZI.

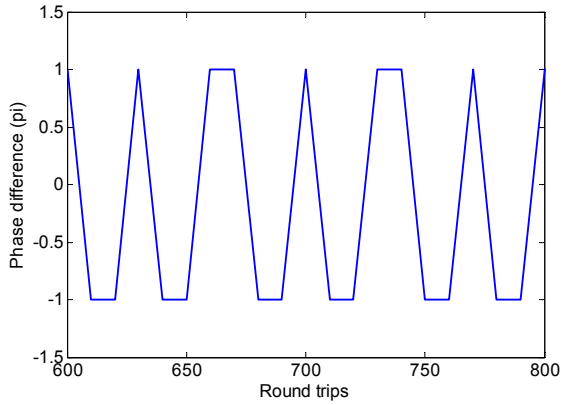

Figure 4-21 Periodic variation of the phase difference of triple-bound soliton over 200 round trips which is simulated in Figure 4-15(b).

4.6 CONCLUDING REMARKS

The important mechanisms as well as interactions in bound soliton formation of mode-locked fibre lasers have been reviewed. Formation of multi-bound solitons in active mode locking has been also explained to show the role of phase modulation in the balanced interplay between interactions of multi-bound solitons.

The generation of stable multi-soliton bound states in a FM mode-locked fibre laser has been experimentally and numerically demonstrated. It has been demonstrated that it is possible to generate the bound states from dual to sextuple states provided that there is sufficient optical energy circulating in the fibre ring. Multi-bound soliton states in a phase modulated fibre ring are rigorously explained

based on the phase matching and chirping effects of the lightwave and the velocity variation of the optical pulses in a dispersive fibre ring. Experimental and numerical results have confirmed the stable existence of multi-bound solitons with phase difference of $\pm\pi$ between neighbouring solitons. However it is more sensitive to the cavity settings as well as the external perturbations at the higher order multi-bound soliton states.

Chapter 5

Effect of the phase modulator on multi-bounding in soliton formation

5.1 ELECTRO-OPTIC PHASE MODULATORS

Integrated-optic modulators including the electro-optic (EO) phase modulators have become essential components in optical transmission systems and photonic signal processing because of their advantages such as free- or adjustable-chirp, small size and compatibility with other optical fibre components [184]. For an actively mode-locked fibre laser, an EO phase modulator acts as the mode-locker, hence its characteristics influence significantly to the performance as well as the operation modes of pulses in the fibre cavity. In this thesis we have used two models of integrated EO phase modulators: one is a PM-315P (Crystal Technology) and the other is a Mach-40-27 (Covega). This chapter first characterises these types of modulators, then reports on their effects on soliton formation.

Depending on the geometry of the electrodes, an integrated LiNbO3 modulator can belong to one of two types: lumped-type modulator or travelling-wave type modulator.

5.1.1 Lumped-type modulator

A $LiNbO_3$ phase modulator consists of a titanium-diffused single-mode waveguide and a pair of oriented electrodes [107]. Titanium waveguides can support both transverse electric (TE) and transverse magnetic (TM) optical polarisations. Due to the crystal symmetry in LiNbO3, there are two useful crystal orientations Z-cut and X-cut, which take advantage of the strongest EO coefficient. For an X-cut device, the waveguide is symmetrically located between two electrodes as shown in Figure 5-1. In a Z-cut device with the optical axis perpendicular to the surface, one of the electrodes is directly placed on the waveguide and an optical isolation layer is inserted between the waveguide and the electrode to avoid increased optical losses. Application of the electrical driving voltage to the electrodes causes a small change in the refractive index of the waveguide, and the phase of the optical signal passing through the modulator can be consequently changed as [185]

$$\Delta\varphi = \pi \frac{V}{V_\pi} = \frac{\pi L}{\lambda} r_{eff} n_{eff}^3 \frac{V}{d} \Gamma \qquad (5\text{-}1)$$

where V is the applied voltage, V_π is called half-wave voltage or the voltage required for inducing a phase change of π, L is the length of the electrode, λ is the wavelength, r_{eff} is the appropriate electro-optic coefficient, n_{eff} is the unperturbed refractive index, d is the separation between electrodes, and Γ is the overlap factor between the electric field and the optical mode field, which is an important parameter to optimize the modulator design.

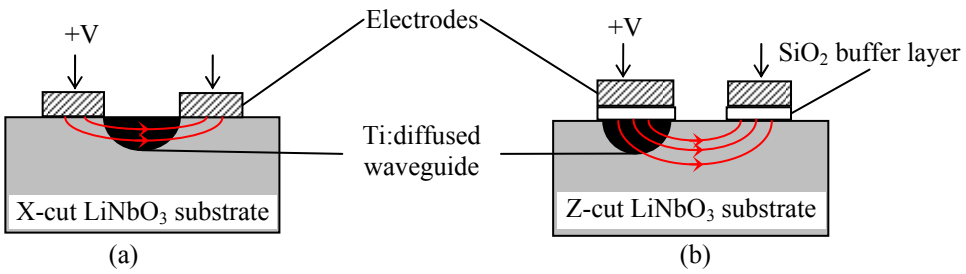

Figure 5-1 Geometries of $LiNbO_3$ phase modulators

A lumped-type EO phase modulator is illustrated in Figure 5-2. In this configuration, the RF driving voltage is directly fed to the electrodes whose lengths are small compared to the drive-signal wavelength, and the modulation bandwidth is limited by the *RC* time constant of the electrode capacitance (*C*) and the parallel termination resistance (*R*), as follows

$$f_{3dB} = \frac{1}{\pi RC} \tag{5-2}$$

The termination resistance is normally set to 50Ω to allow broadband matching to a 50Ω driving source. For low operating voltage, the modulator of longer interactive lengths is required, but the capacitance of the electrode increases, which limits the maximum frequency of operation. It is difficult to fabricate a lumped-type EO phase modulator with a broad bandwidth and low operating voltage. On other words, lumped-type EO phase modulators can operate at frequency of a few GHz with the expense of low V_π.

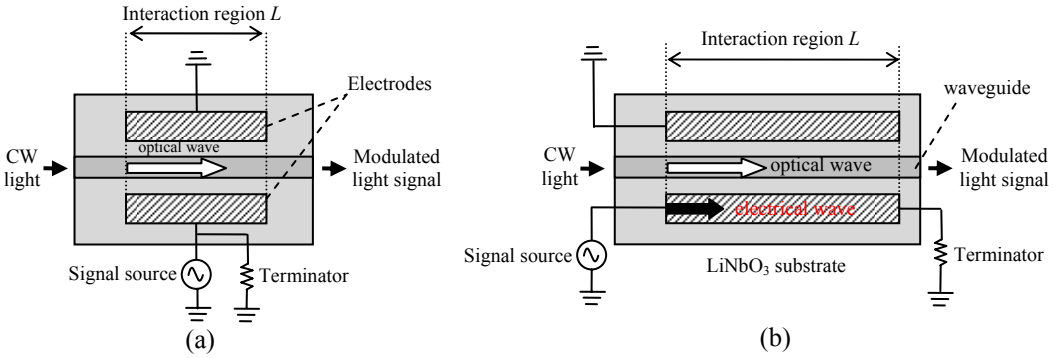

Figure 5-2 Two types of EO phase modulator: (a) Lumped-type, (b) Travelling-wave type

5.1.2 Travelling-wave modulator

In order to increase the modulation bandwidth, travelling-wave electrodes are preferably used. Travelling-wave electrodes are designed as transmission lines, fed at one end and terminated with a resistive load at the other end as shown in Figure 5-2(b). The optical signal in the waveguide and the electrical signal in the electrode propagate the same direction. Because the effective refractive index of the electrical wave n_m is about twice that of the optical wave n_o, there is a velocity mismatch between the electrical wave and the optical wave that limits the modulation bandwidth as follows [186]

$$f_{3dB} = \frac{1.4c}{\left[L(n_o - n_m)\right]} \tag{5-3}$$

where c is the velocity of light in vacuum, L is the length of the electrode.

Much effort has been put into designing travelling-wave modulators to match the velocities of the electrical and optical waves, and thus to improve the frequency response characteristics [187-189]. To obtain the velocity matching, the effective index of the electric wave n_m is lowered by using effectively a dielectric buffer layer between the electrode and the waveguide. Based on this concept, many structures of

the travelling-wave electrode have been proposed to produce the EO modulators with broad bandwidth of tens GHz and low V_π [187-189]. Note that the modulator only works well if the lightwave propagates in the same direction as the electric wave.

5.2 CHARACTERIZATION MEASUREMENTS

5.2.1 Half-wave voltage

In some options for half-wave voltage (V_π) measurement, the direct optical spectrum analysis offers an accurate and simple solution, in the case where the modulation sidebands can be resolved by the OSA. When CW light passes through a phase modulator, its spectrum is broadened by generation of modulation sidebands. The strength of sidebands is proportional to the modulation index and the sideband positions. The optical field in frequency domain of a phase modulated CW signal can be mathematically expressed by Fourier expansion as

$$E_o(\omega) = E_i \exp(j\omega_0 t) \sum_{k=-\infty}^{\infty} (j)^k J_k(m) \exp(jk\omega_m t) \qquad (5\text{-}4)$$

where ω_0, ω_m are the carrier frequency and RF modulation frequency respectively, $\omega = \omega_0 + k\omega_m$, k is the sidemode index which is an integer, J_k is the kth-order Bessel function of first kind, and E_o, E_i are the output and input fields of the phase modulator respectively. Thus, the intensity of each sidemode measured on an OSA is

$$I_o(\omega_0 + k\omega_m) = I_i J_k^2(m) \qquad (5\text{-}5)$$

where m is the modulation index and related to the V_π by (5-1) and $I = |E|^2$.

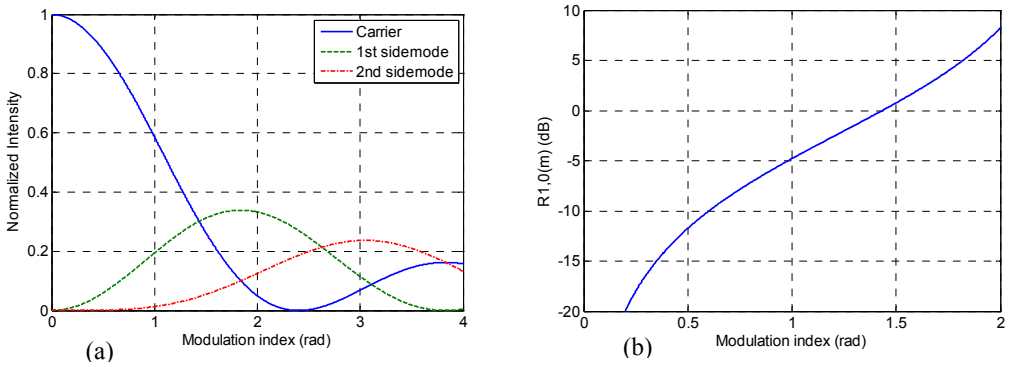

Figure 5-3 Variation of (a) normalized optical intensity for carrier and sidemodes, and (b) ratio $R_{1,0}$ as a function of phase modulation index m.

Expression (5-5) shows a relationship between the modulation index and the intensity at a specific sideband that varies as a Bessel function as shown in Figure 5-3. Based on optical spectrum analysis, there are some approaches for the V_π measurement such as the carrier nulling method [190] and the relative sideband/carrier intensity ratio method [191]. Because RF amplifiers generally do not produce a sufficient drive voltage, the relative first sideband/carrier intensity ratio is the most suitable method for small signal modulation that is used for our measurement.

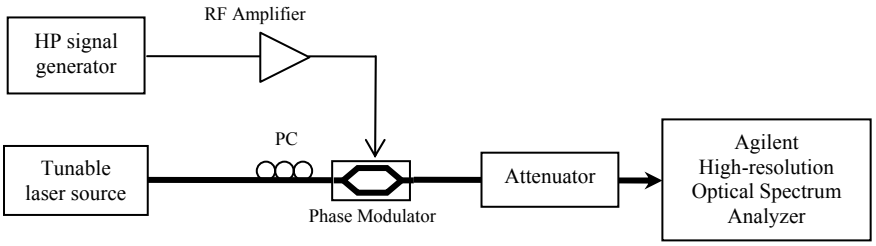

Figure 5-4 The OSA-based V_π measurement setup

The measurement setup and the components are depicted in Figure 5-4. The two phase modulators (PM-315P and Mach-40-27) were characterised by OSA at modulation frequency of 1 GHz. For a conventional OSA, the resolution is limited to

resolve the modulation sidemodes at such a low frequency. Thus a high-resolution spectrum analyser (Agilent 83453B) was used for this measurement. This OSA has a resolution of 20 MHz, so the intensity of the 1 GHz sidemodes can be clearly displayed as shown in Figure 5-5. At a specific RF driving power the modulation index m is calculated from the relative intensity ratio between the carrier and the first sidemode $R_{1,0}$:

$$R_{1,0}(m) = \frac{I_o(\omega_0 \pm \omega_m)}{I_o(\omega_0)} = \frac{J_1^2(m)}{J_0^2(m)} \tag{5-6}$$

which is measured by the OSA. By varying the RF driving voltages, the V_π of two phase modulators can be then determined from the slope of the linear fit line as shown in Figure 5-6. The estimated V_π of PM-315 was 8.87 V and the V_π of Mach-40-27 was 3.93 V. These results agree with the specifications provided by the manufacturers.

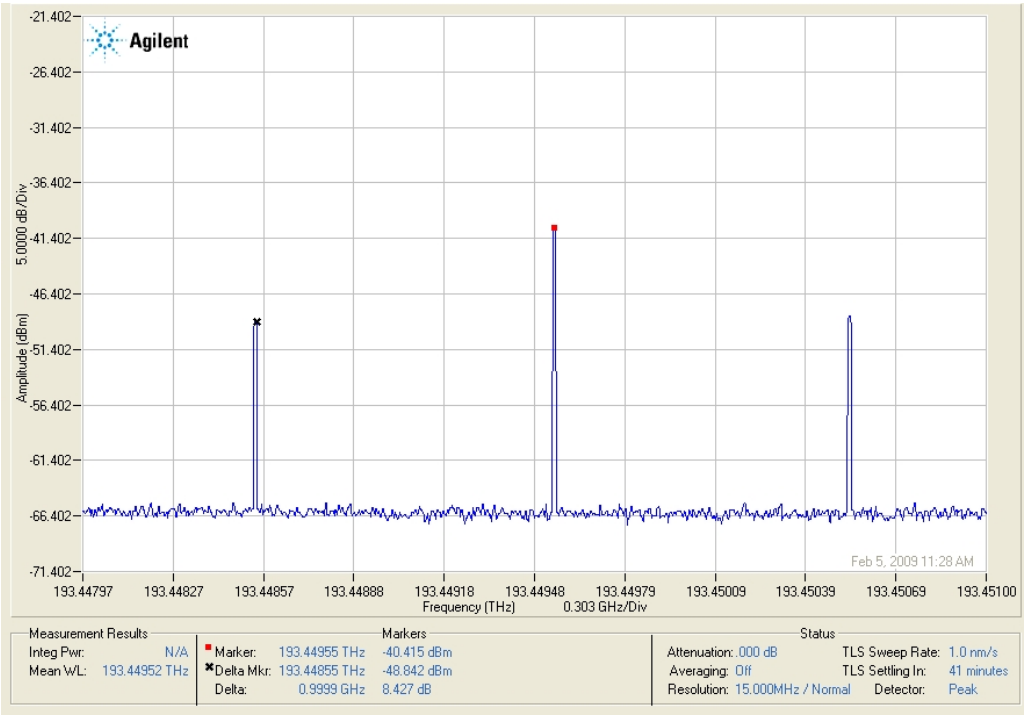

(a)

Figure 5-5 Optical spectra of the signal modulated by phase modulators: (a) PM-315P, (b) Mach-40-27 at the same RF driving level of 19 dBm.

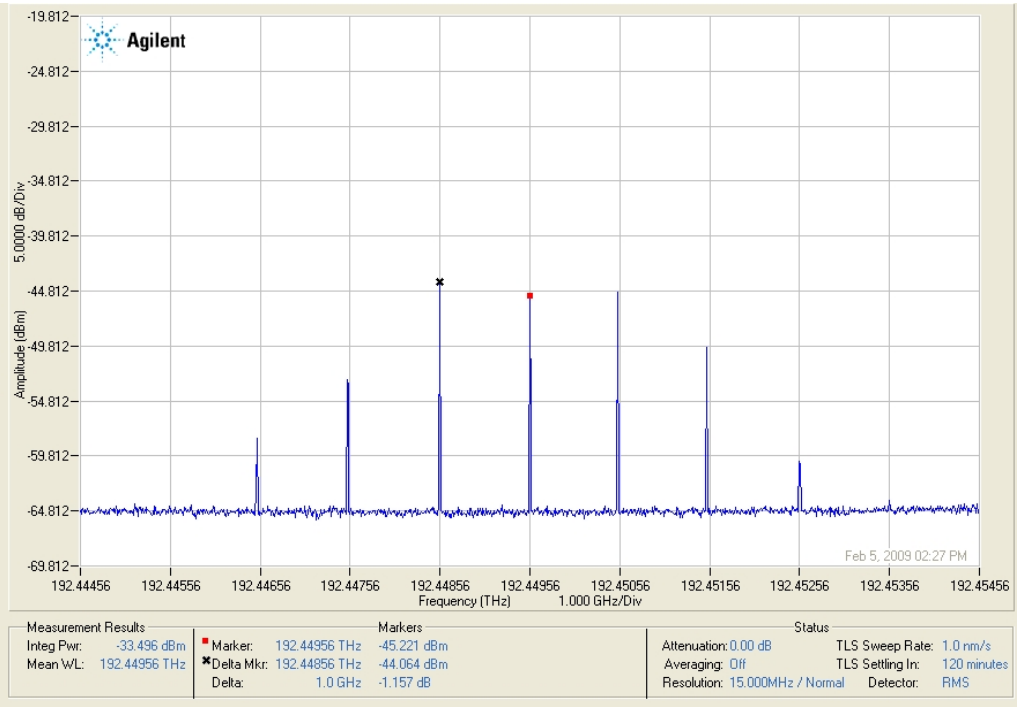

(b)

Figure 5-5 Continued. (Note the different scales).

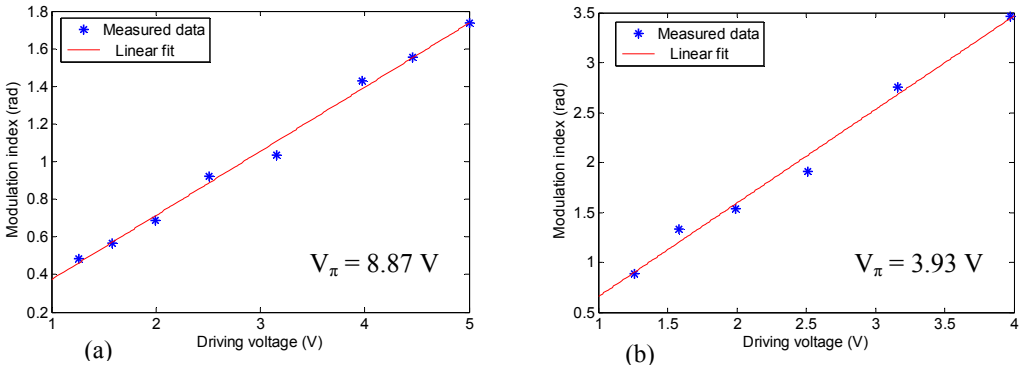

Figure 5-6 Phase modulation index calculated from measured relative intensity ratio $R_{1,0}$ at 1 GHz as a function of RF driving voltage for two models: (a) PM-315P, and (b) Mach-40-27.

5.2.2 Frequency response

The frequency response of the EO phase modulator is an important characteristic which indicates the variation of the modulation efficiency over a range of frequencies. Because optical phase modulators only modulate the phase of optical carrier, it is impossible to measure the modulator's response with a direct-detection photodiode. A

conversion of phase modulation into amplitude modulation needs to be done for this measurement. There are several techniques which have been proposed to implement this operation: using a Mach-Zehnder interferometer [190], using a Fabry-Perot interferometer as an optical discriminator [192], and using a Sagnac loop configuration [193]. However the Mach-Zehnder interferometer technique and the Fabry-Perot interferometer technique are limited in use due to their complexity and reliability, the last technique provides an efficient and simple way of measuring the dynamic response for all types of EO phase modulators with high resolution. Especially, various types of the phase modulator can be identified through this measurement.

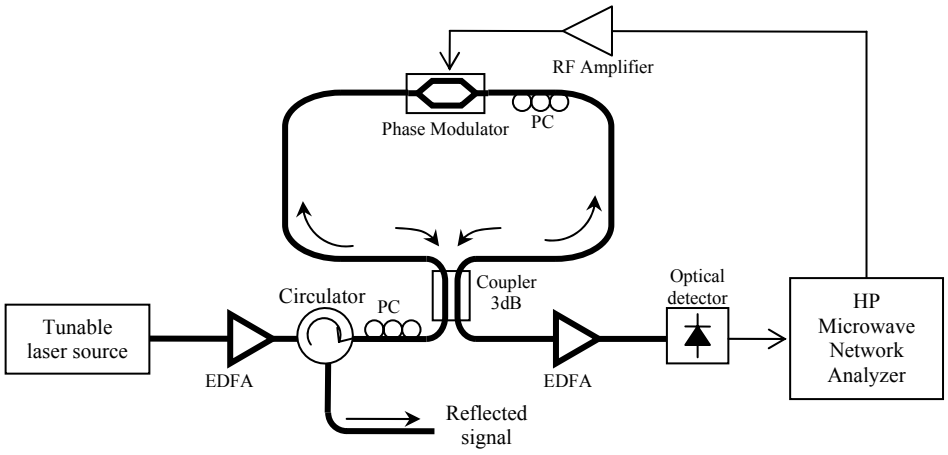

Figure 5-7 The measurement setup of the frequency response

The setup of the frequency response measurement based on a Sagnac loop is shown in Figure 5-7. This configuration is similar to the configuration of PMSL described in Chapter 3. Only main difference is the position of the phase modulator in the Sagnac loop is off-centre. Two counter-propagating optical waves are phase modulated and then coherently summed at the output 3-dB coupler. This process converts phase modulation into intensity modulation, so that the response of phase

modulator can be measured by a network analyser (Agilent HP8753D) and an S-parameter test set (Agilent HP85046A). The polarization is optimized by the polarization controller to maximize the optical power passing through the lithium niobate optical waveguide. Thus the transfer function for this structure, which can be detected by the network analyser, is given by [193]

$$H(f) = \frac{1}{2} l_{PM}^2 K_0(f) \Re \left[\left(1 + \eta^2(f)\right) - 2\eta(f)\cos\phi(f) \right] R_0 \qquad (5\text{-}7)$$

where: l_{PM} is the insertion loss of phase modulator, $K_0(f)$ is the modulation response parameter, R_0 is the load resistance, $\Re$ is the detector responsivity, $\phi(f)$ is the phase difference and $\eta(f)$ is the ratio of backward to forward phase modulation index which relates to the signal transit time τ_L [186] as follows

$$\eta(f) = \frac{\sin(2\pi f \tau_L)}{2\pi f \tau_L} \qquad (5\text{-}8)$$

This structure is also a notch filter applied in photonic signal processing [194], so that the frequency response of the phase modulator should be the envelope of the periodic notch filter response. The free spectral range (FSR) of the notch response relates to the phase difference by

$$\phi(f) = 2\pi f \tau \text{ and } \tau = \frac{1}{FSR_{notch}} = \frac{\Delta L}{c/n} \qquad (5\text{-}9)$$

where τ, ΔL are the time delay and the length difference between two sides of the Sagnac loop respectively. In order to measure accurately the frequency response of the modulator, FSR of the notch response must be as small as possible to give a high resolution, which is the reason why the phase modulator must be located off-centre of

the loop. In our setup, the length difference ΔL is about 3.5 m that gives a FSR of 58 MHz.

With a frequency range up to 3 GHz, the network analyser may not cover whole bandwidth of the phase modulators. However this measurement allows an identification of different types of the phase modulator. Figure 5-8 shows the frequency responses for two phase modulators, and indicates the difference between them. For a lumped-type modulator such as PM-315P, the ratio η keeps unchanged over the bandwidth of the phase modulator, so the notch response shows deep notches and a flat passband within the bandwidth as shown in Figure 5-8(a). The envelope of this response gives exactly the dynamics response of the phase modulator with the measured 3-dB bandwidth of 2.7 GHz. For a travelling-wave modulator, the velocity mismatch effect causes the notch depth to disappear at certain frequencies, f_k, which are related to the transit time τ_L as follows [186]

$$f_k = \frac{k}{2\tau_L} \qquad \text{with } k = 1,2,... \tag{5-10}$$

The measured notch response of the phase modulator Mach-40-27 with the null frequency f_1 of 2.27 GHz is shown in Figure 5-8 that indicates a response of the travelling-wave modulator. And the net dynamic response of the modulator can be also obtained by a correction of the envelope of the measured notch response from the known function $\eta(f)$. More importantly, the interactive length of the electrode in the travelling-wave modulator can be estimated from the transit time τ_L. For the Mach-40-27 modulator, the interactive length about 32 mm is calculated from the transit time of 0.455 ns. The length of waveguide in this modulator would be much longer than that of the electrode due to a polarizer integrated in the phase modulator [195].

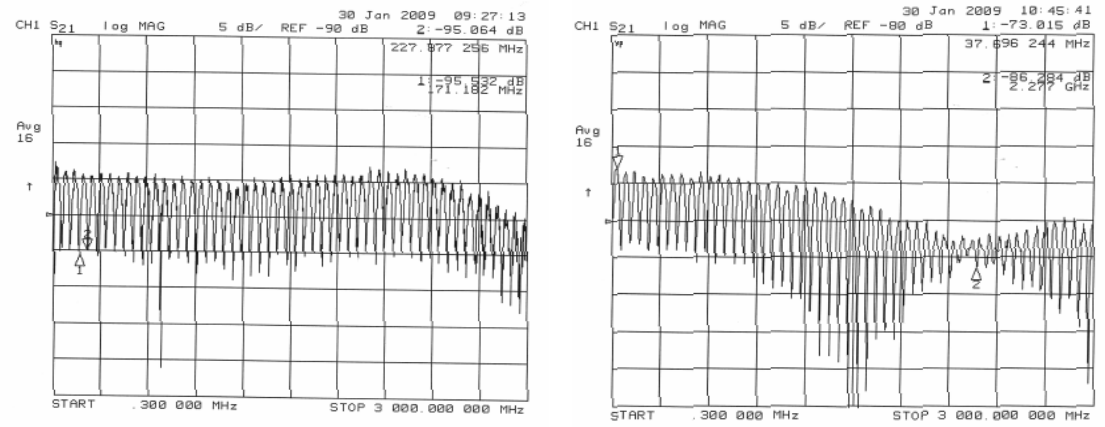

(a) (b)

Figure 5-8 Measured frequency notch response of the phase modulators (a) lumped-type PM-315P, (b) travelling-wave type Mach-40-27 within measured frequency range up to 3 GHz.

Thus from the characterization measurements of two phase modulators, the difference between lumped-type modulator and travelling-wave modulator has been identified. For the modulator PM-315P, a lumped type, the short length of electrodes has been verified by its high V_π and flat frequency response over the measurement bandwidth. Similarly, for the modulator Mach-40-27, a travelling-wave type, long electrodes and waveguide have been verified by its low V_π and the velocity mismatch in frequency response measurement.

5.3 COMB SPECTRUM OF AN ACTIVELY FIBER RING RESONATOR USING A PHASE MODULATOR

5.3.1 Birefringence and comb spectrum in the fibre ring using phase modulator

Because the integrated EO modulators normally contain polarizing elements, the birefringence effect always exists in an actively fibre ring laser, even if the birefringence of other components such as optical fibres can be ignored. In fact, a Ti:diffused electro-optic $LiNbO_3$ phase modulator (PM) can support both TE and TM

modes propagating at different ordinary and extraordinary effective indices. Although the polarization state is usually controlled by the polarization controller, especially at input of integrated EO modulator so as only one polarized state can be preferred through the modulator and hence the forcing of the matching condition of this polarized state, there is still an asymmetrically simultaneous existence of two polarization modes in the ring, especially in the Ti:diffused waveguide. Thus these modes with different phase delays can couple and interfere at the output of the modulator to form an artificial birefringence filter, known as a Lyot filter, in the ring cavity [196]. Hence the output spectral response of the ring cavity is similar to that of a Mach-Zehnder interferometer, the all-pass filter with nulls and maxima [197-198]. The output transmittance of the ring cavity using EO phase modulator is simply given by [197]

$$T = \Gamma_g \cos^2(\Delta\phi / 2) \tag{5-11}$$

where Γ_g is the insertion loss of waveguide depending on the input polarization states and the gain bandwidth of the EDFA, $\Delta\phi$ - the effective phase difference between TE and TM modes. Because no polarization maintaining (PM) fibre is used, the effective phase difference in the cavity is dominated by the birefringence of the Ti:diffused waveguide. Therefore, the phase difference is given as

$$\Delta\phi = \frac{2\pi l \Delta n_{eff}}{\lambda} \tag{5-12}$$

where l is the waveguide length, Δn_{eff} is the effective index difference between TE and TM modes. The interference between two polarization modes generates a comb-like spectrum with spacing or free spectral range (FSR)

$$\delta\lambda = \lambda^2 / l\Delta n_{eff} \qquad (5\text{-}13)$$

On the other hand, the gain spectrum in the fibre cavity is modulated when the waves propagate through the phase modulator.

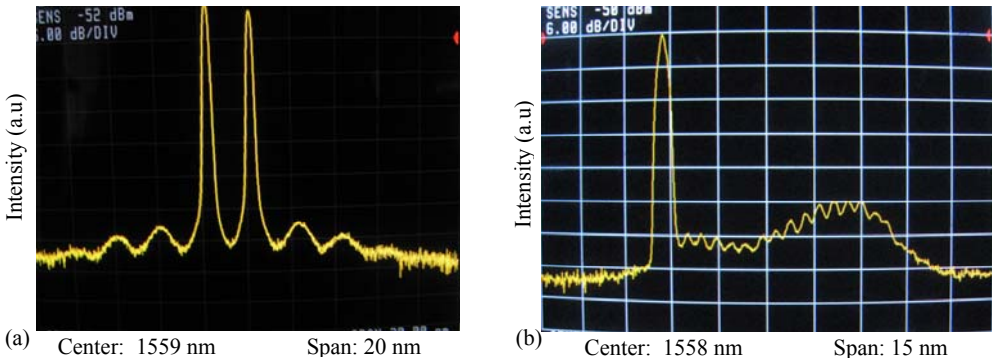

Figure 5-9 The comb-like optical spectra in two setups of the fibre ring laser using (a) model PM-315P and (b) model Mach-40-27 respectively.

With two models of phase modulator are used in the experiment, the comb-like optical spectra were measured by appropriate setting to display in OSA. Figure 5-9 shows the optical spectra in CW operation mode of the ring cavities using models PM-315P and Mach-40-27 respectively. The emission wavelength is located on one of the maxima of the comb-like response where the gain is maximized. For the ring using model PM-315P, the average FSR is 2.15 nm in a bandwidth of about 12 nm, while the average FSR of the ring using model Mach40-027 is only 0.45 nm in a bandwidth of about 10 nm as observed in Figure 5-9. Based on the characterization and the physical dimensions of two these models, the waveguide lengths of PM-315P and Mach-40-27 are assumed to be 16 mm and 64 mm respectively. Thus the FSRs of comb-like spectral response in cases of two models, calculated by Eq. (5-13), are 2.0254 nm and 0.4668 nm respectively when the effective index difference of TE and TM modes of 0.08 is used [199]. We have examined the birefringence of the ring

cavity in both cases by changing the optical fibres of different lengths. The FSRs remain unchanged in all cases that has proven that the birefringence is mainly determined by the Ti:diffused waveguide. These results are reasonable and agree with the results obtained from OSA. The existence of parasitic birefringence in the integrated EO phase modulators forms naturally a comb-like filter which affects to mode locking schemes and characteristics of mode-locked pulse train.

5.3.2 Discrete wavelength tuning

One of the influences of the comb-like filtering effect is a discrete wavelength tuning in the FM mode-locked fibre ring laser. In our mode-locked fibre lasers, the mode locking happens only at the peaks of the comb-like optical spectrum where the lightwaves acquire sufficient energy gain to satisfy the mode locking condition. The wavelength of the sequence of the mode-locked pulses can be tuned by only changing the modulation frequency of the phase modulator. Thus the wavelength tuning is based on the matching of the dispersed spectrum of the pulse sequence, hence tuning of the pulse central passband [200-202]. Hence the tuning range of the laser depends on the profile of gain spectrum and the total dispersion of the cavity. Because the gain spectrum is modulated by the interference between two polarization modes, so the modulation frequency tuning is required by amount of [200]

$$\delta f_m = -\frac{f_m^2 D L_{cav} \delta\lambda}{m} \tag{5-14}$$

where f_m is the modulation frequency, m is the harmonic order, D and L_{cav} are the average dispersion and the total length of the ring cavity respectively. The tuning is only achieved in a specific range of wavelengths to prevent the competition of the

CW modes which suppress the mode locking at other matched wavelengths although the comb-like spectrum can be observed in most of phase modulators.

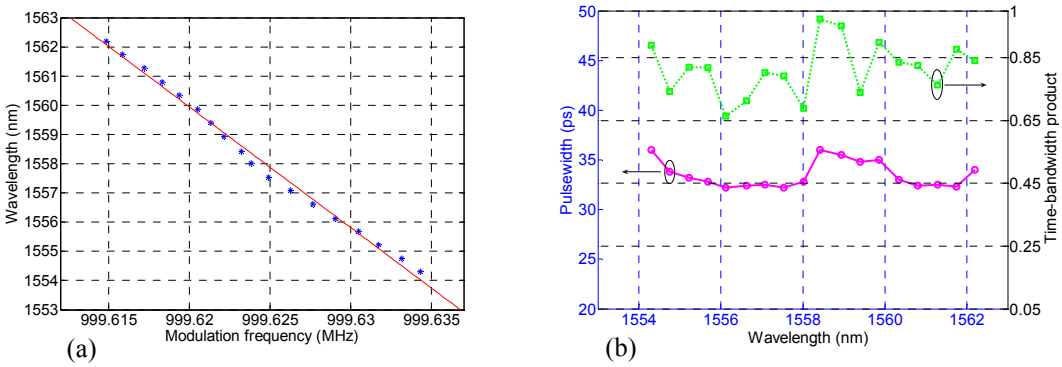

Figure 5-10 (a) The mode-locked wavelength versus modulation frequency and (b) Measured characteristics of mode-locked pulse over the tuning range.

In the setup using the phase modulator Mach-40-027 with an integrated polarizer at its output, mode locking is achieved at modulation frequency of about 1 GHz. A 100m long Corning SMF-28 fibre is inserted after the PM to ensure that the average dispersion in the loop is anomalous. The total loop length is 190 m corresponding to a mode spacing of 1.075 MHz. By tuning the modulation frequency, the light-waves in the cavity are mode-locked to generate a short pulse sequence at the wavelength corresponding to one of the peaks of the comb spectrum as shown in Figure 5-9. A 0.46 nm average spacing between two adjacent mode-locked wavelengths is achieved. By adjusting the PC to optimize the gain spectrum, we can tune over 18 different wavelengths (1554-1562 nm) by simply changing the modulation frequency of 1.35 kHz as shown in Figure 5-10(a). These measured parameters agree with the theoretically predicted values, which are of 0.4578 nm and 1.27 kHz respectively. Figure 5-10(b) shows the pulsewidth and time-bandwidth product (TBP) of mode-locked pulse at 18 wavelengths. The average TBP of 0.8 indicates that the output pulses are highly chirped and they can be compressed by

using a suitable dispersive fibre at the output of the laser. In wavelength tunable harmonically mode-locked fibre laser, the supermode noise is normally an important issue which requires some methods of suppression to improve performance of the generated pulse train [202]. It is worth noting that the mode-locked pulses at all 18 wavelengths are very clean which is seen from the time trace and its corresponding RF spectrum shown in Figure 5-11. When the f_m is tuned by amount of $\delta f_m/2$ the mode competition occurs strongly which degrades the waveform of the output as shown in Figure 5-12. On the other hand, this is the transition state for switching to adjacent spectral peak, the mode locking cannot be totally achieved. When the wavelength is tuned to the edge of gain spectrum, multi-wavelengths operation of the laser can be easily excited and it also affects the performance of mode-locked pulses as shown in Figure 5-13.

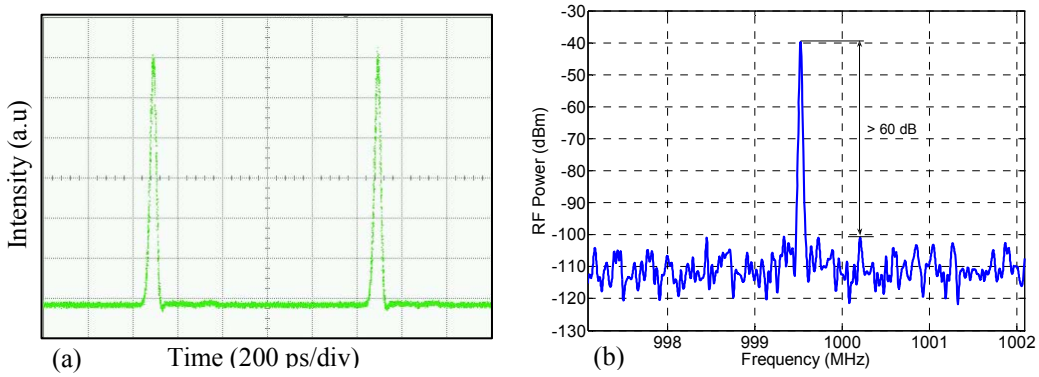

Figure 5-11 An example of (a) the time trace and (b) RF spectrum of the mode-locked pulse sequence at one of tuned wavelengths.

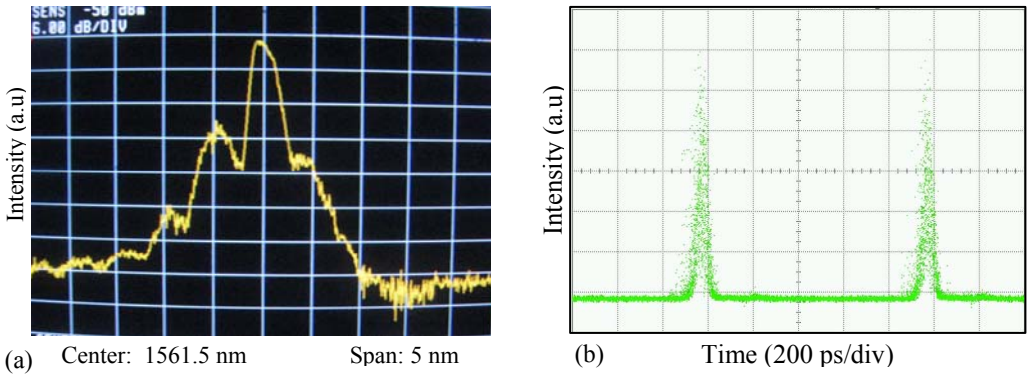

Figure 5-12 (a) Optical spectrum and (b) time trace of the output when modulation frequency f_m is tuned by $\pm\delta f_m/2$.

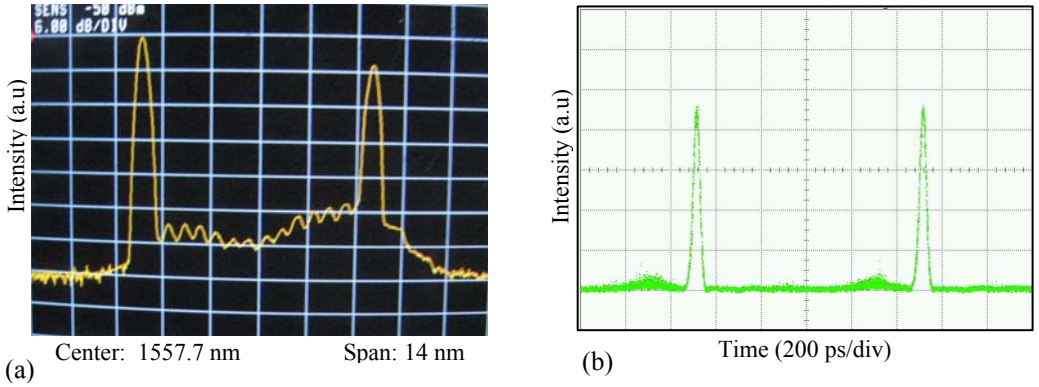

Figure 5-13 (a) Optical spectrum and (b) time trace of mode-locked pulse when the wavelength is tuned at the edge of gain spectrum.

Similarly, wavelength tuning operation is also observed in the setup using the phase modulator PM-315P although it is more difficult in adjustment of the polarization controller to obtain a sufficient gain bandwidth covering the tuning range of wavelength because of a wide spacing between comb peaks. Only three wavelengths at the peaks of the comb-like spectrum are tuned with changing the modulation frequency of 3.1 kHz in this setup to obtain a high-quality pulse train with characteristics summarised in Table 5-1.

Table 5-1 Pulse characteristics at tuned wavelengths of the FM mode-locked laser using the modulator PM-315P

{Wavelengths (nm)	1555.98	1558.03	1560.14
Pulse width (ps)	11.9	13	11.3
Spectral width (nm)	0.237	0.24	0.26
TB product	0.3525	0.405	0.3672

5.4 INFLUENCE OF PHASE MODULATOR ON MULTI-BOUND SOLITONS

5.4.1 Formation of multi-bound solitons

The existence of comb-like filtering effect in the cavity using EO phase modulator influences remarkably to the characteristics of generated pulses. The artificial filter based on the birefringence of the cavity limits the gain bandwidth and contributes to the mechanism of pulse broadening due to the limitation of pulse spectrum. This effect has been experimentally demonstrated by the results of pulse width obtained from two setups of the mode-locked fibre lasers using the modulators PM-315P and Mach-40-27. Although the modulator Mach-40-27 is driven at much higher modulation index compared to the modulator PM-315P because of lower V_π, the pulse generated from the setup using Mach-40-27 modulator is more than twice as wide as that generated from the setup using PM-315P modulator. With a much smaller width due to broader gain bandwidth, the pulse generated in the case of PM-315P has a high peak power to create a sufficiently nonlinear phase shift which is necessary for pulse splitting in the cavity. Moreover the effective interactions between pulses in bound states also depend on the pulse width through the overlap of long pulse tails and the chirping caused by phase modulation. In the case of PM-315P, the chirp imposed on the generated pulses with sufficient small width allows an effective attraction to

balance the repulsion to generate a stable bound state. In contrast, a distinct bound state cannot be observed in the case of Mach-40-27 with wider generated pulses as mentioned in Chapter 3. In this case wider pulses obtain higher chirp from phase modulator to result in a stronger attraction. At once the repulsion force from direct interaction becomes weaker. Therefore, a balanced interaction cannot be achieved in this case to generate a bound state with obviously resolved pulses although the cavity is strongly pumped. A state of mode-locked pulse with two-hump generated from the setup using Mach-40-27 has been observed as shown in Figure 5-14. This result may be a new solution of the fibre laser system, yet the time separation between two humps less than 20 ps may also indicate a strong attraction between two adjacent pulses.

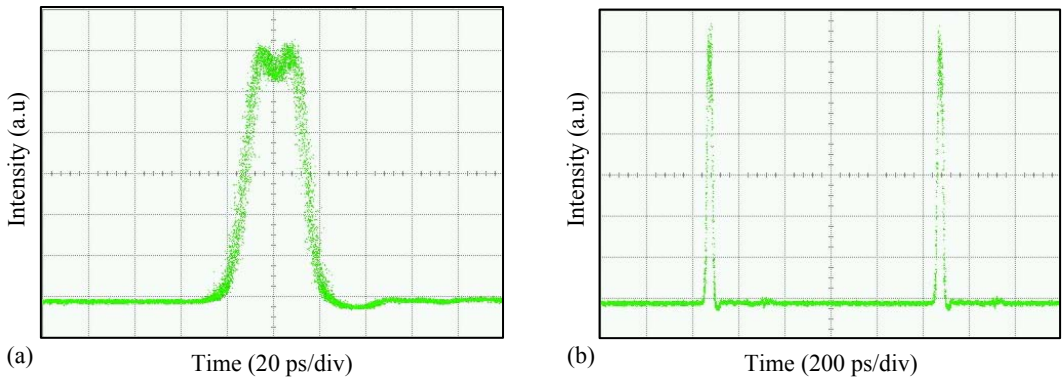

Figure 5-14 A mode-locked state generating a two-hump pulse in the cavity using the phase modulator Mach-40-27. (a) Single pulse trace, (b) Pulse train trace.

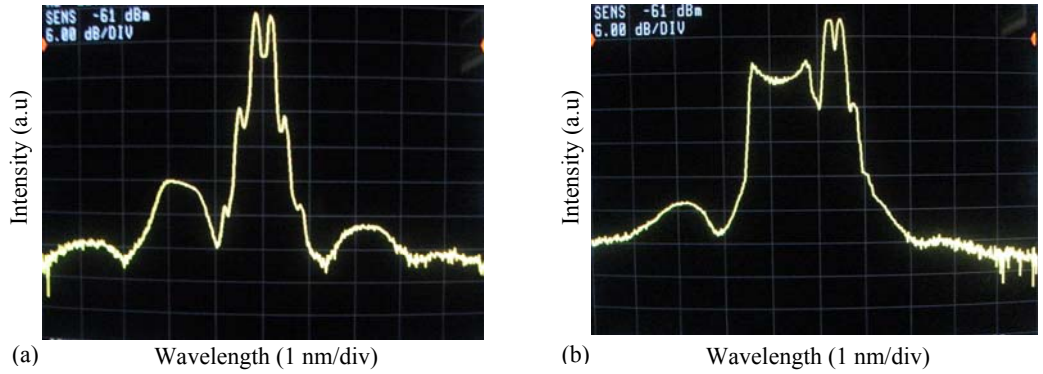

Figure 5-15 A switching from the triple-bound soliton into the dual-bound soliton after an adjustment of the polarization controller. (a) Spectrum of triple-bound soliton, (b) Spectrum of dual-bound soliton with an adjacent wavelength in FM mode.

Furthermore, the polarization sensitivity of the cavity also increases because of the inherently birefringence of the waveguide. Under strong pumping scheme, some effects such as spectral hole burning (SHB) and polarization hole burning (PHB) are enhanced in the gain medium, and these make polarization-dependent loss and gain become more complex [203-206]. Inhomogeneous broadening of the gain spectrum associated with SHB and PHB effects excites multi-wavelength emission in the fibre ring laser which results in a gain competition between different emission wavelengths. Normally only one of emission wavelengths satisfies the phase locking condition in the cavity to generate a pulse train, while other wavelengths may operate in CW mode or FM mode depending on the polarization setting in the cavity. Thus if the polarization setting is not optimized, the gain of the mode-locked wavelength can be reduced that results in a switching from higher-order bound solitons to lower-order bound solitons. Figure 5-15 shows a typical example of switching from the triple-bound soliton into the dual-bound soliton after the polarization controller is slightly adjusted. The gain reduction of the mode-locked wavelength always accompanies with the gain enhancement of adjacent wavelengths as shown in Figure 5-15(b).

Therefore, it is understandable that the higher-order bound states are more sensitive to polarization settings. However, the polarization dependent gain effect also provides a flexible mechanism for stabilization of bound state by adjusting the input polarization state of the phase modulator. If the gain is too high, multi-bound solitons can fall into unstable state because of the phase fluctuation which leads to a breakdown of interactive balance between pulses. Therefore, a reduction of gain from tuning the polarization state can pull the ring laser back to the stable operation region.

5.4.2 Limitation of multi-bound soliton states

According to the interaction mechanism of bound solitons in the actively mode-locked fibre ring laser, an effective repulsion is induced by linear chirping caused by periodic phase modulation or a balanced interaction between solitons is only achieved around the extreme of modulation cycle where approximates as a parabolic function. However, this approximation is no longer valid if the width of the bunch is so wide. Deviation from linear chirping increases when number of solitons in bound states increases. Thus the pulses at edge of the bunch would experience a nonlinear chirping rather than linear chirping which influences the balanced interaction of bound solitons. This explains why the trace of sextuple-bound solitons looks noisy because of oscillation of solitons in the bound state and the spectrum is slightly modulated due to change in the relative phase difference. It has also shown that the higher-order multi-bound solitons are more sensitive to environmental perturbations such as temperature variation. When the fluctuation of cavity length due to causes a slight detuning, the outer pulses in multi-bound state would be most affected by the frequency shifting which breaks the balance in soliton interaction.

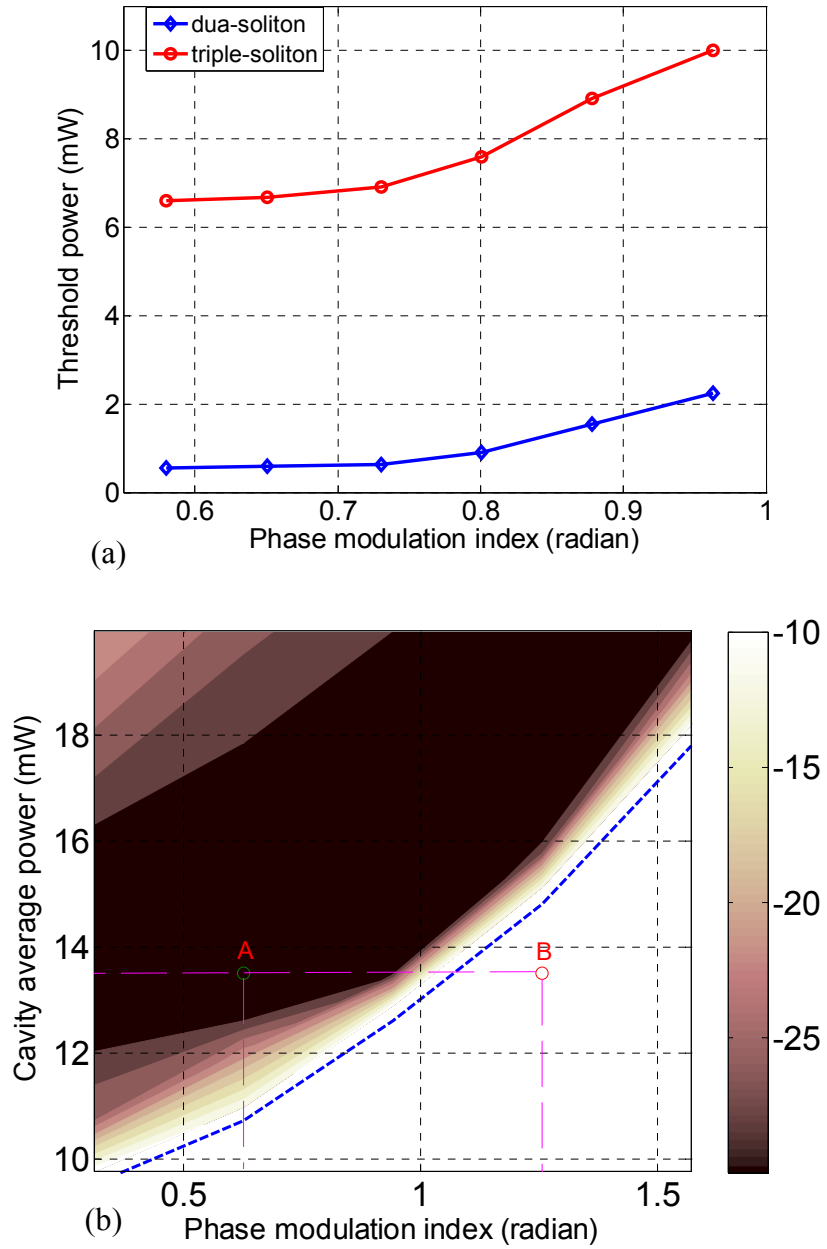

Figure 5-16 (a) Experimentally measured variation of threshold splitting power with the phase modulation index of the bound soliton states. (b) Simulated variation of the peak power in dB of the triple-bound state with the phase modulation index.

The chirping rate determines the separation between bound solitons as described in Chapter 3. The chirp effect and the number of soliton in the bound states are also correlated. Figure 5-16(a) depicts the experimental threshold power for the creation of dual- and triple-soliton bound states against the phase modulation index,

which indicates the increase of required splitting optical power when the chirping is increased. An increase in the chirp rate requires a higher threshold power to maintain a specific number of pulses in the bound state. When the phase modulation index increases, the expansion of signal spectrum is enhanced. This is advantageous in not only shortening the pulse width, but also in more tightly binding the pulses due to the increase in number of phase-locked modes. However, the increase in chirping rate also causes an energy transfer to sidebands stronger which can degrade the soliton content of pulse sequence. Although the up-chirped pulse is further compressed by anomalous dispersion of the fibre ring at higher modulation index, larger frequency chirp at pulse edges also may require higher energy contained in the pulses. This tendency agrees with the theoretical analysis of soliton production from the chirped pulses in [207-208]. At a low phase modulation index, the chirping is almost unaffected by the threshold power due to weak binding of the bound solitons. Consequently, the waveforms of the bound states are noisier and more sensitive to phase fluctuations caused by the amplification stimulated emission (ASE) noise or the random polarization variation of the guided medium. A simulation result of the power limit of the cavity to maintain the bound state is shown in Figure 5-16(b). The rates of increasing and decreasing of peak power of bound solitons are indicated showing two distinct regions of operations, the triple and the double bound separated by the dashed bold line. This limit line (dashed bold line) is obtained when a minimum power level circulating in the cavity is required to maintain the bound state that divides the graph into the triple and double bound regions. At a specific modulation index, when the average power of the cavity decreases, the variation of the peak power is stronger. When the power is lower than the limit line, the higher order soliton bound state

switches to the lower order soliton bound state. This tendency also indicates that the increase in chirping diminishes the number of solitons in the bound state at a specific optical power level as shown in Figure 5-17(a) & (b). These figures show the evolution of the triple-soliton bound state in the cavity at the same average power level but different phase modulation indices which correspond to the points A and B respectively in Figure 5-16(b).

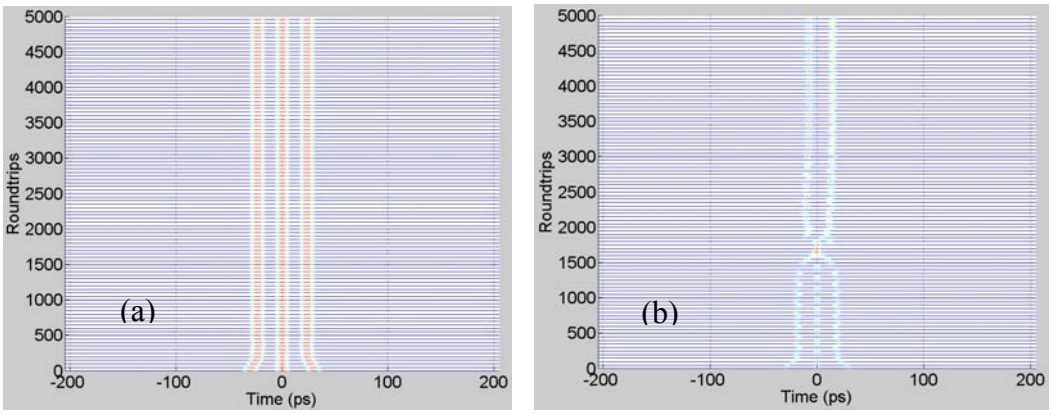

Figure 5-17 (a) & (b) Simulated evolution of the triple-soliton bound state at operation points A & B respectively in Figure 5-16(b).

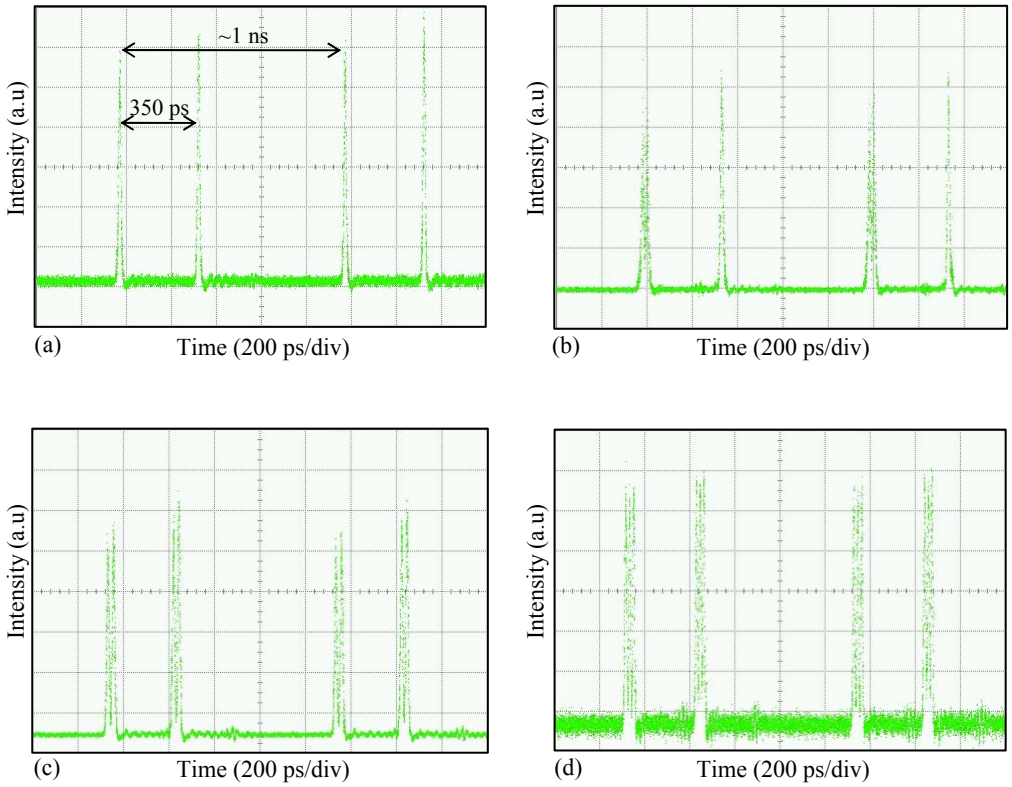

Figure 5-18 Splitting of multi-bound solitons: (a) dual-bound soliton, (b) triple-bound soliton, (c) quadruple-bound soliton, and (d) sextuple-bound soliton, into lower-order bound solitons.

Thus, the phase modulation profile affects significantly to multi-bound soliton states. In other words, multi-bound states can be modified by variation of modulation curve of the phase modulator. Enhancement of higher-order harmonics in the modulation signal is the simplest way to modify the phase modulation profile. Similar to the rational harmonic mode locking, the higher-order harmonics of modulation frequency is strongly enhanced by saturation of the RF power amplifier. When the levels of the second- and the third-harmonics are sufficiently high to distort the phase modulation profile, multiple linear chirps in each modulation cycle can be created. In particular, there are two linear chirps in each modulation cycle created by increase in the input power of the RF amplifier higher than 2 dBm in our setup. In fact a sub-modulation cycle would appear aside the main cycle due to the enhancement of the

second harmonics in the modulation signal. When the laser is locked in harmonic mode locking scheme instead of rational harmonic mode locking at the same optical power level of various multi-bound solitons, the multi-bound solitons with smaller number of solitons are formed at two linear chirp positions as shown in Figure 5-18. The distortion of phase modulation profile splits higher-order bound solitons into two groups of lower-order bound solitons within the same cycle. Moreover the change in the higher-order harmonics level also changes the distortion which varies the chirp rate between two groups of solitons. Figure 5-19 shows a variation of time separation between two solitons split from the dual-bound soliton state as a function of the RF input power. Thus the time separation reduces according to the reduction of the higher harmonic level in the modulation signal. When the RF input power is decreased to 2 dBm, two groups of bound soliton emerge together to form higher-order multi-bound soliton with number of solitons equal to total of solitons in two groups. The emergence of two bound soliton groups is due to the almost disappearance of sub-modulation cycle generated by the second harmonic RF signal. It is interesting to show that the change in temporal separation is a complete linear function of the second harmonic RF power as shown in Figure 5-20.

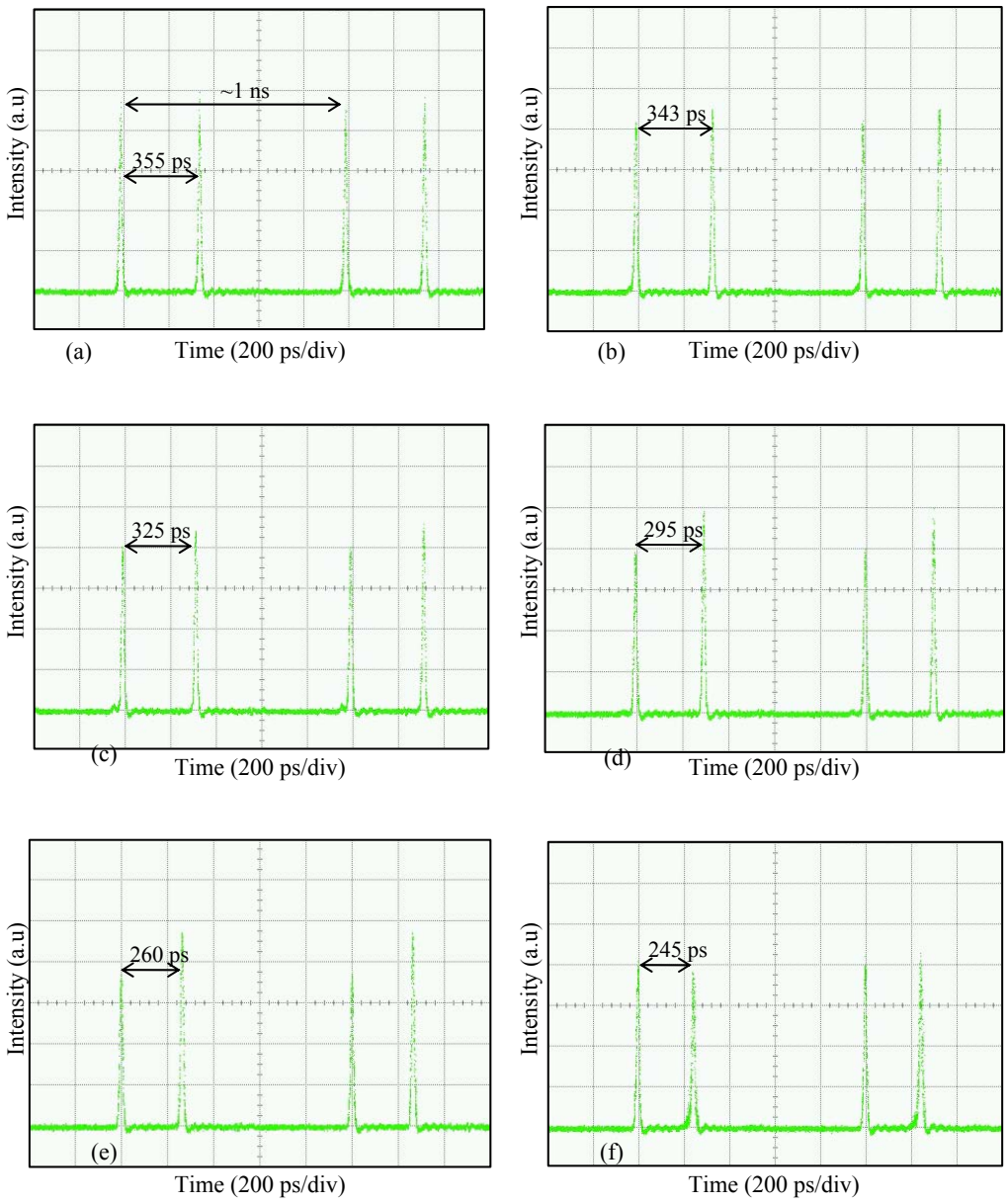

Figure 5-19 Time traces shows the variation of time separation between two solitons split from dual-bound soliton versus the change in RF input power: (a) 7 dBm, (b) 6 dBm, (c) 5 dBm, (d) 4 dBm, (e) 3 dBm, and (f) 2.5 dBm.

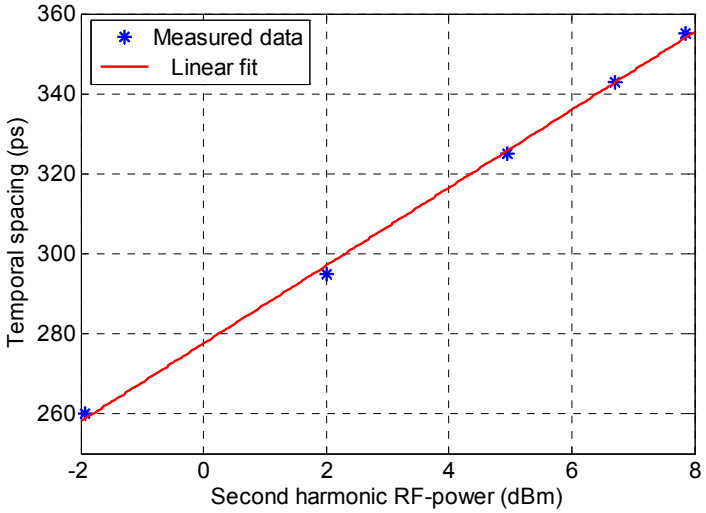

Figure 5-20 Correlation between the temporal spacing between two groups of bound soliton and the second harmonic RF power.

5.5 CONCLUDING REMARKS

In this chapter, we have demonstrated the influence of the EO phase modulator on multi-bound solitons. The influence is reflected through two aspects of the phase modulator which consists of the inherent birefringence in the Ti:$LiNbO_3$ waveguide and the phase modulation profile or chirp rate caused by the modulation signal. Two typical phase modulators have been described and characterized to indicate a difference in structure between the lumped-type and the travelling-wave type that influence to operation modes of the mode-locked fibre laser. Because an artificial comb-like response can be formed in the ring cavity by the birefringence of the integrated phase modulators, a narrow FSR in the response for the phase modulator with long waveguide can limit the pulse shortening and multi-bound soliton formation. Moreover, the ability of discrete wavelength tuning can be implemented in the fibre laser through simple tuning of modulation frequency.

Mode-locking and multi-bound soliton operation in the actively FM-MLFRL is supported by linear chirping which can be approximated by a sinusoidal modulation. Besides the temporal separation of adjacent pulses, the optical power threshold for splitting the solitons and the number of solitons in the bound states are influenced by the chirp rate induced by this phase modulation. When the modulation profile is modified by the enhancement of higher order harmonic in the driving modulation signal, higher order multi-bound solitons can be split into lower order multi-bound solitons with controllable temporal separation between them. More importantly, the experimental results have demonstrated the ability of control through the active device such as EO phase modulator that is important in potential applications.

Chapter 6

Transmission of multi-bound solitons in fibres

6.1 INTRODUCTION

Temporal solitons are attractive for long haul fibre transmission systems due to their preservation of shape during propagation in nonlinear dispersive medium. In theory, the soliton only remains unchanged in ideal transmission medium without any perturbation such as loss and noise. Therefore, the understanding of soliton propagation characteristics in real fibre systems is of significance to the design of an optical communication link. Moreover, there is a difference between the propagation of solitons in a ring such as a mode-locked fibre laser and a real fibre transmission link. It must be noted that the length of the mode-locked fibre ring is much shorter than the dispersion length of the fibre, L_D, and the pulse sequence is thus operating in the near field region in which the chirp of the lightwave occurs significantly, especially at the edges of the pulses; While the distance of each span in the fibre link is longer than the dispersion length. Therefore distinct transmission conditions are required to ensure that solitons can be recovered at the end of the link.

Although a number of reports on bound soliton states in mode-locked fibre lasers have been published [30, 45, 144-152, 160], to date there is no report on the propagation dynamics of multi-bound solitons in optical fibre. The difficulty of the

generation of stable bound soliton sequence in passive mode-locked fibre laser may have prevented the investigation of their propagation and related dynamics. As described in above chapters the actively FM mode-locked fibre laser offers significant advantage in generation of ultra-stable multi-bound soliton sequence at modulation frequency that would be important for propagation in optical fibre. Dynamics of multi-bound solitons are an important issue for investigation. The obtained results are significant to possibly potential applications of bound soliton lasers.

6.2 SOLITON PROPAGATION IN OPTICAL FIBRES

6.2.1 Loss management

Because the dispersion or GVD value is unchanged along optical fibres, the balance between GVD and SPM in soliton transmission would be only achieved if the soliton pulse was not attenuated during propagation. For a lossy fibre in the real transmission system, a reduction of the peak power over distance leads to a soliton broadening. The broadening of a soliton can be understood by the reduction of SPM effect resulting from the reduced peak power that makes the impact of dispersion effect stronger during propagation. When the fibre loss is assumed as a weak perturbation of NLSE, a change in soliton parameters under the influence of the fibre loss has been investigated by using the variation method [209]. Variations of soliton amplitude and phase along the fibre can be given by

$$\eta(\xi) = \exp\left(-\Gamma\xi\right) \text{ and } \phi(\xi) = \phi(0) + \left[1 - \exp(-2\Gamma\xi)\right]/(4\Gamma) \qquad (6\text{-}1)$$

where $\Gamma = \alpha L_D$ and $\xi = z/L_D$, α is the loss coefficient of the fibre. An exponential decrease in soliton amplitude weakens the SPM effect; hence soliton is also broadened with the same manner [60]:

$$T(z) = T_0 \exp(\Gamma \xi) = T_0 \exp(\alpha z) \qquad (6\text{-}2)$$

where T_0 is the initial width of unperturbed soliton, T is the width of soliton at distance z. It notes that a linear increase in pulse width occurs in the linear propagation scheme [60]. When the peak power is considerably attenuated at long distance, the SPM effect can be negligible and solitons behave like non-solitary pulses. Therefore the exponential dependence of soliton width over the distance is only valid at the distance where αz is less than 1 [210].

In order to overcome the broadening problem due to fibre loss, periodic amplification of soliton is required to maintain the soliton's energy. A lumped amplification scheme can be used in fibre link for this purpose [211]. Solitons which propagate in this scheme are called "path-average solitons" [210]. Similar to the mode-locked fibre ring system, the adjustment of soliton in the fibre following the amplifier can lead to a shedding a part of soliton energy as dispersive waves which are accumulated to a considerable level over a large number of amplifiers. In order to keep the variations of the soliton's shape and power negligible, two conditions to operate in the average-soliton regime must be satisfied [60, 210]

- The amplifier spacing L_A must be much smaller than the dispersion length L_D ($L_A << L_D$). This condition is required to keep radiation of dispersive waves negligibly small because the energy of dispersive waves is inversely proportional to the dispersion length L_D.
- The input peak power of soliton must be larger than that of fundamental soliton by a factor

$$\frac{P_s}{P_0} = \frac{G \ln G}{G - 1} \qquad (6\text{-}3)$$

where P_s, P_0 are the peak powers of the path-average soliton and the unperturbed soliton respectively, G is the amplifier gain factor. This condition is to make certain that the average peak power over the L_A is sufficient to balance the GVD effect.

The soliton energy varies periodically in each span due to the fibre loss, hence other parameters of soliton such as the width and the phase also change accordingly. However the soliton still remains unchanged at ultra-long distances if the above conditions are satisfied.

It is impractical to satisfy the first condition when conventional transmission fibres with L_D of about 10 – 20 km are used for the long-haul transmission system [212-213]. If the L_A is short, there are some disadvantages such as high cost and large accumulated ASE noise resulting from compensating a large loss. To facilitate the first condition, a distributed amplification scheme such as Raman amplification can be employed [214-215]. The variation of peak power along each span is considerably reduced by Raman amplification because the amplification process takes place along the transmission fibre, allowing a transmission with $L_A >> L_D$. However an unstable soliton transmission can occur due to the resonance of the dispersive waves and solitons when $L_A / L_D \geq 4\pi$, which needs to be considered carefully in the design of soliton transmission system [216].

6.2.2 Dispersion management

The problem of soliton broadening in lossy fibre can be also overcome by using dispersion-decreasing-fibre (DDF), which has its dispersion decreasing exponentially

corresponding to the attenuation of the fibre. From the variation of soliton amplitude in (6-1), the variation of the GVD in DDF follows a function as

$$\left|\beta_2(z)\right| = \left|\beta_2(0)\right| \exp(-\alpha z) \tag{6-4}$$

Thus the reduction of the GVD is proportional to the reduction of the SPM effect; hence solitons can remain unchanged during propagation in the DDF. However, the use of DDF in practical transmission systems is not feasible because of the availability of the DDF as well as the complexity of the system design. Furthermore, the performance would be degraded because the average dispersion along the link is large. Although this scheme is disadvantageous to the system, it is commonly applied for pulse compression based on soliton effect [217-218].

Therefore, another option is the use of dispersion management which uses alternating positive and negative GVD fibres. This arrangement is commonly employed in high speed transmission systems today because it offers a relatively improvement in performance [219-220]. Hence using periodic dispersion map along the fibre link has attracted extensive attention for its ability in soliton transmission. Both theoretical and experimental research has shown the advantages of dispersion-managed (DM) solitons [221-223]. Owing to alternating the sign of the fibre dispersion in one map period, average GVD of whole link can be kept in small value while the GVD of each section is large enough to suppress the impairments such as four-wave mixing and third order dispersion. Two important parameters of the map are the average GVD of the whole link $\overline{\beta}_2$ and the map strength S_m which are defined as follows [60]

$$\overline{\beta}_2 = \frac{\beta_{2n} l_n + \beta_{2a} l_a}{l_n + l_a}, \qquad S_m = \frac{\beta_{2n} l_n - \beta_{2a} l_a}{\tau_{FWHM}^2} \tag{6-5}$$

where β_{2n}, β_{2a} are the GVD parameters in the normal and anomalous sections of lengths l_n and l_a respectively, τ_{FWHM} is the full width at half of maximum (FWHM) . It has been shown [224] that the shape of DM solitons is closer to a Gaussian pulse rather than a "sech" shape and their parameters such as the width, peak power and chirp vary considerably in each map period. Therefore depending on the map configuration, input parameters of DM solitons should be carefully chosen to ensure that the pulse can recover its state after each map period [225]. In addition, the peak power enhancement of DM soliton compared to the constant-GVD soliton allows an improvement of performance in terms of signal to noise ratio while suppression of timing jitter by reducing the average GVD. Interestingly, it has been confirmed that DM solitons exist not only in anomalous average dispersion ($\overline{\beta}_2 < 0$) but also in normal average dispersion scheme ($\overline{\beta}_2 > 0$) [226]. However the existence of DM soliton in the map with $\overline{\beta}_2 > 0$ is obtained only when the strength of map S_m is greater than a critical value S_{cr} which is approximately 4 [223]. Hence it is not surprising to observe the existence of solitons in the mode-locked fibre laser with normal average dispersion.

Interaction between solitons is an important issue in practice. Because the properties of DM solitons are different from the average-GVD solitons, the evolution and dynamics of DM solitons have become more attractive [227-233]. Theoretical studies have shown that a strong interaction prevents the DM solitons in a positive average GVD map from practical high speed transmission applications, although they can exist [227]. This also indicates a complexity in dynamics of DM solitons in propagation, beside a single soliton solution some complex solutions of DM soliton

can exist in specific dispersion maps. In one study on a high-order DM soliton [228] a stable evolution of antisymmetric (antiphase) solitons occurred along the fibre even for ultra-long distances. Recently, dispersion management has been also proposed to support a transmission of a bisoliton which consists of two DM solitons with zero-(in-phase) or π-(antiphase) phase difference [229]. By selecting appropriate parameters of DM map and input pulse, a stable propagation of in-phase bisoliton for single channel and antiphase bisoliton for WDM has been confirmed through numerical simulation [229]. In other studies, a structure called "soliton molecules" consisting of one dark and two bright solitons, which is similar to an asymmetrical soliton, has been numerically and experimentally demonstrated [230-233].

We can see that the soliton complexes in above studies have a structure similar to pairs of bound solitons generated from the mode-locked fibre lasers. Stable propagation of the soliton complexes can offer new coding schemes for soliton transmission systems. In conventional coding scheme, data bits "1" or "0" is represented by presence or absence of a soliton pulse in each time slot. In one proposal, using the soliton complex such as bisoliton for new coding scheme provides code states with a redundant bit for error prevention [229]. Therefore it is necessary to have a new optical source which can generate the complex soliton like a bisoliton, for new coding schemes. With ability of multi-bound solitons generation, the actively FM-MLFRL offers more states for coding scheme that allows an improvement of performance and transmission of more than one data bit in each time slot. Hence the propagation characteristics of multi-bound solitons generated from the actively FM mode-locked fibre laser is of significant for potential applications of multi-bound soliton lasers in telecommunication systems.

6.3 TRANSMISSION OF MULTI-BOUND SOLITONS

6.3.1 Experimental setup

To investigate the propagation dynamics of multi-bound solitons, various multi-bound solitons with ultra-high stability from dual- to quintuple- states are generated by carefully optimizing the locking conditions of the fibre ring. These states are then propagated through standard single mode optical fibres (SSMF) to investigate their propagation dynamics, as shown in Figure 6-1. The length of the fibre is varied to prove the interaction between the soliton pulses. The estimated full width half-maximum (FWHM) of individual pulse of original dual-bound soliton (DBS), triple-bound solitons (TBS) and quadruple-bound solitons (QBS) are 7.9, 6.9 and 6.0 ps respectively. The time separation between two adjacent pulses is about 3 times of FWHM pulse width. The repetition rate of these multi-bound soliton sequences is about 1 GHz.

In this setup, a booster EDFA is used before the transmission section to specify the power of multi-bound solitons launched into the SSMF. Through adjustment of the launched power, the multi-bound solitons can propagate under various transmission conditions from linear to nonlinear schemes. Two rolls of standard single mode fibre with lengths of 1 km and 50 km are used for the investigation. After propagation, the outputs such as time trace and spectrum are monitored by the oscilloscope and the OSA respectively.

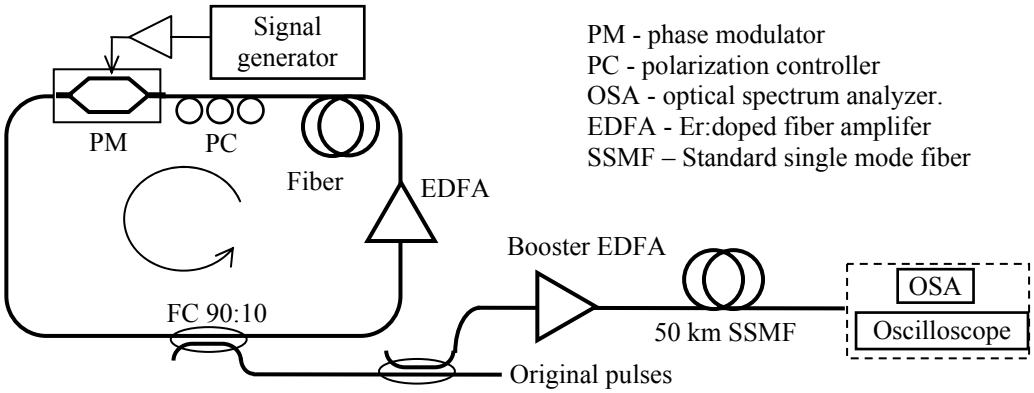

Figure 6-1 Experimental setup for propagation of multi-bound solitons in standard single fibre.

6.3.2 Results and discussion

It is obvious, but worth mentioning, that the binding property of the solitons circulating in the fibre ring, is different under the case when they are propagating through the optical fibre. In the propagation these individual solitons would be interacting with each other and naturally they are no longer supported by periodic phase modulation as when circulating in the ring laser. When propagating through a dispersive fibre, the optical carrier under the envelope of generated multi-bound solitons are influenced by the chirping effects, thence the overlapping between the soliton pulses. When the accumulated phase difference of adjacent pulses is π, the solitons repel each other [173-175]. In other words, the solitons in their multi-bound states acquire the down chirping effect when propagating in SSMF due to its group velocity dispersion (GVD) induced phase shift. Hence, within the group of multi-bound solitons the front-end soliton would travel with higher positive frequency shift, thus higher group velocity than those at back-end of the multi-bound group which is influenced with lower negative frequency shift. Therefore, the time separation between adjacent pulses varies with the propagation distance. The variation of the time separation between pulses depends on their relative frequency difference. Figure

6-2 shows the waveforms and their corresponding spectra of triple-bound solitons after propagating over 50 km fibre with different launched powers.

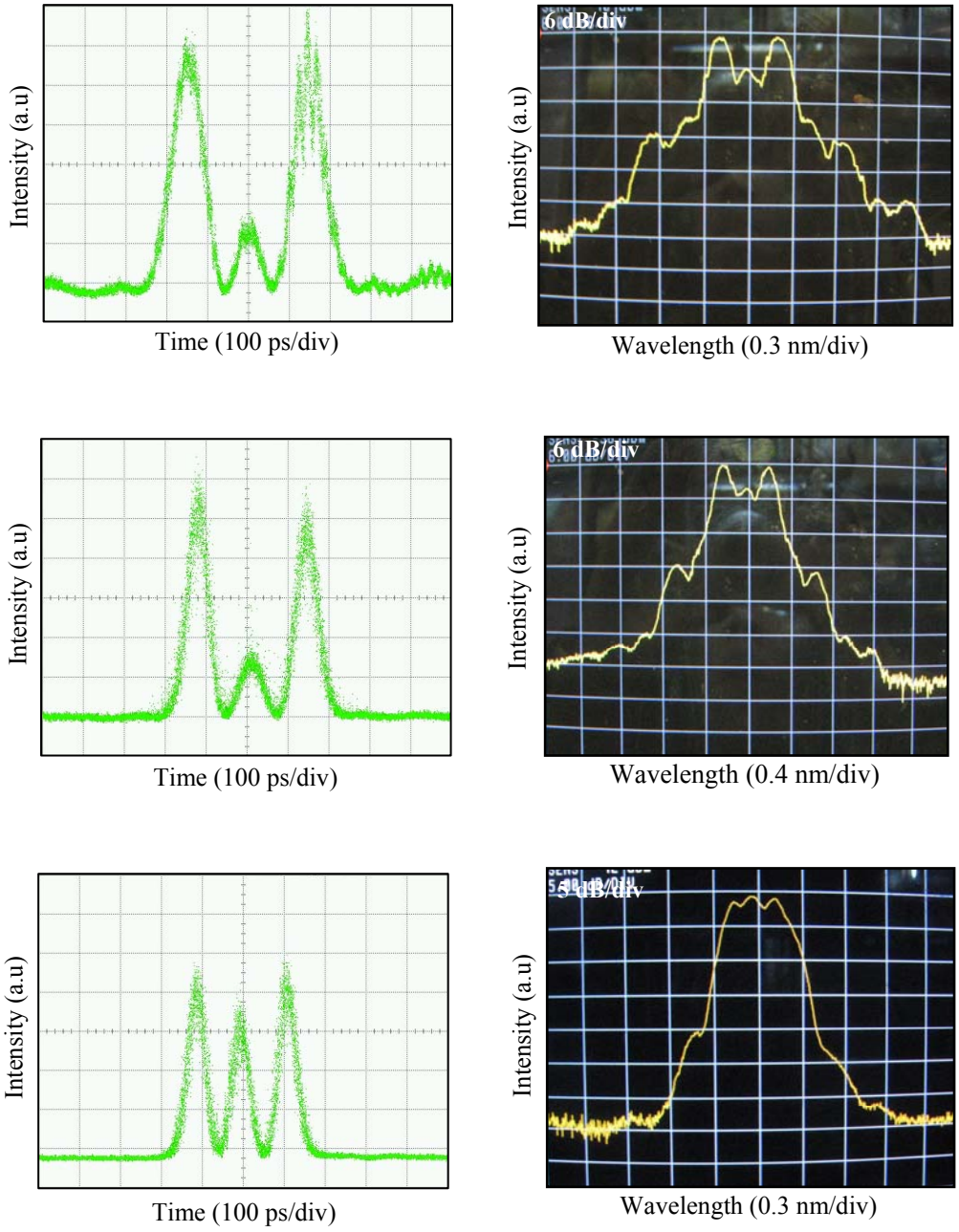

Figure 6-2 The waveforms and corresponding spectra of the triple-bound soliton at launching powers of (a-d) 4.5 dBm ($P_l < P_{sol}$), (b-e) 10.5 dBm ($P_l < P_{sol}$) and (c-f) 14.5 dBm ($P_l > P_{sol}$) respectively.

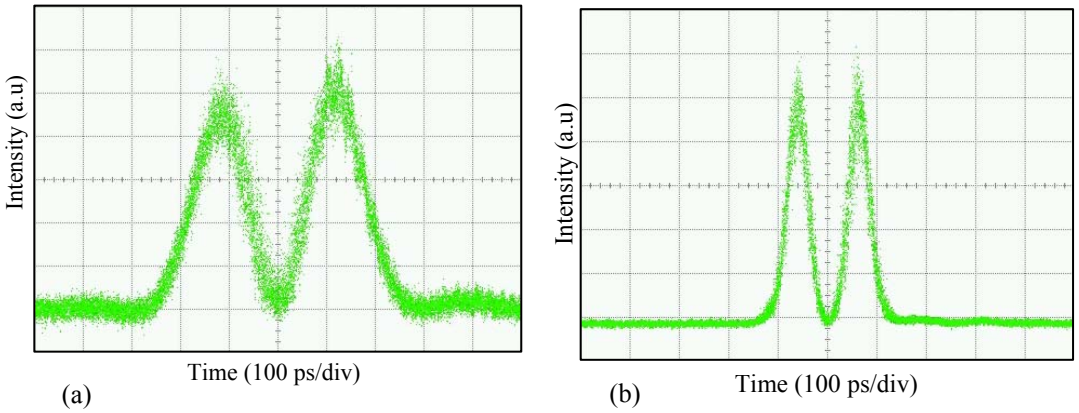

Figure 6-3 The waveforms of the dual-bound soliton at launching powers of (a) 4.5 dBm ($P_l < P_{sol}$), and (b) 17 dBm ($P_l > P_{sol}$) respectively after propagating through 50 km SSMF.

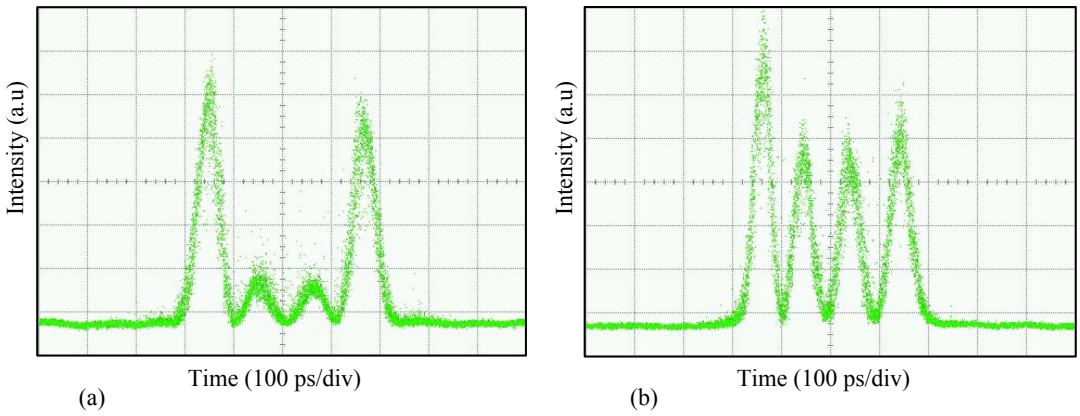

Figure 6-4 The waveforms of the quadruple-bound soliton at launching powers of (a) 5 dBm ($P_l < P_{sol}$), and (b) 16.5 dBm ($P_l > P_{sol}$) respectively after propagating through 50 km SSMF.

In all cases, the time separation significantly increases compared to the initial state due to the repulsion. In the ideal condition of propagation, direct interaction is the only factor that influences to the time position and the pulse shape of solitons in bound states. However, propagation in a real optical fibre is considerably influenced by perturbations such as loss of fibre and the initial launched powers (P_l) of solitons. The loss of fibre always leads to the broadening of bound solitons. Figure 6-5(a) and (b) shows the dependence of pulse width and temporal separation of various multi-bound solitons with the launched power as a parameter. We observe similar dynamics

in the propagation of dual, quadruple and quintuple groups of solitons. In general, an increase in launched power leads to a enhanced shortening of the pulsewidth or a broadening of bound solitons at lower rate, thence a reduction of the pulse temporal separation due to the enhancement of nonlinear self-phase-modulation phase shift. Unlike the nearly linear variation of the pulsewidth, curves of the temporal separation show a nonlinear dependence on launch power. As observed in Figure 6-5(b), two distinct areas of the curves can be observed as separated at points A, B and C. The intersection points A, B, C of the two tangential curves corresponds to the average soliton power (P_{sol}) of the bound state. On the other hand, the points A, B & C correspond to the minimum powers to launch the bound pulses for soliton propagation. For the transmission over standard single mode fibre, it is observed that with the experimental parameters of the multi-bound solitons, the estimated average soliton powers for DBS, TBS and QBS are 11, 13.5 and 15.2 dBm respectively.

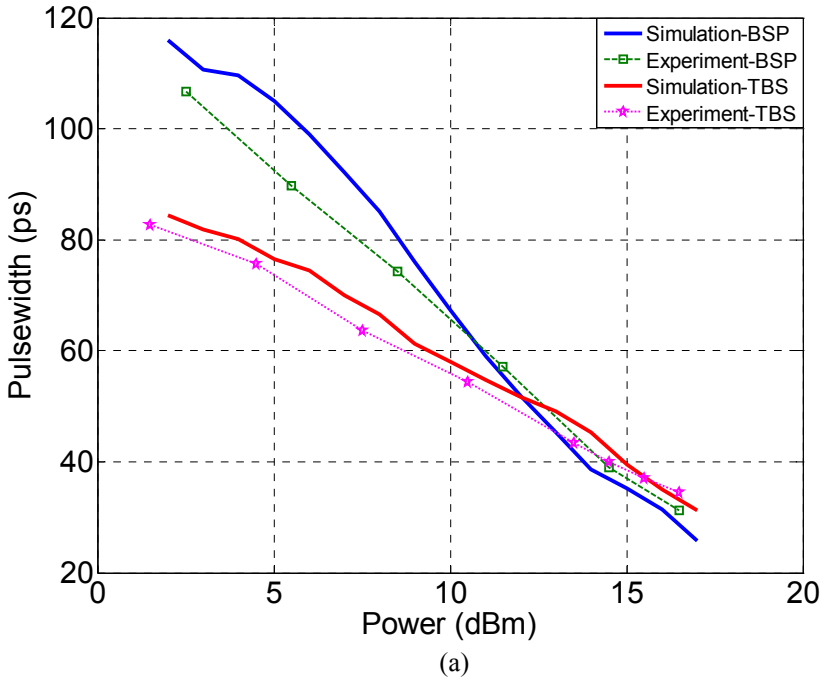

(a)

Figure 6-5 The launching power dependent variation of (a) pulsewidth, and (b) time separation, and (c) peak power ratio of different multi-soliton bound states after 50 km propagation distance.

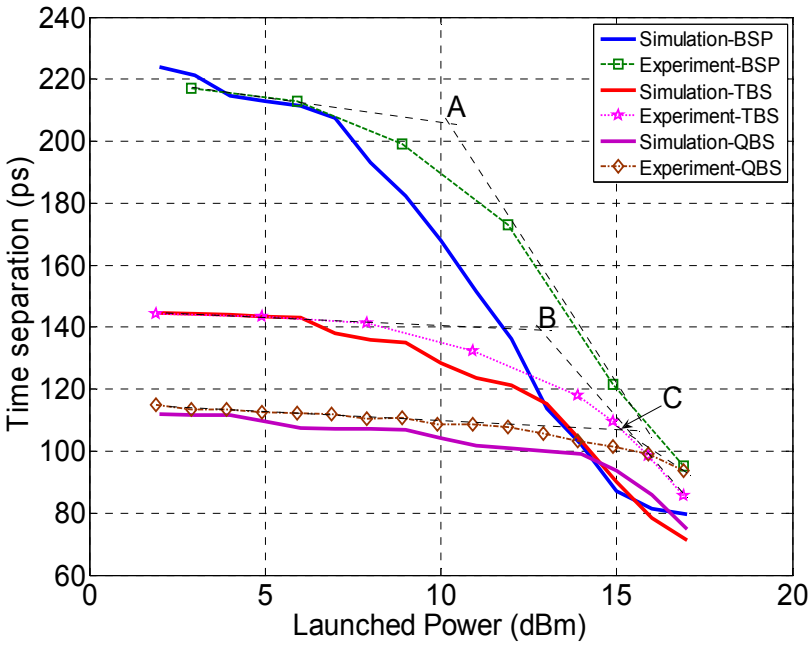

(b)

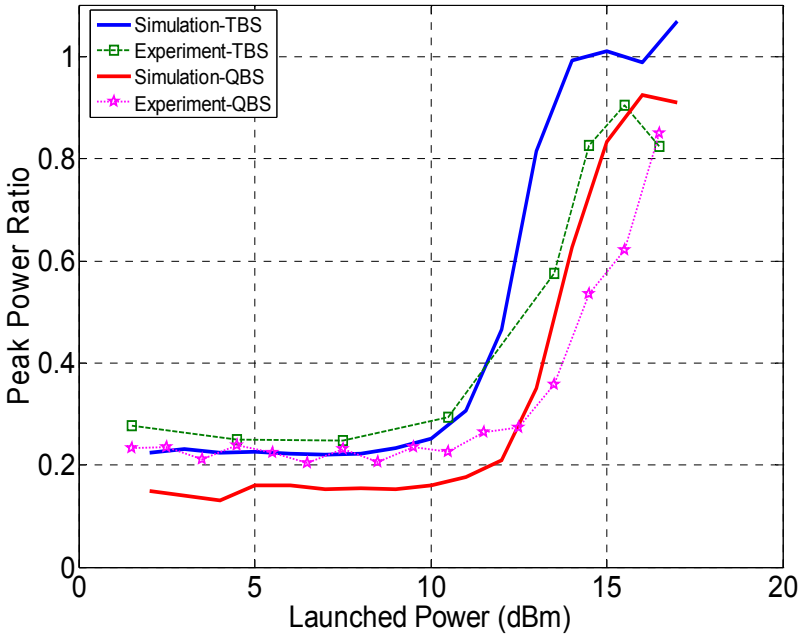

(c)

Figure 6-5 Continued.

At P_l lower than P_{sol}, and in addition to the fibre attenuation, the power of multi-bound soliton is not sufficient to balance the GVD effect. As a result, the pulse widths are rapidly broadened by self- alignment of the multi-bound solitons due to the perturbations accompanied by partly shading their energy in form of dispersive waves

[60]. The broadening of such dispersive wave is accumulated along the transmission fibre and oscillations are formed around the multi-bound solitons as shown by the ripple of the tail of the soliton group in Figure 6-2(a1). Furthermore, the rate of broadening of the pulses is faster than that of the temporal separation at low launched powers leading to the enhancement of the overlapping between pulses. Therefore, the pulse envelope is consequently modulated by the interference of waves with the phase modulation effect due to the GVD that is the same as the fractional temporal Talbot effect [234-235]. Because of the parabolic symmetry of the anomalous GVD-induced phase shift profile around multi-bound solitons with a relative phase difference of π, the energy of the inner pulses is shifted to the outer pulses, hence decreases of the amplitude of inner pulses. The frequency components of the inner pulses obtain a higher relative velocity or propagate faster than those of the edge pulses that result in the energy transfer from the inner to the outer. This pattern also reconfirms the relative phase difference of π in the bound state.

In contrast, at $P_l > P_{sol}$, the multi-bound states operate in nonlinear transmission scheme where the solitary waves are supported because the SPM phase shift is increased to balance the GVD effect. The pulse width becomes narrower and the ripple of the pulse envelope is lower with higher level of launched power. For the dual-bound soliton, there is no difference in peak power of two pulses in bound state. For the bound states with the number of solitons greater than two, however, there is high difference between the inner and the outer pulses because of the energy transfer at $P_l < P_{sol}$. Owing to the soliton content in pulses is enhanced at the average soliton power, hence there is a jump of peak power ratio between inner and outer pulses as shown in Figure 6-5(c).

6.4 DYNAMICS OF MULTI-BOUND SOLITONS IN TRANSMISSION

To verify the experimental results as well as to identify the evolution of multi-bound solitons propagation in the fibre, we model the multi-bound solitons as [236]

$$u_{bs} = \sum_{i=1}^{N} u_i(z,t) \tag{6-6}$$

with N is number of solitons in bound state, and

$$u_i = A_i \, sec\, h\{[t - iq_0]\} \, exp(j\theta_i), \tag{6-7}$$

where A_i and q_0 are amplitude and time separation of solitons respectively and the phase difference $\Delta\theta = \theta_{i+1} - \theta_i = \pi$. The propagation of multi-bound solitons in SSMF is governed by the nonlinear Schrödinger equation with the input parameters as those obtained from the experiment. Shown together with experimental results in Figure 6-5 (a)-(c) is the simulation evolution of the parameters (solid curves) over 50 km propagation of various orders of multi-soliton bound states. The simulated evolution of the triple-bound soliton is shown in Figure 6-6 over 50 km SSMF, while Figure 6-7 shows the pulse shape and corresponding spectrum of the outputs at various launched power levels. The simulated results generally agree well with those obtained in the experiment (see Figure 6-2 and Figure 6-5 for comparison). The small residual chirp caused small difference between the experimental and numerical results.

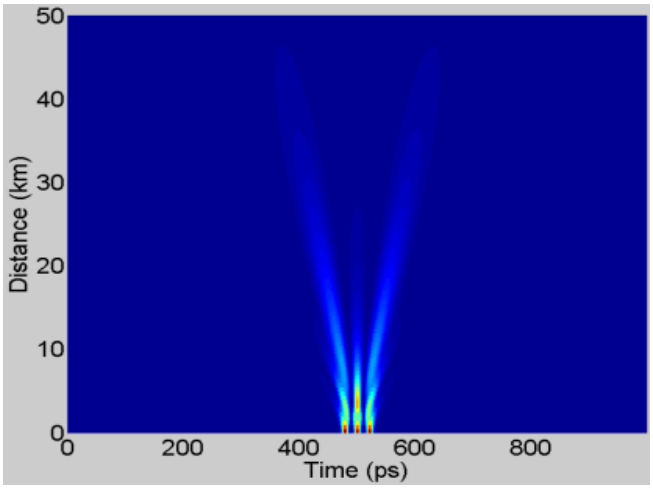

(a)

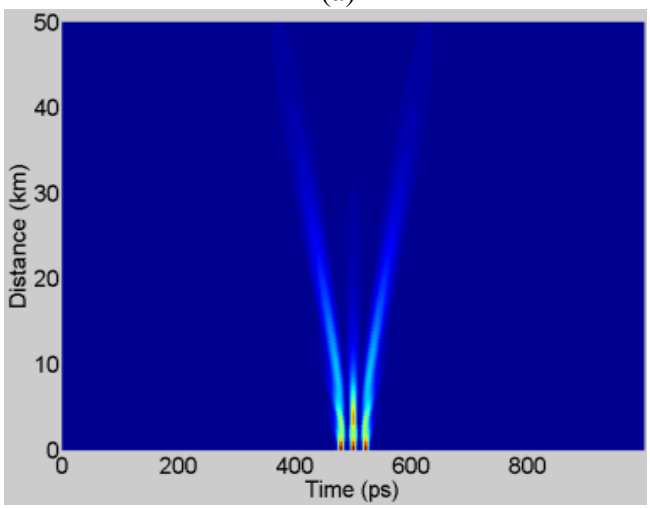

(b)

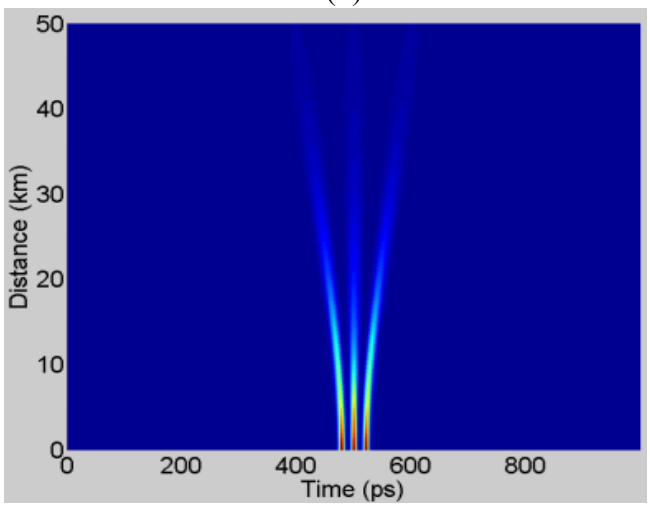

(c)

Figure 6-6 Numerically simulated evolutions of the triple-bound soliton over 50 km SSMF propagation at P_1 of respectively (a) 5 dBm, (b) 10 dBm and (c) 14 dBm

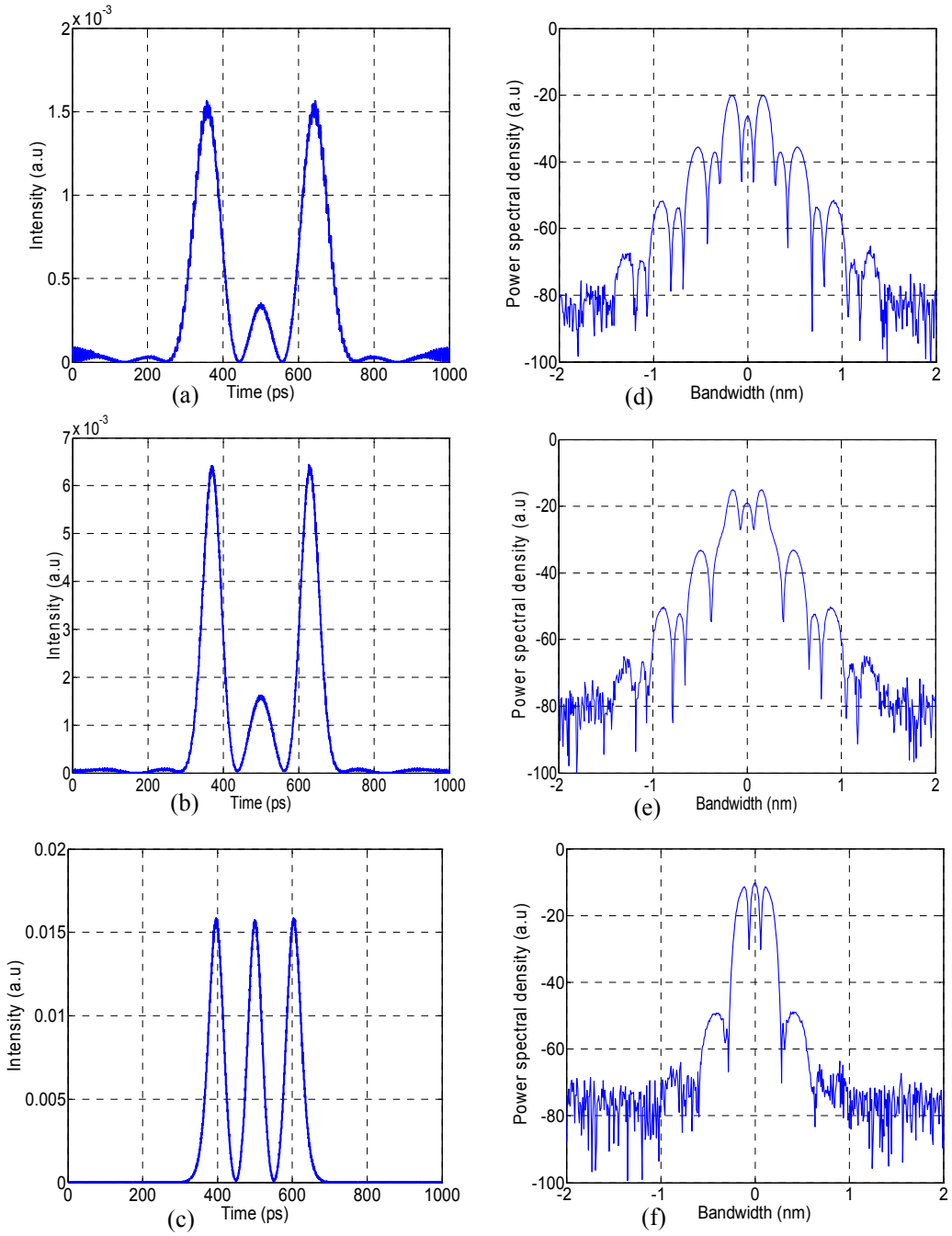

Figure 6-7 Row (a) Numerically simulated output pulse shape and Row (c) optical spectrum of triple-soliton bound state over 50 km SSMF propagation at P_1 of respectively 5 dBm, 10 dBm and 14 dBm.

The simulated dynamics of multi-bound solitons consisting of DBS and TBS during propagation are shown from Figure 6-8 to Figure 6-9. In each figure the evolution of multi-bound solitons parameters such as the pulse width, the temporal separation between solitons, the ratio between the pulse width and the pulse

separation and the peak power of the solitons, is simulated along the transmission fibre with different launched powers. The difference between lower and higher launching powers also obviously exhibit in simulated results. When the launched powers is far from the soliton power P_{sol}, there is oscillation or rapid variation of parameters at initial propagation distance due to the adjustment of multi-bound solitons to perturbations of propagation conditions as mentioned above. The pulses are compressed at P_ls higher than P_{sol}, while they are rapidly broadened at P_ls lower than P_{sol}. The slow variation of parameters occurs at P_l close to P_{sol}. However, the time separation of solitons remains unchanged in the propagation distance of one soliton period. We have validated this prediction in our experiment by using 1 km SSMF for transmission.

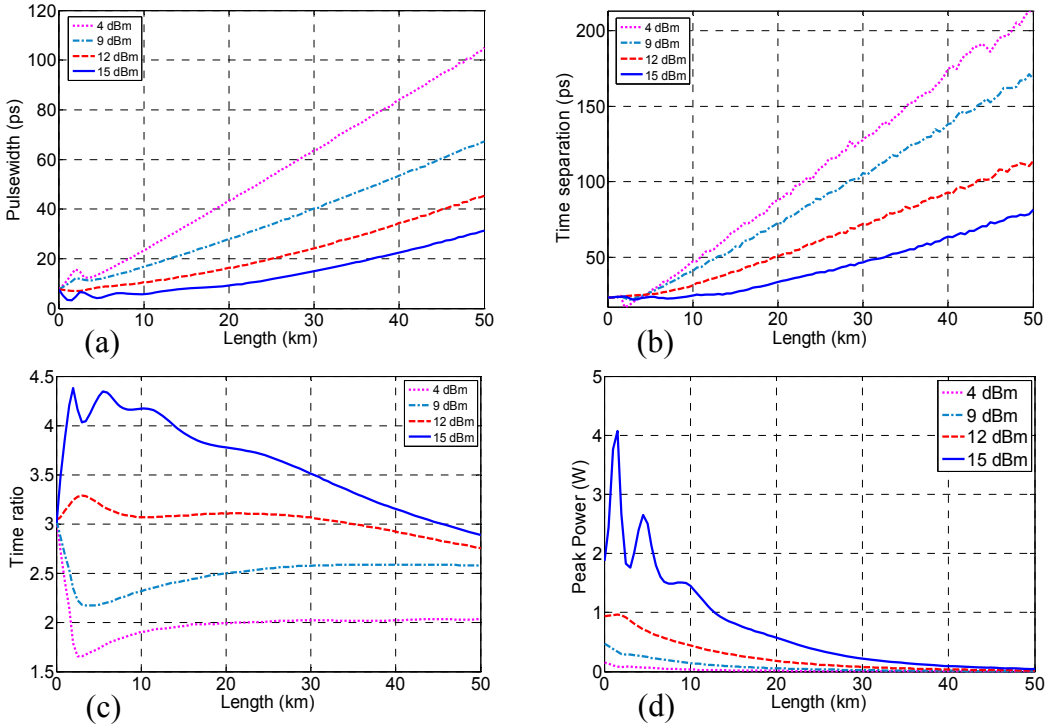

Figure 6-8 Evolution of numerically simulated dual-soliton bound state after 50 km propagation distance of SMF-28 fibre: (a) pulse width, (b) temporal separation, (c) ratio between pulse width and separation, and (d) peak power.

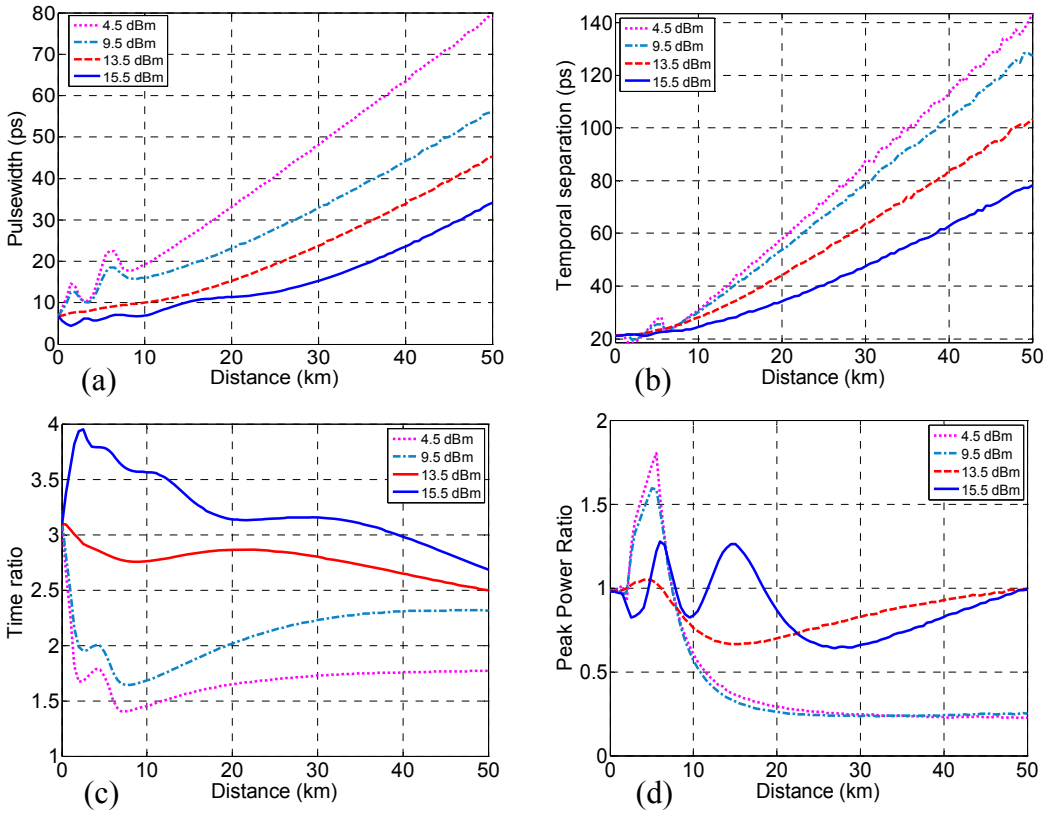

Figure 6-9 Evolution of numerically simulated triple-soliton bound state after 50 km propagation distance of SMF-28 fibre: (a) pulse width (b) temporal separation (c) ratio between pulse width and separation (d) peak power ratio between inner pulse and outer pulse.

Another important property of multi-bound solitons is the phase difference between the pulses that can be determined by the shape of the spectrum. We have monitored the optical spectrum of the multi-bound solitons at both the launched end and the output of the fibre length. The modulated spectrum of multi-bound solitons is symmetrical with carrier suppression due to a relative phase relationship of π between adjacent solitons. After 50-km propagation at low P_l, both experimental and simulated results show that the spectrum of multi-bound solitons is nearly same as that at the launched end (see Figure 6-2(d) and Figure 6-7(d)). In a linear-like scheme where the SPM effect is negligible, the GVD only modulates the spectral phase which modifies the temporal profile, but does not modify the spectrum of the bound state. The

modulation of spectrum is modified with increase in P_l. At sufficient high P_l, the nonlinear phase shift induced chirp is increased at the edges of pulses. Although, the nonlinear phase shift reduces the GVD effect, the phase transition between adjacent pulses is changed due to direct impact of the nonlinear phase shift. Hence the small humps in the spectra of multi-bound states are strengthened and they may be comparable to main lobes due to enhancement of the far interaction between pulses as shown in Figure 6-2(f) and Figure 6-7(f). Figure 6-10 shows the variation of the relative phase difference between adjacent pulses in various multi-bound soliton states over 50 km propagation. The simulated results also indicate that the relative phase difference varies differently between two adjacent pulses in propagation. Although the phase difference of π between two central pulses in even-soliton bound states such as DBS and QBS can remain unchanged, it varies in general along propagation distance. At low P_l in all cases, the phase difference is varied to zero or π/2 value, then recovered to π at the output of the 50-km fibre. When the SPM phase shift becomes significant, the phase difference varies in the same manner in the first 40 km propagation, and then it tends to π/2 that modifies the corresponding spectrum.

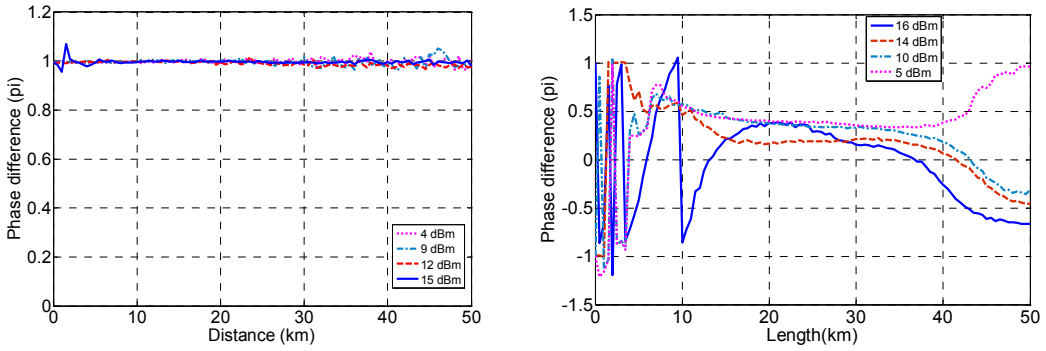

(a) (b)

Figure 6-10 Evolution of the phase difference between adjacent pulses over 50 km propagation in various bound states: (a) dual-bound soliton, (b) triple-bound soliton.

6.5 CONCLUDING REMARKS

Characteristics of multi-bound soliton in propagation over 50 km SSM fibre have been investigated in this chapter. Depending on the launched power level, the variation of multi-bound states parameters can divide into two propagation schemes: linear and soliton schemes. At low launched power in linear propagation scheme, the modulated spectrum of multi-bound states remains unchanged due to the preservation of the phase difference of π, yet the temporal shape is modified that can be used to reconfirm the phase difference. At high launched power in soliton propagation scheme, the modulated spectrum of multi-bound states is modified due to the enhancement of SPM effect; however, the pulses in bound state behave similarly to the single soliton transmission in perturbed conditions.

However, the time separation between pulses can remain unchanged at distances shorter than the soliton period. Thus it is possible to remain the binding of solitons in a DM fibre transmission link where the dispersion length is longer than the length of span. Therefore, multi-bound solitons generated from the FM-MLFRL are potentially new data coding sources for communication systems, but require further study.

Chapter 7

Bispectrum estimation and photonic signal processing

7.1 BISPECTRUM OF MULTI-BOUND SOLITONS

7.1.1 Bispectrum

In signal processing, the power spectrum estimation showing the distribution of power in frequency domain is a useful and popular tool to analyse or characterise a signal or process, however the phase information between frequency components is suppressed in the power spectrum. Therefore it is necessarily useful to exploit higher order spectra known as multi-dimensional spectra instead of the power spectrum in some cases, especially in nonlinear processes or systems [93-94]. In contrast to the power spectrum, the Fourier transform of higher-order autocorrelations gives multi-dimensional spectra, hence they provide us with the phase information [94].

In particular, the two-dimensional spectrum also called bispectrum is, by definition, the Fourier transform of the triple correlation, or the third order statistics [94]. For a signal *x(t)* its triple-correlation function C_3 is defined as:

$$C_3(\tau_1,\tau_2) = \int x(t)x(t-\tau_1)x(t-\tau_2)dt \qquad (7\text{-}1)$$

where τ_1, τ_2 are the time-delay variables. Thus the bispectrum can be estimated through the Fourier transform of C_3 as follows

$$B_i(f_1, f_2) \equiv F\{C_3\} = \iint C_3(\tau_1, \tau_2) \exp(-2\pi j(f_1\tau_1 + f_2\tau_2)) d\tau_1 d\tau_2 \qquad (7\text{-}2)$$

where $F\{\}$ is the Fourier transform, and f_1, f_2 are the frequency variables. From the definitions (7-1) and (7-2), both the triple-correlation and the bispectrum are represented in a 3D graph with two variables of time and frequency respectively. Figure 7-1 shows the regions of power spectrum and bispectrum respectively and their relationship. The cut-off frequencies f_c are determined by intersection between the noise and spectral lines of the signal. These frequencies also determine the distinct areas which are basically bounded by a hexagon in bispectrum. The area inside the hexagon shows the relationship between frequency components of the signal only, otherwise the area outside shows the relationship between the signal components and noise. Due to a two-dimension representation in bispectrum, the variation of the signal and the interaction between signal components can be easily identified.

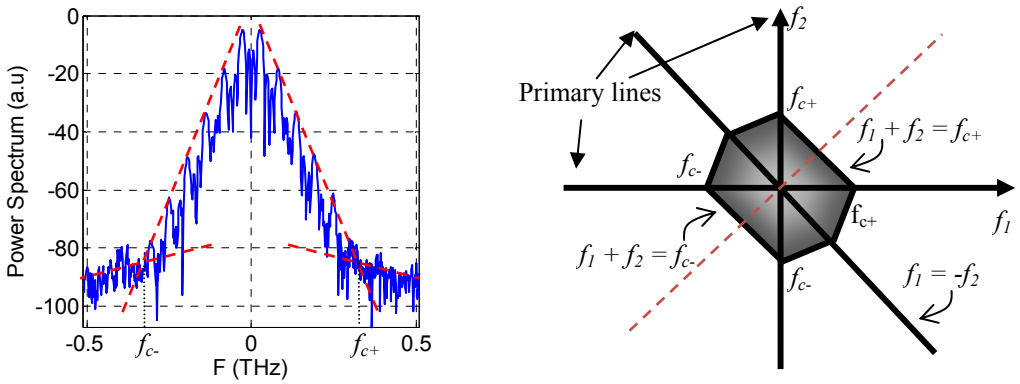

Figure 7-1 A description of (a) power spectrum regions and (b) bispectrum regions for explanation.

Because of unique features of the bispectrum (See Appendix C for more details), it is useful in characterizing the non-Gaussian or nonlinear processes and applicable in many various fields such as signal processing [93-94], biomedicine [237] and image reconstruction [238-239]. Extension of number of representation

dimensions makes the bispectrum become more easily and significantly in representation of different types of signals and differentiation of various processes, especially nonlinear processes such as doubling and chaos. Hence multi-dimensional spectra is proposed as a useful tool to analyse the behaviours of signals generated from these systems such as multi-bound solitons, especially transition states in formation process of multi-bound solitons. This section will illustrate that the triple-correlation and bispectrum reveal certain features of the pulse train that cannot be easily seen by autocorrelation method.

7.1.2 Various states of bound solitons

For multi-bound solitons, the optical power spectrum is modulated with the appearance of main lobes and sub-lobes due to the phase relationship between bound pulses as demonstrated in Chapter 3. Therefore, various multi-bound states generated from the FM mode-locked fibre laser can be distinguished by the optical power spectrum analysis. However, as a result the bispectrum of each multi-bound soliton state obviously exhibits a distinct structure for characterization. In this section, various multi-bound solitons in steady state obtained from simulation are used to estimate their bispectra. Moreover, some interesting information of the MBS can be obtained from the bispectrum.

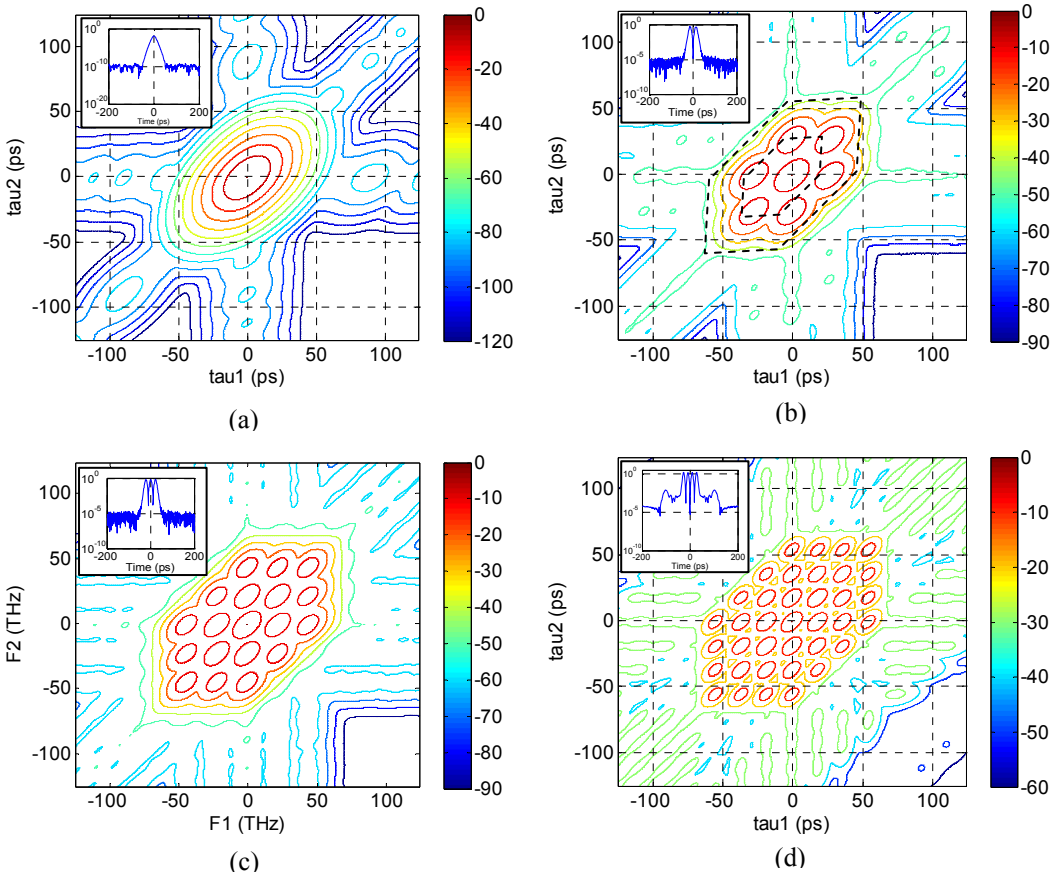

Figure 7-2 Triple-correlations in contour plot view of various bound soliton states: (a) Single soliton, (b) dual-bound solitons, (c) triple-bound solitons and (d) quadruple-bound solitons respectively. (Insets: The temporal waveforms in logarithm scale showing the enhancement of the pedestal in higher order multi-bound solitons).

Firstly, the triple-correlations of various multi-bound solitons are calculated as shown in Figure 7-2. The triple-correlation of a pulse can be represented by the elliptical contour lines corresponding to its magnitude as shown in Figure 7-2(a). Depending on the number of solitons in the bound state, the triple-correlation of the multi-bound soliton is represented by the layers of elliptical contour lines bounded in a hexagon as shown in Figure 7-2(b)-(d). The quality and symmetry of pulses can be reflected by the uniformity of the ellipsis in the same layer. In the triple-correlation, the presence of pedestals, which is commonly characterized by the high dynamic

range autocorrelation measurement [240], can be easily observed by the contour lines outside the hexagon. As shown in Figure 7-2(d), when the gain is enhanced in the cavity for the higher multi-bound state, the pulses are not only shortened but also possibly degraded by the increase in pedestal energy which is proportional to the level of the lines outside the hexagon area.

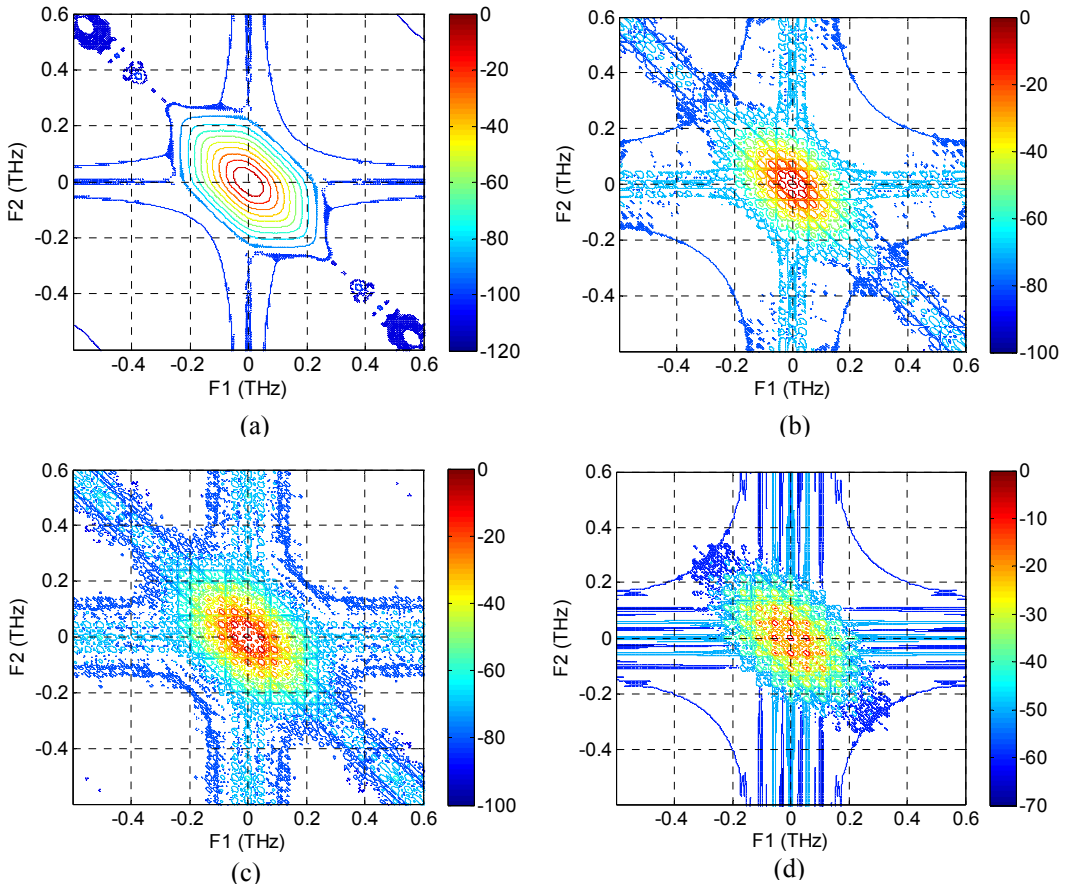

Figure 7-3 The magnitude bi-spectra in logarithm scale of different multi-bound soliton states: (a) single soliton, (b) dual-bound solitons, (c) triple-bound solitons and (d) quadruple-bound solitons respectively.

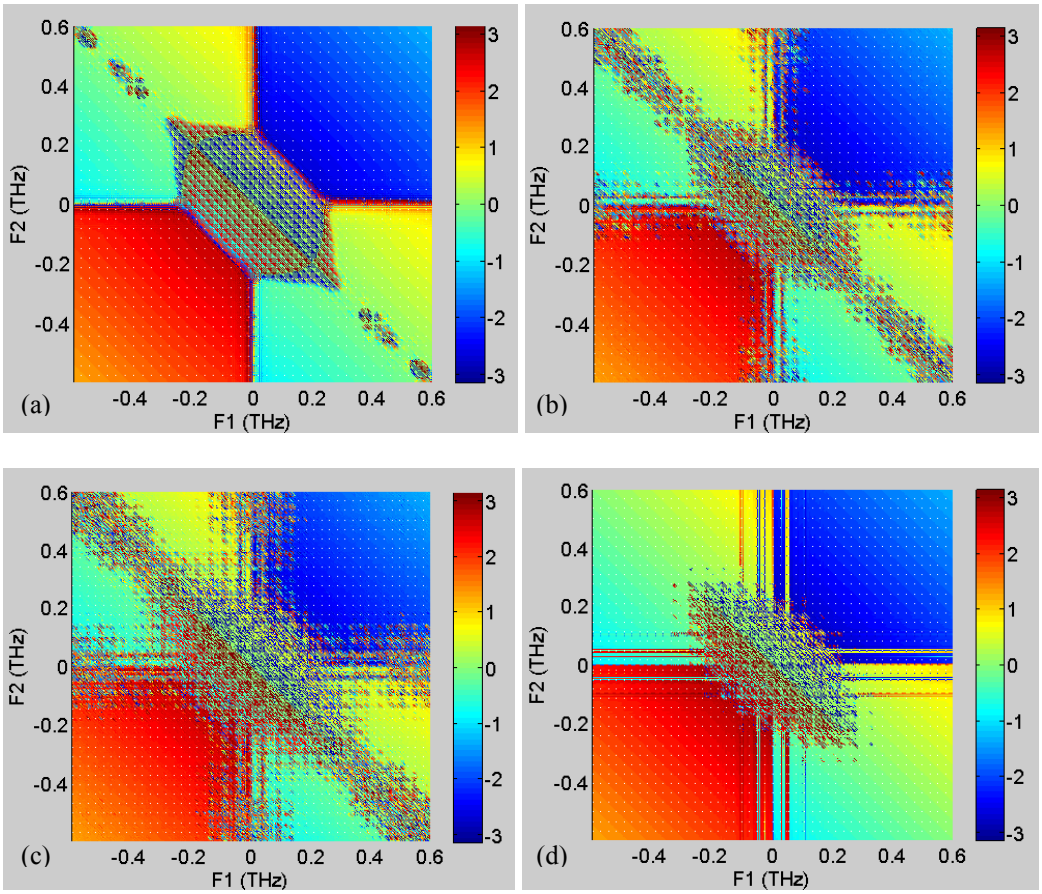

Figure 7-4 The phase bi-spectra of different multi-bound soliton states: (a) single soliton, (b) dual-bound solitons, (c) triple-bound solitons and (d) quadruple-bound solitons respectively.

The Fourier transform of the triple-correlations results in the bispectra of multi-bound solitons which consist of the magnitude and the phase representations. Figure 7-3 shows the magnitude in contour plot view of different multi-bound soliton states with π phase difference which circulate stably in the FM mode-locked fiber laser cavity. In single soliton state only, the magnitude bispectrum contour is only closed contour lines inside the area bounded by the hexagon as shown in Figure 7-3(a). Whilst the bispectra of higher order bound solitons from dual- to quadruple bound states exhibit a periodic structure inside this area as shown in Figure 7-3(b)-(d). Depending on the number of pulses in bound states, the periodic structures of both phase and magnitude spectra vary correspondingly. When number of pulses in bound

state increases the periodic structure of its bispectra becomes more sophisticated because the interactive relationship between sidelobes or various frequency components. Moreover, the hexagonal area in bispectrum that is broader at higher order bound state reflects the bandwidth of the signal which is broadened by the pulse compression due to the enhancement of the gain or power in the fibre cavity. Similar to the observation in the triple-correlation, the stability of the bound states also exhibits obviously in the bispectrum. A lower stability of higher order bound states is shown by the blurred contour lines inside the hexagon and the enhancement of the contour ridges outside the hexagon.

The phase bispectra provide additional information about status and quality of the bound state. Figure 7-4 shows the phase bispectra of various soliton states from the single pulse to quadruple-pulse. For the phase bispectrum, with periodic phase variation of a stable state in frequency domain is easily exhibited in two dimensions. The sharply periodic structure of phase bispectrum inside the hexagon with two distinct regions which are complex conjugate of each other and separated by the line $f_1=-f_2$ as shown in Figure 7-4(a) indicates high stability of the single soliton state. On the other hand, the periodic structure of stable multi-bound state is corrupted by the change in operating conditions of multi-bound state such as gain, noise level in the fibre cavity. At higher order bound soliton state, the phase variation in the bispectrum is more blurred in the hexagon, however two conjugate regions can be still obviously identified.

7.1.3 Transitions in multi-bound soliton formation

One of important advantages of the bispectrum representation is to differentiate the linear and nonlinear responses or processes, therefore it is specially useful in

analysing the transition processes from the noise to the steady state or from the unstable state to the stable. In transition processes of multi-bound soliton, the signal experiences strong fluctuations in phase and magnitude like a chaotic state before reaching to a new steady state. Therefore, the average bispectrum of these processes also exhibit clearly the variation in terms of both phase and magnitude, which can be used to analyse multi-bound soliton at this stage. One of the most important transition processes is the formation of multi-bound solitons from the noise in the fibre cavity which has been numerically investigated in Chapter 4. The evolution of the signal from the noise into the multi-bound solitons can be split into three stages in which the first stage is the process that the noise builds up into the pulses, yet the amplitude and phase of the signal fluctuate strongly during circulating inside the cavity like a chaotic state. In order to analyse this stage, the bispectrum is averaged over the first 1000 round trips in the evolution of the multi-bound soliton formation which was simulated in Chapter 4. Figure 7-5 shows the magnitude and phase bispectra of the dual-bound soliton and the triple-bound soliton evolutions respectively. For the case of dual-bound soliton, the bispectra in Figure 7-5(a)-(b) show non-periodic structure in a hexagon with small area that corresponds to the rapid variation of magnitude and phase of the signal from roundtrip to roundtrip. In particular, the phase structure shows a uniform distribution indicating an independence of the frequency components in the signal envelope because the signal behaviour in this stage is similar to a chaotic state. While the magnitude bispectrum for the case of the triple-bound soliton shows the closed contours in low frequency region and the phase bispectrum has a periodic structure due to the existence of two dominant short pulses in this first stage. However the state of these two pulses is unstable that expresses by the ridges in the hexagon of

the magnitude bispectrum and the unclarity of two distinct regions in phase structure of the bispectrum.

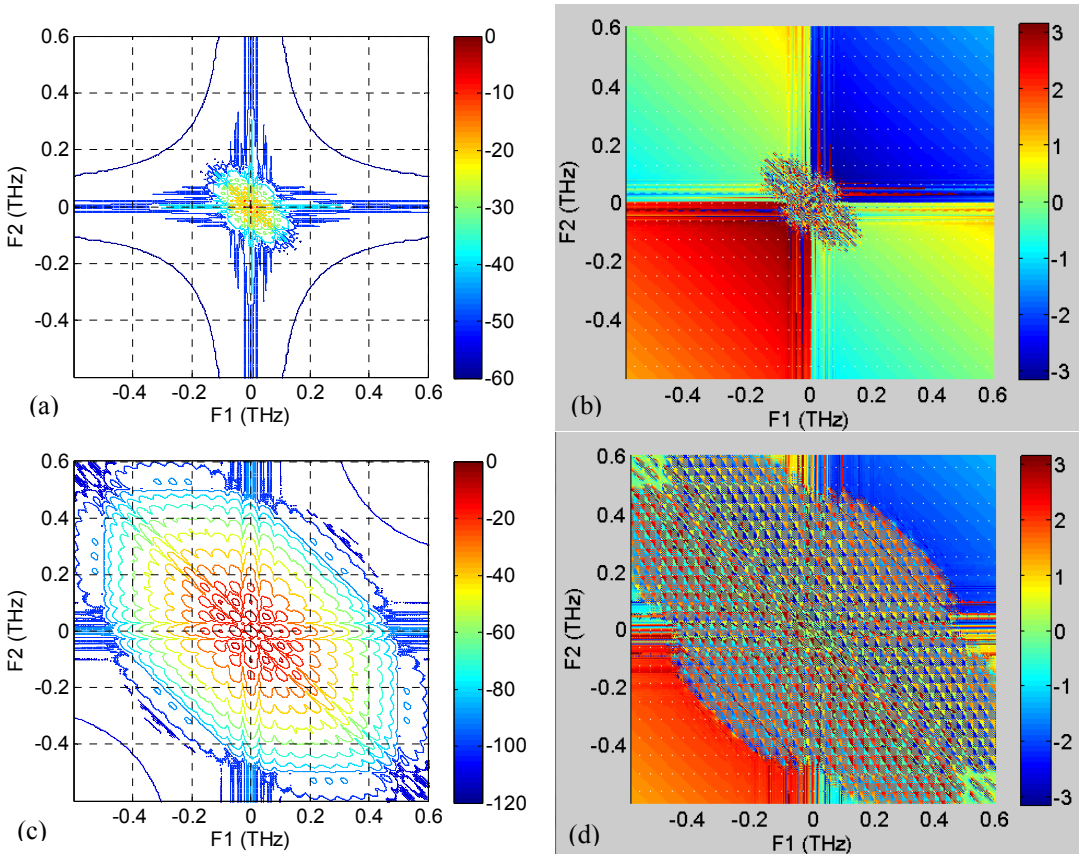

Figure 7-5 Magnitude and phase bispectra averaged over 1000 roundtrips of evolution of the signal at the first stage in formation process from the noise of various multi-bound solitons: (a)-(b) Dual-bound soliton, and (c)-(d) Triple-bound soliton.

The second stage in next 1000 round trips is the process that the built-up pulses interact and bind together to form the multi-bound soliton. For the evolution of dual-bound soliton, therefore the elliptical contours in magnitude bispectrum and the periodic structure in phase bispectrum in this stage appear obviously because of the presence of periodic components as shown in Figure 7-6(a)-(b). The structure of closed contours in magnitude bispectrum becomes finer and extended due to the appearance of three solitons in the evolution of triple-bound soliton as shown in

Figure 7-6(c). However the bound state in this stage is unstable during circulating in the cavity because the operating condition such as gain factor is not optimized. Hence, the contamination in phase bispectra still exists and the structure of ridges is dominant in the hexagon of the magnitude spectra. The transition process between different bound states due to the change in operating conditions behaves similar to the evolution in this stage which is easily identified by the bispectral representation. When the fluctuations of multi-bound soliton occurs, the periodic lines of bispectrum at that process are varied and smeared, before another periodic structure of the bispectrum is formed when a new stable state is established.

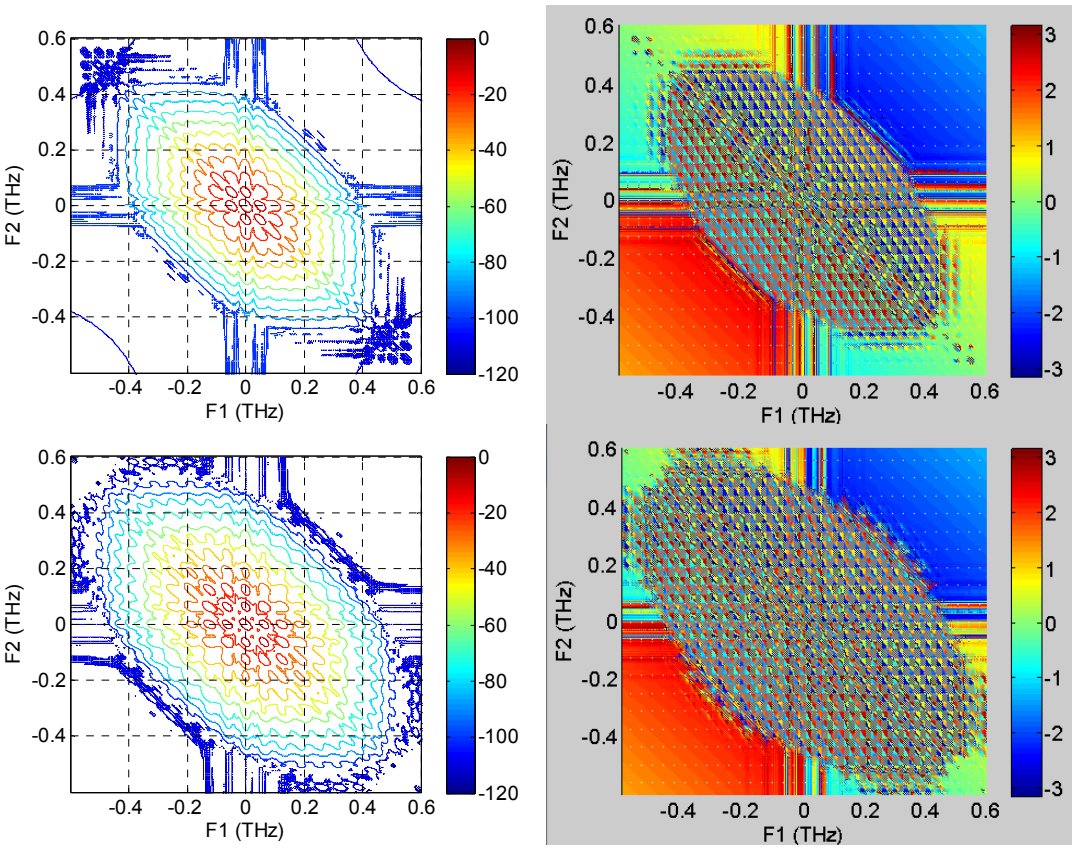

Figure 7-6 Magnitude and phase bispectra averaged over 1000 roundtrips of evolution of the signal at the second stage in formation process of various multi-bound solitons: (a)-(b) Dual-bound soliton, and (c)-(d) Triple-bound soliton.

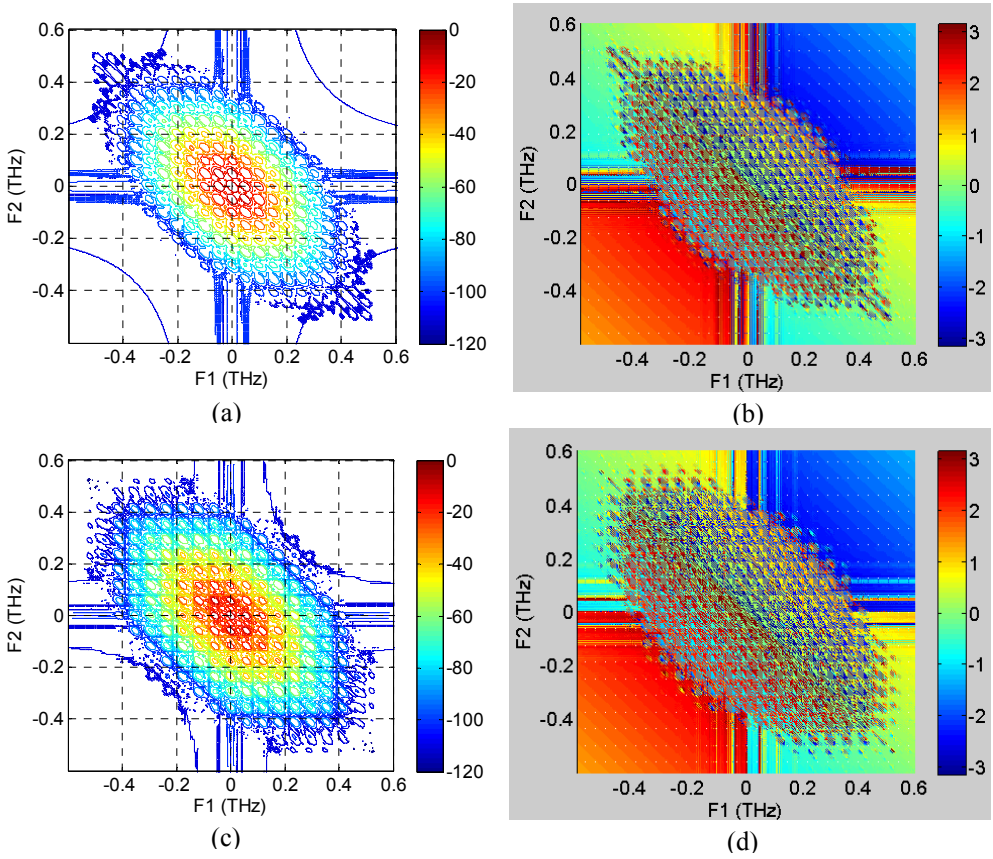

Figure 7-7 Magnitude and phase bispectra averaged over the last 1000 roundtrips of evolution of the signal at the third stage in formation process of various multi-bound solitons: (a)-(b) Dual-bound soliton, and (c)-(d) Triple-bound soliton.

The last stage in the evolution of multi-bound soliton is the process in which the pulses do self-adjustments until multi-bound soliton reaches a steady state after the gain of the cavity is optimally adjusted. Although there is still existence of small fluctuations of the phase and amplitude in this process, the pulses in bound states are well-defined in a periodic evolution. Therefore the magnitude bispectra in both the dual- and the triple-bound solitons show the periodic structure with the closed elliptical contours dominant in the hexagon as shown in Figure 7-7(a)&(c). Figure 7-7(b)&(d) show the phase bispectra with periodic relationship between frequency components of pulses and two clearly distinct conjugate regions separated by the diagonal f_1=-f_2. On the other way, the periodic structure in the bispectra is

progressively widened until a stably final state during transition from the unstable to the stable states.

Another state of multi-pulse in the fibre cavity can be obtained when the gain factor is not optimized for higher multi-bound soliton state. Therefore the magnitude and the phase fluctuate strongly during circulation in the cavity. Non-uniformity and deviation of the phase difference between pulses from the value of π result in collision of pulses in this state and formation of new pulses. Figure 7-8 shows both the magnitude and the phase bispectra of this state averaged over 2000 round trips. The presence of both the closed contours and the ridges in a jumble indicate the presence of multipulsing operation and its dynamic state with the rapid variation in time due to the collision and the interaction of pulses in the cavity. The chaos in this state also exhibits through the uniform distribution of phase in the bispectrum as observed in Figure 7-8(b).

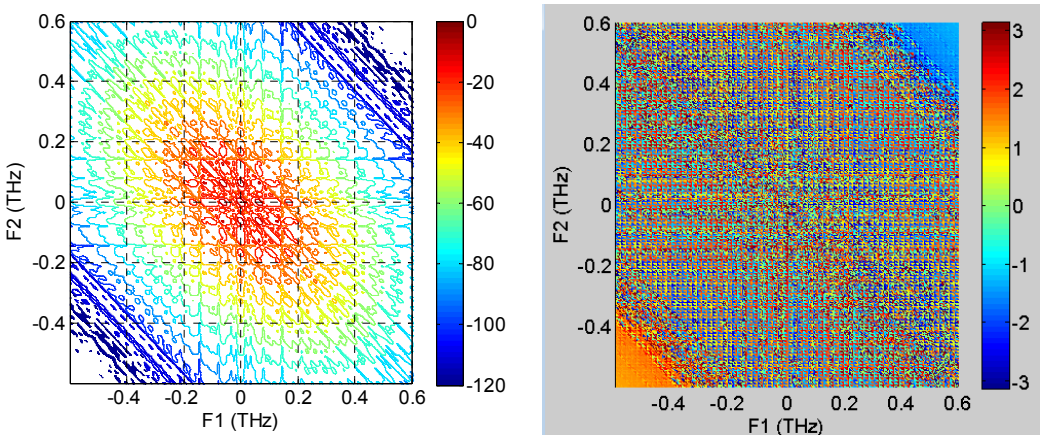

(a) (b)

Figure 7-8 (a) Magnitude spectrum and (b) phase bispectra averaged over 2000 roundtrips of the unstable multi-pulse state in the FM fibre ring cavity.

7.2 THIRD-ORDER NONLINEARITY FOUR WAVE MIXING FOR PHOTONIC SIGNAL PROCESSING

When the processing speed is over that of the electronic limit or requires massive parallel and high speed operations, the processing in the optical domain offers significant advantages. Thus all-optical signal processing is a promising technology for future optical communication networks. An advanced optical network requires a variety of signal processing functions including optical regeneration, wavelength conversion, optical switching and signal monitoring. An attractive way to realize these processing functions in transparent and high speed mode is to exploit the third-order nonlinearity in optical waveguides, particularly parametric processes.

7.2.1 Four-wave mixing in nonlinear waveguides

Four-wave mixing (FWM) is a parametric process through the third-order susceptibility $\chi^{(3)}$. In the FWM process, the superposition and generation of the propagating of the waves with different amplitudes A_k, frequencies ω_k and wave numbers k_k through the waveguide can be represented as

$$A = \sum_k A_k e^{[j(k_k z - \omega_k \tau)]} \quad \text{with } k = 1,..,4 \tag{7-3}$$

The propagation and interaction between different waves in nonlinear waveguides can be described by the system of coupled differential equation which is derived by the introduction of Eq. (7-3) into the NSE with ignoring some linear and scattering effects for simplification [60]. The coupled differential equations, each of which is responsible for one distinct wave in the optical waveguide are as follows [60]:

$$\frac{\partial A_1}{\partial z}+\frac{\alpha}{2}A_1 = j\gamma A_1\left[|A_1|^2+2\sum_{k\neq 1}|A_k|^2\right]+j\gamma 2A_3A_4A_2^*\exp(-j\Delta k_1 z)$$

$$\frac{\partial A_2}{\partial z}+\frac{\alpha}{2}A_2 = j\gamma A_2\left[|A_2|^2+2\sum_{k\neq 2}|A_k|^2\right]+j\gamma 2A_3A_4A_1^*\exp(-j\Delta k_2 z)$$

$$\frac{\partial A_3}{\partial z}+\frac{\alpha}{2}A_3 = j\gamma A_3\left[|A_3|^2+2\sum_{k\neq 3}|A_k|^2\right]+j\gamma 2A_1A_2A_4^*\exp(-j\Delta k_3 z) \qquad (7\text{-}4)$$

$$\frac{\partial A_4}{\partial z}+\frac{\alpha}{2}A_4 = j\gamma A_4\left[|A_4|^2+2\sum_{k\neq 4}|A_k|^2\right]+j\gamma 2A_1A_2A_3^*\exp(-j\Delta k_4 z)$$

where $\Delta k = k_1 + k_2 - k_3 - k_4$ is the wave vector mismatch. In Eqs. (7-4) the last term represents for the interaction which can generate new waves. For three waves with different frequencies, a fourth wave can be generated at frequency $\omega_4 = \omega_1 + \omega_2 - \omega_3$. The waves at frequencies ω_1 and ω_2 are called pump waves, whereas the wave at frequency ω_3 is the signal and generated wave at ω_4 is called idler wave as shown in Figure 7-9(a).

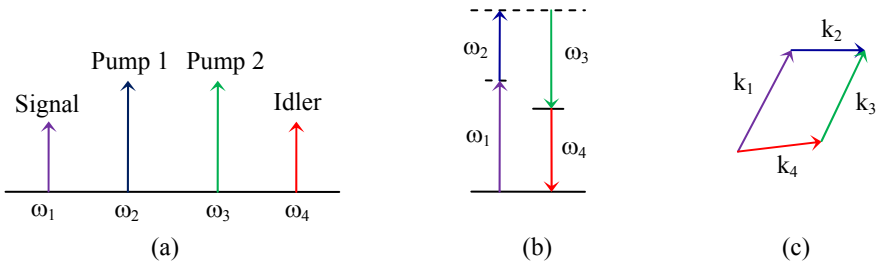

Figure 7-9 (a) Position and notation of the distinct waves, (b) Diagram of energy conservation, and (c) Diagram of momentum conservation in FWM.

If all three waves have the same frequency $\omega_1 = \omega_2 = \omega_3$, the interaction is called a degenerate FWM with the new wave at the same frequency. If only two of the three wave are at the same frequency ($\omega_1 = \omega_2 \neq \omega_3$), the process is called partly degenerate FWM which is important for some applications like the wavelength converter and parametric amplifier.

7.2.2 Phase matching

In parametric nonlinear processes such as FWM, the energy conservation and momentum conservation must be satisfied to obtain a high efficiency of the energy transfer as shown in Figure 7-9(b)-(c). The phase matching condition for the new wave requires:

$$\begin{aligned}\Delta k = k_1 + k_2 - k_3 - k_4 &= \frac{1}{c}(n_1\omega_1 + n_2\omega_2 - n_3\omega_3 - n_4\omega_4) \\ &= 2\pi\left(\frac{n_1}{\lambda_1} + \frac{n_2}{\lambda_2} - \frac{n_3}{\lambda_3} - \frac{n_4}{\lambda_4}\right)\end{aligned} \tag{7-5}$$

where n_i is the refractive index of the wave at the wavelength λ_i. During propagation in optical waveguides, the relative phase difference $\theta(z)$ between four involved waves is determined by [241-242]:

$$\theta(z) = \Delta kz + \phi_1(z) + \phi_2(z) - \phi_3(z) - \phi_4(z) \tag{7-6}$$

where $\phi_k(z)$ relates to the initial phase and the nonlinear phase shift during propagation. An approximation of phase matching condition can be given as follows [243]:

$$\frac{\partial\theta}{\partial z} \approx \Delta k + \gamma(P_1 + P_2 - P_3 - P_4) = \kappa \tag{7-7}$$

where P_k is the power of the waves and κ is the phase mismatch parameter. Thus the FWM process has maximum efficiency for $\kappa = 0$. The mismatch comes from the frequency dependence of the refractive index and the dispersion of optical waveguides. Depending on the dispersion profile of the nonlinear waveguides, it is very important in selection of pump wavelengths to ensure that the phase mismatch parameter is minimized.

7.3 APPLICATIONS OF FWM IN PHOTONIC SIGNAL PROCESSING

Based on the Simulink® platform for optical fibre communication systems, a range of signal processing applications based on parametric process will be demonstrated through simulations in which the model of nonlinear waveguide is used as a functional block. Details of the Simulink® models are presented in Appendix D.

7.3.1 Signal processing based on parametric amplification

One of important applications of the $\chi^{(3)}$ nonlinearity is parametric amplification. The optical parametric amplifiers (OPA) offer a wide gain bandwidth, high differential gain and optional wavelength conversion and operation at any wavelength [242-245]. These important features of OPA are obtained because the parametric gain process does not rely on energy transitions between energy states, but it is based on highly efficient FWM in which two photons at one or two pump wavelengths will interact with a signal photon. A fourth photon, the idler, will be formed with a phase such that the phase difference between the pump waves and the signal and idler waves satisfies a phase matching condition. A typical scheme of the fibre-based parametric amplifier is shown in Figure 7-10(a).

For parametric amplifier using one pump source, from the coupled equations (7-4) with $A_1 = A_2 = A_p$, $A_3 = A_s$ and $A_4 = A_i$, it is possible to derive three coupled equations for complex field amplitude of the three waves $A_{p,s,i}$:

$$\begin{aligned}
\frac{\partial A_p}{\partial z} &= -\frac{\alpha}{2}A_p + i\gamma A_p\left[\left|A_p\right|^2 + 2\left(\left|A_s\right|^2 + \left|A_i\right|^2\right)\right] + i2\gamma A_s A_i A_p^* \exp(-i\Delta kz) \\
\frac{\partial A_s}{\partial z} &= -\frac{\alpha}{2}A_s + i\gamma A_s\left[\left|A_s\right|^2 + 2\left(\left|A_p\right|^2 + \left|A_i\right|^2\right)\right] + i\gamma A_p^2 A_i^* \exp(-i\Delta kz) \\
\frac{\partial A_i}{\partial z} &= -\frac{\alpha}{2}A_i + i\gamma A_i\left[\left|A_i\right|^2 + 2\left(\left|A_s\right|^2 + \left|A_p\right|^2\right)\right] + i\gamma A_p^2 A_s^* \exp(-i\Delta kz)
\end{aligned} \tag{7-8}$$

The analytical solution of these coupled equations determines the gain of the amplifier [241]:

$$G_s(L) = \frac{|A_s(L)|^2}{|A_s(0)|^2} = 1 + \left[\frac{\gamma P_p}{g}\sinh(gL)\right]^2 \tag{7-9}$$

with L is the length of the highly nonlinear fibre/waveguide, P_p is the pump power, and g is the parametric gain coefficient:

$$g^2 = -\Delta k\left(\frac{\Delta k}{4} + \gamma P_p\right) \tag{7-10}$$

where the phase mismatch Δk can be approximated by extending the propagation constant in a Taylor series around ω_0:

$$\Delta k = -\frac{2\pi c}{\lambda_0^2}\frac{dD}{d\lambda}(\lambda_p - \lambda_0)(\lambda_p - \lambda_s)^2 \tag{7-11}$$

Here, $dD/d\lambda$ is the slope of the dispersion at the zero-dispersion wavelength, $\lambda_k = 2\pi c/\omega_k$ is the optical wavelength.

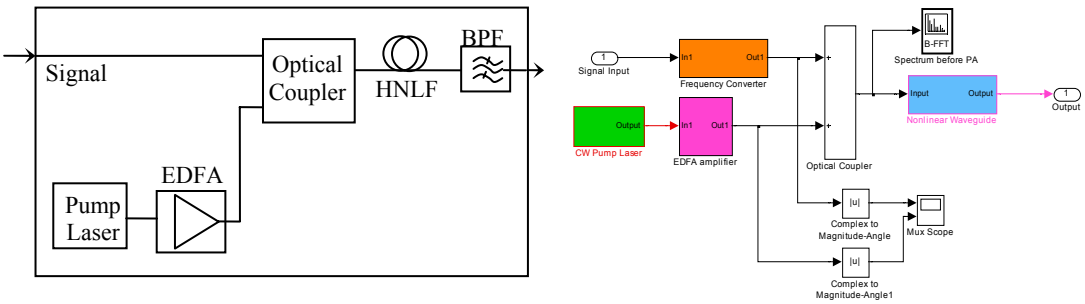

(a) (b)

Figure 7-10 (a) A typical setup of an optical parametric amplifier [242]; (b) The Simulink model of optical parametric amplifier.

A setup of the 40 Gbit/s RZ transmission system using parametric amplifier has been implemented in the Simulink® platform. The setup contains a 40 Gbit/s optical RZ transmitter, an optical receiver for monitoring, a parametric amplifier

block and a bandpass filter that filters the desired signal from the total field output of the amplifier. Details of the parametric amplifier block can be seen in Figure 7-10(b). The block setup of parametric amplifier consists of a continuous wave (CW) pump laser source, an optical coupler to combine the signal and the pump, a highly nonlinear fibre block which contains the embedded MATLAB model for nonlinear propagation. The important simulation parameters of the system are shown in Table 7-1.

Table 7-1 Important parameters of the parametric amplifier in 40Gbps system.

RZ 40 Gbit/s Transmitter
λ_s = 1520 nm – 1600 nm, λ_0 = 1559 nm Modulation: RZ-OOK, P_s = 0.01 mW (peak), B_r = 40 Gbit/s
Parametric Amplifier
Pump source: P_p = 1 W (after EDFA), λ_p = 1560.07 nm HNLF: L_f = 500 m, D = 0.02 ps/km/nm, S = 0.09 ps/nm^2/km, α = 0.5 dB/km, A_{eff} = 12 μm^2, γ = 13 1/W/km. BPF: $\Delta\lambda_{BPF}$ = 0.64 nm

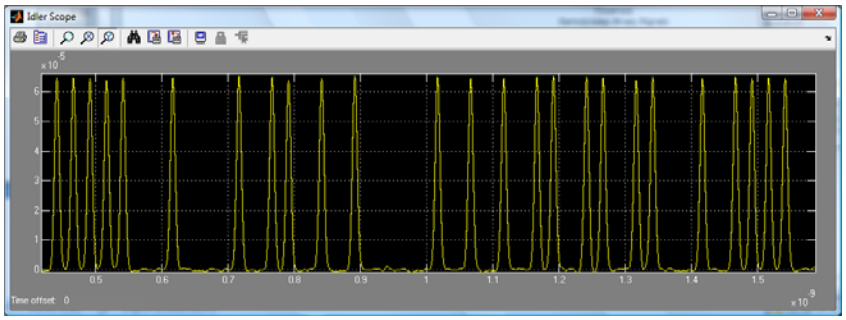

(a)

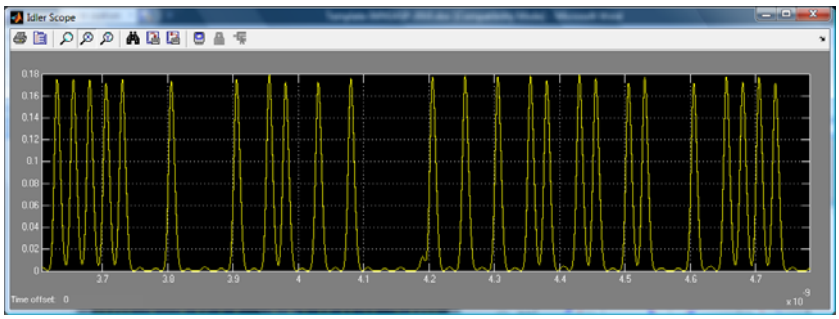

(b)

Figure 7-11 Time traces of the 40 Gbit/s signal before (a) and after (b) the parametric amplifier.

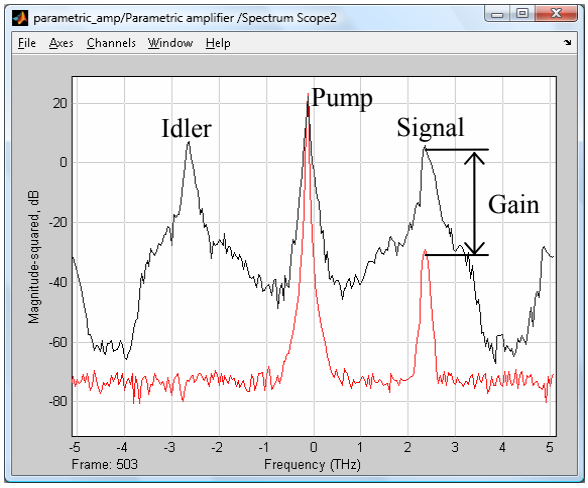

Figure 7-12 Optical spectra at the input (red) and the output (black) of the OPA

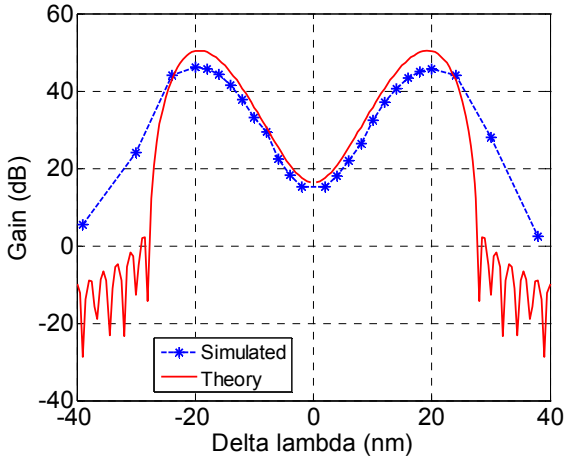

Figure 7-13 Calculated and simulated gain of the OPA at P_p = 30 dBm.

Figure 7-11 shows the signals before and after the amplifier in time domain. The time trace indicates the amplitude fluctuation of the amplified signal as a noisy source from wave mixing process. Their corresponding spectra are shown in Figure 7-12. The noise floor of the output spectrum of amplifier shows the gain profile of OPA. Simulated dependence of OPA gain on the wavelength difference between the signal and the pump is shown in Figure 7-13 together with theoretical gain using Eq. (7-9). The plot shows an agreement between theoretical and simulated results. The

peak gain is achieved at phase matched condition where the linear phase mismatch is compensated by the nonlinear phase shift.

In fact, the parametric amplifier is not popularly applied in the transmission systems because of some disadvantages [242]. However, the structure of parametric amplifier is prospectively applied to signal processing function such as wavelength conversion which can be obtained from the idler after wave mixing process. Due to very fast response of the third-order nonlinearity, the wavelength conversion based on this effect is transparent to the modulation format and the bit rate of signals. For a flat wideband converter which is a key device in wavelength-division multiplexing (WDM) networks, a short length HNLF with a low dispersion slope is required in design. By a suitable selection of the pump wavelength, the wavelength converter can be optimized to obtain a bandwidth of 200 nm [244]. Therefore, the wavelength conversion between bands such as C and L bands can be performed in WDM networks. Figure 7-14 shows an example of the wavelength conversion for four WDM channels at C-band. The important parameters of the wavelength converter are shown in Table 7-2. The WDM signals are converted into L-band with the conversion efficiency of -12 dB.

Table 7-2 Important parameters of the wavelength converter.

RZ 40 Gbit/s Signal
λ_0 = 1559 nm, λ_s = {1531.12, 1537.4, 1543.73, 1550.12} nm, P_s = 1 mW (peak), B_r = 40 Gbit/s
Parametric Amplifier
Pump source: P_p = 100 mW (after EDFA), λ_p = 1560.07 nm HNLF: L_f = 200 m, D = 0.02 ps/km/nm, S = 0.03 ps/nm^2/km, α = 0.5 dB/km, A_{eff} = 12 μm^2, γ = 13 1/W/km BPF: $\Delta\lambda_{BPF}$ = 0.64 nm, λ_i = {1587.91, 1581.21, 1574.58, 1567.98} nm

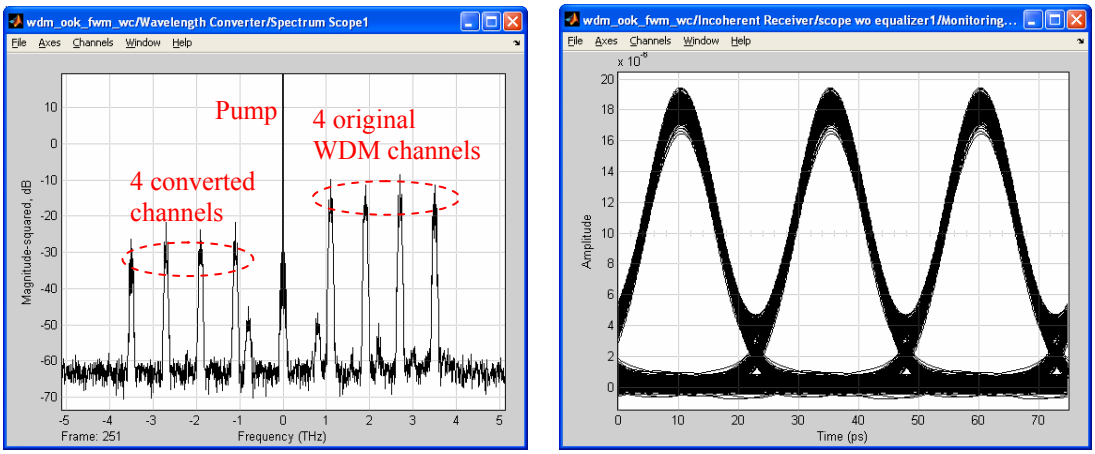

(a) (b)

Figure 7-14 (a) The wavelength conversion of 4 WDM channels, (b) Eyediagram of the converted 40 Gbit/s signal after BPF.

Another important application with the same setup is the nonlinear phase conjugation (NPC). A phase conjugated replica of the signal wave can be generated by FWM process. From Eq. (7-8), the idler wave is approximately given in case of degenerate FWM for simplification: $E_i \sim A_p^2 A_s^* e^{-j\Delta kz}$ or $E_i \sim r A_s^* e^{[j(-kz-\omega\tau)]}$ with the signal wave $E_s \sim A_s e^{[j(kz-\omega\tau)]}$. Thus the idler field is complex conjugate of the signal field. In appropriate conditions, optical distortions can be compensated by using NPC and optical pulses propagating in the fibre link can be recovered. The basic principle of distortion compensation with NPC refers to spectral inversion. When an optical pulse propagates in an optical fibre, its shape will be spread in time and distorted by the group velocity dispersion. The phase conjugated replica of the pulse is generated in the middle point of the transmission link by the nonlinear effect. On the other hand, the pulse is spectrally inverted where spectral components in the lower frequency range are shifted to the higher frequency range and vice versa. If the pulse propagates in the second part of the link with the same manner in the first part, it is inversely distorted again that can cancel the distortion in the first part to recover the pulse shape

at the end of the transmission link. With using NPC for distortion compensation, a 40-50 % increase in transmission distance compared to a conventional transmission link can be obtained [246-248]. However NPC for distortion compensation has been mostly implemented by exploiting the second order susceptibility of nonlinear crystals such as KTP and periodically poled $LiNbO_3$ (PPLN) [247]. Recently, planar nonlinear waveguides based on AsS_3 glass have emerged as promising devices for ultra-high speed photonic processing [80-81, 249]. These nonlinear waveguides offer a lot of advantages such as no free-carrier absorption, stable at room temperature, no requirement of quasi-phase matching and possibility of dispersion engineering.

Table 7-3 Important parameters of the long-haul transmission system using NPC for distortion compensation.

RZ 40 Gbit/s Transmitter
λ_s = 1547 nm, λ_0 = 1559 nm Modulation: RZ-OOK, P_s = 1 mW (peak), B_r = 40 Gbit/s
Fiber transmission link
SMF: L_{SMF} = 100 km, D_{SMF} = 17 ps/nm/km, α = 0.2 dB/km EDFA: Gain = 20 dB, NF = 5dB; Number of spans: 10 (5 in each section), L_{link} = 1000 km
NPC based on OPA
Pump source: P_p = 500 mW (after EDFA), λ_p = 1560.07 nm NW: L_w = 7 cm, D = 28 ps/km/nm, S = 0.03 ps/nm^2/km, α = 5 dB/cm, A_{eff} = 1 μm^2, γ = 10000 1/W/km BPF: $\Delta\lambda_{BPF}$ = 0.64 nm

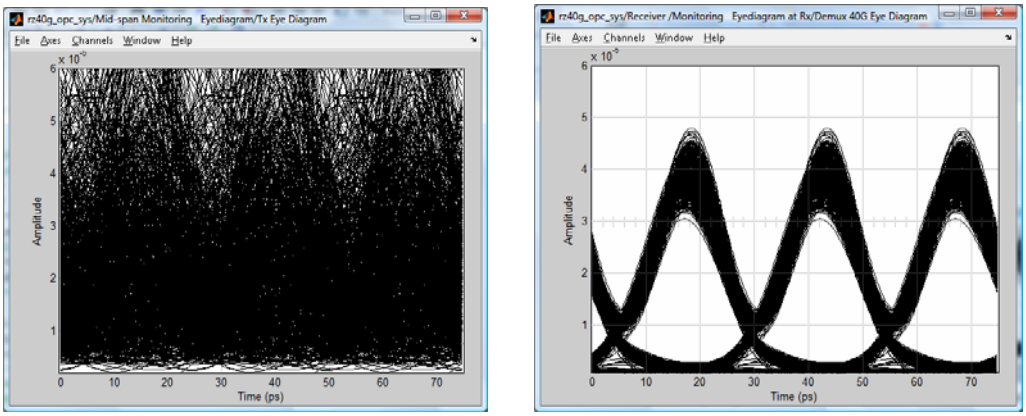

(a) (b)

Figure 7-15 Eye-diagrams of the 40Gbit/s signal at the end (a) of the first section and (b) of the transmission link.

Details of the Simulink® setup of a long-haul 40 Gbit/s transmission system demonstrating the distortion compensation using NPC are shown in Appendix D. The fibre transmission link of the system is divided into two sections by an NPC based on parametric amplifier. Each section consists of five spans with 100 km standard single mode fibre (SSMF) in each span. Figure 7-15(a) shows the eyediagram of the signal after propagating through the first fibre section. After the NPC at the midlink, the idler signal, a phase conjugated replica of the original signal, is filtered for transmission in next section. The signal in the second section suffers the same dispersion as in the first section. At the end of the transmission link the optical signal is totally regenerated as shown in Figure 7-15(b). It is noted that due to change in wavelength of the signal after the NPC, a tunable dispersion compensator can be required to compensate the residual dispersion after transmission in real systems.

7.3.2 Ultra-high speed optical switching

When the pump is an intensity modulated signal instead of the CW signal, the gain of the OPA is also modulated due to its exponential dependence on the pump power in a phase matched condition. The width of gain profile in time domain is inversely

proportional to the product of the gain slope (S_p) or the nonlinear coefficient and the length of the nonlinear waveguide (L) [241]. Therefore an OPA with high gain or large S_pL operates as an optical switch with an ultra-high bandwidth which is very important in some signal processing applications such as pulse compression or short-pulse generation [250-251]. A Simulink® setup for a 40 GHz short-pulse generator is built with the configuration as shown in Figure 7-16. In this setup, the input signal is a CW source with low power and the pump is amplitude modulated by a Mach-Zehnder intensity modulator which is driven by a RF sinusoidal wave at 40 GHz. The waveform of the modulated pump is shown in Figure 7-17(a). Important parameters of the FWM-based short-pulse generator are shown in Table 7-4. Figure 7-17(b) shows the generated short-pulse sequence with the pulsewidth of 2.6 ps at the signal wavelength after the optical BPF.

Table 7-4 Parameters of the 40 GHz short pulse generator

Short-pulse generator
Signal: P_s = 0.7 mW, λ_s = 1535 nm, λ_0 = 1559 nm,
Pump source: P_p = 1W (peak), λ_p = 1560.07 nm, f_m = 40 GHz
HNLF: L_f = 500 m, D = 0.02 ps/km/nm, S = 0.03 ps/nm^2/km,
α = 0.5 dB/km, A_{eff} = 12 μm^2, γ = 13 1/W/km. BPF: $\Delta\lambda_{BPF}$ = 3.2 nm

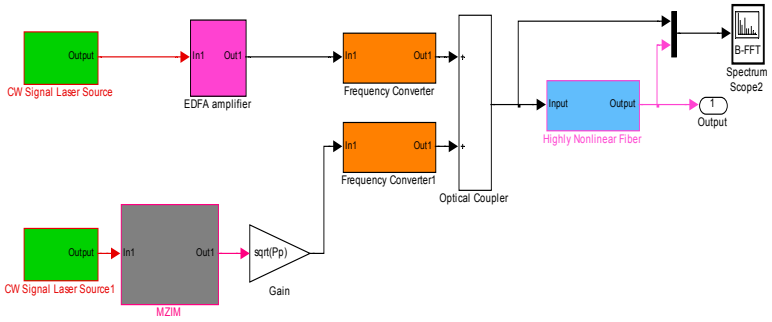

Figure 7-16 Simulink setup of the 40 GHz short-pulse generator to demonstrate ultra-high speed switching based on parametric amplification with using of a intensity-modulated source for pump.

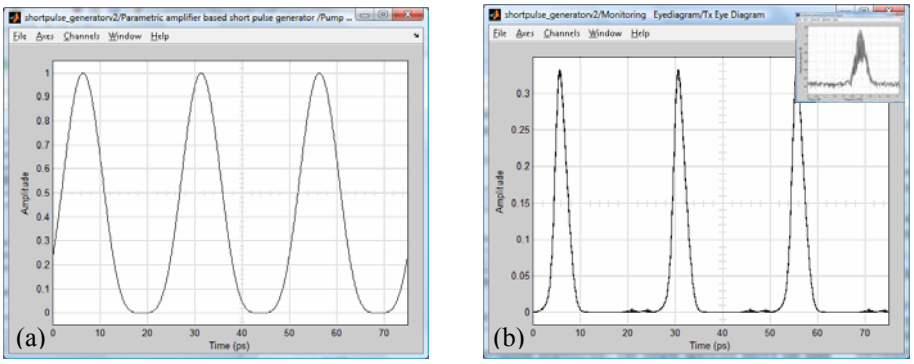

Figure 7-17 Time traces of (a) the sinussoidally amplitude modulated pump, and (b) the generated short-pulse sequence (Inset: The corresponding pulse spectrum).

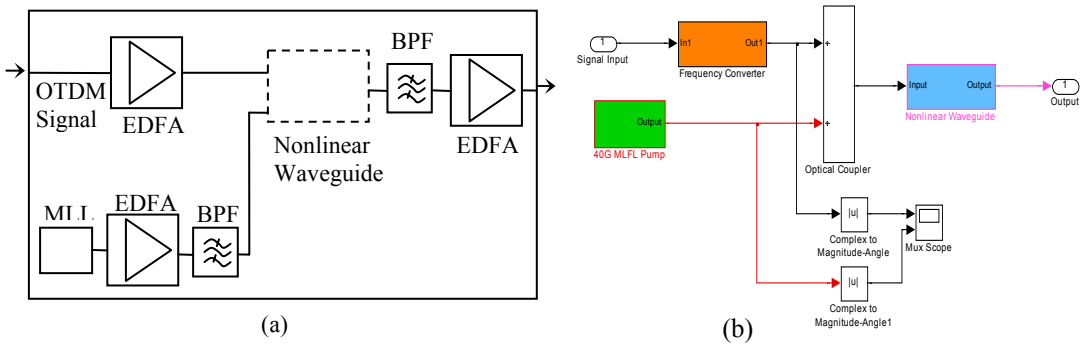

Figure 7-18 (a) A typical setup of the FWM-based OTDM demultiplexer, (b) Simulink model of the OTDM demultiplexer.

Another important application of the optical switch based on FWM process is the demultiplexer a key component in ultra-high speed optical time division multiplexing (OTDM) systems. OTDM is a key technology for Tb/s Ethernet transmission which can meet the increasing demand of traffic in future optical networks. A typical scheme of OTDM demultiplexer in which the pump is a mode-locked laser (MLL) to generate short pulses for control is shown in Figure 7-18(a). The working principle of the FWM-based demultiplexing is described as follows: The control pulses generated from a MLL at tributary rate are pumped and co-propagated with the OTDM signal through a nonlinear medium such as HNLF or nonlinear waveguide. Mixing process between the control pulses and the OTDM signal during

propagation through the nonlinear medium converts the desired tributary channel to a new idler wavelength. Then the demultiplexed signal at the idler wavelength is extracted by a band pass filter before going to a receiver as shown in Figure 7-18(a).

Table 7-5 Important parameters of the FWM-based OTDM demultiplxer using a nonlinear waveguide.

OTDM Transmitter
MLL: P_0 = 1 mW, T_p = 2.5 ps, f_m = 40 GHz
Modulation formats: OOK and DQPSK; OTDM multiplexer: 4x40Gsymbols/s
FWM based demultiplexer
Pumped control: P_p = 500 mW, T_p = 2.5ps, f_m = 40GHz, λ_p = 1556.55 nm
Input signal: P_s = 10 mW (after EDFA), λ_s = 1548.51 nm
Waveguide: L_w = 7cm, D_w = 28 ps/km/nm, S_w = 0.003 ps/nm^2/km
α = 0.5 dB/cm, $\gamma = 10^4$ 1/W/km
BPF: $\Delta\lambda_{BPF}$ = 0.64 nm

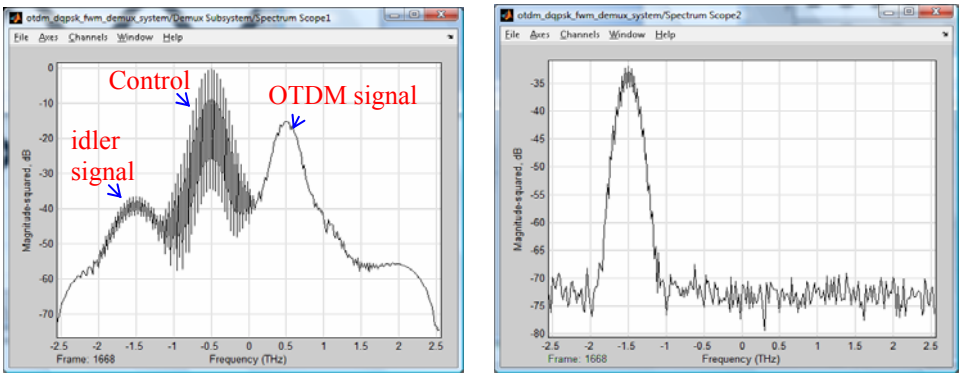

(a) (b)

Figure 7-19 Spectra at the outputs (a) of nonlinear waveguide and (b) of BPF.

Using HNLF is relatively popular in structures of OTDM demultiplexer [245, 252]. However its stability, especially the walk-off problem is still a serious obstacle. With the same operational principle, planar waveguide-based OTDM demultiplexers are very compact and suitable for photonic integrated solutions [81]. Figure 7-18(b) shows the Simulink setup of the FWM-based demultiplexer of the on-off keying (OOK) 40Gbit/s signal from the 160 Gbit/s OTDM signal using a highly nonlinear

waveguide instead of HNLF. The important simulation parameters of the OTDM system are given in Table 7-5. Figure 7-19(a) shows the spectrum at the output of the nonlinear waveguide. Then the demultiplexed signal is extracted by the bandpass filter as shown in Figure 7-19(b). The developed model of OTDM demultiplexer can be applied not only to the conventional OOK format but also to advanced modulation formats such as DQPSK which increases the data load of the OTDM system without increase in bandwidth of the signal. By using available blocks developed for DQPSK system [253], a Simulink® model of DQPSK-OTDM system is also setup for demonstration. The bitrate of the OTDM system is doubled to 320 Gbit/s with the same pulse repetition rate. Figure 7-20 shows the simulated performance of the demultiplexer in both 160 Gbit/s OOK- and 320 Gbit/s DQPSK-OTDM systems. The BER curve in case of the DQPSK-OTDM signal shows a low error floor which may be resulted by the influence of nonlinear effects on phase-modulated signals in the waveguide.

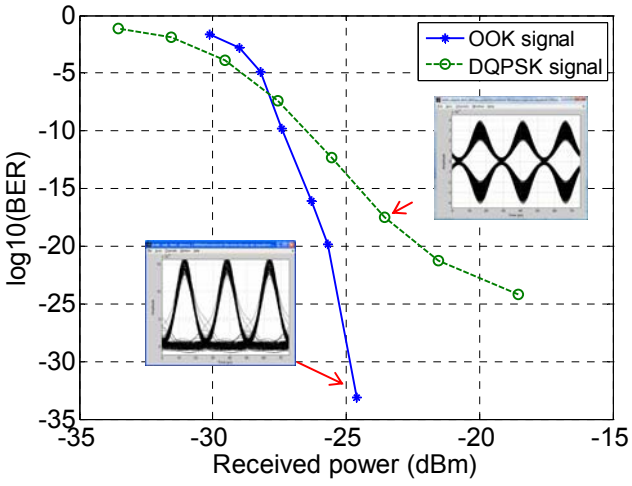

Figure 7-20 Simulated performance of the demultiplexed signals for 160 Gbit/s OOK- and 320 Gbit/s DQPSK-OTDM systems (Insets: Eyediagrams at the receiver).

7.3.3 FWM based triple-correlation and bispectrum

One of promising possibilities exploiting the $\chi^{(3)}$ nonlinearity is implementation of triple-correlation in optical domain. To implement the triple correlation in optical domain, thus the product of three signals including different delayed versions of original signal need to be generated, and then detected by an optical photodiode to perform the integral operation. From the representation of nonlinear polarization vector [60], this triple-product can be generated by the $\chi^{(3)}$ nonlinearity. One conventional way to generate the triple correlation is based on third harmonic generation (THG) where the generated new wave containing the triple-product is at the frequency of three times of original carrier frequency. Thus if the signal wavelength is in the 1550 nm band, the new wave need to be detected at around 517 nm. The triple-optical autocorrelation based on single stage third harmonic generation has been demonstrated in direct optical pulse shape measurement [254-255]. However this way is hard to obtain high efficiency in the wave mixing process due to the difficulty of phase matching between three signals. Moreover, the triple-product wave is in 517 nm where wideband photo-detectors are not available for high-speed communication applications. Therefore a possible alternative to generate the triple product is based on other nonlinear interactions such as FWM. From Eq.(7-4), the fourth wave is proportional to the product of three waves $A_4 \sim A_1 A_2 A_3^* e^{-j\Delta kz}$. If A_1 and A_2 are the delayed versions of the signal A_3, the mixing of three waves results in the fourth wave A_4 which is obviously the triple product of three signals. As mentioned in section 7.2.1, all three waves can have the same frequency, however these waves should propagate into different directions to possibly distinguish the new generated wave in a diverse propagation direction which requires a strict arrangement of the

signals in spatial domain for phase matching. An alternative way we propose is to convert the three signals into different frequencies (ω_1, ω_2 and ω_3). Then the triple-product wave can be extracted at the frequency $\omega_4 = \omega_1 + \omega_2 - \omega_3$ which is still in the 1550 nm band.

Table 7-6 Important parameters of the FWM based triple-product generator using a nonlinear waveguide.

Signal generator
Single-pulse: P_0 = 200 mW, T_p = 5 ps, f_m = 5 GHz Dual-pulse: P_p = 200 mW, T_p = 5 ps, f_m = 5 GHz
FWM based triple-product generator
Original signal: λ_{s1} = 1552.52 nm Delayed τ_1 signal: λ_{s2} = 1553.32 nm, Delayed τ_2 signal: λ_{s3} = 1551.5 nm Waveguide: L_w = 7cm, D_w = 28 ps/km/nm, S_w = 0.003 ps/nm^2/km α = 0.5 dB/cm, $\gamma = 10^4$ 1/W/km BPF: $\Delta\lambda_{BPF}$ = 0.64÷1 nm

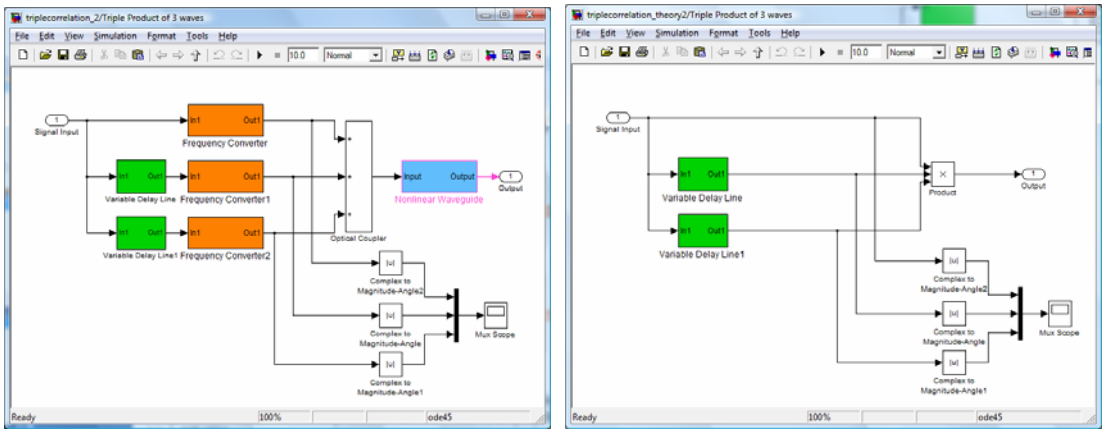

(a) (b)

Figure 7-21 (a) Simulink setup of the FWM-based triple-product generation, (b) Simulink setup of the theory-based triple-product generation.

A Simulink® model for the triple-correlation estimation based on FWM in nonlinear waveguide is setup for investigation. The structural block consists of two variable delay lines to generate delayed versions of the original signal and frequency

converters to convert the signal into different three waves before combining at the optical coupler to launch into the nonlinear waveguide as shown in Figure 7-21(a). Then the fourth wave signal generated by FWM is extracted by the passband filter. To verify the triple-product based on FWM, another model shown in Figure 7-21(b) to estimate the triple-product by a mathematical function block is also implemented for comparison. The integration of the generated triple-product signal is then performed at photo-detector in the optical receiver to estimate the triple-correlation of the signal. Repetitive signals with different patterns are generated for investigation. Important parameters of the setup are shown in Table 7-6. The triple-correlation is represented by 3D plot as an image with hot colours corresponding to the intensity of the triple-correlation. The axes (X&Y) of the image are the time-delay variables (τ_1 and τ_2) in terms of samples with step-size of $T_m/32$ where T_m is the pulse period. Various patterns of pulse sequence are used to estimate the FWM-based triple-correlation as shown in Figure 7-22.

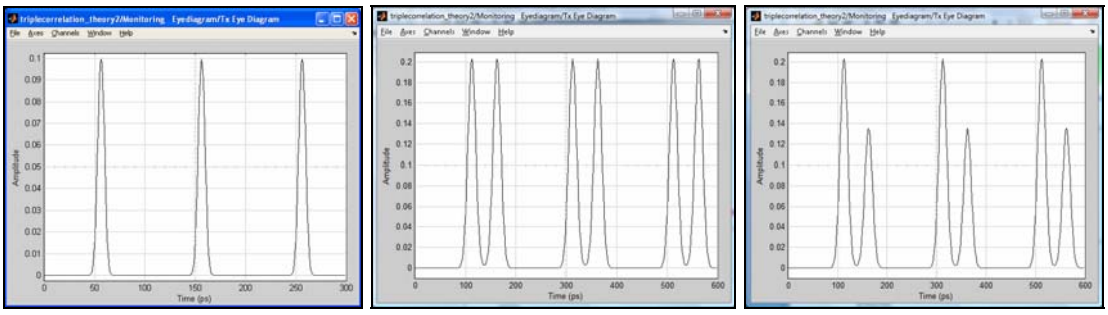

(a) (b) (c)

Figure 7-22 Pulse sequence patterns: (a) Single pulse, (b) Dual-pulse with equal amplitudes, and (c) Dual-pulse with unequal amplitudes.

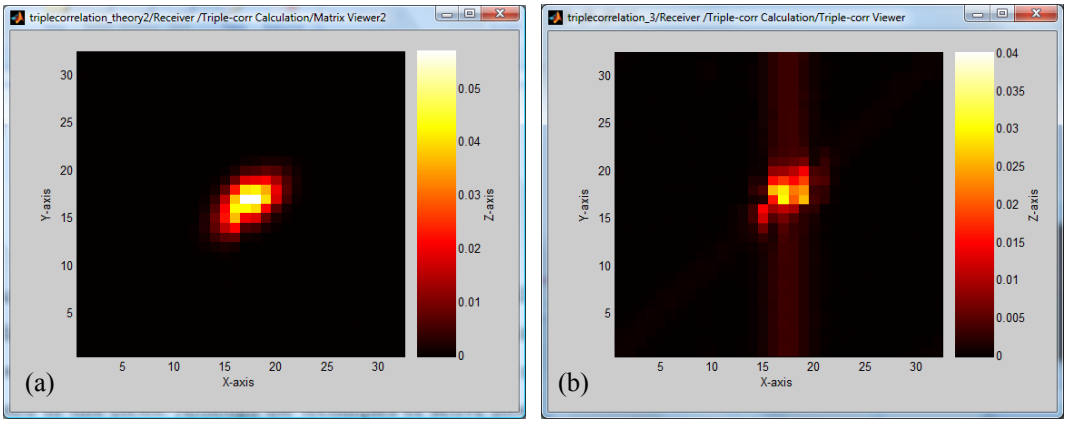

Figure 7-23 Triple correlation of the single-pulse signal based on (a) theoretical estimation, (b) FWM in nonlinear waveguide.

In the simple case, a single Gaussian pulse sequence at 5 GHz is generated for investigation. Figure 7-23 shows the triple-correlations of the signal in both models which are based on the FWM process and the theory for comparison with the same resolution. The intensity of the triple-correlation based on the FWM is focused in a spot similar to that shown in Figure 7-23(a). By changing into another pattern, the triple-correlations of dual-pulse with equal and unequal amplitudes in both models are obtained as shown in Figure 7-24. Because of the presence of second pulse in the pattern, a layer of spots in a hexagonal shape appears in the triple-correlation based on the FWM process. When the amplitude of the second pulse is lower, the intensity of the spots outside is also reduced correspondingly.

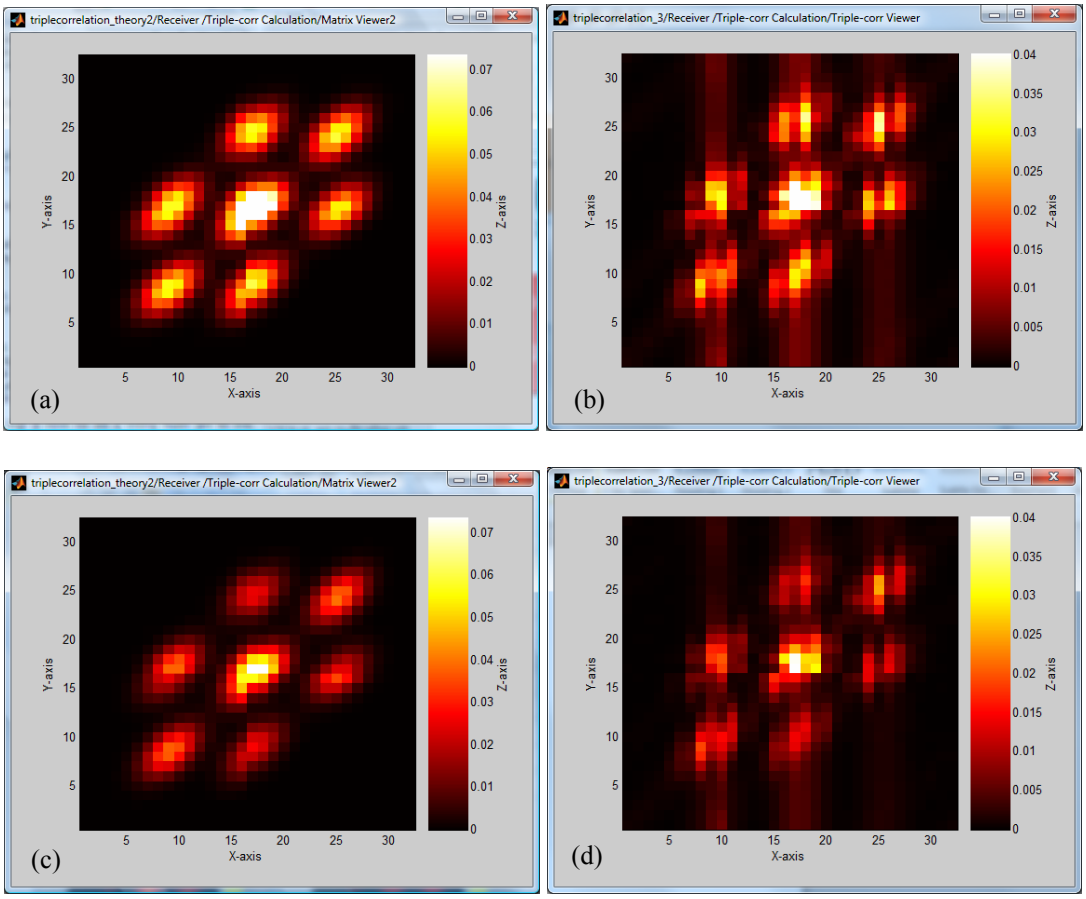

Figure 7-24 Triple correlations based on (a) theoretical estimation, and (b) FWM in nonlinear waveguide of the dual-pulse signal with equal amplitudes, and triple correlations based on (c) theoretical estimation, and (d) FWM in nonlinear waveguide of the dual-pulse with unequal amplitudes (Peak power of the second pulse $P_2=2/3P_p$).

In general, the triple-correlation patterns are still distinguishable as compared to the theory. However the FWM-based triple correlations are contaminated by noise which is mainly generated by other mixing processes and crosstalk from neighbour wavelengths similar to those in WDM systems. If the wavelength spacing between three waves is equal, the noise level from undesired mixing processes is enhanced as demonstrated in Figure 7-25(a). Furthermore if the bandwidth of the signal is broadened, the crosstalk noise increases correspondingly as demonstrated in Figure 7-25(b). In all triple-correlations obtained by the FWM, the noise is deterministic that

is enhanced only at certain vertical lines in the image. We note that the noise can be reduced by the optical bandpass filter, however the bandwidth of optical filter can distort the triple-correlation. Depending on the bandwidth of the signal, hence the wavelength positions as well as the bandwidth of the filter need to be carefully chosen to obtain the best results.

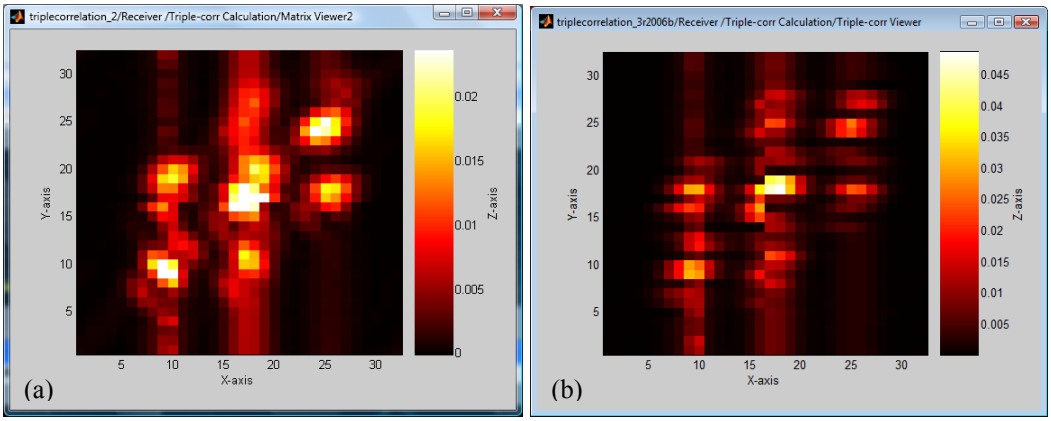

Figure 7-25 Triple-correlations of the dual-pulse signal based on FWM process in various conditions: (a) with double the bandwidth of the signal, (b) with equal wavelength spacing.

7.4 CONCLUDING REMARKS

Bispectrum estimation, a Fourier transform of triple-correlation, has been proposed to characterise various states of multi-bound solitons. Owing to distinct representation of the bispectrum, dynamic aspects of the multi-bound solitons can be identified. Specially, the stability and the transition from a chaotic state to a steady state or vice versa were obviously distinguished by variation of the periodic structure in the magnitude bispectrum and the phase distribution in the phase bispectrum.

The triple-correlation based on FWM process has been examined by the Simulink model which was developed for signal processing using nonlinear waveguides. The validity of the model has been demonstrated through important applications of FWM process such as wavelength conversion, nonlinear phase

conjugation and ultrafast switching. The obtained results showed that the triple-correlation based on FWM is still distinguishable although it is noisy due to other mixing processes. However the complexity of properly selection of parameters such as in this technique can prevent it from practical applications.

Chapter 8

Conclusion

Optical solitons could become more significant in fibre communications and signal processing applications; therefore short-pulse generators such as mode-locked fibre lasers have attracted a lot attention in research on soliton generation and the dynamic behaviour of solitons in a mode-locked fibre laser. Together with passively mode-locked fibre lasers, actively mode-locked fibre ring lasers show new behaviours that can be explored for potential applications. Especially, multi-pulse operation which results in multi-bound solitons can occur in strongly-nonlinear fibre cavities. Therefore some research issues about multi-bound solitons generated from actively FM mode-locked fibre ring laser have been addressed in this thesis. Both experimental and numerical investigations of multi-bound solitons during generation, propagation and detection have been performed.

The existence of multi-bound solitons having more than two pulses in an actively FM mode-locked fibre laser has been reported for the first time. By properly setting the parameters of the cavity, various multi-soliton bound states from the dual- to the sextuple-order have been experimentally generated at modulation frequency of 1 GHz. Together with experimental results, numerical simulations have been shown that multi-bound solitons with the relative phase difference of π are stable solutions of the FM mode-locked fibre laser in specific conditions of the cavity. When the cavity

parameters deviate from the optimum value, the multi-bound solitons would become a quasi-stable state with a periodic variation of pulse parameters or unstable state with strong fluctuations in amplitude and temporal position due to the variation of the phase difference. Both experimental and simulated results showed that the higher order bound state becomes more sensitive to the environment fluctuations and the changes in cavity settings.

In contrast to passive mode locking, the EO phase modulator allows active mode locking of a fibre laser. The influence of the phase modulator on multi-soliton bound states can exhibit on two aspects which are the artificial filtering response of the cavity and the chirping caused by phase modulation. By characterization measurements the inherent birefringence in the Ti-waveguide of the EO phase modulators was identified through the formation of the artificial Lyot-based filtering response. This response not only relates to the discrete wavelength tunable function but also limits the pulse shortening in the cavity that is very important in multi-bound soliton formation. Multi-bound solitons were only obtained in the cavity using the lumped-type phase modulator PM-315P, while it is difficult to generate multi-bound solitons in the cavity using the traveling-wave phase modulator Mach-40-27. In another aspect, the chirp rate induced by phase modulation from the EO phase modulator significantly affects important parameters of the multi-bound solitons such as temporal separation and the optical power level for stabilization. At higher chirps, the temporal separation is reduced and the optical power level required for stability is increased. It has been also demonstrated that at the same optical power in the cavity a switching from higher-order bound state to lower-order one can occur when the modulation index is increased sufficiently. Moreover the bound solitons are split into

lower-order bound states with controllable separation by the distortion of the phase modulation profile. The distortion is caused by the enhancement of higher order harmonics in the driving signal which is useful not only for rational harmonic mode locking but also for soliton control inside the cavity.

The transmission characteristics of multi-bound solitons have been experimentally and numerically investigated in 50 km of standard single mode fibre. Depending on the launched power of the multi-bound soliton, the obtained results showed two distinct areas of the soliton parameters after transmission. Multi-bound solitons are influenced by strong repulsive interaction that varies along the fibre. The changes in soliton parameters depend on the launching powers, which can be lower or higher than the power essential to form a single soliton. Although the soliton parameters such as the width, the time separation varies strongly due to the perturbation of loss and dispersion, the phase difference of π still remains almost unchanged at low launching power after 50 km transmission. By contrast the variation of soliton parameters is reduced at sufficiently high launching powers, yet the phase difference deviates from the value of π.

Dynamic states of the multi-bound solitons have been also analysed by the triple-correlation and its Fourier transform, called bispectrum. The bispectrum analysis showed distinguishable representation of various multi-bound soliton states that can be used to estimate their stability. In an effort to find an alternative way in estimation of the triple-correlation in optical domain, the FWM parametric process has been examined for this purpose. The simulation results have shown that the limitations of this approach in practical applications.

Having demonstrated the existence of stable multi-bound solitons in the actively FM mode-locked fibre lasers, an interesting avenue to explore is the behaviour of multi-bound solitons as data carriers in communication systems. As observed in the passively mode-locked fibre laser [256], vector solitons also may exist in an actively mode-locked cavity. Furthermore the polarization-dependent phase modulation of the $LiNbO_3$ modulators can affect to the interaction and the coupling between two distinct polarization components that produce new dynamic states. In order to enhance the controllability of the multi-bound solitons in the cavity, a different guided-wave medium could be used. It has been shown that gap solitons propagating in a fibre Bragg grating (FBG) have a local interaction which is different from that in conventional fibres [257-258]. Hence, the insertion of an FBG in the cavity could allow a variation of propagation velocity of the pulses that could influence effective interaction in the bound state. In addition, photonic crystal fibres (PCF) have recently emerged as a new class of optical fibre which offers interesting features such as highly nonlinearity with optimized dispersion properties [259]. Therefore, PCFs can be another option for the nonlinear guided-wave medium in generation of the multi-bound soliton.

Although the triple-correlation based on FWM process showed the complexity of this technique and the limited performance due to the noise of other mixing processes, the FWM parametric effect still plays a key role in a variety of signal processing functions in future photonic networks. Moreover, distinct representation of the triple-correlation and the bispectrum for a signal or process can be significantly applied for monitoring the signal in optical transmission systems. For an ultra-high speed long-haul transmission system, impairments such as dispersion and nonlinear

phase noise can result in a non-Gaussian distribution of the distortions of the signal that can be easily identified by the bispectrum. Owing to the insensitivity of the bispectrum to a Gaussian random process, it has been demonstrated that the bispectrum is useful to reconstruct the signal corrupted by noise [260]. By this approach, we have numerically shown the potential of the signal recovery for Gaussian white noise corrupted BPSK system by using the bispectrum estimation in digital domain instead of optical domain [253]. By rapid development of high speed analog-to-digital converters for optical receivers, the bispectrum estimation in digital domain is becoming feasible to expand its ability to practical transmission systems.

Appendix A

List of publications

A.1 JOURNAL PAPERS

[N1] **N. D. Nguyen** and L. N. Binh, "Generation of bound solitons in actively phase modulation mode-locked fiber ring resonators," *Optics Communications,* vol. 281, pp. 2012-2022, 2008.

[N2] T. L. Huynh, L. N. Binh, **N. D. Nguyen**, "Fast-processing statistical methods for measurement of BER in optical fiber communication systems," *Optics Communications,* vol. 281, pp. 2750-2754, 2008.

[N3] **N. D. Nguyen** and L. N. Binh, "Generation of high order multi-bound solitons and propagation in optical fibers," *Optics Communications,* vol. 282, pp. 2394-2406, 2009.

[N4] L. K. Dang, H. P. Nguyen, L. N. Binh, **N. D. Nguyen**, "Simulink model and FPGA-based OFDM communication system: A simulation and hardware integrated platform," *International Journal of Modeling, Simulation, and Scientific Computing (IJMSSC),* vol. 1, pp. 369-404, 2010.

A.2 BOOK CHAPTER

[N5] Le Nguyen Binh, **Nhan Duc Nguyen**, Wenn Jing Lai, "Nonlinear Photonic Fibre Ring Lasers: Stability, Harmonic Detuning, Temporal Diffraction and Bound States," in *PROGRESS IN NONLINEAR OPTICS RESEARCH*, M. Takahashi and H. Goto, Eds., ed New York: Nova Science Publishers, Inc., 2008, pp. 1-62.

A.3 CONFERENCE PAPERS

[N6] **N. D. Nguyen**, L. N. Binh, K. K. Pang, T. Vo, T. L. Huynh, "Temporal imaging and optical repetition multiplication via quadratic phase modulation," in *Information, Communications & Signal Processing, 2007 6th International Conference on*, 2007, pp. 1-5.

[N7] T. L. Huynh, L. N. Binh, T. Sivahumaran, K. K. Pang, **N. D. Nguyen**, "MLSE equalizers for incoherent optical MSK systems based on optical frequency discrimination detectionequation," in *Information, Communications & Signal Processing, 2007 6th International Conference on*, 2007, pp. 1-5.

[N8] L. N. Binh, **N. D. Nguyen**, T. L. Huynh, "Multi-bound Solitons in a FM Mode-locked Fiber Laser," in *Optical Fiber communication/National Fiber*

Optic Engineers Conference, 2008. OFC/NFOEC 2008. Conference on, 2008, pp. 1-3.

[N9] **N. D. Nguyen**, L. N. Binh, T. L. Huynh, "Bound-soliton states under a periodic phase modulation," in *Lasers and Electro-Optics, 2008 and 2008 Conference on Quantum Electronics and Laser Science. CLEO/QELS 2008. Conference on*, 2008, pp. 1-2.

[N10] L. N. Binh and **N. D. Nguyen**, "Active multi-bound soliton lasers: Generation of dual to sextuple states," in *Optical Fiber Communication - incudes post deadline papers, 2009. OFC 2009. Conference on*, 2009, pp. 1-3.

[N11] **N. D. Nguyen**, L. N. Binh, K. K. Pang, "Propagation of multi-bound soliton states in optical fibers," in *Optical Fiber Communication - incudes post deadline papers, 2009. OFC 2009. Conference on*, 2009, pp. 1-3.

[N12] **N. D. Nguyen** and L. N. Binh, "Solitonic interactions in actively multi-bound soliton fiber lasers," in *Lasers and Electro-Optics, 2009 and 2009 Conference on Quantum electronics and Laser Science Conference. CLEO/QELS 2009. Conference on*, 2009, pp. 1-2.

[N13] **N. Nguyen** and L. N. Binh, "Demultiplexing Techniques of 320 Gb/s OTDM-DQPSK Signals: A Comparison by Simulation," presented at the IEEE International Conference on Communication Systems, Singapore, 2010.

[N14] L. N. Binh, L. H. Binh, **N. Nguyen**, "Burst Switching in Ultra-high Speed All-optical IP over DWDM Network With and Without Buffers under Linear and Nonlinear Effects," presented at the IEEE International Conference on Communication Systems, Singapore, 2010.

[N15] L. N. Binh, **N. Nguyen**, Martin Firus, M. Steve, L. Dang, "Nonlinear Photonic Pre-Processing Bi-Spectrum Optical Receivers For Long Haul Optically Amplified Transmission Systems," presented at the IEEE International Conference on Communication Systems, Singapore, 2010.

Appendix B

MATLAB code for soliton propagation

```
%%%%%%%%%%%%%%%%%%%%%%%%%%%%%%%%%%%%%%%%%%%%%%%%%%%%%%%%%%%%%%%%%%%%%%%%%%%%
%        O P T I C A L   S O L I T O N   P R O P A G A T I O N
%
%
% This is the Matlab program to simulate soliton propagation in
% optical fibers using the split-step Fourier method in Agrawal's
% book.
% Written by Nguyen Duc Nhan - 2005. Revised - 2010.
cla reset

%--- Physics constant ---------------------------------
c       = 3e8 ; % speed of light - m/s
OpLamda = 1.550e-6 ; % Wavelength - m

%--- Soliton parameters -------------------------------
N = 2; % Soliton order
To = 10e-12; % Soliton width - s
Ci = 0; % Chirp parameter
%--- Fiber parameters ---------------------------------
Dp = 17e-6 ; % Dispersion - s/m^2
ro      = 5e-6 ; % Core radius - m
Aeff    = pi*ro^2; % Core area - m^2
n2      = 2.6e-20 ; % Nonlinear refractive index
alphadB = 0; % attenuation factor - dB/km
Beta2   = -(Dp*OpLamda^2)/(2*pi*c) ; % GVD
Beta3   = 0; % Third order dispersion
Ld      = To^2/abs(Beta2) ; % Dispersion length
Zo      = pi*Ld/2 ; % Soliton period
Gamma   = (2*pi*n2)/(OpLamda*Aeff) ; % Nonlinear coefficient
Po      = N^2/(Gamma*Ld); % Soliton peak power - W

Alpha=log(10)*alphadB/(10*1000);     % fiber loss per meter

%--- Simulation parameters ----------------------------
h = 100; % Stepsize - m
Phi_nl = Gamma*Po*h; % Nonlinear phase shift
while Phi_nl > 0.05 % Keep the nonlinear phase shift lower the upper
limit
    h = h/2;
    Phi_nl = Gamma*Po*h;
end
Num_steps = round(2*Zo/h); % Number of steps in 2 soliton periods
SegNum
Num_blk = 20; % Size of data array for display
BlockSize     = round(Num_steps/Num_blk);
```

```
Lb = BlockSize*h; % Distance

Ns = 256; % FFT number of points

Ts      =To/20; % sampling time
t       = Ts*(-Ns/2:1:Ns/2-1);
w       = fftshift((2*pi/((Ns-1)*Ts))*(-Ns/2:1:Ns/2-1));
%-------------------------------------------------------------
Usol        = sqrt(Po).*sech(t/To).*exp(-j*Ci*t.^2./2/To.^2) ; %
Input field
ARR = abs(Usol).^2;
%---- Algorithm for Soliton Beam Propagation Method : Split Step
Model -----%

for k = 1:Num_steps
  D     = -j/2*Beta2.*(j.*w).^2 + 1/6*Beta3.*(j.*w).^3 - Alpha/2 ; %
Linear operator
  N1    = j*Gamma.*(abs(Usol)).^2 ;  % Nonlinear operator
  N2    = N1 ;
  % First half interval : dispersion operator only
    Udisp   = ifft( exp(h/2.*D) .* fft(Usol) ) ;
  % Iteration process to find N2
    for c = 1:2 % two iterations
      Utmp  = ifft( exp(h/2.*D) .* fft(Usol) ) ;
      UnonTmp  = exp(h/2.*(N1+N2)) .* Utmp ;
      U2tmp    = ifft( exp(h/2.*D) .* fft(UnonTmp) ) ;
      N2    = j*Gamma.*(abs(U2tmp)).^2 ;
    end
  % Second half interval : non linear operator only
    Unon    = exp(h/2.*(N1+N2)) .* Udisp ;
  % Whole segment propagation
    U2  = ifft(exp(h/2.*D).*fft(Unon));
    Usol=U2;

  if mod(k,BlockSize)==0
           ARR = [ARR ; abs(U2).^2]; % Store numerical data in an
array for plotting
  end
end
%---- Plotting ----------------------------------------------------
-------%
z = 0:Lb:2*Zo;
znorm = z./Zo; % Normalized distance
tnorm = t./To; % Normalized time window
ARR = ARR./Po; % Normalized intensity
[tp,zp] = meshgrid(tnorm,znorm);
mesh (tp,zp,ARR,'meshstyle','row','facecolor','none');
axis tight;
view(-25,42)
xlabel('t/To');ylabel('Z/Zo');
zlabel('Normalized intensity');
```

Appendix C

Calculation procedures of triple-correlation, bispectrum and examples

C.1 TRIPLE CORRELATION AND BISPECTRUM ESTIMATION

Definitions of triple-correlation and bispectrum for continuous signal *x(t)* are given in Chapter 7. However, calculation of both triple-correlation and bispectrum is normally achieved in discrete domain. Thus the discrete triple-correlation is estimated as follows:

$$C_3(\tau_1,\tau_2)=\sum_k x(kdt)x(kdt-\tau_1)x(kdt-\tau_2) \qquad \text{(C-1)}$$

where *x(kdt)* is the discrete version of *x(t)*, *k* is integer number, $dt = 1/f_s$ is the sampling period, f_s is the sampling frequency, the delay variables are also discretized as $\tau_i = mdt$, *m*= 0,1,2 ..., N/2-1. Although *x(t)* can be a complex signal, in this thesis, *x(t)* is the intensity of pulse from direct detection through a photodiode.

Similarly, the discrete bispectrum is estimated by the discrete Fourier transform of C_3

$$B_i(f_1,f_2)=\sum_m\sum_n C_3(mdt,ndt)\exp(-2\pi j(f_1 mdt+f_2 ndt)) \qquad \text{(C-2)}$$

where *m,n* are integers and the frequency variables $f_i = Kdf$, $K = 0,1,2...N/2-1$, and the frequency resolution $df = 2/(Ndt)$, *N* is the total number of samples in each computation window.

In this thesis, the following steps are used to estimate the bispectrum:

- A discrete process or signal is divided into *M* computation frames in which the number of samples *N* in each frame chosen is 1024. The sampling time dt is properly selected to ensure that whole significant frequency components of *x(kdt)* are in the range from *–B* to *B*, where *B = 1/(2dt)*.
- The triple-correlation of each data frame is computed by using (C-1). The result obtained is an array with the size 512x512. Each value in the array is represented for the amplitude of the triple-correlation.
- The bispectrum of each frame is then calculated by using discrete Fourier transform (C-2). Thus the bispectrum is also an array with the same size. Finally, the bispectrum is averaged over M data frames via the following expression:

$$B(f_1, f_2) = \frac{1}{M}\sum_{i=1}^{M} B_i(f_1, f_2) \qquad \text{(C-3)}$$

- Both the triple-correlation and the bispectrum can be displayed in a 3D graph as shown in Figure C-1 in which the magnitude is normalized in logarithmic scale. However, the contour representation is selected to display effectively the variation in the bispectrum structure.

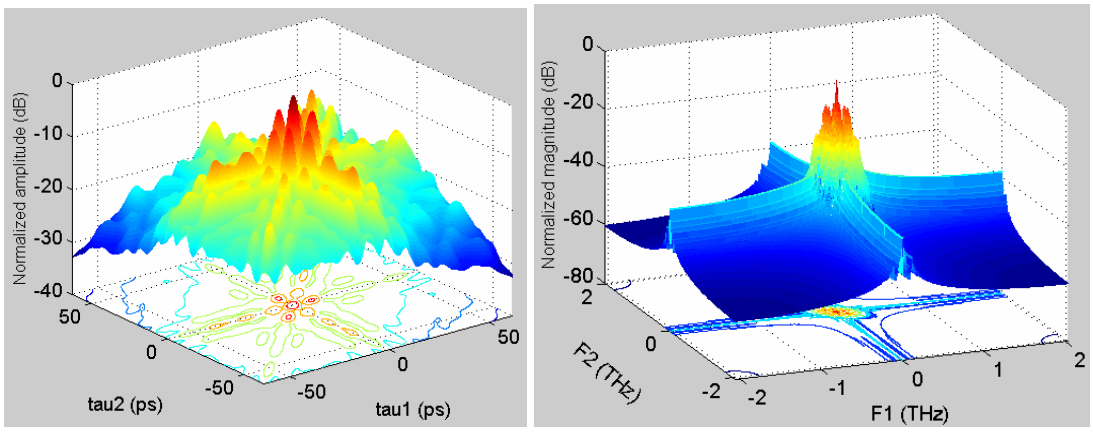

(a) (b)

Figure C-1 Graphical representations of (a) triple-correlation, and (b) magnitude bispectrum. (Bottoms: Corresponding contour representations).

C.2 PROPERTIES OF BISPECTRA

Important properties of the bispectrum are briefly summarized as follows [93]:

- The bispectrum is generally complex. It contains both magnitude and phase information which is important for signal recovery as well as identifying nonlinear response and processes. This property can be easily seen from estimation of bispectrum in frequency domain as follows:

  $$B_i(f_1, f_2) = X(f_1)X(f_2)X^*(f_1 + f_2) \qquad (3\text{-}4)$$

  where $X(f)$ is the Fourier transform of $x(t)$.

- The bispectrum has the lines of symmetry $f_1 = f_2$, $2f_1 = -f_2$ and $2f_2 = -f_1$ corresponding to permutation of the frequencies f_1, f_2.
- The bispectrum of a stationary, zero-mean Gaussian process is zero. Thus a non-zero bispectrum indicates a non-Gaussian process.
- The bispectrum suppresses linear phase information or constant phase shift information.
- The bispectrum is flat for non-Gaussian white noise and is zero for Gaussian white noise.

C.3 BIPSECTRUM OF OPTICAL PULSE PROPAGATION

In this section, the propagation of optical pulses through optical fibre is used as an example of triple-correlation and its bispectrum. Figure C-3, Figure C-4 and Figure C-5 show respectively the triple-correlations and the bispectra of the 6.25 ps Gaussian pulse propagating at different lengths of the optical fibre with the second-order GVD coefficient β_2 = -21.6 ps^2/km. Figure C-7, Figure C-8 and Figure C-9 show respectively the triple-correlations and the bispectra of the 6.25 ps Super-Gaussian pulse propagating at different lengths of the same fibre.

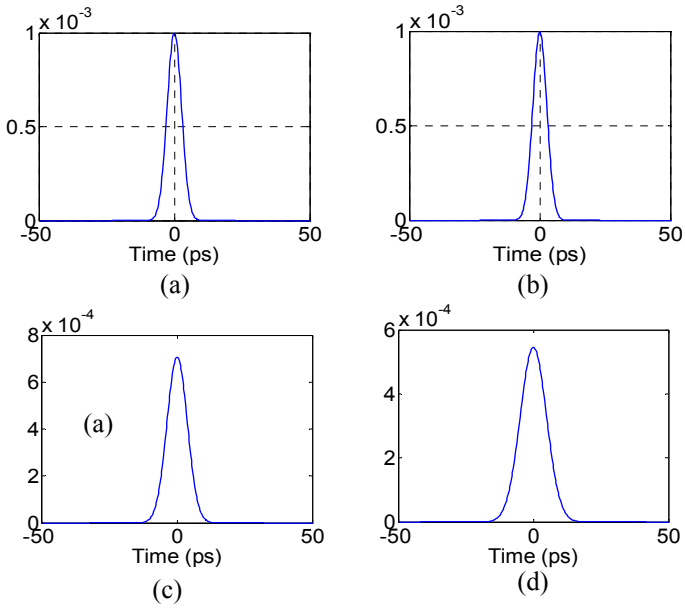

Figure C-2 Time traces of a Gaussian pulse propagating in the fibre with β_2 = -21.6 ps^2/km at different distances (a) z = 0, (b) z = 50 m, (c) z= 650 m, (d) z = 1 km.

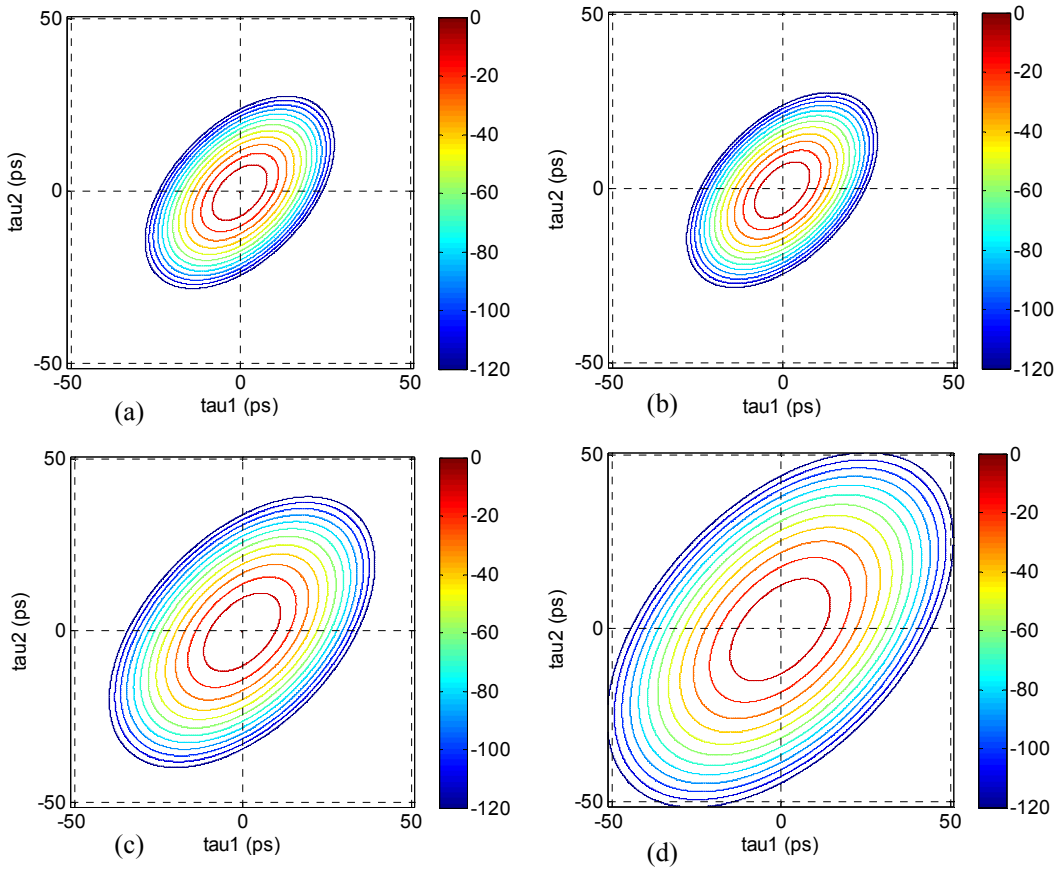

Figure C-3 Triple-correlations of a Gaussian pulse at different distances (a) z = 0, (b) z = 50 m, (c) z= 650 m, (d) z = 1 km.

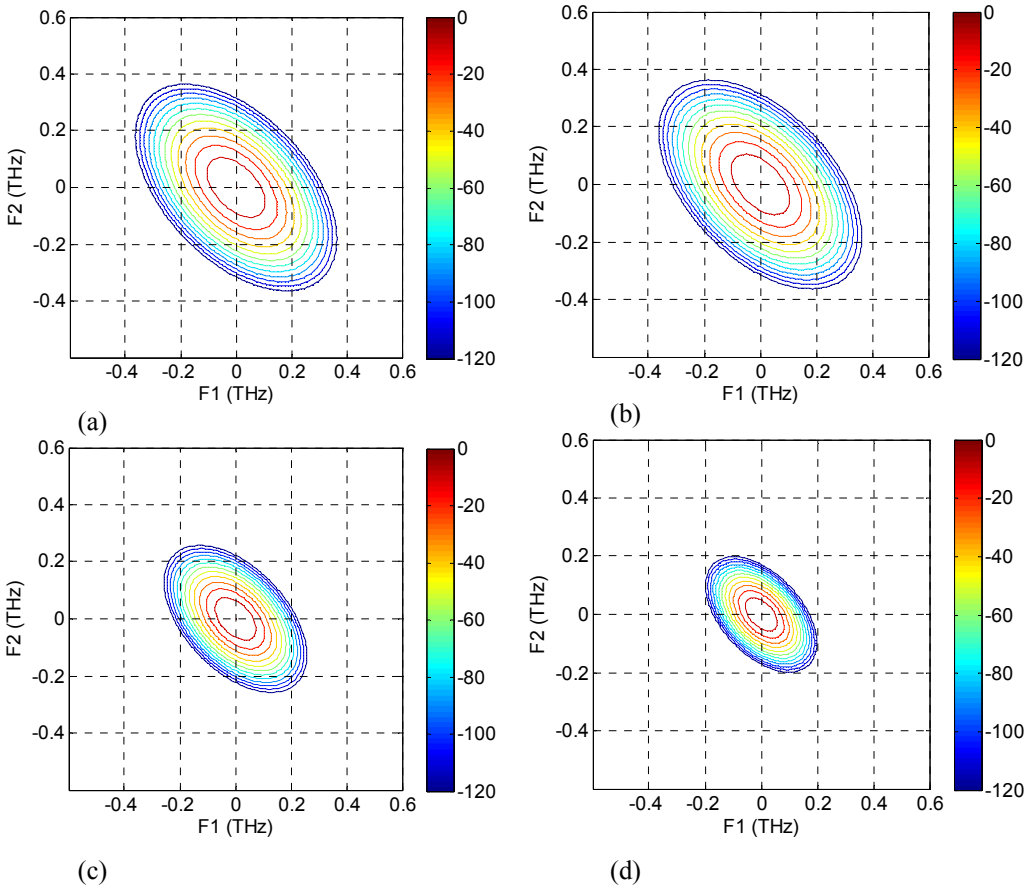

Figure C-4 Corresponding bispectra of a Gaussian pulse propagating in the fibre at different distances (a) z = 0, (b) z = 50 m, (c) z= 650 m, (d) z = 1 km.

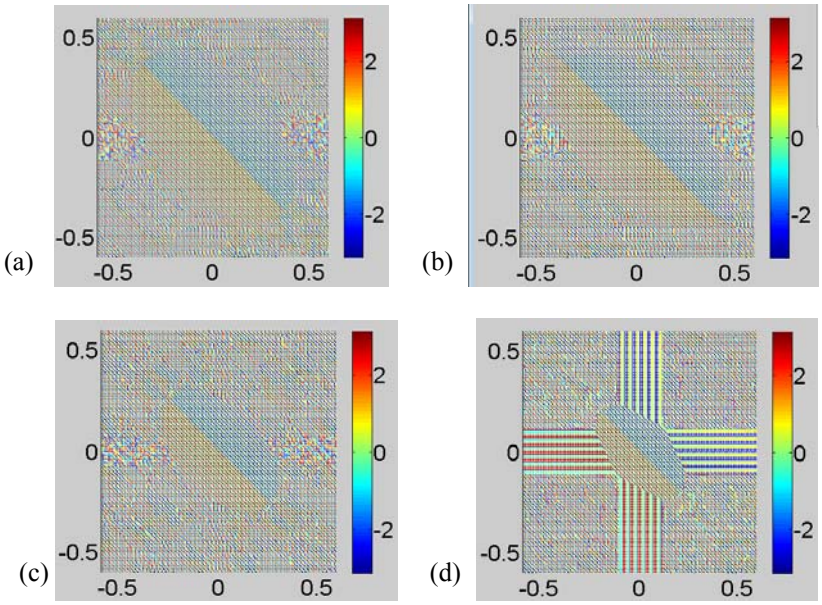

Figure C-5 Corresponding phase bispectra of a Gaussian pulse propagating in the fibre at different distances (a) z = 0, (b) z = 50 m, (c) z= 650 m, (d) z = 1 km.

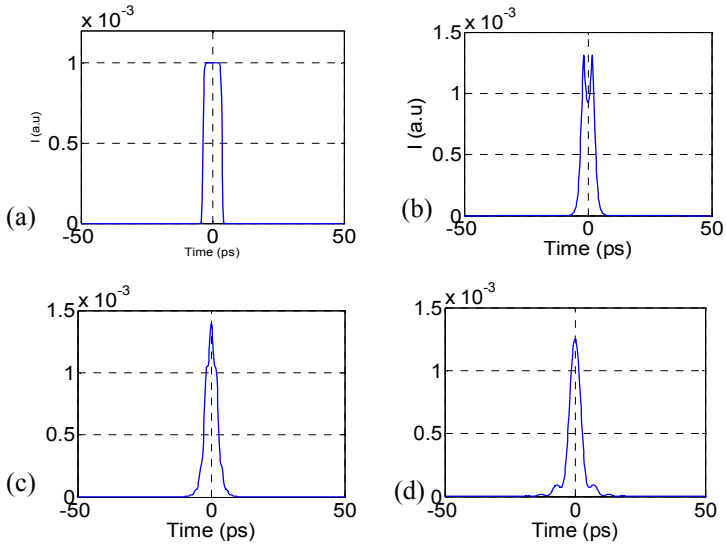

Figure C-6 Time traces of a Super-Gaussian pulse propagating in the fibre with β_2 = -21.6 ps^2/km at different distances (a) z = 0, (b) z = 50 m, (c) z= 100 m, (d) z = 300 m.

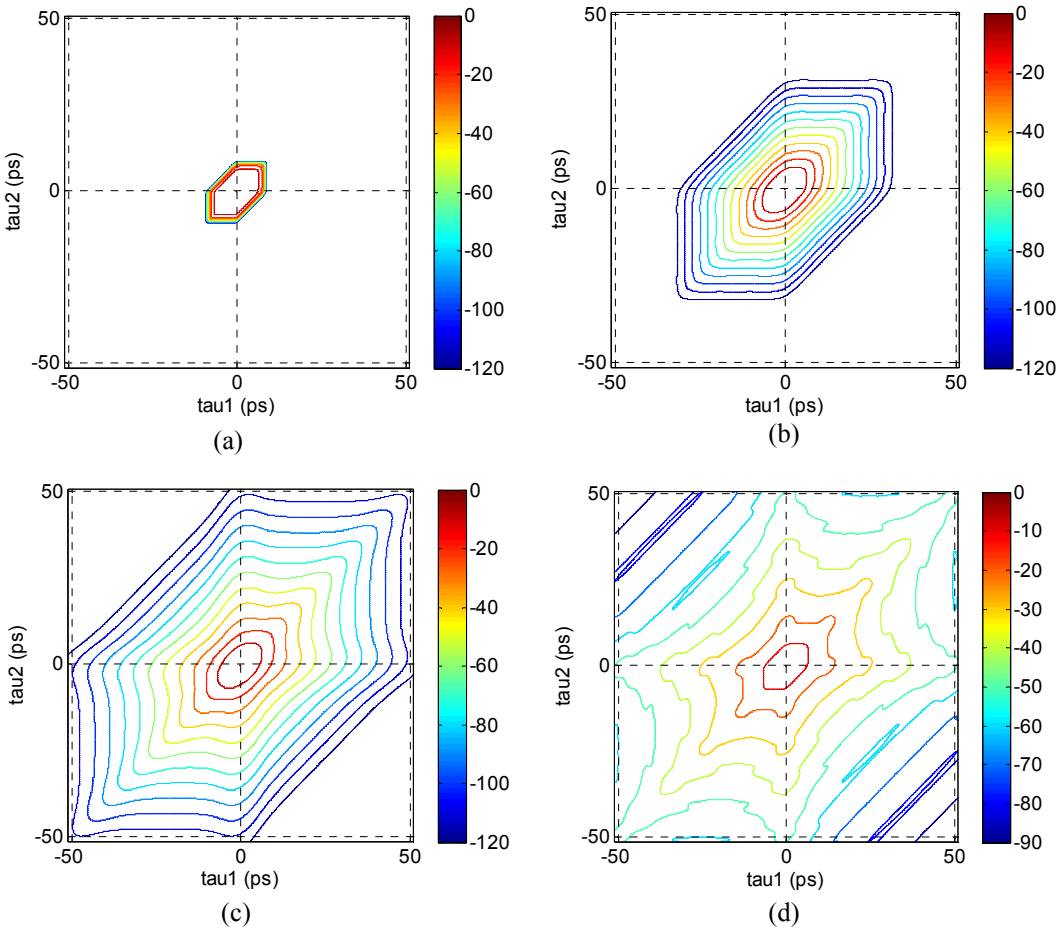

Figure C-7 Triple-correlations of a Super-Gaussian pulse propagating in the fibre at different distances (a) z = 0, (b) z = 50 m, (c) z= 100 m, (d) z = 300 m.

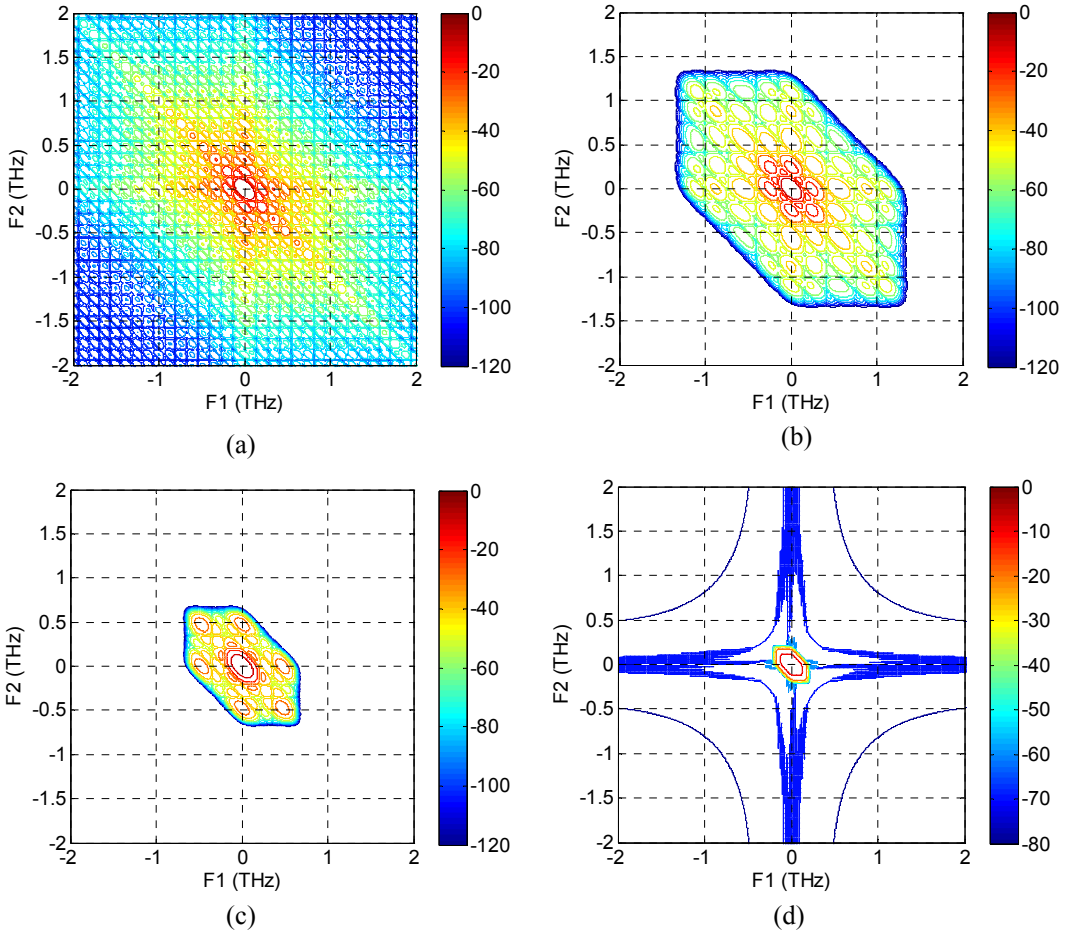

Figure C-8 Corresponding bispectra of the Super-Gaussian pulse propagating in the fibre at different distances (a) z = 0, (b) z = 50 m, (c) z= 100 m, (d) z = 300 m.

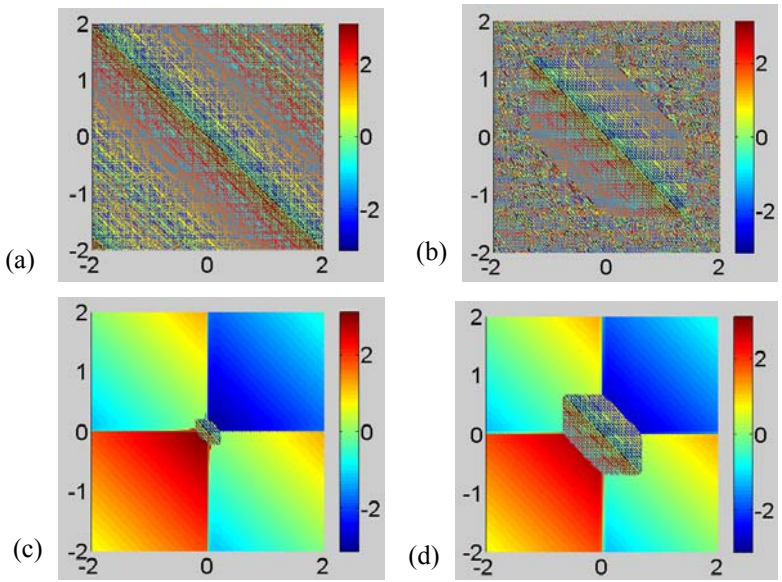

Figure C-9 The corresponding phase bispectra at (a) z = 0, (b) z = 50 m, (c) z= 100 m, (d) z = 300 m.

More important, the triple-correlation can detect easily the asymmetrical distortion of the pulse that is impossible in autocorrelation estimation. Figure C-10 and Figure C-11 show respectively the triple-correlations and the bispectra of the Super-Gaussian pulse propagating through the fibre with the third-order dispersion coefficient $\beta_3 = 0.133$ ps^3/km.

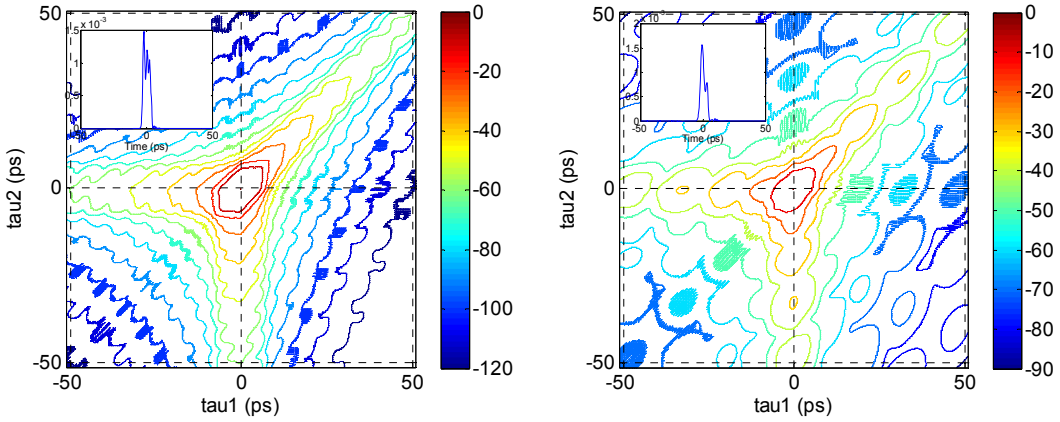

Figure C-10 Triple-correlations of a Super-Gaussian pulse propagating in the fibre with $\beta_2 = 0$, $\beta_3 = 0.133$ ps^3/km at different distances (a) z = 100 m, (b) z = 500 m. (Insets: The waveforms in time domain).

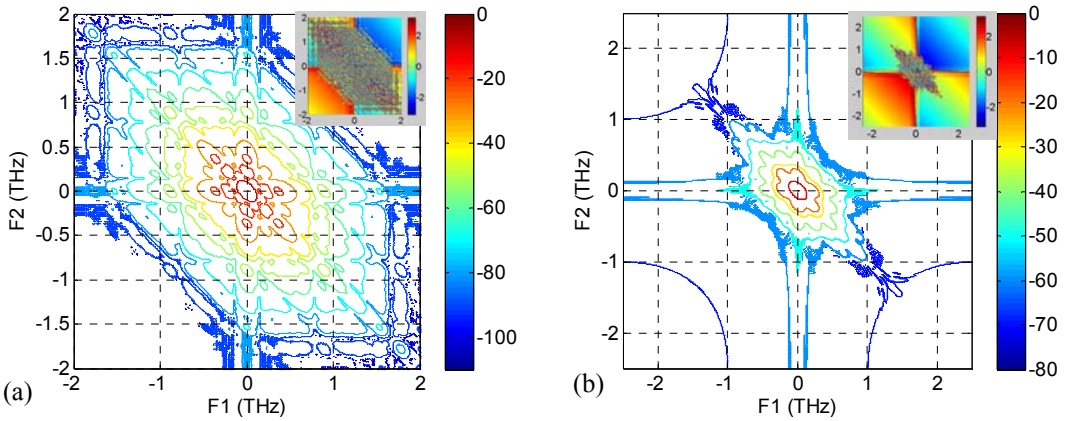

Figure C-11 Corresponding bispectra of the Super-Gaussian pulse propagating in the fibre at different distances (a) z = 100 m, (b) z = 500 m. (Insets: The corresponding phase bispectra).

Appendix D

Simulink models

D.1 MATLAB® and Simulink® modelling platforms

A modelling and simulation platform for optical fibre transmission systems has been developed using MATLAB and Simulink, an environment for simulation and model-based design [253]. There are some advantages of the Simulink modelling platform:

- Subsystem blocks for a complicated transmission system can be setup from the basic blocks available in the toolboxes and block-sets of the Simulink. It is noted that there is no block-sets for optical communication in Simulink. Therefore, the main functional blocks of the optical communication system in the Simulink platform have been developed for years. Details of operational principles as well as examples of the optical components and transmission systems can be found in [253].
- Signals can be easily monitored at any point along the simulation system by available scopes in Simulink block-sets.
- Numerical data can be stored for post-processing in MATLAB to estimate the performance of the system.

D.2 Simulink® model for FWM in optical waveguides

To model the parametric FWM process between multi-waves, the basic propagation equations are used. There are two approaches to simulate the interaction between waves. The first approach is to use the coupled equations system (7-4) which is called the separating channels approach [261]. In this approach, interactions between

different waves are obviously modelled by certain coupling terms in each coupled equation. Thus each optical wave considered as one separated channel is represented by a vector. The coupled equations system will be solved for solutions of the FWM process. The outputs of the nonlinear waveguide are also represented by separated vectors, hence the desired signal can be extracted without using a filter as described in Figure D-12(a).

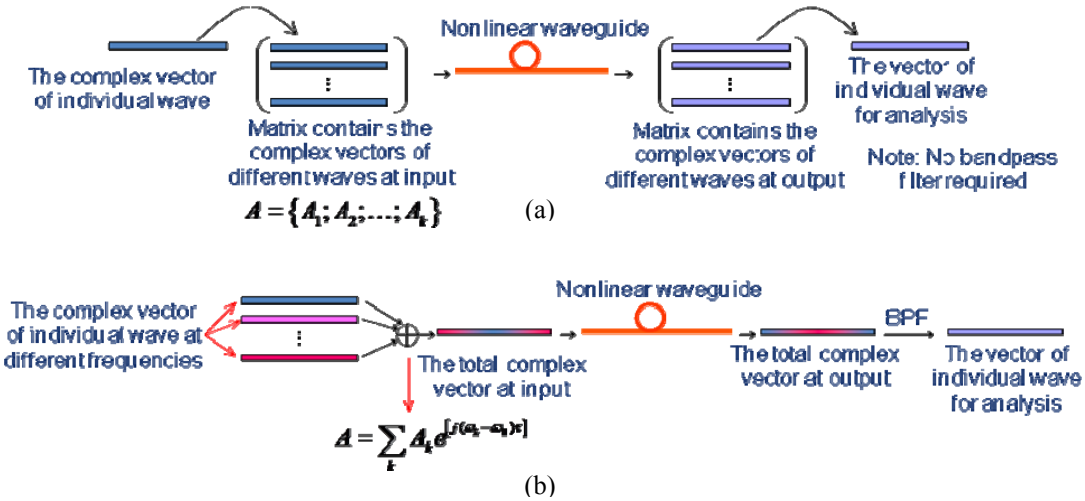

Figure D-12 A description of two approaches in modelling the parametric FWM process in nonlinear waveguides: (a) The separating wave approach, (b) the total complex field approach.

The second approach is to use the NLSE as described in Chapter 2 which can allow us to simulate all evolution effects of optical waves in the nonlinear waveguides. In this approach a total field is used instead of separated waves [60]. The total complex envelope A is represented by only one vector which is summation of individual complex amplitudes of different waves:

$$A=\sum_{k=1}^{N_c} A_k e^{[j(\omega_k-\omega_0)\tau]} \qquad (3\text{-}5)$$

where ω_0 is the defined angular central frequency, A_k, ω_k are the complex envelope and the carrier frequency of individual waves respectively. Hence, various waves at

different frequencies are combined into only a total signal vector which facilitates integration of the nonlinear waveguide model into the Simulink® platform. By this approach, the NLSE is numerically solved by the split-step method and then the block of nonlinear waveguide is developed by an embedded MATLAB program. Because only complex envelopes of the optical waves are considered in the simulation, each of different optical waves is shifted by a frequency difference between the central frequency and the frequency of the wave to allocate the wave in the frequency band of the total field. Then the summation of individual waves, which is equivalent to the combination process at optical coupler, is performed before the block of nonlinear waveguide as shown in Figure D-12(b). The output of nonlinear waveguide will be selected by an optical bandpass filter (BPF). In this way, the model of nonlinear waveguide can easily connect to other Simulink® blocks which are available in the platform for simulation of optical fiber communication systems [253].

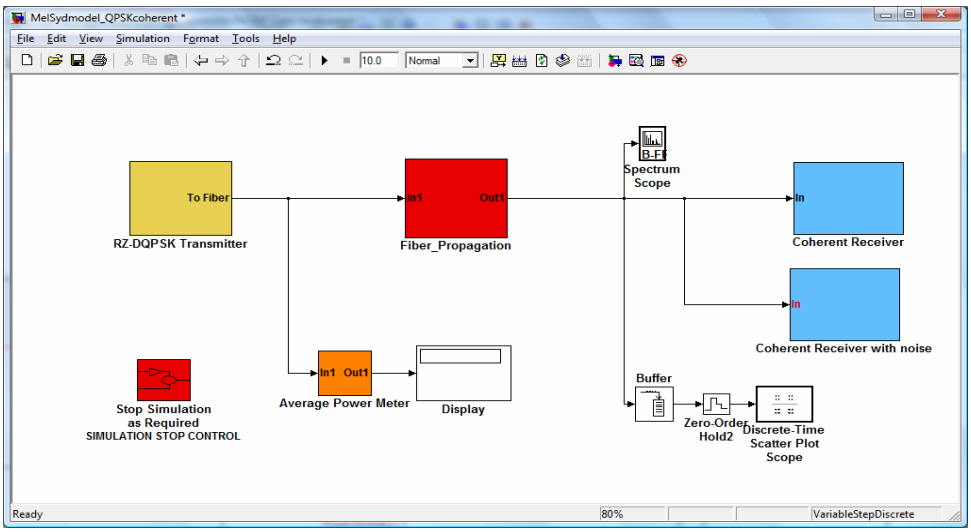

Figure D-2 An example of an optical fibre transmission system consisting of main blocks: optical transmitter, fibre transmission link and optical receiver.

An example of an optical fibre transmission system is shown in Figure D-2. Depending on different problems or targets, various Simulink models are setup for investigation in this thesis.

D.3 Wavelength converter in WDM system

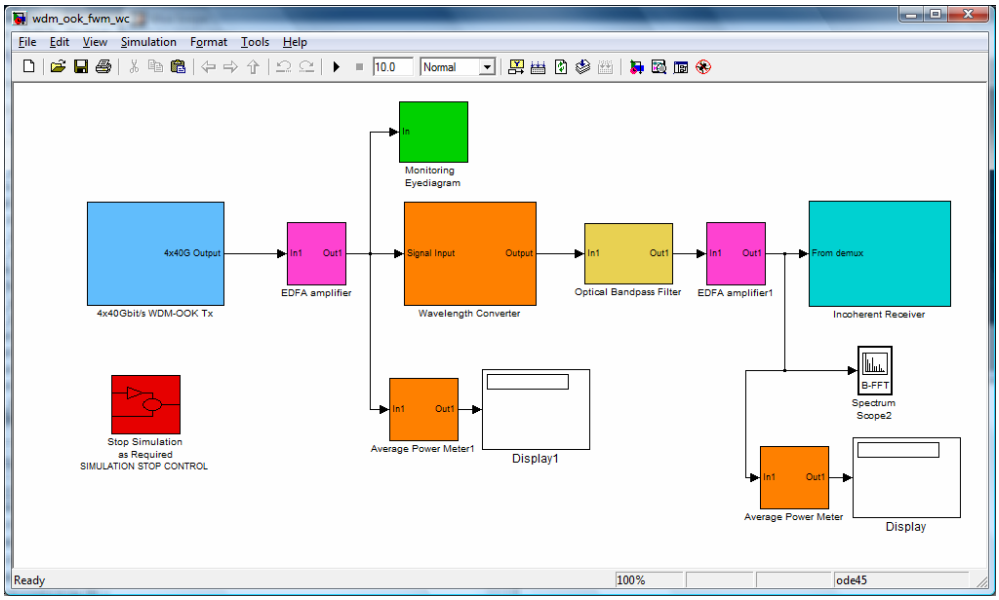

Figure D-3 The Simulink model of optical parametric amplifier used as a wavelength converter in WDM system.

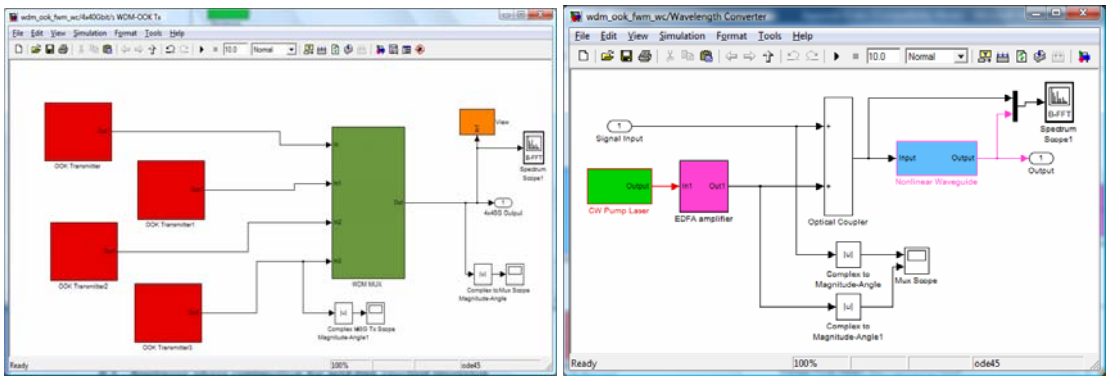

(a) (b)

Figure D-4 (a) Simulink model of WDM transmitter consisting of 4 optical transmitters at different wavelengths and a wavelength multiplexer. (b) Simulink setup of the parametric amplifier using the model of nonlinear waveguide used for wavelength conversion in WDM system.

D.4 Nonlinear phase conjugation for mid-link spectral inversion

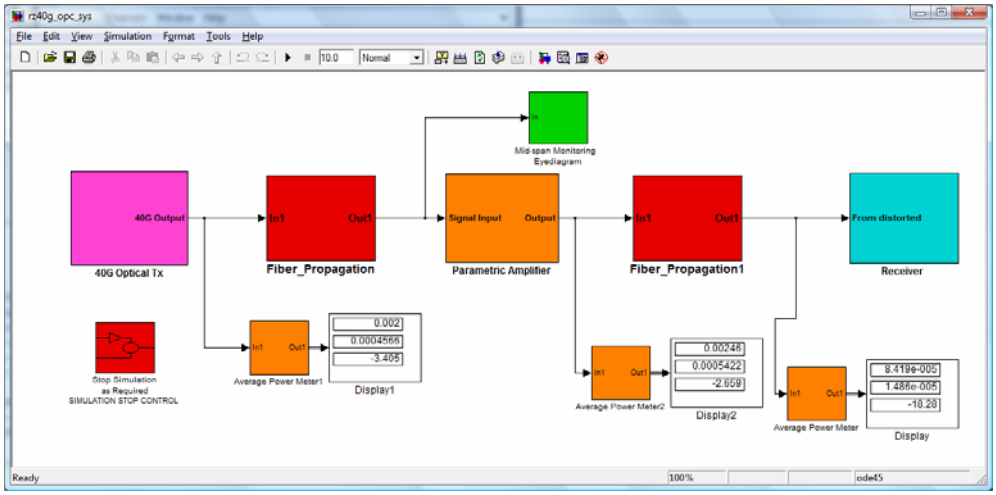

Figure D-5 Simulink setup of a long-haul 40 Gbit/s transmission system using NPC for distortion compensation.

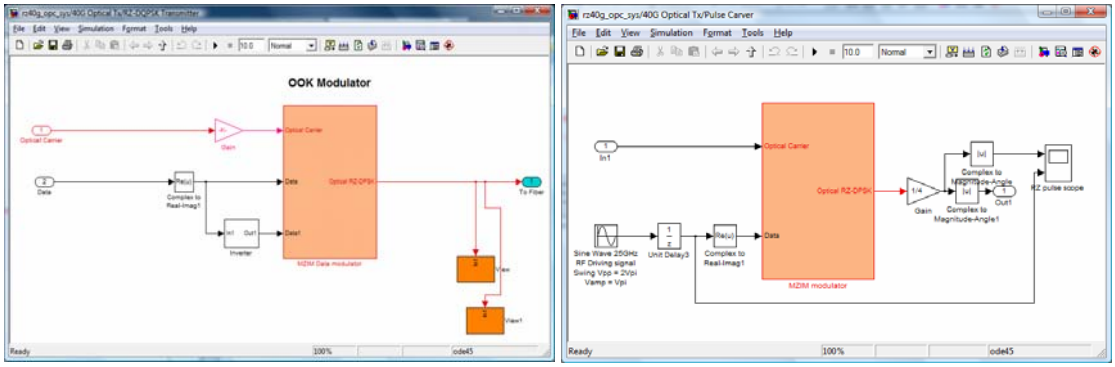

(a) (b)

Figure D-6 (a) Simulink model of an intensity optical modulator driven by data, (b) Simulink model of an optical pulse carver driven by a sinusoidal signal for RZ pulse generation.

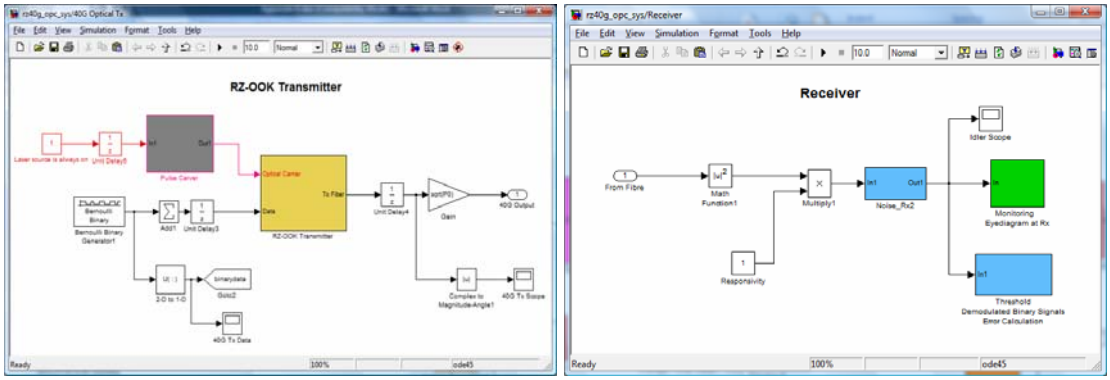

(a) (b)

Figure D-7 (a) Simulink model of an optical transmitter for RZ-OOK modulation scheme. (b) Simulink model of an optical receiver for OOK signal.

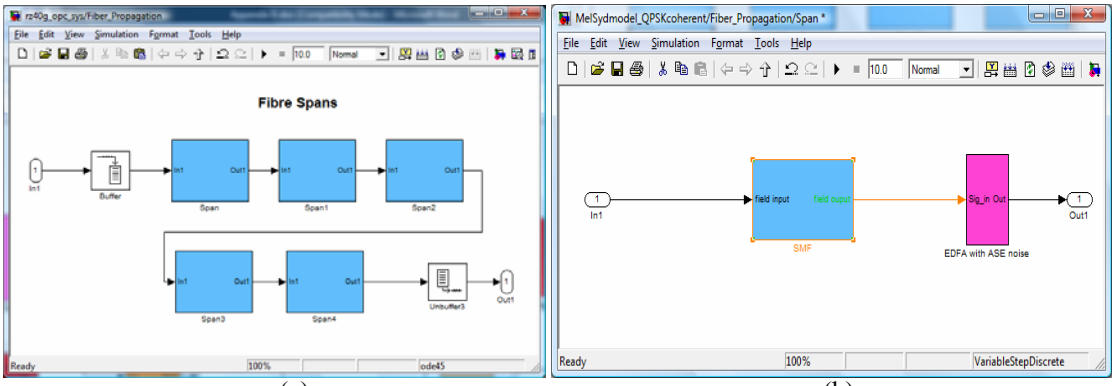

(a) (b)

Figure D-8 (a) Simulink model of each fibre transmission section consisting of 5 spans, (b) Simulink model of each span consisting of one SMF fibre and one EDFA for loss compensation.

D.5 Pulse generator

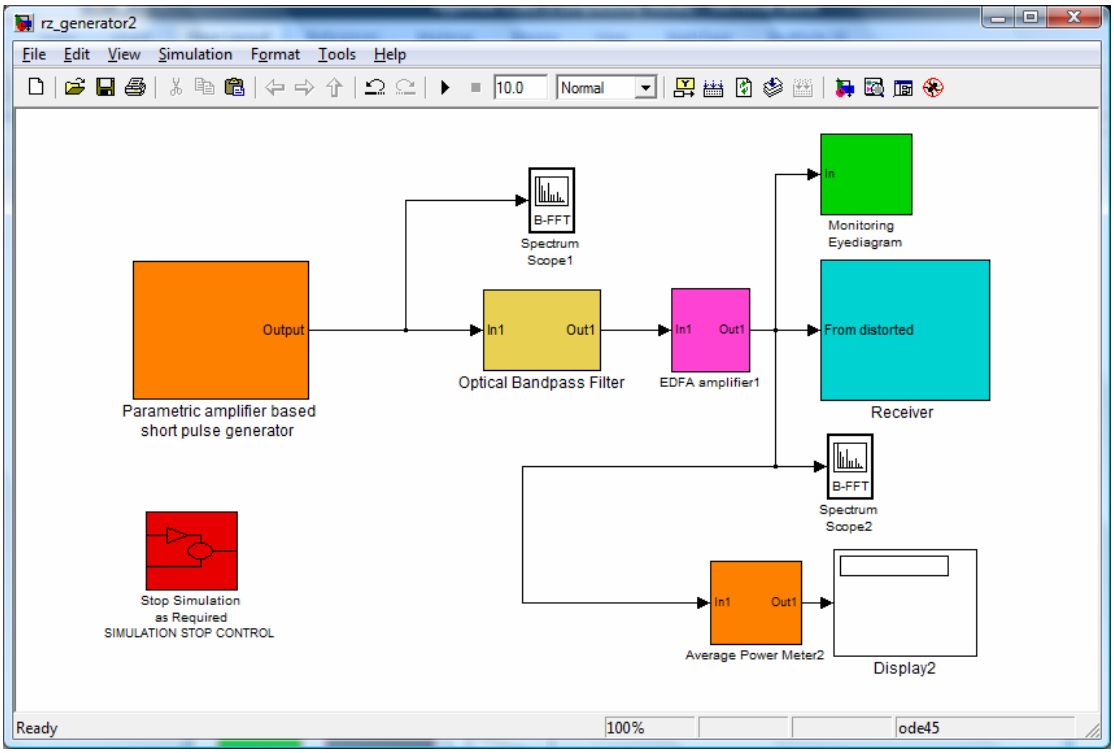

Figure D-9 Simulink setup of a short pulse generator at 40 GHz based on the parametric amplifier.

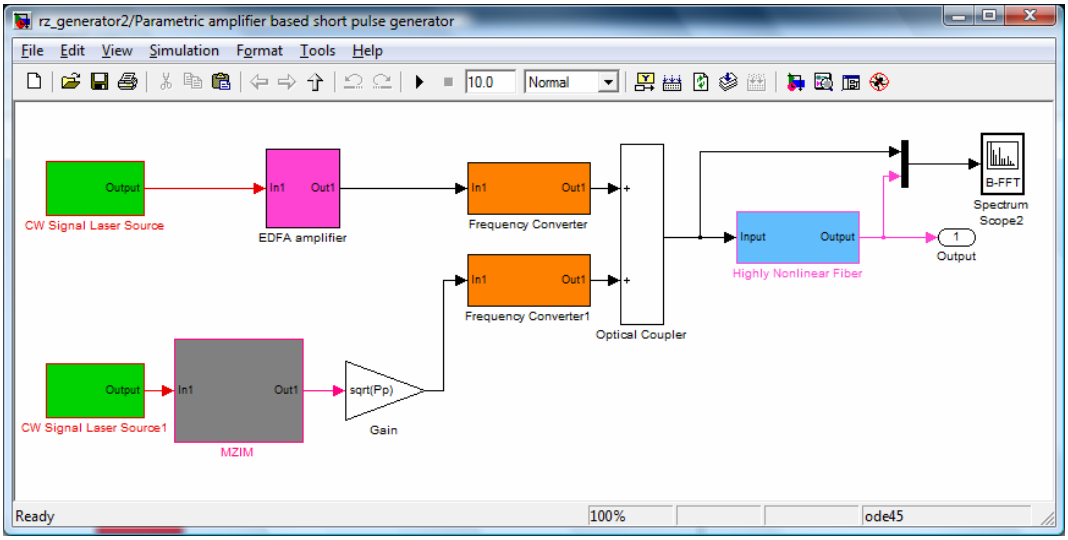

Figure D-10 Simulink blocks inside the 40 GHz short-pulse generator to demonstrate ultra-high speed switching based on parametric amplification.

D.6 OTDM demultiplexer

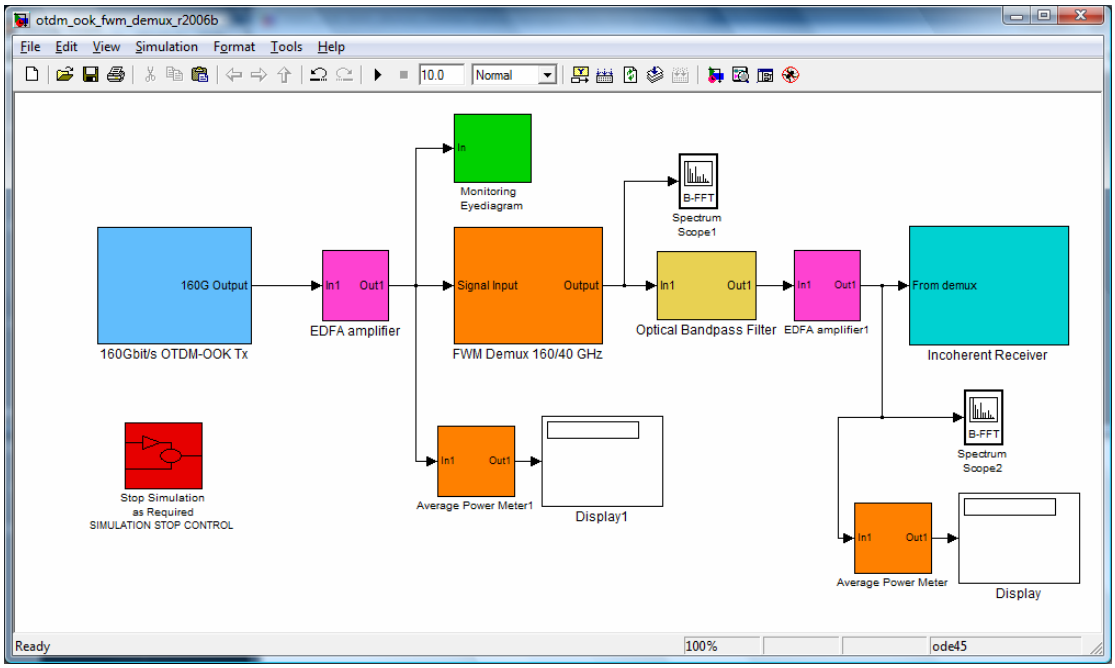

Figure D-11 Simulink setup of the 160 Gbit/s OTDM system using FWM process for demultiplexing.

For the OTDM system using OOK scheme, the Simulink models of the transmitter and receiver are similar to those shown in Figure D- with using a MLFL

instead of a carver. Figure D- shows the Simulink models of the transmitter and receiver in the OTDM system using DQPSK modulation scheme.

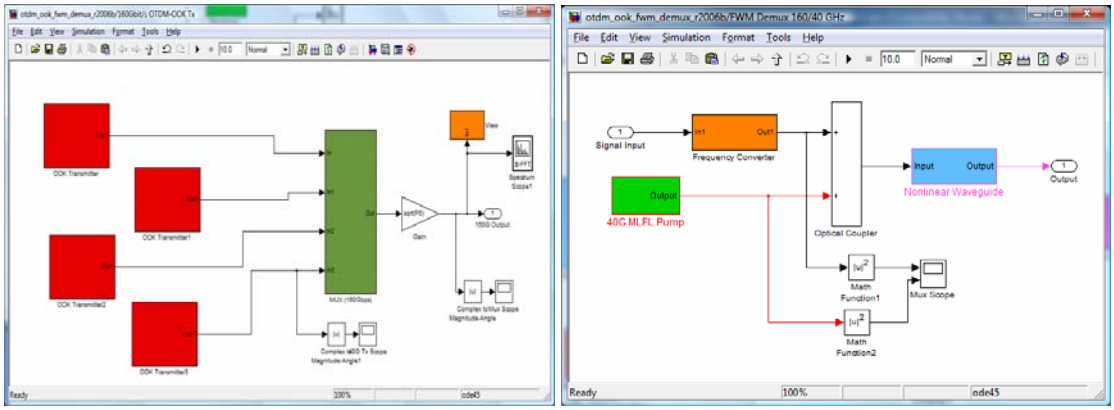

(a) (b)

Figure D-12 (a) Simulink model of OTDM transmitter consisting of 4 optical transmitter and an OTDM multiplexer, (b) Simulink model of the FWM-based demultiplxer.

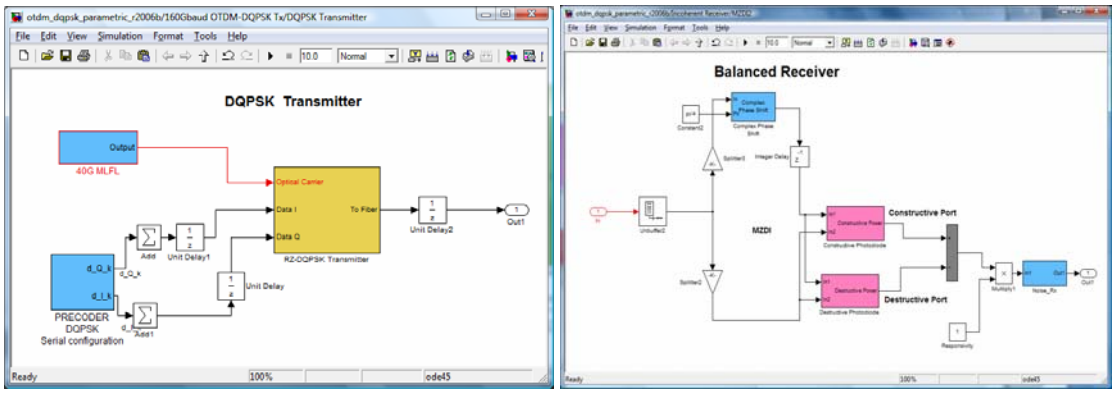

(a) (b)

Figure D-13 (a) Simulink model of an optical transmitter for DQPSK modulation scheme. (b) Simulink model of an optical balanced receiver for DQPSK signal.

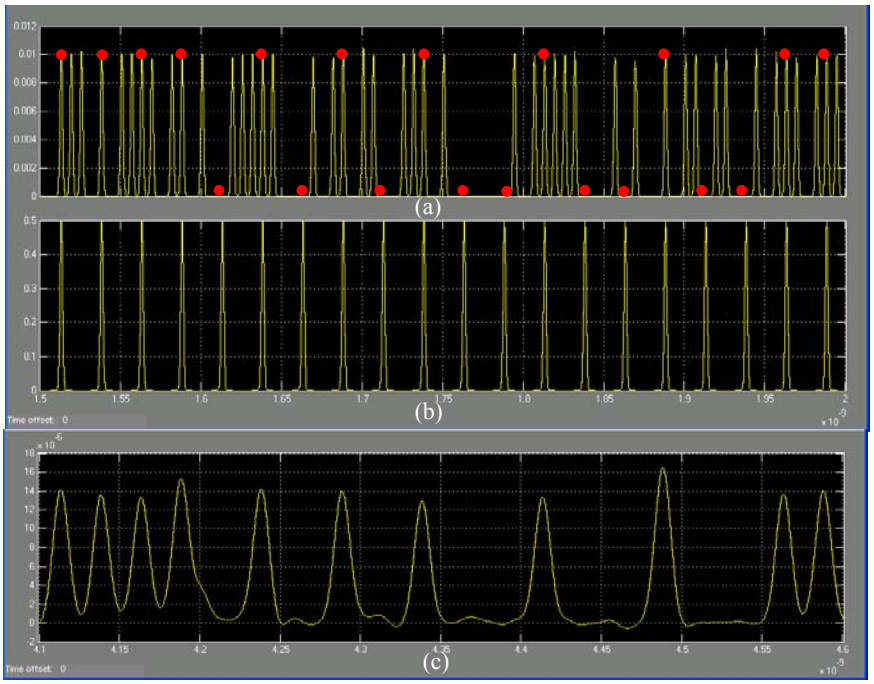

Figure D-14 Time traces of (a) the 160 Gbit/s OTDM signal, (b) the control signal, and (c) the 40 Gbit/s demultiplexed signal.

D.7 Triple correlation

Figure D- shows the Simulink® model for the triple correlation based on FWM in nonlinear waveguide. The structural block consists of two variable delay lines to generate delayed versions of the original signal as shown in Figure D- and frequency converters to convert the signal into different three waves before combining at the optical coupler to launch into the nonlinear waveguide.

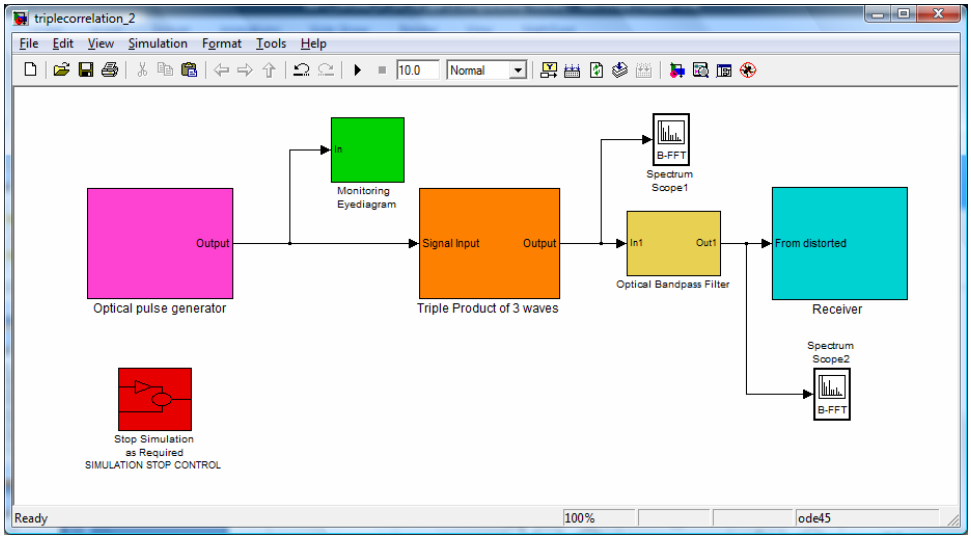

Figure D-15 Simulink setup for investigation of the triple-correlation based on FWM process.

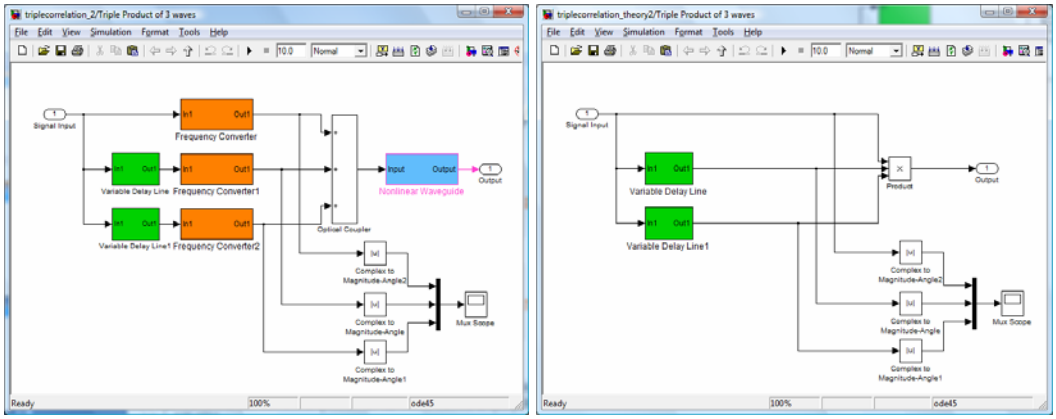

Figure D-16 (a) Simulink setup of the FWM-based triple-product generation, (b) Simulink setup of the theory-based triple-product generation.

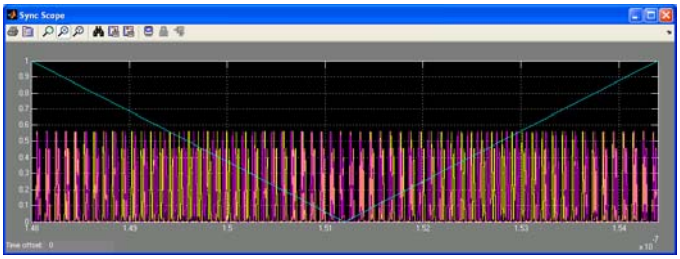

Figure D-17 The variation in time domain of the time delay variable (cyan), the original signal (violet) and the delayed signal (yellow).

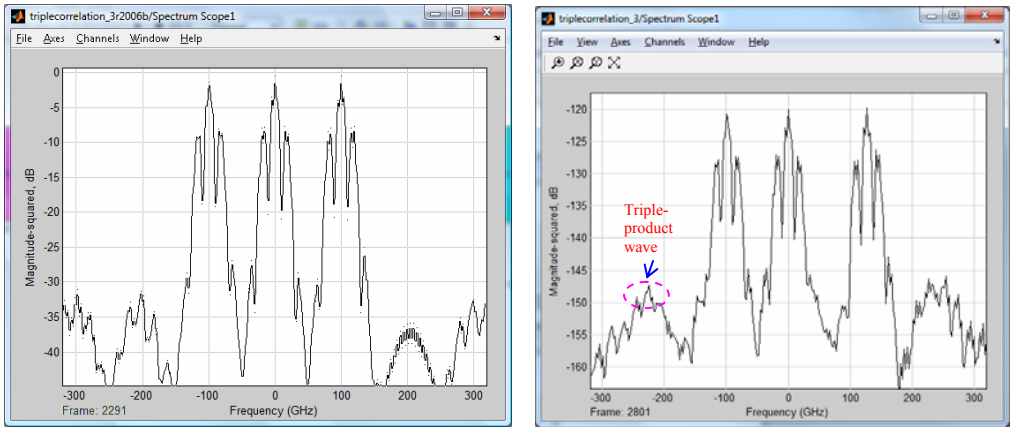

Figure D-18 (a) Spectrum with equal wavelength spacing at the output of the nonlinear waveguide, (b) Spectrum with unequal wavelength spacing at the output of the nonlinear waveguide.

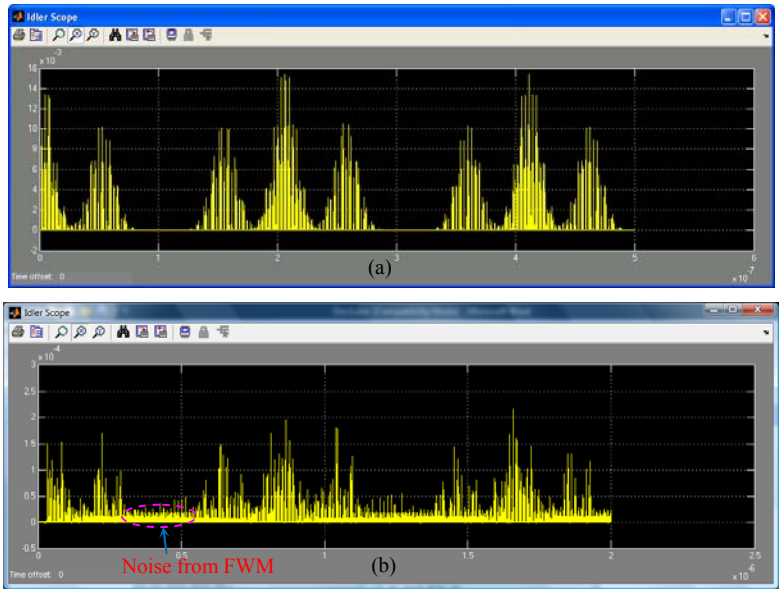

Figure D-19 Generated triple-product waves in time domain of the dual-pulse signal based on (a) theory, and (b) FWM in nonlinear waveguide.

References

[1] M. Nakazawa*, et al.*, "1.28 Tbit/s-70 km OTDM transmission using third- and fourth-order simultaneous dispersion compensation with a phase modulator," *Electronics Letters,* vol. 36, pp. 2027-2029, 2000.

[2] F. Kiyoshi*, et al.*, "10.92-Tb/s (273 x 40-Gb/s) triple-band/ultra-dense WDM optical-repeatered transmission experiment," in *Optical Fiber Communication Conference (OFC)*, Anaheim, California, 2001, p. PD24.

[3] A. H. Gnauck*, et al.*, "2.5 Tb/s (64x42.7 Gb/s) Transmission Over 40x100 km NZDSF Using RZ-DPSK Formatand All-Raman-Amplified Spans," in *Optical Fiber Communication Conference (OFC)*, Anaheim, California, 2002, p. FC2.

[4] A. D. Ellis*, et al.*, "Approaching the Non-Linear Shannon Limit," *Lightwave Technology, Journal of,* vol. 28, pp. 423-433, 2010.

[5] P. J. Winzer and R.-J. Essiambre, "Advanced Modulation Formats for High-Capacity Optical Transport Networks," *J. Lightwave Technol.,* vol. 24, pp. 4711-4728, 2006.

[6] S. Akihide*, et al.*, "69.1-Tb/s (432 x 171-Gb/s) C- and Extended L-Band Transmission over 240 Km Using PDM-16-QAM Modulation and Digital Coherent Detection," in *Optical Fiber Communication Conference (OFC)*, San Diego, California, 2010, p. PDPB7.

[7] A. Sano*, et al.*, "13.4-Tb/s (134 x111-Gb/s/ch) no-guard-interval coherent OFDM transmission over 3,600 km of SMF with 19-ps average PMD," in *Optical Communication, 2008. ECOC 2008. 34th European Conference on*, 2008, pp. 1-2.

[8] B. J. C. Schmidt*, et al.*, "100 Gbit/s transmission using single-band direct-detection Optical OFDM," in *Optical Fiber Communication - incudes post deadline papers, 2009. OFC 2009. Conference on*, 2009, pp. 1-3.

[9] W. Shieh, "High spectral efficiency coherent optical OFDM for 1 Tb/s Ethernet transport," in *Optical Fiber Communication - incudes post deadline papers, 2009. OFC 2009. Conference on*, 2009, pp. 1-3.

[10] HillerkussD*, et al.*, "26 Tbit s^{-1} line-rate super-channel transmission utilizing all-optical fast Fourier transform processing," *Nat Photon,* vol. 5, pp. 364-371, 2011.

[11] E. Ip*, et al.*, "Coherent detection in optical fiber systems," *Opt. Express,* vol. 16, pp. 753-791, 2008.

[12] M. Nakazawa, "Solitons for breaking barriers to terabit/second WDM and OTDM transmission in the next millennium," *Selected Topics in Quantum Electronics, IEEE Journal of,* vol. 6, pp. 1332-1343, 2000.

[13] M. Nakazawa, *et al.*, "Single-channel 80 Gbit/s soliton transmission over 10000 km using in-line synchronous modulation," *Electronics Letters,* vol. 35, pp. 162-164, 1999.

[14] K. L. Hall and K. A. Rauschenbach, "All-optical buffering of 40-Gb/s data packets," *Photonics Technology Letters, IEEE,* vol. 10, pp. 442-444, 1998.

[15] W. Lijun, *et al.*, "All-optical picosecond-pulse packet buffer based on four-wave mixing loading and intracavity soliton control," *Quantum Electronics, IEEE Journal of,* vol. 38, pp. 614-619, 2002.

[16] M. J. Potasek and Y. Yang, "Multiterabit-per-second all-optical switching in a nonlinear directional coupler," *Selected Topics in Quantum Electronics, IEEE Journal of,* vol. 8, pp. 714-721, 2002.

[17] F. Leo, *et al.*, "Temporal cavity solitons in one-dimensional Kerr media as bits in an all-optical buffer," *Nat Photon,* vol. 4, pp. 471-476, 2010.

[18] M. Nakazawa, *et al.*, "Ultrahigh-speed long-distance TDM and WDM soliton transmission technologies," *Selected Topics in Quantum Electronics, IEEE Journal of,* vol. 6, pp. 363-396, 2000.

[19] H. G. Weber, *et al.*, "Ultrahigh-Speed OTDM-Transmission Technology," *Lightwave Technology, Journal of,* vol. 24, pp. 4616-4627, 2006.

[20] C. Schmidt-Langhorst, *et al.*, "Generation and coherent time-division demultiplexing of up to 5.1 Tb/s single-channel 8-PSK and 16-QAM signals," in *Optical Fiber Communication - incudes post deadline papers, 2009. OFC 2009. Conference on*, 2009, pp. 1-3.

[21] C. C. Chang, *et al.*, "Code-division multiple-access encoding and decoding of femtosecond optical pulses over a 2.5-km fiber link," *Photonics Technology Letters, IEEE,* vol. 10, pp. 171-173, 1998.

[22] K. Mori, *et al.*, "Flatly broadened supercontinuum spectrum generated in a dispersion decreasing fibre with convex dispersion profile," *Electronics Letters,* vol. 33, pp. 1806-1808, 1997.

[23] P. W. Juodawlkis, *et al.*, "Optically sampled analog-to-digital converters," *Microwave Theory and Techniques, IEEE Transactions on,* vol. 49, pp. 1840-1853, 2001.

[24] C. Dorrer, *et al.*, "Linear optical sampling," *Photonics Technology Letters, IEEE,* vol. 15, pp. 1746-1748, 2003.

[25] Y. Han and B. Jalali, "Photonic time-stretched analog-to-digital converter: fundamental concepts and practical considerations," *Lightwave Technology, Journal of,* vol. 21, pp. 3085-3103, 2003.

[26] C. Schmidt-Langhorst and H.-G. Weber, "Optical sampling techniques," *Journal of Optical and Fiber Communications Research,* vol. 2, pp. 86-114, 2005.

[27] P. A. Andrekson and M. Westlund, "Nonlinear optical fiber based high resolution all-optical waveform sampling," *Laser & Photonics Reviews,* vol. 1, pp. 231-248, 2007.

[28] G. C. Valley, "Photonic analog-to-digital converters," *Opt. Express,* vol. 15, pp. 1955-1982, 2007.

[29] D. Y. Tang*, et al.*, "Observation of bound states of solitons in a passively mode-locked fiber laser," *Physical Review A,* vol. 64, p. 033814, 2001.

[30] D. Y. Tang*, et al.*, "Bound-soliton fiber laser," *Physical Review A,* vol. 66, p. 033806, 2002.

[31] P. Grelu*, et al.*, "Phase-locked soliton pairs in a stretched-pulse fiber laser," *Opt. Lett.,* vol. 27, pp. 966-968, 2002.

[32] L. M. Zhao*, et al.*, "Period-doubling and quadrupling of bound solitons in a passively mode-locked fiber laser," *Optics Communications,* vol. 252, pp. 167-172, 2005.

[33] A. Haboucha*, et al.*, "Coherent soliton pattern formation in a fiber laser," *Opt. Lett.,* vol. 33, pp. 524-526, 2008.

[34] H. A. Haus, "Mode-locking of lasers," *Selected Topics in Quantum Electronics, IEEE Journal of,* vol. 6, pp. 1173-1185, 2000.

[35] P. M. Anandarajah*, et al.*, "System-Performance Analysis of Optimized Gain-Switched Pulse Source Employed in 40- and 80-Gb/s OTDM Systems," *Lightwave Technology, Journal of,* vol. 25, pp. 1495-1502, 2007.

[36] H. Murata*, et al.*, "Optical pulse generation by electrooptic-modulation method and its application to integrated ultrashort pulse generators," *Selected Topics in Quantum Electronics, IEEE Journal of,* vol. 6, pp. 1325-1331, 2000.

[37] M. Horowitz*, et al.*, "Theoretical and experimental study of harmonically modelocked fiber lasers for optical communication systems," *Lightwave Technology, Journal of,* vol. 18, pp. 1565-1574, 2000.

[38] M. Zirngibl*, et al.*, "1.2 ps pulses from passively mode-locked laser diode pumped Er-doped fibre ring laser," *Electronics Letters,* vol. 27, pp. 1734-1735, 1991.

[39] I. N. Duling, III, "Subpicosecond all-fibre erbium laser," *Electronics Letters,* vol. 27, pp. 544-545, 1991.

[40] K. Tamura*, et al.*, "Self-starting additive pulse mode-locked erbium fibre ring laser," *Electronics Letters,* vol. 28, pp. 2226-2228, 1992.

[41] M. Nakazawa*, et al.*, "Low threshold, 290 fs erbium-doped fiber laser with a nonlinear amplifying loop mirror pumped by InGaAsP laser diodes," *Applied Physics Letters,* vol. 59, pp. 2073-2075, 1991.

[42] K. Tamura*, et al.*, "77-fs pulse generation from a stretched-pulse mode-locked all-fiber ring laser," *Opt. Lett.,* vol. 18, pp. 1080-1082, 1993.

[43] K. Tamura*, et al.*, "Technique for obtaining high-energy ultrashort pulses from an additive-pulse mode-locked erbium-doped fiber ring laser," *Opt. Lett.,* vol. 19, pp. 46-48, 1994.

[44] G. Lenz*, et al.*, "All-solid-state femtosecond source at 1.55 μm," *Opt. Lett.,* vol. 20, pp. 1289-1291, 1995.

[45] D. Y. Tang and L. M. Zhao, "Generation of 47-fs pulses directly from an erbium-doped fiber laser," *Opt. Lett.,* vol. 32, pp. 41-43, 2007.

[46] K. Tamura*, et al.*, "Unidirectional ring resonators for self-starting passively mode-locked lasers," *Opt. Lett.,* vol. 18, pp. 220-222, 1993.

[47] F. Krausz and T. Brabec, "Passive mode locking in standing-wave laser resonators," *Opt. Lett.,* vol. 18, pp. 888-890, 1993.

[48] A. B. Grudinin and S. Gray, "Passive harmonic mode locking in soliton fiber lasers," *J. Opt. Soc. Am. B,* vol. 14, pp. 144-154, 1997.

[49] M. Nakazawa and E. Yoshida, "A 40-GHz 850-fs regeneratively FM mode-locked polarization-maintaining erbium fiber ring laser," *Photonics Technology Letters, IEEE,* vol. 12, pp. 1613-1615, 2000.

[50] Y. J. Kim*, et al.*, "Pulse stabilisation in harmonically FM modelocked erbium fibre ring laser with DFBLD," *Electronics Letters,* vol. 41, pp. 837 - 838, 2005.

[51] N. G. Usechak*, et al.*, "FM mode-locked fiber lasers operating in the autosoliton regime," *Quantum Electronics, IEEE Journal of,* vol. 41, pp. 753-761, 2005.

[52] D. Kuizenga and A. Siegman, "FM and AM mode locking of the homogeneous laser--Part I: Theory," *Quantum Electronics, IEEE Journal of,* vol. 6, pp. 694-708, 1970.

[53] K. Tamura and M. Nakazawa, "Pulse energy equalization in harmonically FM mode-locked lasers with slow gain," *Opt. Lett.,* vol. 21, pp. 1930-1932, 1996.

[54] Y. Shiquan and B. Xiaoyi, ""Rational harmonic mode-locking" in a phase-modulated fiber laser," *Photonics Technology Letters, IEEE,* vol. 18, pp. 1332-1334, 2006.

[55] M. E. Grein*, et al.*, "Quantum-limited timing jitter in actively modelocked lasers," *Quantum Electronics, IEEE Journal of,* vol. 40, pp. 1458-1470, 2004.

[56] C. R. Doerr*, et al.*, "Asynchronous soliton mode locking," *Opt. Lett.,* vol. 19, pp. 1958-1960, 1994.

[57] W.-W. Hsiang*, et al.*, "Direct generation of a 10 GHz 816 fs pulse train from an erbium-fiber soliton laser with asynchronous phase modulation," *Opt. Lett.,* vol. 30, pp. 2493-2495, 2005.

[58] S. B. Eduardo*, et al.*, "396 fs, 2.5-12 GHz Asynchronous Mode-Locking Erbium Fiber Laser," 2007, p. CMC2.

[59] K. R. Tamura and M. Nakazawa, "54-fs, 10-GHz soliton generation from a polarization-maintaining dispersion-flattened dispersion-decreasing fiber pulse compressor," *Opt. Lett.,* vol. 26, pp. 762-764, 2001.

[60] G. P. Agrawal, *Nonlinear fiber optics* 3rd ed. San Diego Academic Press, 2001.

[61] Y. G. (Yili), *Nonlinear photonics : nonlinearities in optics, optoelectronics, and fiber communications* Hong Kong : Chinese University Press ; Berlin ; New York : Springer, 2002.

[62] T. Schneider, *Nonlinear optics in telecommunications* Berlin ; New York :: Springer, 2004.

[63] P. Bayvel and R. Killey, "Nonlinear Optical Effects in WDM Transmission," in *Optical Fiber Telecommunications IV B*, I. P. Kaminow and T. Li, Eds., ed: Academic Press, 2002, pp. 611-641.

[64] G. P. Agrawal, *Applications of nonlinear fiber optics*: San Diego : Academic Press, 2001.

[65] Y. S. Kivshar and G. P. Agrawal, *Optical solitons from fibers to photonic crystals*. Amsterdam ; Boston: Academic Press, 2003.

[66] F. Ilday*, et al.*, "Self-Similar Evolution of Parabolic Pulses in a Laser," *Physical Review Letters,* vol. 92, p. 213902, 2004.

[67] A. Chong*, et al.*, "Properties of normal-dispersion femtosecond fiber lasers," *J. Opt. Soc. Am. B,* vol. 25, pp. 140-148, 2008.

[68] F. X. Kärtner*, et al.*, "Solitary-pulse stabilization and shortening in actively mode-locked lasers," *J. Opt. Soc. Am. B,* vol. 12, pp. 486-496, 1995.

[69] T. F. Carruthers and I. N. Duling Iii, "10-GHz, 1.3-ps erbium fiber laser employing soliton pulse shortening," *Opt. Lett.,* vol. 21, pp. 1927-1929, 1996.

[70] A. Zeitouny*, et al.*, "Stable operating region in a harmonically actively mode-locked fiber laser," *Quantum Electronics, IEEE Journal of,* vol. 41, pp. 1380-1387, 2005.

[71] M. Nakazawa*, et al.*, "Supermode noise suppression in a harmonically modelocked fibre laser by selfphase modulation and spe," *Electronics Letters,* vol. 32, p. 461, 1996.

[72] S. Yang*, et al.*, "Experimental study on relaxation oscillation in a detuned FM harmonic mode-locked Er-doped fiber laser," *Optics Communications,* vol. 245, pp. 371-376, 2005.

[73] K. W. DeLong*, et al.*, "Frequency-resolved optical gating with the use of second-harmonic generation," *J. Opt. Soc. Am. B,* vol. 11, pp. 2206-2215, 1994.

[74] D. Meshulach*, et al.*, "Measurement of ultrashort optical pulses by third-harmonic generation," *J. Opt. Soc. Am. B,* vol. 14, pp. 2122-2125, 1997.

[75] C. Dorrer and D. N. Maywar, "RF Spectrum Analysis of Optical Signals Using Nonlinear Optics," *J. Lightwave Technol.,* vol. 22, p. 266, 2004.

[76] M. D. Pelusi*, et al.*, "Terahertz bandwidth RF spectrum analysis of femtosecond pulses using a chalcogenide chip," *Opt. Express,* vol. 17, pp. 9314-9322, 2009.

[77] G.-W. Lu*, et al.*, "Experimental Demonstrations of All-Optical Phase-Multiplexing Using FWM-Based Phase Interleaving in Silica and Bismuth-

Oxide HNLFs," *Lightwave Technology, Journal of,* vol. 27, pp. 409 - 416, 2009.

[78] H. Murai*, et al.*, "Regenerative SPM-Based Wavelength Conversion and Field Demonstration of 160-Gb/s All-Optical 3R Operation," *J. Lightwave Technol.,* vol. 28, pp. 910-921, 2010.

[79] G.-W. Lu, "Optical signal processing for advanced optical modulation format," presented at the Photonics Society Summer Topical Meeting Series, 2010 IEEE, Playa del Carmen, 2010.

[80] M. D. Pelusi*, et al.*, "Wavelength Conversion of High-Speed Phase and Intensity Modulated Signals Using a Highly Nonlinear Chalcogenide Glass Chip," *Photonics Technology Letters, IEEE,* vol. 22, pp. 3-5, 2010.

[81] D. V. Trung*, et al.*, "Photonic Chip Based 1.28 Tbaud Transmitter Optimization and Receiver OTDM Demultiplexing," 2010, p. PDPC5.

[82] M. Takahashi*, et al.*, "Low-loss and low-dispersion-slope highly nonlinear fibers," *Lightwave Technology, Journal of,* vol. 23, pp. 3615-3624, 2005.

[83] J. C. Knight*, et al.*, "Anomalous dispersion in photonic crystal fiber," *Photonics Technology Letters, IEEE,* vol. 12, pp. 807-809, 2000.

[84] J. K. Ranka*, et al.*, "Optical properties of high-delta air silica microstructure optical fibers," *Opt. Lett.,* vol. 25, pp. 796-798, 2000.

[85] S. Naoki*, et al.*, "Bismuth-based optical fiber with nonlinear coefficient of 1360 $W^{-1}km^{-1}$," 2004, p. PD26.

[86] R. E. Slusher*, et al.*, "Large Raman gain and nonlinear phase shifts in high-purity As_2Se_3 chalcogenide fibers," *J. Opt. Soc. Am. B,* vol. 21, pp. 1146-1155, 2004.

[87] M. R. Lamont*, et al.*, "Dispersion engineering of highly nonlinear As2S3 waveguides for parametric gain and wavelength conversion," *Opt. Express,* vol. 15, pp. 9458-9463, 2007.

[88] K. Vu and S. Madden, "Tellurium dioxide Erbium doped planar rib waveguide amplifiers with net gain and 2.8dB/cm internal gain," *Opt. Express,* vol. 18, pp. 19192-19200, 2010.

[89] S. T. Cundiff, "Soliton Dynamics in Mode-Locked Lasers," in *Dissipative Solitons*. vol. 661, N. Akhmediev and A. Ankiewicz, Eds., ed: Springer Berlin / Heidelberg, 2005, pp. 183-206.

[90] J. J. O'Neil*, et al.*, "Theory and simulation of the dynamics and stability of actively modelocked lasers," *Quantum Electronics, IEEE Journal of,* vol. 38, pp. 1412-1419, 2002.

[91] N. Akhmediev*, et al.*, "Dissipative soliton interactions inside a fiber laser cavity," *Optical Fiber Technology,* vol. 11, pp. 209-228, 2005.

[92] J. G. Proakis and D. G. Manolakis, *Digital signal processing : principles, algorithms, and applications* 2nd ed. ed. New York: Maxwell Macmillan International, 1992.

[93] C. L. Nikias and M. R. Raghuveer, "Bispectrum estimation: A digital signal processing framework," *Proc. IEEE,* vol. 75, pp. 869-891, 1987.

[94] C. L. Nikias and J. M. Mendel, "Signal processing with higher-order spectra," *Signal Processing Magazine, IEEE,* vol. 10, pp. 10-37, 1993.

[95] N. Akhmediev and A. Ankiewicz, Eds., *Dissipative Solitons* (Lecture Notes in Physics 661). Berlin Springer, 2005, p.^pp. Pages.

[96] G. P. Agrawal, "Optical pulse propagation in doped fiber amplifiers," *Physical Review A,* vol. 44, p. 7493, 1991.

[97] S. C. Mancas and S. R. Choudhury, "The complex cubic-quintic Ginzburg-Landau equation: Hopf bifurcations yielding traveling waves," *Math. Comput. Simul.,* vol. 74, pp. 281-291, 2007.

[98] H. A. Haus*, et al.*, "Structures for additive pulse mode locking," *J. Opt. Soc. Am. B,* vol. 8, pp. 2068-2076, 1991.

[99] J. N. Kutz, "Mode-Locked Soliton Lasers," *SIAM Review,* vol. 48, pp. 629-678, 2006.

[100] B. E. A. Saleh and M. C. Teich, "Laser amplifiers," in *Fundamentals of photonics*, ed New York: Wiley, 1991, pp. 460-493.

[101] N. G. Usechak and G. P. Agrawal, "Rate-equation approach for frequency-modulation mode locking using the moment method," *J. Opt. Soc. Am. B,* vol. 22, pp. 2570-2580, 2005.

[102] C. Menyuk, "Nonlinear pulse propagation in birefringent optical fibers," *Quantum Electronics, IEEE Journal of,* vol. 23, pp. 174-176, 1987.

[103] D. Y. Tang*, et al.*, "Subsideband generation and modulational instability lasing in a fiber soliton laser," *J. Opt. Soc. Am. B,* vol. 18, pp. 1443-1450, 2001.

[104] K. M. Spaulding*, et al.*, "Nonlinear dynamics of mode-locking optical fiber ring lasers," *J. Opt. Soc. Am. B,* vol. 19, pp. 1045-1054, 2002.

[105] V. E. Zakharov and A. B. Shabat, "Exact theory of two-dimensional self-focusing and one-dimensional self-modulation of waves in nonlinear media " *Soviet Physics-JETP,* vol. 34, pp. 62-69, 1972.

[106] Y. S. Kivshar and B. Luther-Davies, "Dark optical solitons: physics and applications," *Physics Reports,* vol. 298, pp. 81-197, 1998.

[107] L. N. Binh, *Photonic signal processing: techniques and applications* Boca Raton, USA CRC Press, 2008.

[108] H. A. Haus and A. Mecozzi, "Long-term storage of a bit stream of solitons," *Opt. Lett.,* vol. 17, pp. 1500-1502, 1992.

[109] H. Haus, "A theory of forced mode locking," *Quantum Electronics, IEEE Journal of,* vol. 11, pp. 323-330, 1975.

[110] N. J. Doran and D. Wood, "Nonlinear-optical loop mirror," *Opt. Lett.,* vol. 13, pp. 56-58, 1988.

[111] M. E. Fermann, *et al.*, "Nonlinear amplifying loop mirror," *Opt. Lett.,* vol. 15, pp. 752-754, 1990.

[112] C. J. Chen, *et al.*, "Soliton fiber ring laser," *Opt. Lett.,* vol. 17, pp. 417-419, 1992.

[113] E. P. Ippen, *et al.*, "Additive pulse mode locking," *J. Opt. Soc. Am. B,* vol. 6, pp. 1736-1745, 1989.

[114] O. E. Martinez, *et al.*, "Theory of passively mode-locked lasers including self-phase modulation and group-velocity dispersion," *Opt. Lett.,* vol. 9, pp. 156-158, 1984.

[115] S. M. J. Kelly, "Characteristic sideband instability of periodically amplified average soliton," *Electronics Letters,* vol. 28, pp. 806-807, 1992.

[116] M. L. Dennis and I. N. Duling, III, "Experimental study of sideband generation in femtosecond fiber lasers," *Quantum Electronics, IEEE Journal of,* vol. 30, pp. 1469-1477, 1994.

[117] H. Sotobayashi and K. Kikuchi, "Design Theory of Ultra-Short Pulse Generation from Actively Mode-Locked Fiber Lasers," *IEICE Transactions on Electronics,* vol. E81-C, pp. 201-207, 1998.

[118] D. J. Jones, *et al.*, "Subpicosecond solitons in an actively mode-locked fiber laser," *Opt. Lett.,* vol. 21, pp. 1818-1820, 1996.

[119] H. A. Haus and A. Mecozzi, "Noise of mode-locked lasers," *Quantum Electronics, IEEE Journal of,* vol. 29, pp. 983-996, 1993.

[120] H. A. Haus, *et al.*, "Theory of soliton stability in asynchronous modelocking," *Lightwave Technology, Journal of,* vol. 14, pp. 622-627, 1996.

[121] K. Tamura, *et al.*, "Forced Phase Modulation and Self Phase Modulation Effects in Dispersion-Tuned Mode-Locked Fiber Lasers," *IEICE Transactions on Electronics,* vol. E81, pp. 195-200, 1998.

[122] S. Longhi and P. Laporta, "Floquet theory of intracavity laser frequency modulation," *Physical Review A,* vol. 60, p. 4016, 1999.

[123] S. Yang and X. Bao, "Experimental observation of excess noise in a detuned phase-modulation harmonic mode-locking laser," *Physical Review A,* vol. 74, p. 033805, 2006.

[124] Z. Ahmed and N. Onodera, "High repetition rate optical pulse generation by frequency multiplication in actively modelocked fib," *Electronics Letters,* vol. 32, p. 455, 1996.

[125] M.-Y. Jeon, *et al.*, "Pulse-amplitude-equalized output from a rational harmonic mode-locked fiber laser," *Opt. Lett.,* vol. 23, pp. 855-857, 1998.

[126] C. G. Lee, *et al.*, "Pulse-amplitude equalization in a rational harmonic mode-locked semiconductor ring laser using optical feedback," *Optics Communications,* vol. 209, pp. 417-425, 2002.

[127] Y. Kim, *et al.*, "Pulse-amplitude equalization in a rational harmonic mode-locked semiconductor fiber ring laser using a dual-drive Mach-Zehnder modulator," *Opt. Express,* vol. 12, pp. 907-915, 2004.

[128] G. Zhu and N. K. Dutta, "Eighth-order rational harmonic mode-locked fiber laser with amplitude-equalized output operating at 80 Gbits/s," *Opt. Lett.,* vol. 30, pp. 2212-2214, 2005.

[129] F. Xinhuan, *et al.*, "Pulse-amplitude equalization in a rational harmonic mode-locked fiber laser using nonlinear modulation," *Photonics Technology Letters, IEEE,* vol. 16, pp. 1813-1815, 2004.

[130] M. L. Dennis, *et al.*, "Inherently bias drift free amplitude modulator," *Electronics Letters,* vol. 32, pp. 547-548, 1996.

[131] M. L. Dennis and I. N. Duling, III, "Polarisation-independent intensity modulator based on lithium niobate," *Electronics Letters,* vol. 36, pp. 1857-1858, 2000.

[132] S. Yang, *et al.*, "80-GHz pulse generation from a repetition-rate-doubled FM mode-locking fiber laser," *Photonics Technology Letters, IEEE,* vol. 17, pp. 300-302, 2005.

[133] Y. Shiquan and B. Xiaoyi, "Repetition-rate-multiplication in actively mode-locking fiber laser by using phase modulated fiber loop mirror," *Quantum Electronics, IEEE Journal of,* vol. 41, pp. 1285-1292, 2005.

[134] H. A. Haus, *et al.*, "Additive-pulse modelocking in fiber lasers," *Quantum Electronics, IEEE Journal of,* vol. 30, pp. 200-208, 1994.

[135] T. F. Carruthers, *et al.*, "Active-passive modelocking in a single-polarisation erbium fibre laser," *Electronics Letters,* vol. 30, pp. 1051-1053, 1994.

[136] C. R. Doerr, *et al.*, "Additive-pulse limiting," *Opt. Lett.,* vol. 19, pp. 31-33, 1994.

[137] N. Onodera, *et al.*, "Cyclic wavelength jitter in actively mode-locked semiconductor lasers," *Electronics Letters,* vol. 27, pp. 220-222, 1991.

[138] B. A. Malomed and A. A. Nepomnyashchy, "Kinks and solitons in the generalized Ginzburg-Landau equation," *Physical Review A,* vol. 42, p. 6009, 1990.

[139] N. N. Akhmediev, *et al.*, "Multisoliton Solutions of the Complex Ginzburg-Landau Equation," *Physical Review Letters,* vol. 79, p. 4047, 1997.

[140] B. A. Malomed, "Bound solitons in the nonlinear Schrödinger&Ginzburg-Landau equation," *Physical Review A,* vol. 44, p. 6954, 1991.

[141] B. A. Malomed, "Bound solitons in coupled nonlinear Schrödinger equations," *Physical Review A,* vol. 45, p. R8321, 1992.

[142] N. H. Seong and D. Y. Kim, "Experimental observation of stable bound solitons in a figure-eight fiber laser," *Opt. Lett.,* vol. 27, pp. 1321-1323, 2002.

[143] Y. D. Gong, *et al.*, "Close spaced ultra-short bound solitons from DI-NOLM Figure-8 fiber laser," *Optics Communications,* vol. 220, pp. 297-302, 2003.

[144] P. Grelu, *et al.*, "Relative phase locking of pulses in a passively mode-locked fiber laser," *J. Opt. Soc. Am. B,* vol. 20, pp. 863-870, 2003.

[145] D. Y. Tang, *et al.*, "Compound pulse solitons in a fiber ring laser," *Physical Review A,* vol. 68, p. 013816, 2003.

[146] B. Zhao, *et al.*, "Energy quantization of twin-pulse solitons in a passively mode-locked fiber ring laser," *Applied Physics B: Lasers and Optics,* vol. 77, pp. 585-588, 2003.

[147] Y. D. Gong, *et al.*, "Regimes of operation states in passively mode-locked fiber soliton ring laser," *Optics & Laser Technology,* vol. 36, pp. 299-307, 2004.

[148] B. Ortac, *et al.*, "Generation of bound states of three ultrashort pulses with a passively mode-locked high-power Yb-doped double-clad fiber laser," *Photonics Technology Letters, IEEE,* vol. 16, pp. 1274-1276, 2004.

[149] B. Zhao, *et al.*, "Passive harmonic mode locking of twin-pulse solitons in an erbium-doped fiber ring laser," *Optics Communications,* vol. 229, pp. 363-370, 2004.

[150] D. Y. Tang, *et al.*, "Multipulse bound solitons with fixed pulse separations formed by direct soliton interaction," *Applied Physics B: Lasers and Optics,* vol. 80, pp. 239-242, 2005.

[151] M. Grapinet and P. Grelu, "Vibrating soliton pairs in a mode-locked laser cavity," *Opt. Lett.,* vol. 31, pp. 2115-2117, 2006.

[152] W.-W. Hsiang, *et al.*, "Stable new bound soliton pairs in a 10 GHz hybrid frequency modulation mode-locked Er-fiber laser," *Opt. Lett.,* vol. 31, pp. 1627-1629, 2006.

[153] D. Y. Tang, *et al.*, "Mechanism of multisoliton formation and soliton energy quantization in passively mode-locked fiber lasers," *Physical Review A,* vol. 72, p. 043816, 2005.

[154] M. J. Lederer, *et al.*, "Multipulse operation of a Ti:sapphire laser mode locked by an ion-implanted semiconductor saturable-absorber mirror," *J. Opt. Soc. Am. B,* vol. 16, pp. 895-904, 1999.

[155] F. X. Kurtner, *et al.*, "Mode-locking with slow and fast saturable absorbers-what's the difference?," *Selected Topics in Quantum Electronics, IEEE Journal of,* vol. 4, pp. 159-168, 1998.

[156] D. Y. Tang, *et al.*, "Stimulated soliton pulse formation and its mechanism in a passively mode-locked fibre soliton laser," *Optics Communications,* vol. 165, pp. 189-194, 1999.

[157] R. P. Davey, *et al.*, "Interacting solitons in erbium fibre laser," *Electronics Letters,* vol. 27, pp. 1257-1259, 1991.

[158] A. B. Grudinin, *et al.*, "Energy quantisation in figure eight fibre laser," *Electronics Letters,* vol. 28, pp. 67-68, 1992.

[159] G. Martel, *et al.*, "On the possibility of observing bound soliton pairs in a wave-breaking-free mode-locked fiber laser," *Opt. Lett.,* vol. 32, pp. 343-345, 2007.

[160] A. Komarov, *et al.*, "Ultrahigh-repetition-rate bound-soliton harmonic passive mode-locked fiber lasers," *Opt. Lett.,* vol. 33, pp. 2254-2256, 2008.

[161] J. N. Kutz, *et al.*, "Stabilized pulse spacing in soliton lasers due to gain depletion and recovery," *Quantum Electronics, IEEE Journal of,* vol. 34, pp. 1749-1757, 1998.

[162] A. N. Pilipetskii, *et al.*, "Acoustic effect in passively mode-locked fiber ring lasers," *Opt. Lett.,* vol. 20, pp. 907-909, 1995.

[163] W. H. Loh, *et al.*, "Soliton interaction in the presence of a weak nonsoliton component," *Opt. Lett.,* vol. 19, pp. 698-700, 1994.

[164] L. Socci and M. Romagnoli, "Long-range soliton interactions in periodically amplified fiber links," *J. Opt. Soc. Am. B,* vol. 16, pp. 12-17, 1999.

[165] D. Y. Tang, *et al.*, "Soliton interaction in a fiber ring laser," *Physical Review E,* vol. 72, p. 016616, 2005.

[166] G. Ph and J. M. Soto-Crespo, "Multisoliton states and pulse fragmentation in a passively mode-locked fibre laser," *Journal of Optics B: Quantum and Semiclassical Optics,* vol. 6, p. S271, 2004.

[167] F. Gutty, *et al.*, "Stabilisation of modelocking in fibre ring laser through pulse bunching," *Electronics Letters,* vol. 37, pp. 745-746, 2001.

[168] D. Krylov, *et al.*, "Observation of the breakup of a prechirped N-soliton in an optical fiber," *Opt. Lett.,* vol. 24, pp. 1191-1193, 1999.

[169] S. Longhi, "Pulse dynamics in actively mode-locked lasers with frequency shifting," *Physical Review E,* vol. 66, p. 056607, 2002.

[170] N. J. Smith, *et al.*, "Suppression of soliton interactions by periodic phase modulation," *Opt. Lett.,* vol. 19, pp. 16-18, 1994.

[171] S. Wabnitz, "Suppression of soliton interactions by phase modulation," *Electronics Letters,* vol. 29, pp. 1711-1713, 1993.

[172] T. Georges and F. Favre, "Modulation, filtering, and initial phase control of interacting solitons," *J. Opt. Soc. Am. B,* vol. 10, pp. 1880-1889, 1993.

[173] J. P. Gordon, "Interaction forces among solitons in optical fibers," *Opt. Lett.,* vol. 8, pp. 596-598, 1983.

[174] Y. Kodama and K. Nozaki, "Soliton interaction in optical fibers," *Opt. Lett.,* vol. 12, pp. 1038-1040, 1987.

[175] F. M. Mitschke and L. F. Mollenauer, "Experimental observation of interaction forces between solitons in optical fibers," *Opt. Lett.,* vol. 12, pp. 355-357, 1987.

[176] N. D. Nguyen and L. N. Binh, "Generation of bound solitons in actively phase modulation mode-locked fiber ring resonators," *Optics Communications,* vol. 281, pp. 2012-2022, 2008.

[177] J. G. Proakis, *Digital communications*. N.Y.: McGraw-Hill, 2001.

[178] J. W. Sulhoff*, et al.*, "Spectral-hole burning in erbium-doped silica and fluoride fibers," *Photonics Technology Letters, IEEE,* vol. 9, pp. 1578-1579, 1997.

[179] J. Sun*, et al.*, "Multiwavelength erbium-doped fiber lasers exploiting polarization hole burning," *Optics Communications,* vol. 182, pp. 193-197, 2000.

[180] G. Das and J. W. Y. Lit, "Room-temperature multiwavelength operation of an elliptical core erbium-doped fiber laser," *Microwave and Optical Technology Letters,* vol. 33, pp. 184-186, 2002.

[181] E. Desurvire, *Erbium-Doped Fiber Amplifiers: Principles and Applications*. New York: John Wiley & Sons, 1994.

[182] E. Lichtman, "Limitations imposed by polarization-dependent gain and loss on all-optical ultralong communication systems," *Lightwave Technology, Journal of,* vol. 13, pp. 906-913, 1995.

[183] L. J. Wang*, et al.*, "Analysis of polarization-dependent gain in fiber amplifiers," *Quantum Electronics, IEEE Journal of,* vol. 34, pp. 413-418, 1998.

[184] W. Sohler, "Integrated optics in LiNbO3," *Thin Solid Films,* vol. 175, pp. 191-200, 1989.

[185] G. s. Lifante, *Integrated photonics fundamentals*: Hoboken, NJ : J. Wiley 2003.

[186] W. Leeb*, et al.*, "Measurement of velocity mismatch in traveling-wave electrooptic modulators," *Quantum Electronics, IEEE Journal of,* vol. 18, pp. 14-16, 1982.

[187] K. Kawano*, et al.*, "A wide-band and low-driving-power phase modulator employing a Ti:LiNbO₃ optical waveguide at 1.5 mu m," *Photonics Technology Letters, IEEE,* vol. 1, pp. 33-34, 1989.

[188] K. Kawano*, et al.*, "New travelling-wave electrode Mach-Zehnder optical modulator with 20 GHz bandwidth and 4.7 V driving voltage at 1.52 mu m wavelength," *Electronics Letters,* vol. 25, pp. 1382-1383, 1989.

[189] K. Noguchi*, et al.*, "A broadband Ti:LiNbO₃ optical modulator with a ridge structure," *Lightwave Technology, Journal of,* vol. 13, pp. 1164-1168, 1995.

[190] R. Tench*, et al.*, "Performance evaluation of waveguide phase modulators for coherent systems at 1.3 and 1.5 µm," *Lightwave Technology, Journal of,* vol. 5, pp. 492-501, 1987.

[191] Y. Shi*, et al.*, "High-Speed Electrooptic Modulator Characterization Using Optical Spectrum Analysis," *J. Lightwave Technol.,* vol. 21, p. 2358, 2003.

[192] R. Regener and W. Sohler, "Loss in low-finesse Ti:LiNbO₃ optical waveguide resonators," *Applied Physics B: Lasers and Optics,* vol. 36, pp. 143-147, 1985.

[193] E. Chan and R. A. Minasian, "A New Optical Phase Modulator Dynamic Response Measurement Technique," *Lightwave Technology, Journal of,* vol. 26, pp. 2882-2888, 2008.

[194] E. H. W. Chan and R. A. Minasian, "Sagnac-loop-based equivalent negative tap photonic notch filter," *Photonics Technology Letters, IEEE,* vol. 17, pp. 1740-1742, 2005.

[195] R. Stubbe*, et al.*, "Polarization selective phase modulator in LiNbO₃," *Photonics Technology Letters, IEEE,* vol. 2, pp. 187-190, 1990.

[196] X. Rejeaunier*, et al.*, "A tunable mode-locked erbium-doped fibre laser using a Lyot-type tuner integrated in lithium niobate," *Optics Communications,* vol. 185, pp. 375-380, 2000.

[197] G. Shabtay*, et al.*, "Tunable birefringent filters - optimal iterative design," *Opt. Express,* vol. 10, pp. 1534-1541, 2002.

[198] C. O'Riordan*, et al.*, "Actively Mode-locked Multiwavelength Fibre Ring Laser Incorporating a Lyot Filter, Hybrid Gain Medium and Birefringence Compensated LiNbO3 Modulator," in *Transparent Optical Networks, 2007. ICTON '07. 9th International Conference on*, 2007, pp. 248-251.

[199] G. J. Sellers and S. Sriram, "Manufacturing of lithium niobate integrated optic devices," *Optics News,* vol. 14, pp. 29-31, 1988.

[200] S. P. Li and K. T. Chan, "Electrical wavelength tunable and multiwavelength actively mode-locked fiber ring laser," *Applied Physics Letters,* vol. 72, pp. 1954-1956, Apr 1998.

[201] Y. Zhao*, et al.*, "Wavelength tuning of 1/2-rational harmonically mode-locked pulses in a cavity-dispersive fiber laser," *Applied Physics Letters,* vol. 73, pp. 3483-3485, Dec 1998.

[202] D. Lingze*, et al.*, "Smoothly wavelength-tunable picosecond pulse generation using a harmonically mode-locked fiber ring laser," *Lightwave Technology, Journal of,* vol. 21, pp. 930-937, 2003.

[203] T. Aizawa*, et al.*, "Effect of spectral-hole burning on multi-channel EDFA gain profile," in *Optical Fiber Communication Conference, 1999, and the International Conference on Integrated Optics and Optical Fiber Communication. OFC/IOOC '99. Technical Digest*, 1999, pp. 102-104 vol.2.

[204] M. Bolshtyansky, "Spectral Hole Burning in Erbium-Doped Fiber Amplifiers," *J. Lightwave Technol.,* vol. 21, p. 1032, 2003.

[205] D. Kovsh*, et al.*, "Gain reshaping caused by spectral hole burning in long EDFA-based transmission links," in *Optical Fiber Communication Conference, 2006 and the 2006 National Fiber Optic Engineers Conference. OFC 2006*, 2006, p. 3 pp.

[206] L. Rapp and J. Ferreira, "Dynamics of Spectral Hole Burning in EDFAs: Dependency on Pump Wavelength and Pump Power," *Photonics Technology Letters, IEEE,* vol. 22, pp. 1256-1258, 2010.

[207] M. Desaix*, et al.*, "Propagation properties of chirped soliton pulses in optical nonlinear Kerr media," *J. Phys. Rev. E,* vol. 65, 2002.

[208] J. E. Prilepsky*, et al.*, "Conversion of a chirped Gaussian pulse to a soliton or a bound multisoliton state in quasi-lossless and lossy optical fiber spans," *J. Opt. Soc. Am. B,* vol. 24, pp. 1254-1261, 2007.

[209] K. J. Blow and N. J. Doran, "The asymptotic dispersion of soliton pulses in lossy fibres," *Optics Communications,* vol. 52, pp. 367-370, 1985.

[210] A. Hasegawa and Y. Kodama, "Guiding-center soliton," *Physical Review Letters,* vol. 66, p. 161, 1991.

[211] M. Nakazawa*, et al.*, "Soliton amplification and transmission with Er^{3+}-doped fibre repeater pumped by GaInAsP diode," *Electronics Letters,* vol. 25, pp. 199-200, 1989.

[212] Y. Kodama and A. Hasegawa, "Amplification and reshaping of optical solitons in glass fiber-II," *Opt. Lett.,* vol. 7, pp. 339-341, 1982.

[213] Y. Kodama and A. Hasegawa, "Amplification and reshaping of optical solitons in glass fiber-III. amplifiers with random gain," *Opt. Lett.,* vol. 8, pp. 342-344, 1983.

[214] A. Hasegawa, "Amplification and reshaping of optical solitons in a glass fiber-IV: Use of the stimulated Raman process," *Opt. Lett.,* vol. 8, pp. 650-652, 1983.

[215] L. F. Mollenauer and K. Smith, "Demonstration of soliton transmission over more than 4000 kmin fiber with loss periodically compensated by Raman gain," *Opt. Lett.,* vol. 13, pp. 675-677, 1988.

[216] L. Mollenauer*, et al.*, "Soliton propagation in long fibers with periodically compensated loss," *Quantum Electronics, IEEE Journal of,* vol. 22, pp. 157-173, 1986.

[217] M. Nakazawa, "Tb/s OTDM technology," in *Optical Communication, 2001. ECOC '01. 27th European Conference on*, 2001, pp. 184-187 vol.2.

[218] L. Ju Han*, et al.*, "Wavelength tunable 10-GHz 3-ps pulse source using a dispersion decreasing fiber-based nonlinear optical loop mirror," *Selected Topics in Quantum Electronics, IEEE Journal of,* vol. 10, pp. 181-185, 2004.

[219] A. Sano and Y. Miyamoto, "Performance evaluation of prechirped RZ and CS-RZ formats in high-speed transmission systems with dispersion management," *Lightwave Technology, Journal of,* vol. 19, pp. 1864-1871, 2001.

[220] J. Fatome*, et al.*, "Practical design rules for single-channel ultra high-speed dense dispersion management telecommunication systems," *Optics Communications,* vol. 282, pp. 1427-1434, 2009.

[221] A. B. Grudinin and I. A. Goncharenko, "Increased amplifier spacing in soliton system with partial dispersion compensation," *Electronics Letters,* vol. 32, pp. 1602-1604, 1996.

[222] M. Nakazawa*, et al.*, "Marked increase in the power margin through the use of a dispersion-allocated soliton," *Photonics Technology Letters, IEEE,* vol. 8, pp. 1088-1090, 1996.

[223] J. H. B. Nijhof*, et al.*, "Energy enhancement of dispersion-managed solitons and WDM," *Electronics Letters,* vol. 34, pp. 481-482, 1998.

[224] M. Nakazawa*, et al.*, "Nonlinear pulse transmission through an optical fiber at zero-average group velocity dispersion," *Photonics Technology Letters, IEEE,* vol. 8, pp. 452-454, 1996.

[225] E. Poutrina and G. P. Agrawal, "Design rules for dispersion-managed soliton systems," *Optics Communications,* vol. 206, pp. 193-200, 2002.

[226] J. H. B. Nijhof*, et al.*, "Stable soliton-like propagation in dispersion managed systems with net anomalous, zero and normal dispersion," *Electronics Letters,* vol. 33, pp. 1726-1727, 1997.

[227] T. Inoue*, et al.*, "Interactions between dispersion-managed solitons in optical-time-division-multiplexed systems," *Electronics and Communications in Japan (Part II: Electronics),* vol. 84, pp. 24-29, 2001.

[228] C. Paré and P. A. Bélanger, "Antisymmetric soliton in a dispersion-managed system," *Optics Communications,* vol. 168, pp. 103-109, 1999.

[229] A. Maruta*, et al.*, "Bisoliton propagating in dispersion-managed system and its application to high-speed and long-haul optical transmission," *Selected Topics in Quantum Electronics, IEEE Journal of,* vol. 8, pp. 640-650, 2002.

[230] M. Stratmann*, et al.*, "Dark solitons are stable in dispersion maps of either sign of path-average dispersion," in *Quantum Electronics and Laser Science Conference, 2002. QELS '02. Technical Digest. Summaries of Papers Presented at the*, 2002, p. 226.

[231] M. Stratmann and F. Mitschke, "Bound states between dark and bright solitons in dispersion maps," in *Quantum Electronics and Laser Science Conference, 2002. QELS '02. Technical Digest. Summaries of Papers Presented at the*, 2002, pp. 226-227.

[232] M. Stratmann*, et al.*, "Experimental Observation of Temporal Soliton Molecules," *Physical Review Letters,* vol. 95, p. 143902, 2005.

[233] I. Gabitov*, et al.*, "Twin families of bisolitons in dispersion-managed systems," *Opt. Lett.,* vol. 32, pp. 605-607, 2007.

[234] J. Azana and M. A. Muriel, "Temporal self-imaging effects: theory and application for multiplying pulse repetition rates," *Selected Topics in Quantum Electronics, IEEE Journal of,* vol. 7, pp. 728-744, 2001.

[235] N. D. Nguyen*, et al.*, "Temporal imaging and optical repetition multiplication via quadratic phase modulation," in *Information, Communications & Signal Processing, 2007 6th International Conference on*, 2007, pp. 1-5.

[236] N. D Nguyen and L. N. Binh, "Generation of bound-solitons in actively phase modulation mode-locked fiber ring resonators," *Opt. Coms.,* vol. 281, pp. 2012-2022, 2008.

[237] J. M. Lipton, *et al.*, "Use of the bispectrum to analyse properties of the human electrocardiograph," *Aust. Phys. Eng. Sci. Med.,,* vol. 21, pp. 1-10, 1998.

[238] A. W. Lohmann, *et al.*, "Speckle masking in astronomy: triple correlation theory and applications," *Appl. Opt.,* vol. 22, pp. 4028-4037, 1983.

[239] M. J. Northcott, *et al.*, "Algorithms for image reconstruction from photon-limited data using the triple correlation," *J. Opt. Soc. Am. A,* vol. 5, pp. 986-992, 1988.

[240] I. D. Jung, *et al.*, "High-dynamic-range characterization of ultrashort pulses," *Applied Physics B: Lasers and Optics,* vol. 65, pp. 307-310, 1997.

[241] M. E. Marhic, *et al.*, "Broadband fiber optical parametric amplifiers," *Opt. Lett.,* vol. 21, pp. 573-575, 1996.

[242] J. Hansryd, *et al.*, "Fiber-based optical parametric amplifiers and their applications," *IEEE J. Select. Topics in Quat. Elect.,,* vol. 8, pp. 506-520, 2002.

[243] R. Stolen and J. Bjorkholm, "Parametric amplification and frequency conversion in optical fibers," *IEEE J. Quantum Electron.,* vol. 18, pp. 1062-1072, 1982.

[244] M.-C. Ho, *et al.*, "200-nm-Bandwidth Fiber Optical Amplifier Combining Parametric and Raman Gain," *J. Lightwave Technol.,* vol. 19, p. 977, 2001.

[245] P. O. Hedekvist, *et al.*, "Fiber four-wave mixing demultiplexing with inherent parametric amplification," *J. Lightwave Technol.,* vol. 15, pp. 2051-2058, 1997.

[246] R. M. Jopson, *et al.*, "Compensation of fiber chromatic dispersion by spectral inversion," *Electron. Lett.,* vol. 29, pp. 576-578, 1993.

[247] S. L. Jansen, *et al.*, "Long-haul DWDM transmission systems employing optical phase conjugation," *IEEE J. Select. Topics in Quat. Elect.,* vol. 12, pp. 505-520, 2006.

[248] C. Lorattanasane and K. Kikuchi, "Design theory of long-distance optical transmission systems using midway optical phase conjugation," *J. Lightwave Technol.,* vol. 15, pp. 948-955, 1997.

[249] M. D. Pelusi, *et al.*, "Applications of Highly-Nonlinear Chalcogenide Glass Devices Tailored for High-Speed All-Optical Signal Processing," *IEEE J. Select. Topics in Quat. Elect.,* vol. 14, pp. 529-539, 2008.

[250] T. Yamamoto and M. Nakazawa, "Active optical pulse compression with a gain of 29.0 dB by using four-wave mixing in an optical fiber," *IEEE Photon. Technol. Lett.,* vol. 9, pp. 1595-1597, 1997.

[251] J. Hansryd and P. A. Andrekson, "Wavelength tunable 40GHz pulse source based on fibre optical parametric amplifier," *Electron. Lett.,* vol. 37, pp. 584-585, 2001.

[252] R. Slavik, *et al.*, "Demultiplexing of 320-Gb/s OTDM Data Using Ultrashort Flat-Top Pulses," *Photonics Technology Letters, IEEE,* vol. 19, pp. 1855-1857, 2007.

[253] B. Le Nguyen, *et al.*, "Nonlinear photonic pre-processing bi-spectrum optical receivers for long haul optically amplified transmission systems," in *Communication Systems (ICCS), 2010 IEEE International Conference on*, 2010, pp. 630-634.

[254] B. Wirnitzer, "Measurement of ultrashort laser pulses," *Optics Communications,* vol. 48, pp. 225-228, 1983.

[255] T.-M. Liu, *et al.*, "Triple-optical autocorrelation for direct optical pulse-shape measurement," *Applied Physics Letters,* vol. 81, pp. 1402-1404, 2002.

[256] D. Y. Tang, *et al.*, "Observation of High-Order Polarization-Locked Vector Solitons in a Fiber Laser," *Physical Review Letters,* vol. 101, p. 153904, 2008.

[257] A. Rosenthal and M. Horowitz, "Bragg-soliton formation and pulse compression in a one-dimensional periodic structure," *Physical Review E,* vol. 74, p. 066611, 2006.

[258] Y. P. Shapira and M. Horowitz, "Optical AND gate based on soliton interaction in a fiber Bragg grating," *Opt. Lett.,* vol. 32, pp. 1211-1213, 2007.

[259] P. Russell, "Photonic Crystal Fibers," *Science,* vol. 299, pp. 358-362, 2003.

[260] H. Bartelt, *et al.*, "Phase and amplitude recovery from bispectra," *Appl. Opt.,* vol. 23, pp. 3121-3129, 1984.

[261] D. Marcuse, *et al.*, "Effect of fiber nonlinearity on long-distance transmission," *Lightwave Technology, Journal of,* vol. 9, pp. 121-128, 1991.